In-situ damage and strain monitoring of large polymer composite structures using carbon nanotube networks

Ali Naghashpour

A thesis
In the Department
Of
Mechanical and Industrial Engineering

Presented in Partial Fulfillment of the Requirements
For the Degree of
Doctor of Philosophy (Mechanical Engineering) at
Concordia University
Montreal, Quebec, Canada

April 2014

CONCORDIA UNIVERSITY
SCHOOL OF GRADUATE STUDIES

This is to certify that the thesis prepared

By: Ali Naghashpour

Entitled: In-situ damage and strain monitoring of large polymer composite structures using carbon nanotube networks

and submitted in partial fulfillment of the requirements for the degree of

Doctor of Philosophy (Mechanical Engineering)

complies with the regulations of the University and meets the accepted standards with respect to originality and quality.

Signed by the final examining committee:

Dr. W.P. Zhu	Chair
Dr. Z. Liang	External Examiner
Dr. A. Bagchi	External to Program
Dr. M. Pugh	Examiner
Dr. R. Sedaghati	Examiner
Dr. S.V. Hoa	Thesis Supervisor

Approved by: ______________________________
Dr. A. Dolatabadi , Graduate Program Director

April 14, 2014 ______________________________
Dr. C. Trueman, Interim Dean
Faculty of Engineering and Computer Science

Abstract

In-situ damage and strain monitoring of large polymer composite structures using carbon nanotube networks

Ali Naghashpour, Ph.D.

Concordia University, 2014

In this work, multiwalled carbon nanotubes (MWCNTs) have been introduced in fiber reinforced polymer composites (FRPC) to enhance their capabilities in terms of sensing and improving electrical properties. Even though there have been extensive studies on incorporating MWCNTs into polymer matrix composites to monitor their integrity, no work has been found to provide a technique to detect, locate and quantify damage in large polymer composite structure (LPCS) and also to investigate electrical resistance behavior of glass fiber/epoxy/MWCNT composites subjected to multi-directional deformation.

The thesis is organized into two major sections: Developing two new structural health monitoring (SHM) techniques to detect, locate and quantify damages in LPCS, and investigating electrical resistance behavior of glass fiber/epoxy/MWCNT composites subjected to multi-directional deformation. In the first part of the thesis, two new, practical and real-time SHM techniques have been developed. One is for LPCS made of electrically non-conducive fibers and MWCNT networks. The other is for LPCS made of electrically conducive fibers and MWCNT networks. In these techniques, MWCNTs are added into epoxy matrix. This modified matrix is then incorporated with long fibers to make large composite plates. Two different strategies have been proposed for measuring electrical properties of LPCS depending on the type of fibers. The large plate is marked with grid points where electrically conductive silver paints are deposited. The electrical resistances and potentials between the grid points for electrically non-conductive fibers and conductive fibers reinforced polymer composite structures containing MWCNT are measured respectively. These values are used as reference sets. It has been shown that the occurrence of the damage makes the electrical properties between the contact points surrounding this damage change. The significant change in the electrical properties between contact points is used as an indication for detection, location and quantification of damage in the large plates. The SHM computer programs are written to provide the facility to detect, locate and quantify damage for the LPCSs in real-time. Two new concepts have been introduced for detecting, locating and quantifying damage in LPCSs using MWCNT networks. One is uniformity of MWCNT distribution. The other is sensitivity to change in electrical resistance. A new model of resistors network has been proposed for composite plates with different electrical conductivity as a result of different quantity of MWCNT. Theoretical analyses are performed based on Ohm's and Kirchhoff's laws using Matlab Simulink. Good agreement is found between experimental and simulation results.

In the second part of the thesis, the behavior of electrical resistance for glass fiber/epoxy composite laminates containing MWCNT subjected to uniaxial stresses along different directions is investigated. An explanation is provided for the electrical resistance behavior of the laminates containing MWCNT subjected to multi-directional deformation.

Acknowledgements

I would like to express my sincere gratitude to my merciful God for blessing me with wonderful family, professional and supportive professor and many more things who gave them to me which I cannot count them one by one. I would like to express my deepest sense of gratitude to my thesis supervisor Professor Suong Van Hoa, for giving me the opportunity to work on this project, and for his continuous guidance and mental support all these years. I am heartily grateful to him, whose encouragement, guidance and support from the initial to the final level enabled me to develop an understanding of the subject. I am also grateful to him for careful reading and minute criticism of this thesis. I would also like to acknowledge my examination committee members, Dr. Zhiyong (Richard) Liang, Dr. Martin Pugh, Dr. Ramin Sedaghati and Dr. Ashutosh Bagchi. My gratitude goes to all (CONCOM), for their professional and technical supports. In addition I wish to thank all friends in particular Mr. Rajan Desai, Dr. Isoif Daniel Rosca, the late Dr. Ming Xie, Mr. Heng Wang, Mr. Saeid Jafari, Mr. Pooya Maghoul, Mr. Pooya Rowghanian, Dr. Mohamad geuchy, Mr. Hossein Ghayoor and Mr. Asgar Khan for their supportive friendship and help. I wish to express my gratitude to my beloved father, mother, brother and sister for their moral support and understanding, and for their solid supports in not leaving me alone in different aspects and facing and solving all obstacles, and to whom, I am greatly indebted.

Last but not least, I want to offer my regards and blessings to all of those who supported me in any respect during the completion of the project and appreciations always stay with them.

Dedication

This thesis is dedicated to my beautiful beloved spouse,

Samira Taherkhani

Table of Contents

Table of Contents vii

List of Figures xi

List of Tables xx

NOMENCLATURE xxi

Chapter 1 Introduction, Literature review, problem statement and objectives 1

- 1.1 Introduction 1
- 1.2 Literature review 2
  - 1.2.1 Ultrasonic 3
  - 1.2.2 Acoustic emission 4
  - 1.2.3 X-Ray 5
  - 1.2.4 Thermography 5
  - 1.2.5 Fiber optics 5
  - 1.2.6 Shearography 6
  - 1.2.7 Electrical conductivity along the direction of carbon fiber 6
  - 1.2.8 Resistance-based sensors 7
  - 1.2.9 Adding carbon nanotubes into the resin to make the resin electrically conductive in composite structures 9
- 1.3 Thesis Objectives 25
- 1.4 Content of the Thesis 26

Chapter 2 Experimental investigation for the development of a structural health monitoring technique for large polymer composite structures made of electrically non-conductive fibers and carbon nanotube networks 28

- 2.1 Introduction 28
- 2.2 Preliminary experimental investigations 31
- 2.3 Experimental method 32
  - 2.3.1 Materials 32
  - 2.3.2 Fabrication of glass fiber/epoxy/ CNT composite plates 32

        2.3.3 Quality control 33
        2.3.4 Electrical resistivity measurements 35
        2.3.5 Variability of electrical resistivity 38
    2.4 Investigation of grid points and grid lines 42
        2.4.1 Grid points 42
        2.4.2 Grid lines 44
    2.5 Electrical resistance measurements 47
        2.5.1 Grid points 47
        2.5.2 Grid lines 47
    2.6 Drilled Holes 49
    2.7 Results and discussion 49
        2.7.1 Grid points: 50
        2.7.2 Grid Lines 57
    2.8 Conclusion 63
Chapter 3 A technique for real-time detection, location and quantification of damages in large polymer composite structures made of electrically non-conductive fibers and carbon nanotube networks 65
    3.1 Experimental Methods 66
        3.1.1 Materials 66
        3.1.2 Methods 66
        3.1.3 Electrical resistance measurements 69
    3.2 Drilled holes and impact tests 70
    3.3 Results and discussion 72
        3.3.1 Glass fabric /epoxy/ MWCNT composite plates 72
        3.3.2 Kevlar fiber/epoxy/MWCNT composite plates 89
    3.4 Conclusions 93
Chapter 4 A technique for real-time detecting, locating and quantifying damage in large polymer composite structures made of carbon fibers and carbon nanotube networks 95
    4.1 Introduction 96

4.2 Experimental methods 99
  4.2.1 Materials 99
  4.2.2 Methods 99
  4.2.3 Electric potential measurements 104
4.3 Drilled holes and impact tests 105
4.4 Result and discussion 106
  4.4.1 Drilled holes and impacted areas 106
  4.4.2 Barely visible impact damage (BVID) 111
4.5 Conclusion 113
Chapter 5 Electrical model of composite plates: Theory and Simulation 114
5.1 Basic definition for electrical conduction 115
  5.1.1 Ohm's law 115
  5.1.2 Kirchhoff's Laws 115
  5.1.3 Current density 116
5.2 Theoretical modeling 116
5.3 Numerical Study 125
  5.3.1 Theoretical formulation of numerical simulation 125
  5.3.2 Numerical simulation 129
5.4 Comparing simulation results with experimental results 138
5.5 Conclusions 139
Chapter 6 Relationship between through-thickness strain and electrical resistance in glass fibers/epoxy composite laminates containing carbon nanotubes 140
6.1 In situ monitoring of through-thickness strain in glass fiber/epoxy composite laminates using carbon nanotube sensors 140
  6.1.1 Introduction 141
  6.1.2 Experimental characterization and materials 144
  6.1.3 Analysis 147
  6.1.4 Experimental methods 151
  6.1.5 Tensile tests along x direction 154

6.1.6 Compression test across the thickness of sample 158
6.1.7 Conclusions 161
6.2 Electrical resistance behavior of Glass fiber/Epoxy/CNTs composite laminates subjected to multi-directional deformation 162
6.2.1 Experiments 163
6.2.2 Explanation for the obtained experimental results 170
6.2.3 Conclusions 177
Chapter 7 Conclusions, contributions and future works 179
7.1 Conclusions 179
7.2 Contributions 182
7.3 Future works 184
7.4 List of Publications 184
7.5 Patent 187

List of Figures

Figure 1.1: A schematic illustration showing the construction of the composite, including the contact locations and the position of the glass fiber plies [47] 8

Figure 1.2: Resistance-based electrically conductive fiber sensors [48] 8

Figure 1.3: A schematic showing system comprising carbon nanofibers reinforced polymeric resin as conductive lines bonded on the surface and connected wires [49] 9

Figure 1.4:Three-dimensional model showing the penetration of nanotubes throughout a fiber array due to their relative scale [5] 10

Figure 1.5: Normalized change in surface resistivity of a) Dry blended and b) Solution cast PMMA/MWCNT at various MWCNT concentrations [57] 11

Figure 1.6: Sensitivity factors for PMMA/MWCNT films [57] 12

Figure 1.7: Comparison of various experimental results [58] 13

Figure 1.8: Gauge factor versus electrical conductivity of sensor [58] 13

Figure 1.9: Tensile results showing a) Five-ply composite with the center ply cut to initiate delamination, b) Cross-ply composite [4] 14

Figure 1.10: Three-points bending results showing a) Span-to-thickness ratio of 4 , b) Span-to-thickness ratio of 8 , Optical microscopic images of c) Interlaminar fracture and d) Fiber and matrix damage for span-to-thickness ratio of 4 and 8 respectively [4] 15

Figure 1.11: Tensile test results resistance versus strain [9, 61] 16

Figure 1.12: Tensile test results showing detection of failure occurred between a) Points 2-3, and b) Points 1-2 [9, 61] 17

Figure 1.13: Tensile test showing a) Sample with mounted electrical contact lines b) Tensile test results [63] 18

Figure 1.14: Fatigue test results showing a) Sample mounted with electrical contact points, b) Change in electrical resistance versus loading cycle and c) Optical image of the $[0_2/90_2]_S$ showing failure [63] 19

Figure 1.15: Impact testing: a) In-plane resistance change, b) Through-thickness resistance change [66] 20

Figure 1.16: Experimental set-up of electric resistance tomography (ERT) and close- up of the sample mounted with electrodes around its periphery[68] 21
Figure 1.17: Volume resistivity for the through-thickness (Z) direction [69] 22
Figure 1.18: Volume resistivity for the in-plane normal to the fibers in transverse (Y) direction and along the fibers (X) direction. In-plane resistivity [69] 23
Figure 1.19: Change in through-thickness electrical resistance across the delamination versus the delamination length [19] 24
Figure 2.1: Schematic illustrating manufacturing process of fiber/epoxy/CNT plate 33
Figure 2.2: TGA result of the composite plate with 1wt% MWCNT after curing 34
Figure 2.3: DSC result of the sample containing 1wt% MWCNT after curing...................... 34
Figure 2.4: Two-probe method for measuring electrical resistivity of sample....................... 35
Figure 2.5: Four-probe method for measuring electrical resistivity of sample...................... 36
Figure 2.6: Van der Pauw fixtures for measuring electrical resistivity by Keithley machines a) Experimental set-up b) Close-up view of sample 37
Figure 2.7: a) Light transmission image of plate 1 containing 1wt% MWCNT.................... 39
Figure 2.8: a) Light transmission image of plate 2 containing 0.3wt% MWCNT................. 39
Figure 2.9: Eight samples cut out from plate 1 containing 1wt% MWCNT a) Volume resistivity measured by the van der pauw and the four-probe methods b) Surface resistivity measured the by two-probe method on both sides 41
Figure 2.10: Plates 3, 4 and 5 specification. The wires attached to black dots, labeled from 1 to 5 are contact-point electrodes 42
Figure 2.11: Specification of plate 6. The wires attached to black dots, labeled from 1 to 9 are contact-point electrodes 43
Figure 2.12: Plate 7 specification. The wires attached to black dots, labeled from 1 to 25 are contact-point electrodes 43
Figure 2.13: Plate 8 specification. The wires attached to black dots, labeled from 1 to 40 are contact-point electrodes 44
Figure 2.14: Plate 9 mounted with twenty eight contact-line electrodes with different spacing 45

Figure 2.15: Plate 10 mounted with five and three contact-line electrodes on top and bottom surfaces respectively 45
Figure 2.16: Specification of plate 11 .The wires attached to black lines labeled from 1 to 5 and 1 to 8 are vertical and horizontal contact-line electrodes respectively 46
Figure 2.17: Plate 3 a) After hole of size (1/4 inch) is drilled b) ERC distribution, plate 4 c) After the hole is drilled d) ERC distribution, plate 5 e) After the hole is drilled f) ERC distribution, g) ERC versus distance between pair of electrodes closest to the hole location 51
Figure 2.18: a) Plate 6 after hole of size (4/16) inch is drilled b) ERC distribution of plate 6 c) ERC versus distance between pair of electrodes and drilled hole (1/4) inch.......................... 52
Figure 2.19: a) Plate 7 after hole of size (4/16) inch is drilled, b) ERC distribution of the composite plate 8. The black dots, labeled from 1 to 25 are representation of contact points 53
Figure 2.20: a) Plate 8 after hole 1(1/16) inch is drilled b) ERC distribution c) Plate 8 after holes 1 and 2 (1/16 and 2/16) inch are drilled d) ERC distribution e) Plate 8 after holes 1, 2, 3, 4, 5 and 6 (1/16, 2/16, 3/16, 4/16, 5/16 and 6/16) inch are drilled f) ERC distribution...... 55
Figure 2.21: Effect of hole volume on ERC (Average electrical resistance: 276,000 ohms) (Data are presented as mean ± standard deviation (SD) from three experiments) 56
Figure 2.22: Plate 9 mounted with twenty eight contact-line electrodes after six holes of sizes (1/16, 2/16, 4/16, 6/16, 8/16 and 12/16) inch are drilled respectively................................... 57
Figure 2.23: ERC versus spacing between contact-line electrodes for drilled holes of sizes 1/16, 2/16, 4/16, 6/16, 8/16 and 12/16 inch 58
Figure 2.24: a) Plate 10 mounted with contact-line electrodes on both sides after hole of size (4/16) inch is drilled. b) AERC distribution after drilling of hole of size 1(4/16) inch. The vertical black lines, labeled from 1 to 5 and the horizontal dash lines, labeled from 1 to 3 are representation of electrical contact lines on top and bottom surfaces of plate 10 respectively 59
Figure 2.25: a) Plate 11 after hole 1(1/16) inch is drilled b) AERC distribution c) Plate 11 after holes 1 and 2 (1/16 and 2/16) inch are drilled d) AERC distribution e) Plate 11 after holes 1, 2, 3, 4, 5 and 6 (1/16, 2/16, 3/16, 4/16, 5/16 and 6/16) inch are drilled f) AERC

distribution. The vertical black lines labeled from 1 to 5 and the horizontal black lines labeled from 1 to 8 are representation of contact lines 61

Figure 2.26: Effect of hole volume on AERC (Average of AER: 54,570 ohms) (Data are presented as mean ± SD from three experiments) 62

Figure 3.1: Viscometer for measuring dynamic viscosity 67

Figure 3.2: Schematic illustration of instrumented plate showing wires attached to the grid points connected to data acquisition (DA) system and computer with program 69

Figure 3.3: Experimental set-up to detect and locate damage due to high velocity impact test 70

Figure 3.4: Light transmission image of glass fiber/epoxy/0.10wt% MWCNT plate 1 mounted with 40 contact points on its surface showing transparent (glass fibers and resin) regions as compared to dark (dispersed MWCNTs) regions 74

Figure 3.5: a) Light transmission image of glass fiber/epoxy/0.20wt% MWCNT plate 2 showing transparent (glass fibers and resin) regions as compared to dark (dispersed MWCNTs) regions b) Distribution of electrical resistance 74

Figure 3.6: a) Light transmission image of glass fiber/epoxy/0.25wt% MWCNT plate 3 showing transparent (glass fibers and resin) regions as compared to dark (dispersed MWCNTs) regions b) Distribution of electrical resistance 75

Figure 3.7: a) Light transmission image of glass fiber/epoxy /0.30wt% MWCNT plate 4 showing dark (dispersed MWCNTs) regions b) Distribution of resistance........................... 75

Figure 3.8: a) Light transmission image of glass fiber/epoxy/0.40wt% MWCNT plate 5 showing dark (dispersed MWCNTs) regions b) Distribution of resistance........................... 76

Figure 3.9: a) Distribution of electrical resistance for glass fiber/epoxy composite plate 6 containing 1.00wt% MWCNT b) Close up view of electrical contact points 76

Figure 3.10: Light transmission optical micrographs of an epoxy composite containing 0.1wt% MWCNT with magnification (4x) a) Liquid uncured sample b) Cured sample. Reagglomeration of MWCNTs is observed by comparing uncured sample with cured sample 78

Figure 3.11: Light transmission optical micrographs of an epoxy composite containing 0.2wt% MWCNT with magnification (4x) a) Liquid uncured sample b) Cured sample. Reagglomeration of MWCNTs is observed by comparing uncured sample with cured sample 79

Figure 3.12: Light transmission optical micrographs of an epoxy composite containing 0.25wt% MWCNT with magnification (4x) a) Liquid uncured sample b) Cured sample. Reagglomeration of MWCNTs is observed by comparing uncured sample with cured sample 80

Figure 3.13: Light transmission optical micrographs of an epoxy composite containing 0.3wt% MWCNT with magnification (4x) a) Liquid uncured sample b) Cured sample. Reagglomeration of MWCNTs is observed by comparing uncured sample with cured sample 81

Figure 3.14: Light transmission optical micrographs of an epoxy composite containing 0.4wt% MWCNT with magnification (4x) a) Liquid uncured sample b) Cured sample. Reagglomeration of MWCNTs is observed by comparing uncured sample with cured sample 82

Figure 3.15: Light transmission optical micrographs of an epoxy composite containing 1wt% MWCNT with magnification (4x) a) Liquid uncured sample b) Cured sample. Reagglomeration of MWCNTs is observed by comparing uncured sample with cured sample 83

Figure 3.16: Dynamic viscosity-shear rate curves of epoxy matrix unfilled and filled with 0.30 wt% MWCNT at a) 25^0C and b) 60^0C 85

Figure 3.17: ERC distribution of glass/epoxy/MWCNT plate 7 after a) Impact damage 1 (78J) , b) Impact damages 1 and 2 (78J each) and c) Plate 7 after impact damages 1 and 2.. 86

Figure 3.18: ERC distribution of glass/epoxy/MWCNT plate 8 after , a) BVI damage 1 (1J), b) BVI damages 1 and 2 (1J and 2J) , c) Impact damages 1, 2,3,4,5 and 6 (1J, 2J, 3J, 4J, 5J and 10J) and d) Effect of energy level on the change in electrical resistance (Data are presented as mean ± SD from three experiments) 87

Figure 3.19: Schematic illustration of 22×13 inch^2 glass fiber/epoxy/0.30wt% MWCNT (plate 8) impacted at six regions using drop weights with impact energies of 1J, 2J, 3J, 4J, 5J and 10J respectively 88

Figure 3.20: ERC distribution for Kevlar fiber/epoxy/0.3wt%MWCNT plate 9 after drilling of a) Hole1 (1/16 inch) b) Holes1 and 2 (1/16 and 2/16 inch), c) Holes1, 2, 3, 4, 5 and 6 (1/16, 2/16, 3/16, 4/16, 5/16 and 6/16 inch) d) Plate 9 after six drilled holes e) Effect of hole volume on the ERC (Data are presented as mean ± SD from three experiments) 90

Figure 3.21: ERC distribution of kevlar fiber/epoxy/0.30wt% MWCNT plate 10 after a) Impact damage 1 (78J), b) Impact damages 1 and 2 (78J each) and c) Plate 10 after two impact damages 1 and 2 91

Figure 3.22: Schematic illustration of 22×13 inch^2 kevlar fiber/epoxy/0.30wt% MWCNT (plate 11) impacted at six regions using drop weights with impact energies of 1J, 2J, 3J, 4J, 5J and 10J respectively 92

Figure 3.23: ERC distribution of plate 11 after a) BVI damage 1 (1J), b) BVI damages 1 and 2 (1J and 2J) c) Impact damages 1, 2,3,4,5 and 6 (1J, 2J, 3J, 4J, 5J and 10J) d) Effect of energy level on the change in electrical resistance (Data are presented as mean ± SD from three experiments) 93

Figure 4.1: Schematic illustrating strategy for EPM using the four-probe method 101

Figure 4.2: Schematic illustration of plate specification and strategy of EPM 102

Figure 4.3: Schematic illustration for describing pairs of electrical contacts corresponding to points 13I and 13V to inject constant electric current (solid red lines) and to measure electric potentials (dashed blue lines) respectively 103

Figure 4.4: Experimental set-up to detect and locate damage due to high velocity impact test 105

Figure 4.5: a) Distribution of electric potential of plate 1. The black dots, labeled 1,., 40 are representations of potential contacts b) Close up view of electrical contact points 106

Figure 4.6: EPC distribution of plate 1 after drilling a) Hole 1 (1/16 in), b) Holes 1 and 2 (1/16 and 2/16 in), c) Holes 1, 2, 3, 4, 5 and 6 (1/16, 2/16, 3/16, 4/16, 5/16, d) plate 1 after six

drilled holes and e) Effect of hole volume on the change in potential (Data are presented as mean ± SD from three experiments) 107

Figure 4.7: Electric potential change distribution of plate 2 after a) Impact damage 1 (78J) and b) Impact damages 1 and 2 (78J each) c) Plate 2 after two impact damages 109

Figure 4.8: a) Schematic illustration of 22×13 inch^2 plate 3 impacted at three regions using drop weights with impact energies of 1, 2 and 3J. Absolute EPC distribution of plate 3 after b) BVI damage 1 (1J), c) BVI damages 1, 2 and 3 (1, 2 and 3J) 112

Figure 5.1: Window (segment B) that can provide sensitivity to ERC and uniformity of electrical conductivity for damage detection, location and quantification 117

Figure 5.2: Example of how damage can cut off a conductive path in aluminum plate. Conduction continues with many conductive paths 117

Figure 5.3: Schematic illustration of CNT clusters dispersed in polymer representing example of how damage can cut off a conductive path in epoxy containing relatively a) Small CNT concentration and b) Large CNT concentration 119

Figure 5.4: An electrical model of network of resistors, representing a) Plate 1 with relatively low conductivity (coarse grid) b) Plate 2 with relatively high conductivity (fine grid) with multiple current paths 120

Figure 5.5: Effect of CNT concentration(wt%) on electrical conductivity [75] 121

Figure 5.6: A network of resistors, showing equivalent resistance of parallel resistances... 122

Figure 5.7: A network of resistors, equivalent resistance of parallel resistances 124

Figure 5.8: A representative resistors network of conductive plate to illustrate formulation125

Figure 5.9: Schematic circuit representing the electrical network in a) Undamaged CFRP structure and damaged CFRP structure b) Increase in resistance change and c) Decrease in resistance change [90] 131

Figure 5.10: Network of resistors each of resistance (R=129,491Ohm), representing plate 1 with low conductivity modeled by a 6×6 network of resistors with contact-point electrodes 132

Figure 5.11: Network of resistors each of resistance (R=812 Ohm), showing plate 2 with high conductivity modeled by a 24×24 resistors network with contact-point electrodes 133

Figure 5.12: Network of resistors each of resistance (R=812 Ohm), showing plate 2 modeled by a 24×24 resistors network with contact-point electrodes 136

Figure 5.13: Network of resistors each of resistance (R=812 Ohm), showing plate 2 with high conductivity modeled by a 24×24 network of resistors with contact-line electrodes 137

Figure 6.1: Experimental set-up for tensile testing of coupons showing typical transverse (90^0) failure for samples a) Unfilled and b) Filled with 0.3wt% MWCNT 145

Figure 6.2: Analysis results for $[0_5, \theta_{n\ (n=6,\ldots,10)}, 0_5]$ laminate under N_x= 43.307 KN 150

Figure 6.3: SEM of laminate section 152

Figure 6.4: Schematic illustration of dimensions and locations of strain gauge and electrical contact points 153

Figure 6.5: Schematic illustration of cross ply glass fiber/epoxy/CNT composite laminate showing out-of-plane deformation and change in through-thickness electrical resistance while it is loaded 154

Figure 6.6: Experimental set-up for tensile test: a) Sample mounted on MTS machine and measurements system. b) Close-up view of strain gauge and electrodes bonded to sample through-thickness 155

Figure 6.7: Tensile result, showing ATTS over 90^0 layers of $[0_5, 90_8, 0_5]$ versus stress 156

Figure 6.8: Variation of ATTS calculated from CLT for the laminate and TTER versus tensile stress along axial direction (initial electrical resistance at the electrodes T1-B1: 165,510 ohms) 157

Figure 6.9: Thicknesswise compression test setup a) Sample placed on MTS machine with load cell to apply compressive load. b) Close-up view of L-shaped support, electrodes and strain gauge bonded to sample and location of loading rod with diameter of 12.7mm 159

Figure 6.10: Thicknesswise compressive load result showing ATTS and TTER versus stress (initial electrical resistance at the electrodes T1-B1:169,100 ohms)) 160

Figure 6.11: Poisson coupling reduces the laminate thickness. Schematic illustrating a) Reduction of the tunneling distance between crossing CNTs (a_1 and a_2 before and after loading), b) One possible explanation for the increase in TTER (b_1 and b_2 before and after loading) 161

Figure 6.12: Schematic illustration of compressive sample details 164
Figure 6.13: Lengthwise compression test set-up a) Sample placed on MTS machine with compression fixture b) Close-up view of the fixture, electrodes and strain gauge bonded to sample 165
Figure 6.14: ATTS and TTER versus compressive stress along axial direction (initial electrical resistance at the electrodes T1-B1: 167,200 ohms)... 166
Figure 6.15: Four-point bending test set-up a) Sample placed on MTS machine with load cell under four-point bending. b) Close-up view of Load span, support span, electrodes and strain gauge bonded to sample 167
Figure 6.16: Four-point bending test results showing load and change in TTER at the electrodes T1-B1versus displacement curves for the specimen 168
Figure 6.17: Four-point bending test results showing change in in-plane electrical resistance at the electrodes T2-T3 measured on compression side of the sample versus stress............ 169
Figure 6.18: Four-point bending test results showing change in in-plane electrical resistance at the electrodes B2-B3 measured on tension side of the sample versus stress.................... 170
Figure 6.19: Simplified representation of the relative motion between a pair of straight CNTs 172
Figure 6.20: Schematic illustration showing a) Cross ply glass fiber/epoxy/CNT composite laminate b) Systematic creation of CNT-CNT contact configurations by rotating one CNT pair with respect to other one.. 174
Figure 6.21: Schematic illustration showing seven CNT-CNT contact configurations (a to g) before loading and after lengthwise and thicknesswise loadings 176

List of Tables

Table 1.1: Peak ΔR/Ro recorded for the maximum load of each loading cycle for the reference and CNT modified laminates [69] 23

Table 2.1: Comparing electrical resistivity, uniformity of MWCNT distribution for plates 1 and 2 containing 1w% and 0.3wt% MWCNT 40

Table 2.2: Specifications and experimental conditions of the plates 49

Table 3.1: Specifications and experimental conditions of large plates 71

Table 3.2: Comparing electrical resistance, uniformity of MWCNT distribution and sensitivity to resistance change for plates containing different MWCNT concentrations...... 72

Table 3.3: The importance of electrical resistance change (ERC) in relation to the severity of damage introduced by impact with different energy levels in plate 8 89

Table 4.1: The pairs of electrical contacts nearest to points 13 I and 13 V 104

Table 5.1: Numerical results for comparing the effect of material's electrical conductivity on the electrical resistance change (ERC) 134

Table 5.2: Numerical results for comparing the effect of the proximity of pair of electrodes to removed resistors on the change in electrical resistance for plate 2 134

Table 5.3: Numerical results for comparing the effect of the number of removed resistors (damage size) on the change in electrical resistance for plate 2. 135

Table 5.4: Numerical results for comparing the effect of spacing between electrodes on the change in electrical resistance for plate 2 with relatively high conductivity 136

Table 5.5: Numerical results for comparing the effect of electrode geometry on the change in electrical resistance for plate 2 with relatively high conductivity 138

Table 6.1: Measured mechanical properties of both glass fiber/epoxy composites without and with 0.3wt% MWCNT with 60% fiber volume fraction based on ASTM D 3039 M-07 and ASTM D3518M 146

Table 6.2: Average thickness of samples 151

NOMENCLATURE

Large polymer composite structure (LPCS)

Structural health monitoring (SHM)

Electrical resistance measurement (ERM)

Carbon nanotubes (CNTs)

Multiwalled Carbon Nanotubes (MWCNTs)

Electrical Resistance Change (ERC)

Average electrical resistance change (AERC)

Carbon Fiber Reinforced Polymer Composites (CFRPCs)

Non-Destructive Evaluation (NDE)

Electric Potential Change Measurement (EPCM)

Electrical Resistance Change Measurement (ERCM)

Electric Potential Change (EPC)

Through-Thickness Strain (TTS)

Through-Thickness Electrical Resistance (TTER)

Fiber Volume Fraction (Vf)

Scanning Electron Microscopy (SEM)

Average Through-Thickness Strain (ATTS)

Classical Lamination Theory (CLT)

Interlaminar (IL)

Chapter 1

Introduction, Literature review, Problem statement and Objectives

1.1 Introduction

Polymer matrix composites have found augmented use in many important engineering structures such as aircrafts. This is due to their light weight, high strength, high stiffness and good fatigue resistance. However, along with their advantages, there are many issues. One of the significant issues is the ability to monitor the integrity of the composite structures, particularly for in-situ process (i.e. detection and location of damage during service). Many techniques have been proposed to address this problem, with limited amount of success. Carbon nanotubes (CNTs) are inherently multifunctional materials that can be used as structural materials and sensing materials due to their small size, high aspect ratios (length to diameter ratio), and exceptional electrical conductivity, thermal conductivity and outstanding mechanical properties [1-3]. Currently many studies have focused on incorporating CNT into polymers as sensors for detecting strain and subsequently failure in polymer matrix composites (PMCs) using electrical methods [4-

9]. However, all works in this area have been limited to monitor in-plane strain and to detect damage in composite laminate samples with small size.

In the first part of this thesis, two new, practical and real-time structural health monitoring (SHM) techniques are developed to detect, locate and quantify damage in large polymer composite structure (LPCS).

In the second part of this thesis, electrical resistance behavior of glass fiber/epoxy/CNTs composites subjected to multi-directional deformation is investigated and this behavior is explained.

1.2 Literature review

Fiber reinforced polymer composites (FRPC) are widely used in many industrial applications due to their high strength-to-weight and stiffness-to-weight ratios. One of the critical challenges in the practical use of structural composite materials in comparison to the traditional metallic structures is to monitor the health of composite structures in real-time. This is due to their susceptibility to different types of damages such as fiber fracture, matrix cracking, and fiber/matrix debonding which occur at different locations of composite structures [10]. There is an urgent need to develop SHM techniques for in-situ health monitoring of large structural composites before catastrophic failure to ensure safety and proper performance of the large structures.

Various non-destructive evaluation (NDE) techniques such as ultrasound scanning, acoustic emissions, X-ray, thermography, fiber optics, shearography, electrical conductivity along the direction of carbon fibers, and resistance-based sensors have been used for health monitoring of structural composites. However, the applications of these techniques to structural health monitoring which is the continuous assessment of structural composite integrity have been limited in practice due to various reasons such as impractical for real-time damage monitoring, local measurement, lack of ability for real-time inspecting large composite structure, high cost, complex data analysis tools, poor spatial resolution, limited in-situ capabilities and equipment requirements [11-16]. Recently CNTs are added into resin to make the resin electrically conductive in the composite structure [4, 17-19]. The descriptions for the above NDE techniques and their limitations are described in the following:

1.2.1 Ultrasonic

In this technique, ultrasonic waves are sent through the thickness of the composite laminate. If the laminate is good, the time of travel of the ultrasonic wave is short. If there are defects in the laminate such as delamination or matrix cracking, the time of the travel of the ultrasonic wave is altered. Scanning over the surface area of the laminate is done and a map of images of the time of travel is displayed. This map of images is compared against a reference map of images taken over a good laminate. Comparison between the actual map of images and the reference map of images can indicate the area of the defect [20-23]. Ultrasonic seems to be the most widely used technique. However, there are many problems:

- The scanning has to be done in a lab (for the case of small sample) or in a shop (for the case of large sample). The fact that the technique cannot be used in-situ, puts a limitation of its usefulness.

- There is a need for a transfer medium to keep the ultrasonic beam coherent. Normally water is used as the transfer medium. This presents the problem of introduction of water and the mess that may be created due to wetness. Recently laser ultrasonic is introduced. This helps the coherence of the beam to some extent. However, the need for scanning still limits the usefulness of the technique.

1.2.2 Acoustic emission

In acoustic emission, an artificial ear (high frequency sensor) is attached to the composite structure. When a crack occurs, this crack creates stress waves that propagate in the structure. When the wave hits the sensor, the sensor records and displays a signal. By reading the signal displayed from the sensor, one may tell whether a crack has been formed. By placing many sensors in a certain geometrical pattern on the surface of the structure, one may be able to locate the crack [12, 24-29]. The problem with this technique is the extraneous noise coming from many sources such as the reflection and reverberation from stiffeners, free edges etc. can interfere with the desired signal. Sometime unloading can also produce signals due to the rubbing of the existing crack surfaces. The interference of other signals confuses the information and makes the technique intractable.

1.2.3 X-Ray

In this technique, the sample is subjected to X-Ray diffraction. Observation of the X-Ray photograph can differentiate the defect from the good material [16, 30]. This technique can only be applied in the lab.

1.2.4 Thermography

Thermography operates on the principle that the heat emitted from the surface of a structure depends on the stress state of the material below the surface [11]. If there are defects in the material below the surface, the temperature distribution on the surface (down to a fraction of a degree) will be non-uniform. By comparing the thermal image of a reference sample to that of the sample studied, one can determine whether there are defects in the sample. Again this technique is applicable in the lab and cannot be used in-situ.

1.2.5 Fiber optics

Optical fibers with gratings (such as Bragg gratings) are either embedded inside the composite structure or bonded on its surface [31-37]. The deformation of the material in the structure is transmitted to the optical fiber. The strain in the optical fiber changes the spacing between the gratings. By sending light waves in the fibers, the reflection of the light wave from the gratings changes. By observing the changes in the reflected wave as compared to referenced signals, one can determine the level of the strain. The technique is interesting in which it can be used in-situ. However the size of the optical fibers is fairly large (52 micrometers). Embedding these fibers in the composite structures with fiber diameters in the order of 10 microns creates stress concentration and may induce damage. Bonding the fibers on the surface of the structure only allows it to detect deformation locally. The difference between the use of optical fibers and strain gauges need to be proven. Besides, the fibers are fragile and the equipment is bulky.

1.2.6 Shearography

Shearography is an optical technique that involves holography and speckle interferometry [38]. An expanded laser beam is used to illuminate the region to be examined on the surface of the object. The surface can be used as is or a layer of paint or powder layer can be applied on top. Light scattered by the surface is recorded using a camera. The camera has a glass wedge or shearing interferometer to generate a double image of the object surface. To detect the deformation of the surface, a reference interferogram is first recorded. Subsequently interferograms are recorded either statically or dynamically as the object is loaded. Either a single camera or multi-camera sensor can be used to obtain the displacement gradient components. The disadvantages of this technique include the fact that a high precision location between the part and the camera is required, which may not be suitable for field applications. Also, it cannot be used for the measurement of the bulk strain in the material.

1.2.7 Electrical conductivity along the direction of carbon fiber

Over the past few years, many researchers have used the electrical conductivity of the carbon fibers as an indication for the presence of damage [39-46]. Since carbon fibers are highly conductive along the fiber direction, by applying an electric current over two probes at two points and measuring electric potential over another two probes along the direction of the fibers, change in electric potential can be taken as an indication of damage in the composite. The problem with this technique is that since the resin is not conductive, one cannot use the technique to detect resin cracks. The majority of damages at the relatively low loads are due to matrix cracking and delamination, rather than due to the fiber breakages. As such, the usefulness of this technique is limited.

1.2.8 Resistance-based sensors

A number of resistance-based sensors have been developed for the sensing of deformation and damage in composite structures. For instance, Hou and Hayes [47] developed a resistance-based sensor consisting of wire contacts embedded at the edge of carbon fiber composite as shown in Figure 1.1. The sensor was shown to be capable of detecting barely visible impact damage, induced by a falling dart impact tester, and accurately providing the damage location. However, the size of the panel is small (12 cm by 10 cm) and only one damage site was created. Hayes et al. [48] presented a composite material system where the fiber reinforcement comprises electrically conductive fibers as illustrated in Figure 1.2. They designed the flexible circuit board connected to the aligned axially conductive fibers for detecting damage.

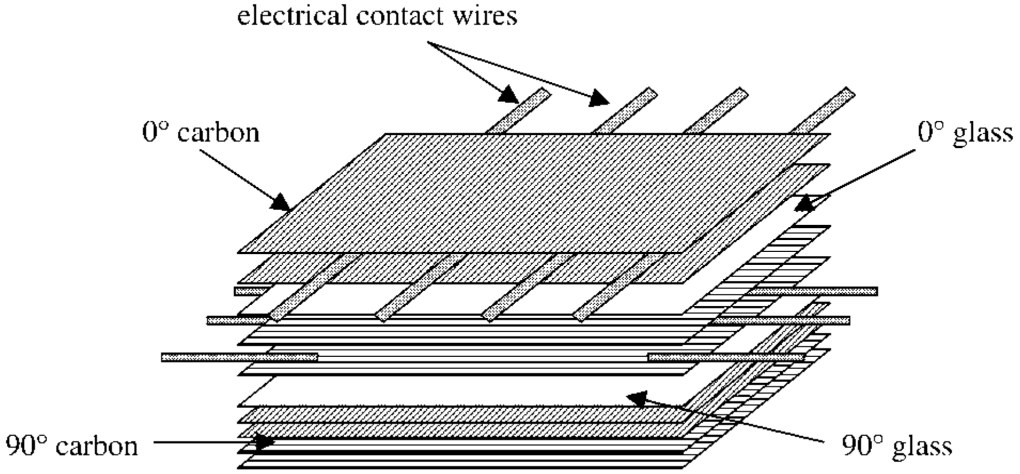

Figure 1.1: A schematic illustration showing the construction of the composite, including the contact locations and the position of the glass fiber plies [47]

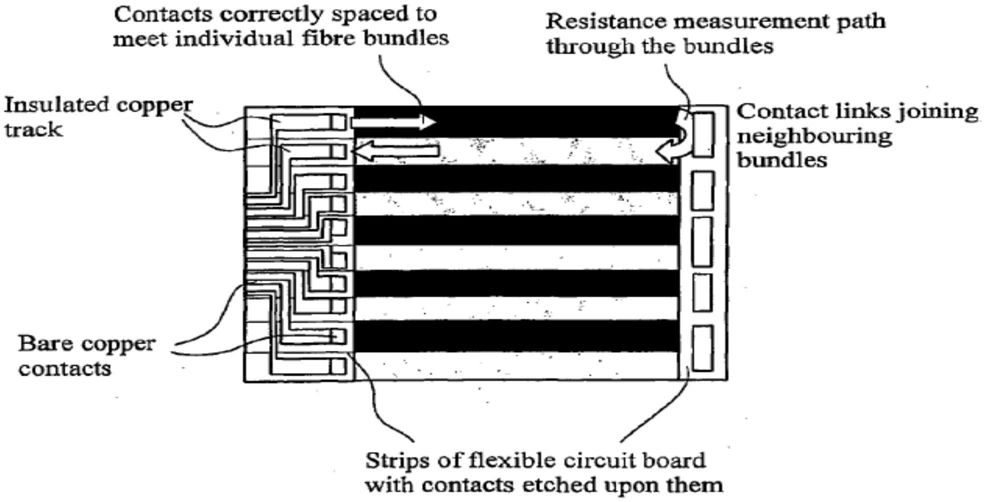

Figure 1.2: Resistance-based electrically conductive fiber sensors [48]

Rice [49] presented a sensing system which consists of depositing lines of conductive ink containing carbon nanofibers and polymeric resin on the surface of the structure in the form of a grid pattern. Electrical wires are connected to the ends of these grid lines for measuring the changes in resistances between grid lines as shown in Figure 1.3.

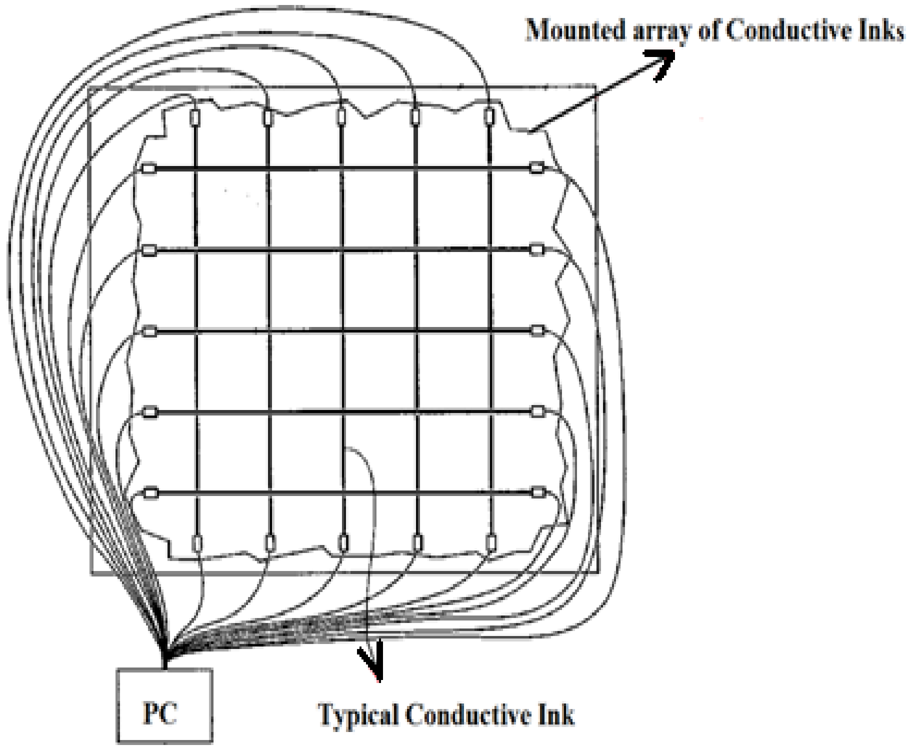

Figure 1.3: A schematic showing system comprising carbon nanofibers reinforced polymeric resin as conductive lines bonded on the surface and connected wires [49]

1.2.9 Adding carbon nanotubes into the resin to make the resin electrically conductive in composite structures

Carbon nanotubes (CNTs) have been introduced as multifunctional fillers because of their small size, high aspect ratios, exceptional electrical conductivity, thermal conductivity and outstanding mechanical properties [1, 17, 50-56]. Recently many researchers have added carbon nanotubes into polymer to make the matrix electrically conductive in fiber reinforced polymer composite structures. This electrical conductivity is due to the formation of a network of the carbon nanotubes. Upon the application of a mechanical load, the network is deformed, the configuration of the network is affected and there is a change in the conductivity. Thostenson and Chou [5] showed that the carbon nanotubes at very small concentrations can penetrate in the matrix-rich reign areas between fibers as well as between plies due to their small size in comparison to the size of advanced fibers as shown in Figure 1.4. This offers CNTs as nonconductors for detecting both deformation and damage in composite laminates.

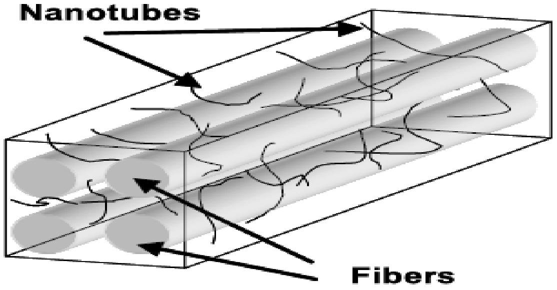

Figure 1.4:Three-dimensional model showing the penetration of nanotubes throughout a fiber array due to their relative scale [5]

Pham et al. [57] investigated the effect of different multiwalled carbon nanotube (MWCNT) concentrations on the sensitivity of composite films made of polymethyl methacrylate (PMMA) and MWCNT using a melt-based process (dry blending of polymer powder and MWCNTs and hot pressed), and a solvent-based method (dispersion has been done ultrasonically). It can be seen from Figures 1.5a and 1.5b that the sensitivity of normalized change in surface resistivity increases with decreasing MWCNT concentrations in PMMA/MWCNT films. They reported the unit of surface resistivity as (Ω/square) to differentiate with the unit of surface resistance (Ω). Even though the unit of surface resistivity is often expressed as (Ω /square), it is not a valid unit from the dimensional analysis point of view.

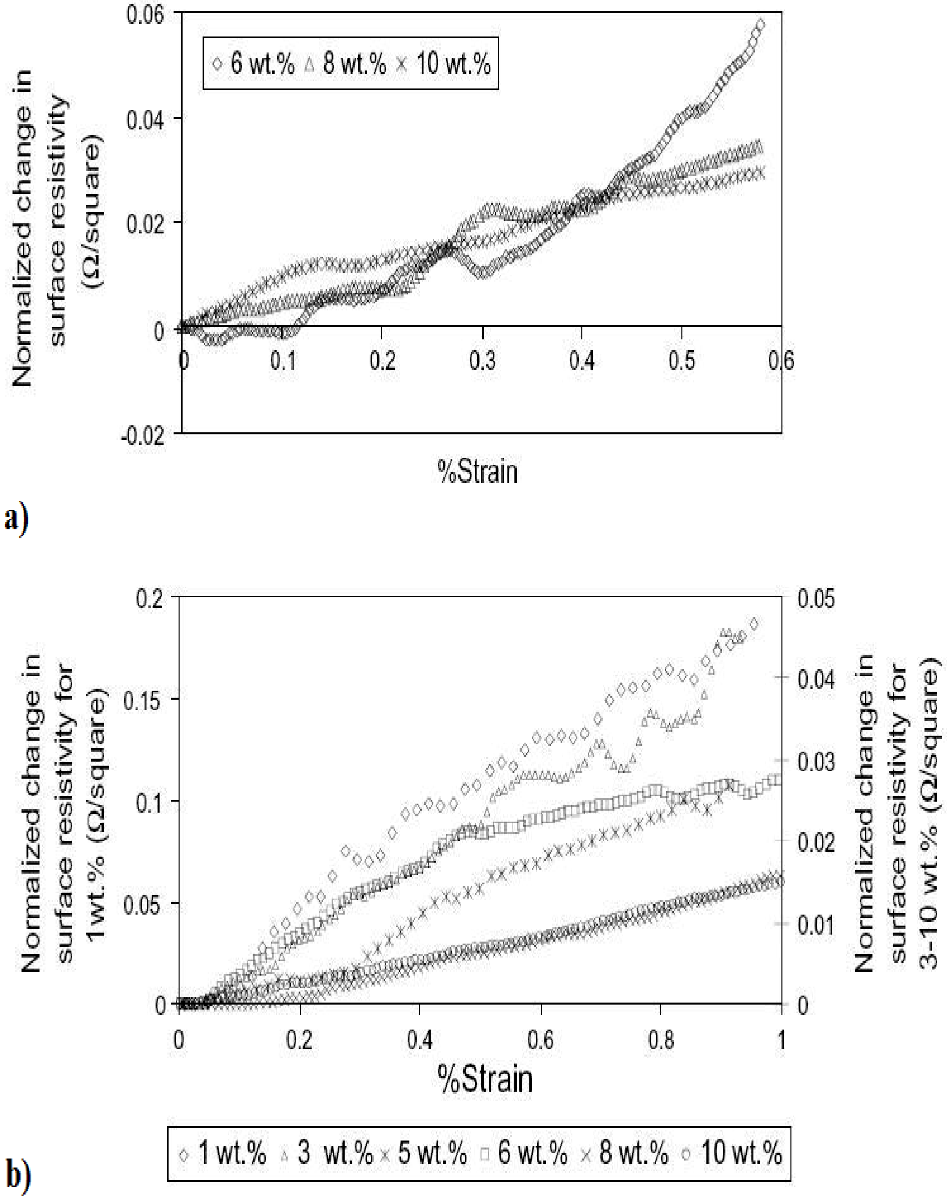

Figure 1.5: Normalized change in surface resistivity of a) Dry blended and b) Solution cast PMMA/MWCNT at various MWCNT concentrations [57]

Figure 1.6 shows the sensitivity factor (SF) which is defined as (SF= ΔR/R ε) for composite films containing different MWCNT concentrations. It is clear that the sensitivity factor decreases as MWCNT concentrations increases.

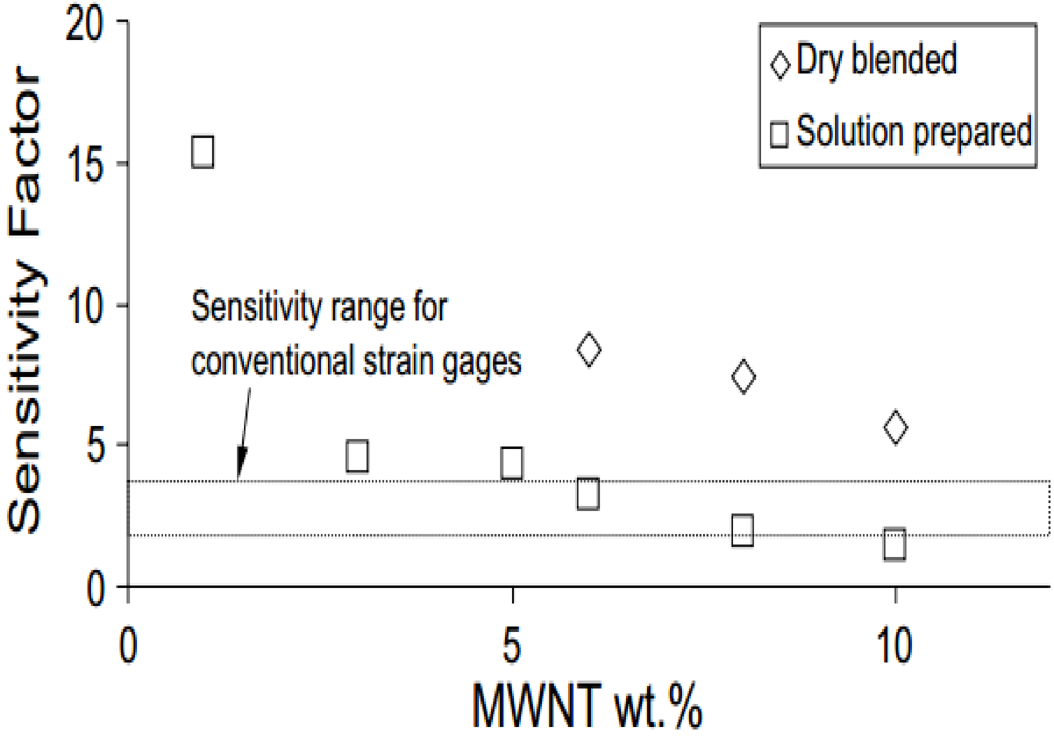

Figure 1.6: Sensitivity factors for PMMA/MWCNT films [57]

Hu et al. [58, 59] investigated the effect of processing conditions and material properties on the sensitivity of an epoxy/MWCNT composite. Gauge factor is defined as a measure of sensor sensitivity. They found that the gauge factor (sensitivity) of the composite increases with decreasing MWCNT concentration as shown in Figure 1.7. Figure 1.8 shows the correlation between the gauge factor (sensitivity) and electrical conductivity of the composite containing different MWCNT concentrations. It is clear that the composite containing 1wt% MWCNT which gives rise to lower electrical conductivity indicates higher gauge factor (sensitivity).

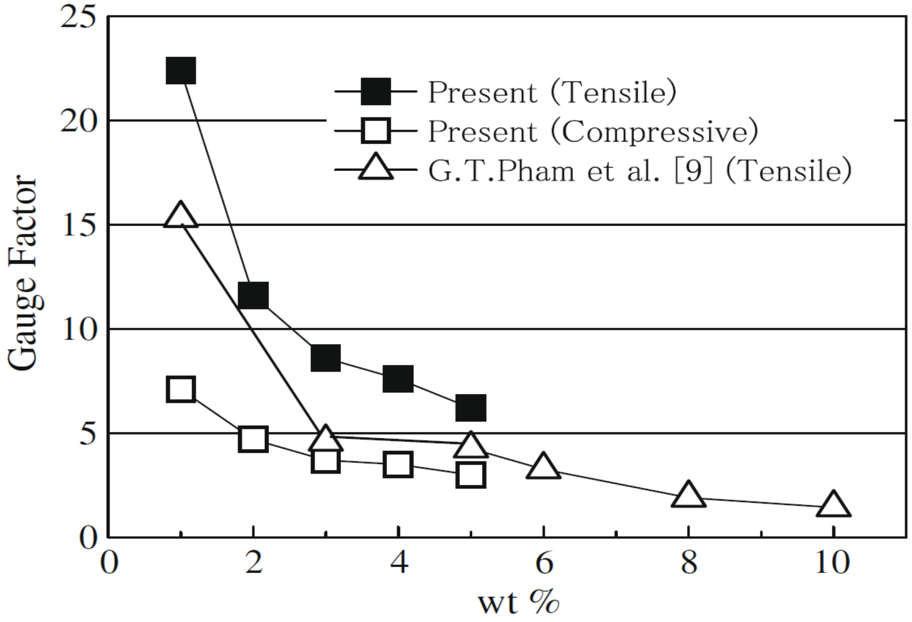

Figure 1.7: Comparison of various experimental results [58]

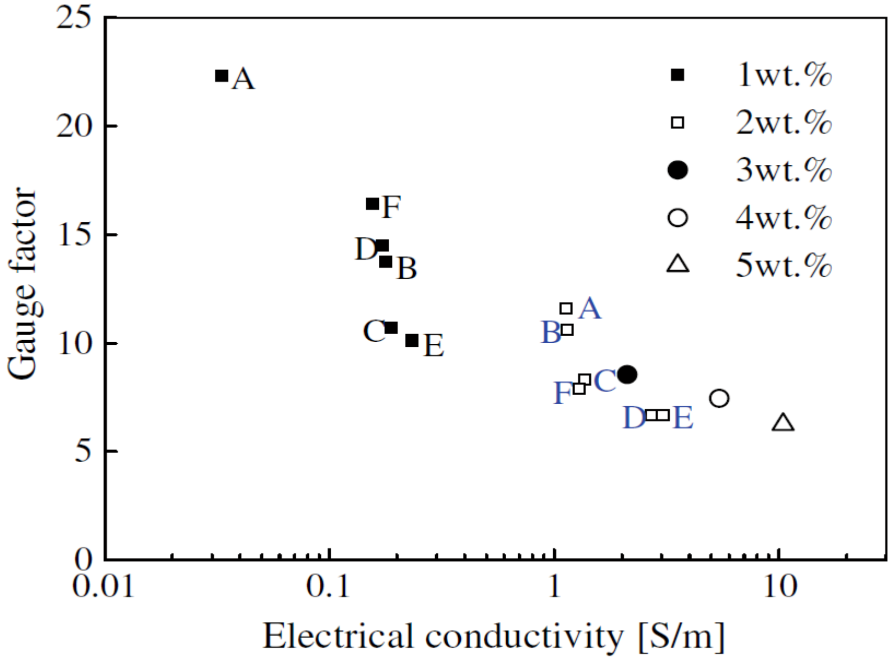

Figure 1.8: Gauge factor versus electrical conductivity of sensor [58]

Thostenson and Chou [4] incorporated CNTs in a five-ply unidirectional glass fiber/epoxy/CNT composite where the center ply was cut to create initiation of ply delamination due to the shear stresses accumulated at the broken fiber ends during tensile loading. Also, they fabricated $[0/90]_s$ cross-ply laminate containing CNTs to investigate transverse damage during tensile loading. They found that significant change in electrical resistance corresponds to delamination extension and damage accumulation as shown in Figure 1.9a and Figure 1.9b respectively. They also performed flexural tests in three-point bending to explore the ability of CNT networks to monitor the through-thickness fracture of plies in the samples. The experiments with two span-to-thickness ratios were carried out to obtain two different types of fracture as shown in Figure 1.10. Comparing Figures 1.10a and 1.10b, it is clear that a sharp change in electrical resistance occurs in the shorter span as a result of complete delamination and electrical resistance increases incrementally at a higher rate in the longer span by creating matrix cracking and local delamination (see Figures 1.10c and 1.10d).

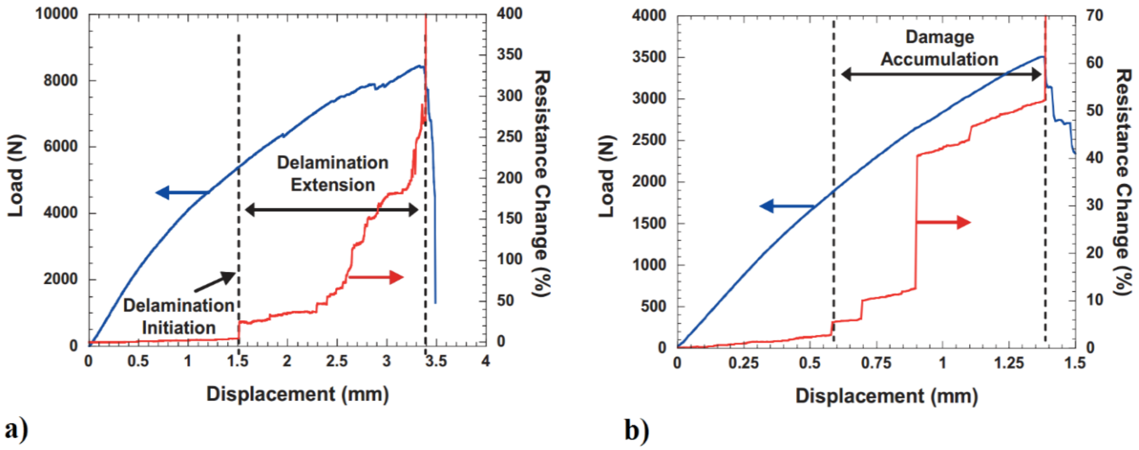

Figure 1.9: Tensile results showing a) Five-ply composite with the center ply cut to initiate delamination, b) Cross-ply composite [4]

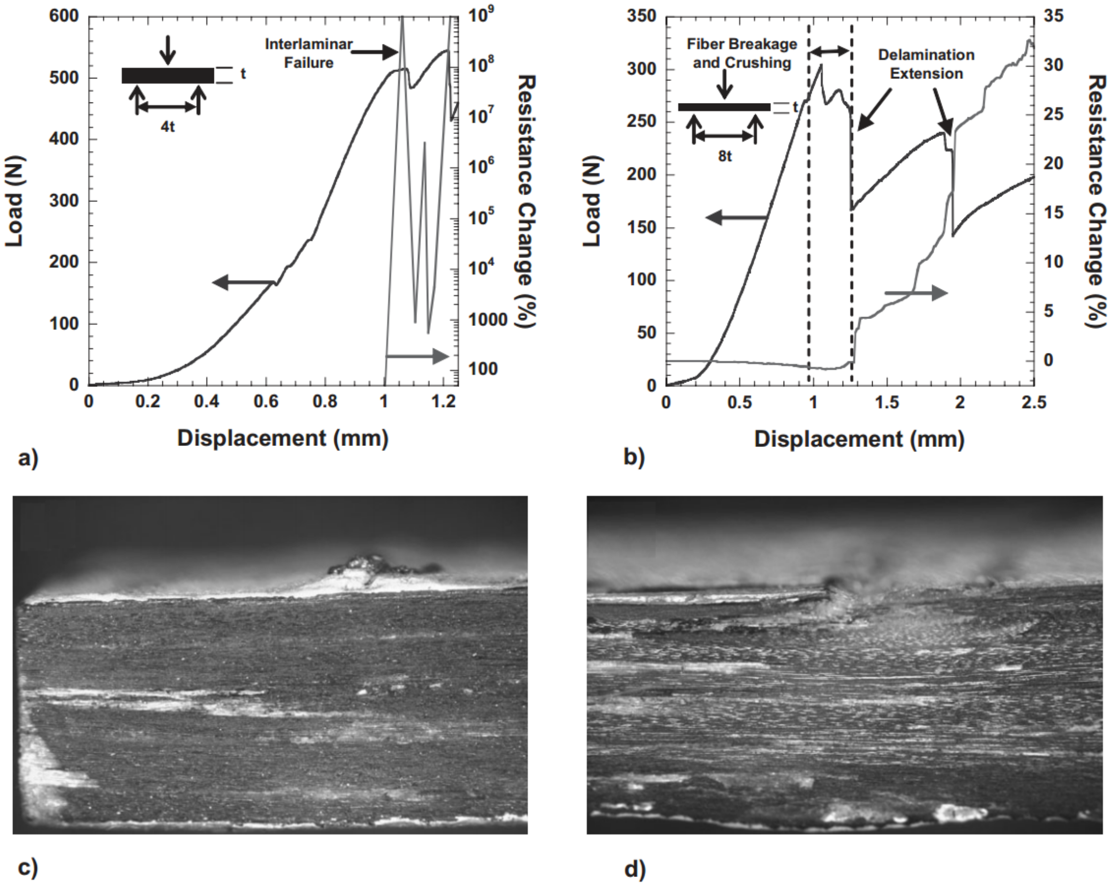

Figure 1.10: Three-points bending results showing a) Span-to-thickness ratio of 4 , b) Span-to-thickness ratio of 8 , Optical microscopic images of c) Interlaminar fracture and d) Fiber and matrix damage for span-to-thickness ratio of 4 and 8 respectively [4]

Böger et al. [8] added CNTs and carbon black in the glass/epoxy composites and found that there is correspondence between the change in in-plane strain and the change in through-thickness electrical resistance during cyclic tensile test. Gao et al. [60] deposited CNT onto glass fiber surfaces and found that epoxy composites made using this fiber system may be used for in-situ sensing of strain and damage. Nofar et al. [9, 61, 62] embedded CNTs in a glass/epoxy composite to detect damage using electrical resistance measurement during tensile and fatigue testing. Electrical resistance measurement was found to be more sensitive than strain gauge measurements for damage monitoring. They found that the point of slope change in load versus strain curve takes place in the range of 2000-3000 N. This change of slope occurs at the same strain value in the resistance versus strain curve shown in Figure 1.11. The sharp increase in electrical resistance may be correlated to the formation of some damage in the sample. They mounted four electrical contact lines made from silver-epoxy on the surface of sample to detect failure at three different zones of the sample. The significant changes in electrical resistances between points 2-3 and points 1-2 show failure regions in the samples as shown in Figure 1.12a and Figure 1.12b respectively.

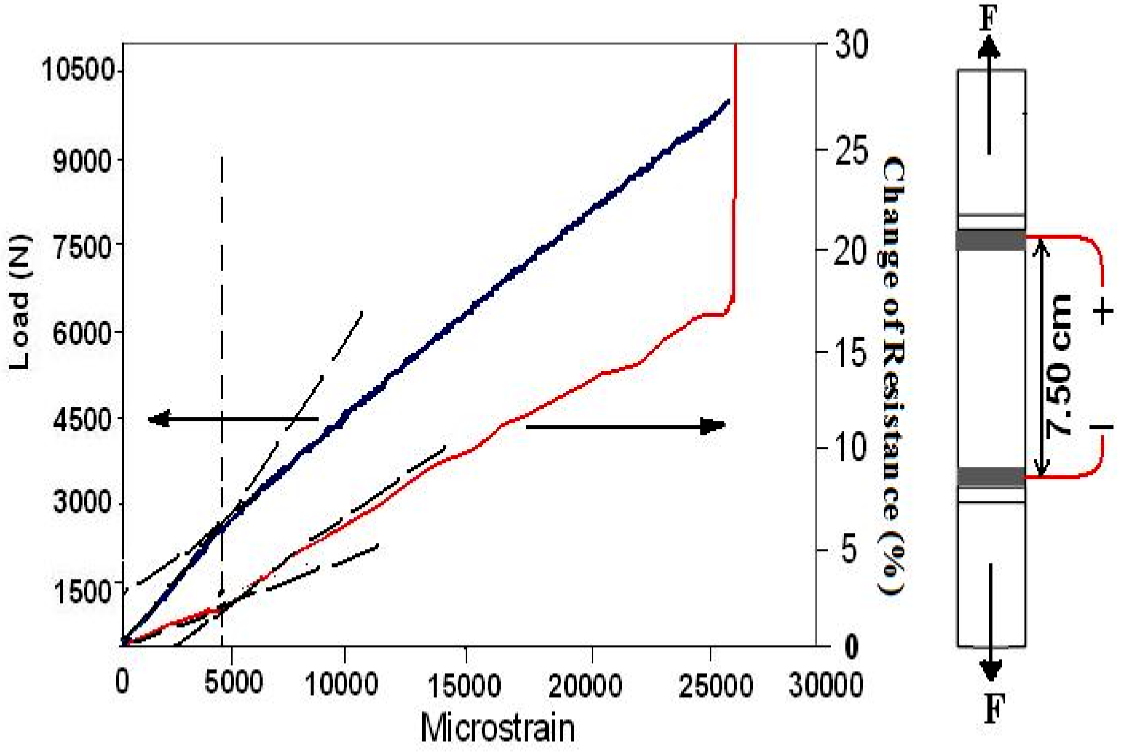

Figure 1.11: Tensile test results resistance versus strain [9, 61]

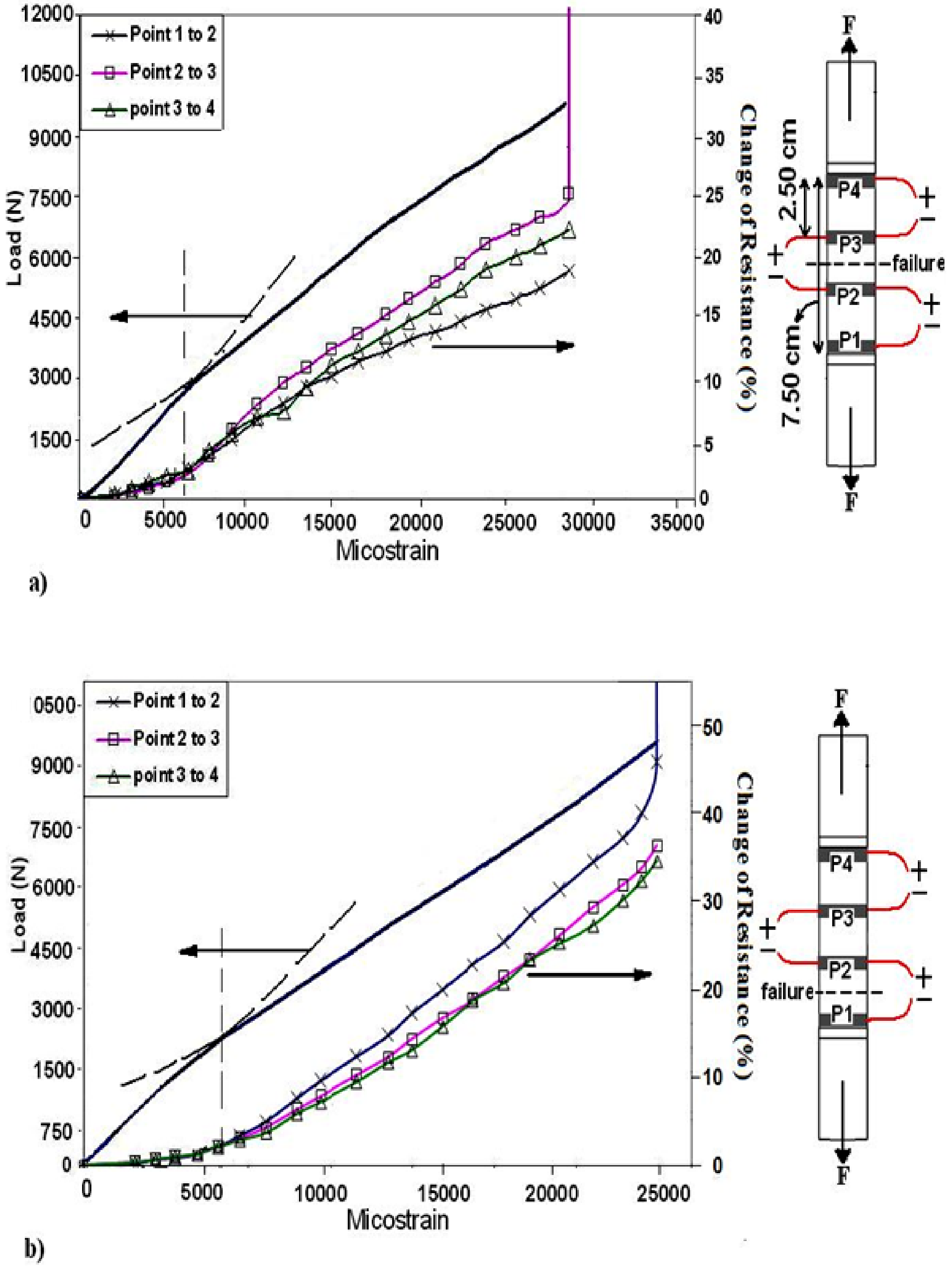

Figure 1.12: Tensile test results showing detection of failure occurred between a) Points 2-3, and b) Points 1-2 [9, 61]

Hena-Zamal and Hoa [63, 64] incorporated CNTs into the epoxy in cross-ply $[0_2/90_2]_S$ glass fiber/epoxy/CNT laminate to detect damage in the laminate. They deposited electrical contact lines and points on both surface of the samples for measuring electrical resistance during tensile and fatigue testing respectively as shown in Figures 1.13a and 1.14a. Figure 1.13b shows load and resistance change versus strain curves for the laminate during tensile test. They indicated that there are three slope changes in the loads of 3500 N, 7000 N and 15000N which may correspond to occurrences of first ply, accumulation of damage and failure of sample respectively as shown in Figure 1.13b. Good correspondence was found between slope change of load and resistance change versus strain (%) curves.

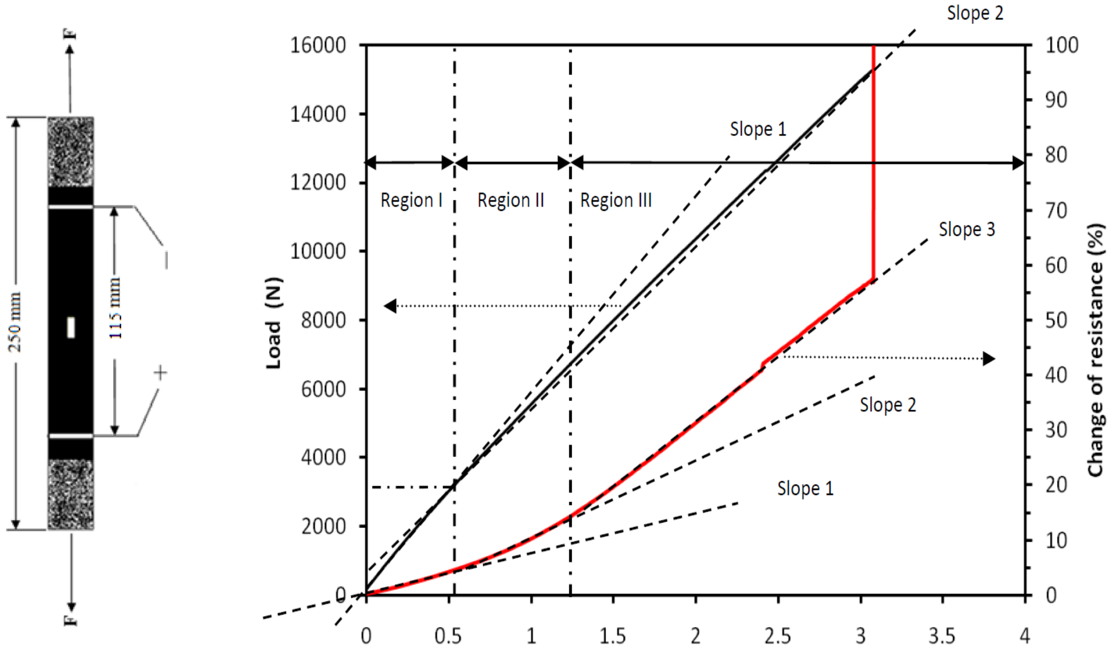

a) **b)**

Figure 1.13: Tensile test showing a) Sample with mounted electrical contact lines b) Tensile test results [63]

Figure 1.14b shows that in-plane and through-thickness electrical resistances increase linearly up-to 500 and 100 cycles respectively. This indicates the effectiveness of through-thickness electrical resistances to detect delamination occurred in the laminate as shown in Figure 1.14c.

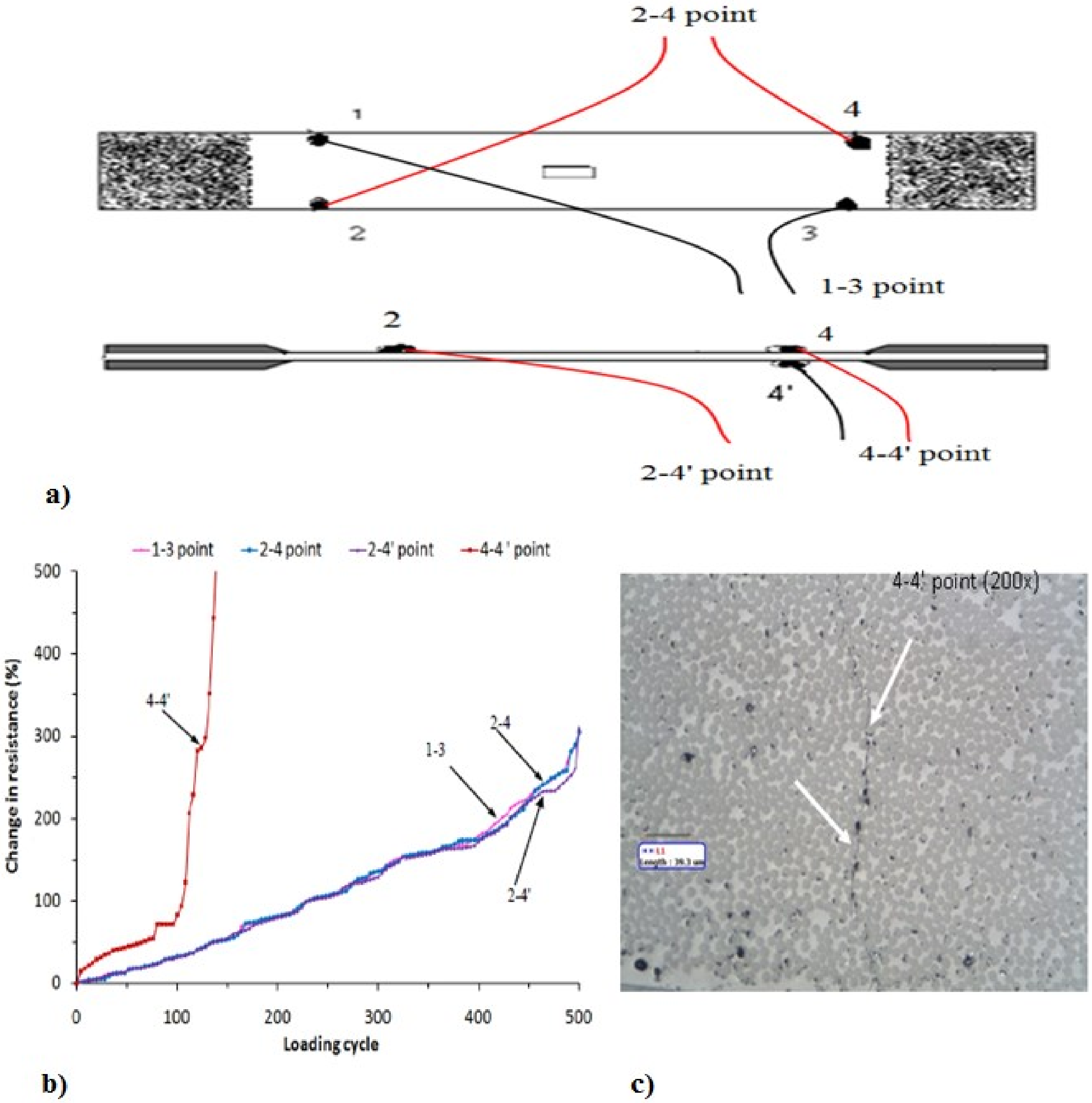

Figure 1.14: Fatigue test results showing a) Sample mounted with electrical contact points, b) Change in electrical resistance versus loading cycle and c) Optical image of the $[0_2/90_2]_S$ showing failure [63]

Gao et al. [65] dispersed CNTs into epoxy to make thick glass fiber/epoxy/CNT composite laminate of 4 inch by 6 inch. They mounted electrical contact lines made from conductive silver-epoxy centered on opposite edges of the 6 inch length of entire sample thickness. They found that the repeated impact loading attributes well with the change in electrical resistance across the electrodes for the laminate. Raghavan et al. [66] developed a system where CNTs were grown radially from fibers made of alumina. Resin was then incorporated into the fibers to make 4.5 × 1 × 0.12 inch^3 composite laminate. They then deposited silver ink to form electrical contact lines spaced 0.118 inches apart on both surface of the laminate. The resistances across the electrodes were measured. A correspondence was found between the changes in in-plane resistance and through-thickness resistance with damages created by impact loading as shown in Figures 1.15a and 1.15b respectively.

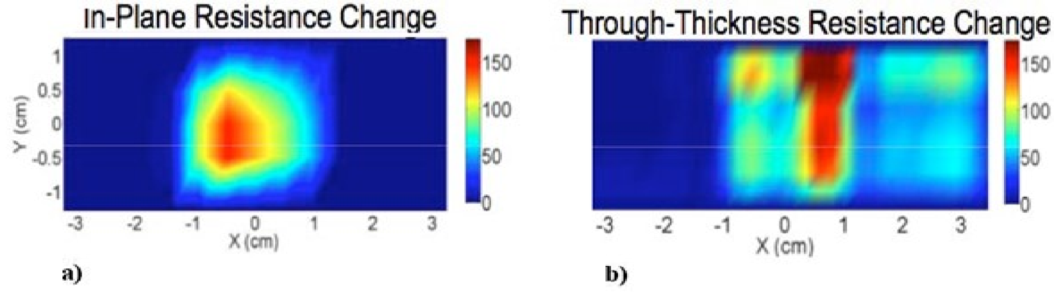

Figure 1.15: Impact testing: a) In-plane resistance change, b) Through-thickness resistance change [66]

Proper et al. [67] modified kevlar fiber/epoxy composite laminate with CNT to make the laminate electrically conductive. They then mounted a grid of points spaced 0.25 inches apart on the surface of 4 inch by 6 inch composite sample. They showed that when the sample is damaged by mechanical impact, there is a correspondence between the change in voltage across the grid and the impact damage. However using a large number of grid points spaced 0.25 inches apart makes the technique impractical. Baltopoulos et al. [68] described the forward and inverse methods for detecting the location of cracks in a small sample ,with size 4 inch by 4 inch , of glass fiber/epoxy/CNT plate using the electric resistance tomography (ERT) technique. They mounted electrodes around the periphery of a square sample as shown in Figure 1.16. They injected a current at one electrode on one side and received the current at another electrode on the opposite side of the square. Then they measured the potential at different electrodes. When damage is created by introducing a small hole in the plate, the electric potentials at the electrodes are measured. They found that when the hole is closer to the center of the square, there is no significant change in the electric potential at the electrodes. When the hole is closer to one of the electrodes, then there is some change in electric potentials. The technique is not strong enough to detect the disturbance at locations far from the electrode. This makes the technique not very efficient.

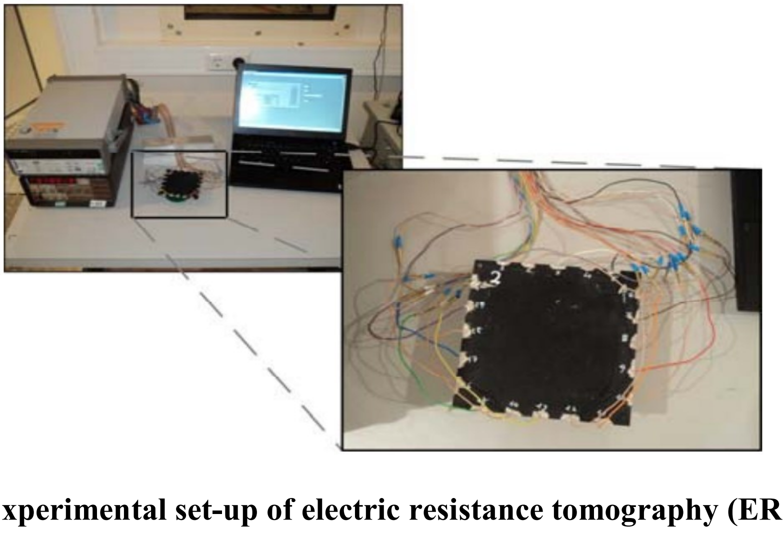

Figure 1.16: Experimental set-up of electric resistance tomography (ERT) and close-up of the sample mounted with electrodes around its periphery[68]

Kostopoulos et al. [69] employed CNTs not only for improving the properties of carbon fibers reinforced epoxy matrix composite but also for detecting matrix cracks in the composites. They applied monotonic and cyclic tensile loading on carbon fiber/epoxy composites unfilled and filled with CNTs while electrical resistance was measured simultaneously. They found that the composite filled with CNTs shows more sensitivity to change in electrical resistance due to matrix damage accumulation compared with the unfilled composite. More sensitivity is obtained due to epoxy matrix modified with CNTs which acts as direct sensors for matrix damage detection. Figure 1.17 shows that electrical resistivity across the thickness of the composites (z direction) increases as the CNT concentration decreases. Figure 1.18 shows that the resistivity along the transverse (Y) direction of the composites increases with decreasing the CNT concentrations while the resistivity along the fiber (X) direction of the composites remains unaffected due to addition of different CNTs concentration.

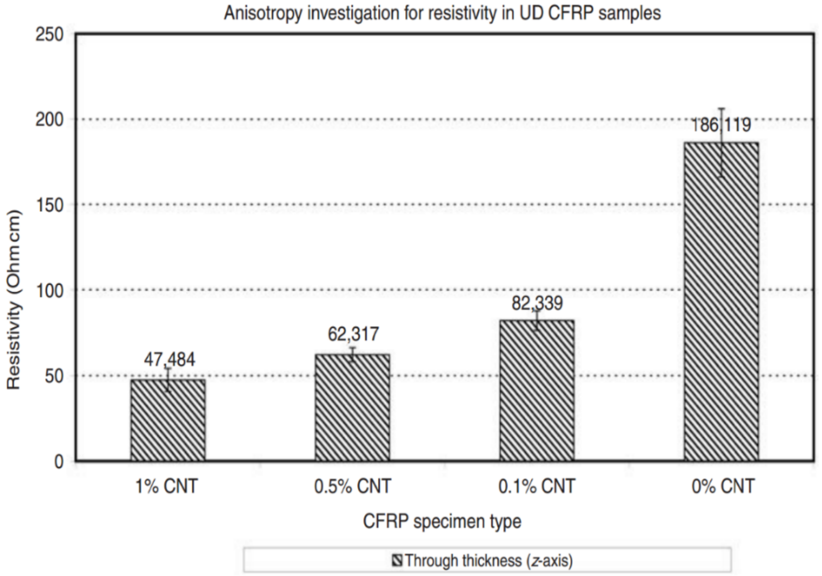

Figure 1.17: Volume resistivity for the through-thickness (Z) direction [69]

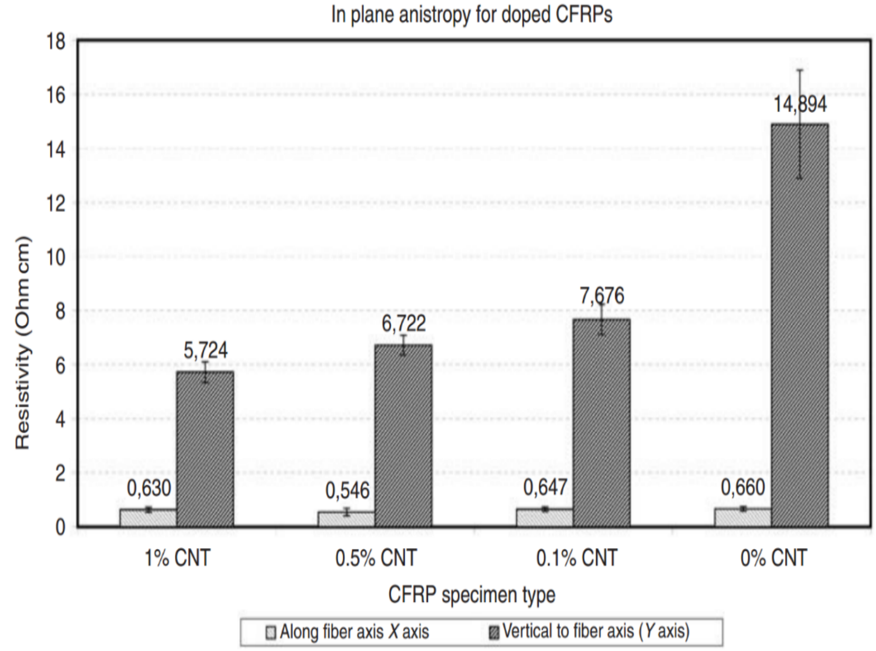

Figure 1.18: Volume resistivity for the in-plane normal to the fibers in transverse (Y) direction and along the fibers (X) direction. In-plane resistivity [69]

Table 1.1 presents sensitivity to change in electrical resistance for carbon fiber/epoxy composites containing different CNT concentrations subjected to cyclic tensile loading. Higher sensitivity is observed for the composite containing 0.5wt% CNTs compared to the composite unfilled. The composite filled with 0.5wt% indicates more sensitivity compared with the composite with 0.1wt% and 1wt% CNTs up to cycle 4.

Table 1.1: Peak ∆R/Ro recorded for the maximum load of each loading cycle for the reference and CNT modified laminates [69]

Cycles	Neat EP	0.1% CINT	0.5% CNT	1% CNT
Cycle 1	0.3 ± 0.04	0.24 ± 0.04	0.35 ± 0.05	0.31 ± 0.06
Cycle 2	0.62 ± 0.05	0.45 ± 0.03	0.89 ± 0.04	0.55 ± 0.03
Cycle 3	0.87 ± 0.04	0.85 ± 0.05	1.33 ± 0.03	1.13 ± 0.02
Cycle 4	1.05 ± 0.03	1.05 ± 0.02	1.89 ± 0.04	2.01 ± 0.12

Zhang et al.[19]embedded CNTs in graphite fiber/epoxy laminates to improve their electrical conductivity in thickness direction. This is because the incorporated CNTs make corrections in interlaminar graphite fibers which provide continuous electrical conduction pathways. This approach was used to detect delamination growth in the laminates. The delamination was created by inserting a Teflon in the laminates. Figure 1.19 shows that there is a good correspondence between the delamination length and changes in through-thickness electrical resistance obtained experimentally and theoretically. The theoretical calculation for the change in resistance was performed by using the classical volume resistance model (R=ρl/A) and the differential form of that (dR/R= dl/l-dA/A) [19]. They assumed that the changes in resistivity (dρ) are negligible and crack growth results in an increase in the conduction path length (dl) coupled with a decrease in cross-section (dA) resulting the resistance to increase.

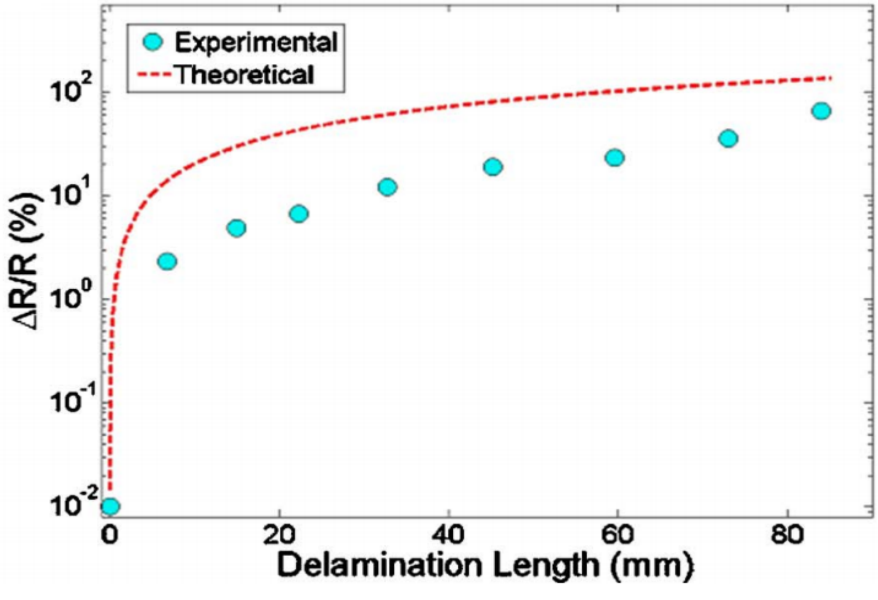

Figure 1.19: Change in through-thickness electrical resistance across the delamination versus the delamination length [19]

1.3 Thesis Objectives

Many sensors and techniques presented in literature have been developed and show promise. However they have disadvantages comprising limited in-situ capabilities and poor spatial resolutions to monitor the failure in composite structures. The incorporation of carbon nanotubes in the epoxy used for the fiber/epoxy composites is very interesting. However, the presented works indicate attempts to monitor in-plane deformation and damage in composite coupons of relatively small sizes (coupons of about 4 inch by 6 inch or smaller). No work has been found to provide a technique to detect, locate and quantify damages that occur in large polymer composite structures using carbon nanotube networks. Moreover, there is a lack of research to investigate the electrical resistance behavior of glass fiber/epoxy/CNT laminates subjected to multi-directional deformation. The main specific objectives of this thesis are devoted in three main categories in the following:

1. Developing a structural health monitoring technique to detect, locate and quantify damage in large polymer composite structures made of electrically non-conductive fibers and carbon nanotube networks

2. Developing a structural health monitoring technique to detect, locate and quantify damage in large polymer composite structures made of electrically conductive fibers and carbon nanotube networks

3. Investigating the electrical resistance behavior of glass fiber/epoxy/carbon nanotube composite laminates subjected to multi-directional deformation

1.4 Content of the Thesis

A general overview of non-destructive evaluation (NDE) techniques and their limitations are described in Chapter 1. This Chapter also presents the motivation of the thesis, literature survey, and thesis objectives.

Experimental aspects for the development of a new structural health monitoring (SHM) technique to detect, locate and quantify damage in electrically non-conductive fiber/epoxy/CNT composite plates are described in Chapter 2. In this chapter, the effects of distance between pair of electrodes closest to damage, proximity of pair of electrodes to the damage, plate size, electrical contact geometry, spacing between electrodes, damage severity and CNT concentration on the change in electrical resistance with respect to damage are studied for the detection, location and quantification of damage in the large plate.

Explanations for the obtained experimental results in Chapter 2 are given in Chapter 3. In this chapter, two new concepts: uniformity of CNTs distribution and sensitivity to change in electrical resistance are introduced to determine an optimal quantity of CNTs that can provide good detection, location and quantification of damages in the large composite plates. These new concepts are demonstrated by optical images and electrical measurements. A new SHM technique is developed to detect, locate and quantify damage in the large composite plates made of electrically non-conductive fibers and carbon nanotube networks. The flowchart of the new SHM technique is presented in Appendix A. A computer program is written for determination of detection, location and quantification of damage in the large composite plates (see Appendix A).

Chapter 4 presents development of a new SHM technique to detect, locate and quantify damage in large polymer composite plates made of electrically conductive fibers and carbon nanotube networks. A new SHM technique is developed for detecting, locating and quantifying damage in the large composite plates. The flowchart of this new SHM technique and the SHM computer program created for this purpose are shown in Appendix B.

A new electrical model of a network of resistors for composite plates containing MWCNT is proposed in Chapter 5. Theoretical simulations are performed to investigate the effects of electrode geometry, spacing between electrodes, proximity of pair of electrodes to damage, plate size, damage severity and MWCNT concentration on change in electrical resistance for damage detection, location and quantification.

Electrical resistance behavior of glass fiber/epoxy/CNT composite laminates subjected to uniaxial stresses along different directions is studied in Chapter 6. In this chapter, an explanation is presented to describe the behavior of electrical resistance measured from MWCNT networks in the composite laminates.

In Chapter 7, a comprehensive conclusion for all of the chapters, contributions, suggested future works and list of publications is presented.

Chapter 2

Experimental investigation for the development of a structural health monitoring technique for large polymer composite structures made of electrically non-conductive fibers and carbon nanotube networks

This chapter explores the possibility to use carbon nanotube (CNT) networks for the development of a structural health monitoring (SHM) technique for large polymer composite structures (LPCSs) made of electrically non-conductive fibers and CNT networks using electrical resistance measurement (ERM). Two types of the electrical contact geometry are examined for ERM. One is electrical contact points and the other is electrical contact lines. The effects of distance between pair of electrodes closest to damage, proximity of pair of electrodes to the damage, plate size, electrical contact geometry, spacing between electrodes, damage severity and CNT concentration on the change in electrical resistance with respect to damage are investigated to develop a SHM technique for detection, location and quantification of damage in large polymer composite structures.

2.1 Introduction

Real-time detection, location and quantification of damage in the LPCSs before catastrophic failure is essential in industrial applications which provide safety and proper performance for LPCSs. This is due to susceptibility of composite materials to different types of damage such as matrix cracking, fiber/matrix interface debonding and inter-ply delamination [10]. Various non-destructive evaluation (NDE) techniques such as X-ray, ultrasound scanning, thermography, acoustic emission, piezoelectric active sensors, fiber optics and resistance-based sensors have been used to detect damage in the LPCSs. However, their applications to SHM have been limited due to poor real-time capabilities and low spatial resolution [11, 12, 26, 30, 37, 70, 71]. Coupling composite technology with nanotechnology is used to provide a solution for sensing challenges in NDE and potentially SHM. Among different types of nanoparticles, carbon nanotubes (CNTs) have been used as a multifunctional additive because of their small size, high aspect ratios, exceptional electrical conductivity [1], thermal conductivity [2] and outstanding mechanical properties [3]. Incorporating CNTs as nanoscale conductors at low concentration into a resin will create electrically conductive networks distributed around the structural fibers which also act as in-situ piezoresistive sensors. Upon application of a mechanical load, the CNTs network is deformed and if the load is high enough to create cracks in the matrix, the configuration of the CNTs network is affected that induces a change in the electrical resistance. This displays their piezoresistive behavior. Recently CNTs were added to glass fiber /epoxy composites and their piezoresistive properties were exploited to assess both deformation and microstructural damage by electrical resistance measurement (ERM) [4, 60, 65, 72-74]. Chou et al. [4, 5, 65, 73] found that cracking in glass /epoxy/CNTs composite coupons of about 4×6 inch^2 or smaller correlates well with the change in electrical resistance. They also reported that the three-roll-milling (TRM) technique provides highly uniform dispersion of CNTs in the composite for damage monitoring while non-uniform dispersion of CNTs is obtained using a nanotube-containing fiber sizing agent. Hoa et al. [9, 75] indicated that the failure region in glass/epoxy/CNTs composite coupons can be detected by a significant change in electrical resistance during tensile and fatigue testing. They also found that more homogeneous dispersion of CNTs in epoxy resin is achieved by the TRM technique compared to ultrasonication. Baltopoulos et al. [68] described the forward and inverse methods for detecting the location of cracks in 4×4 inch^2 glass /epoxy/CNTs composite sample using electric resistance tomography (ERT) technique. They mounted electrodes around the boundary of the sample. They were able to detect damages around the boundary of the sample, but the technique fails to detect damage at the center of the sample. Proper et al. [67] indicated that when a 4×6 inch^2 Kevlar /epoxy/CNTs composite sample is damaged by mechanical impact, there is a correspondence between the change in voltage across the grid points spaced 0.25 inches apart and the impact damage. Wardle et al. [66, 76] developed alumina fiber/epoxy/CNT composites and found that the changes in resistance across the grid lines spaced 0.118 inches apart correspond to impact damage in the 4.5×1 inch^2 sample. In these publications, the use of grid points spaced 0.25 inches and grid lines spaced 0.118 inches make these techniques impractical for LPCSs due to the large number of electrodes required. For large structures, if a small spacing is used, a very large number of electrodes are required and this adds weight and cost to the set up. Wide spacing makes the technique more practical. All the works in this area have been limited to detect damage in composite coupons of about 4 inch by 6 inch or smaller. The cracks and damage will alter the flow of electrical current from one electrical probe to another. For this to happen, the quantity of CNTs in the small sample only needs to be more than the percolation threshold, and this quantity can be large or small. Real engineering structures are large and much bigger than the lab size samples presented in most work. It remains to be observed whether scaling up the technique from small coupons to large structures can win out over traditional NDT and SHM to detect, locate and quantify damage in large composite structures. Here, experimental works are performed to develop sensing technique for large polymer composite structures using CNT networks.

2.2 Preliminary experimental investigations

In many previous works, a quantity of 1.00wt% MWCNT has usually been added in glass fiber/epoxy composites to detect damage in the small samples [9, 62-64]. For the preliminary experiments in this thesis, this quantity was also used initially. Plates of different sizes were made, and electrical resistance changes (ERC) were measured. It was discovered that while 1.00wt% MWCNT could provide uniformity in electrical resistance, it could not provide sufficient sensitivity for damage detection. As such smaller quantities of MWCNT were attempted. These include 0.40wt%, 0.30wt%, 0.25wt%, 0.20wt% and 0.10wt%. Details of the results from these different quantities of MWCNT will be presented in Chapter 3. It was also found that 0.3 wt% MWCNT seems to provide an optimal quantity for both uniformity and sensitivity for the material system used. In this section, the two quantities of MWCNT (1 wt% and 0.3 wt%) are used to study the effect of parameters such as grid lines, grid points, plate size, spacing between probes, and damage severity on ERC. To check the uniformity of CNT distribution, two plates are considered. To examine the effects of plate size and different MWCNT concentration on the ERC, nine composite plates with different sizes containing 1.00wt% and 0.30wt%MWCNT are prepared. Grid points and grid lines spaced at different distances are used to investigate the effect of different parameters on the ERC for damage detection, location and quantification in composite plates. The specifications of twelve plates with different sizes containing two different MWCNT concentrations mounted with grid points and grid lines are shown in Table 2.2.

2.3 Experimental method

2.3.1 Materials

Multiwalled carbon nanotubes (MWCNTs) with 95% of purity, diameters of 2-20 nm and lengths of 1 μm to more than 10 μm were purchased from Bayer Material Science. Plain weave glass fabrics (15 oz/yd2) purchased from HL. plasto company, Epon 862 and EPIKURE W purchased from Miller-Stephenson chemical company were utilized as reinforcement, epoxy resin and curing agent respectively.

2.3.2 Fabrication of glass fiber/epoxy/ CNT composite plates

To fabricate glass fiber/epoxy/MWCNT composite plates, the epoxy resin and curing agent (26.4 wt%) were first mixed. Then two different weight percentages (wt%) of MWCNT comprising 1.00 wt% and 0.30 wt% were added into epoxy matrix. The mixture was processed on three roll milling (EXAKT 80E, EXAKT Technologies Inc.) to disperse the MWCNT within the epoxy matrix. The modified epoxy matrix was heated up to 60^0C for 20 min in a vacuum oven to remove air bubbles. The modified epoxy matrix was dispersed between three layers of woven glass fabrics by hand lay-up method. The plates containing 1.00 wt% and 0.30wt% MWCNT were cured using an autoclave. The manufacturing process of fiber reinforced epoxy composite plates containing carbon nanotube is described as shown in Figure 2.1.

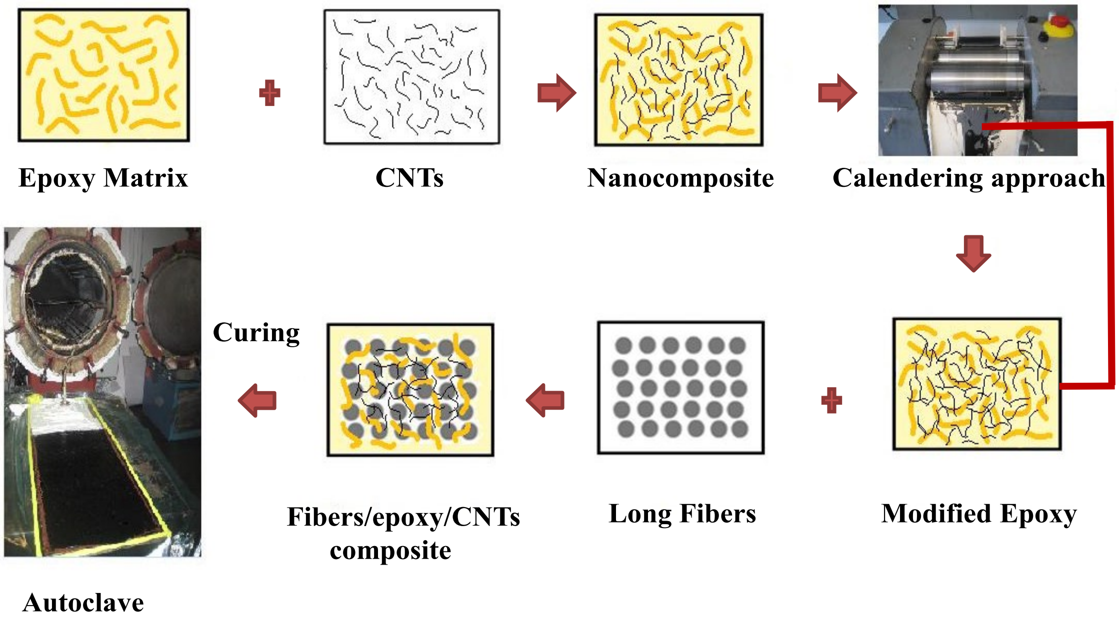

Figure 2.1: Schematic illustrating manufacturing process of fiber/epoxy/CNT plate

2.3.3 Quality control

TGA (Thermo Gravimetric Analysis) and DSC (Differential Scanning Calorimetry) tests were performed to check the quality of samples. In order to determine the volume fraction of fibers, TGA test was carried out for composite samples containing 1wt% and 0.3wt%MWCNT. Figure 2.2 shows the typical TGA results of the composite samples containing 1wt% MWCNT. In this figure, the degradation point of this epoxy is around

389^{o}C. By calculating the weight loss of the sample and by knowing the density of the primary materials, the volume fraction of the fibers in the samples containing 1wt% MWCNT is determined to be almost 69%. From the typical DSC results shown in Figure 2.3, it is observed that the sample containing 1wt% MWCNT is fully cured. Also, Figure 2.3 shows that the heat flow attributed to Tg (Glass transition temperature) is 120.4 ^{0}C.

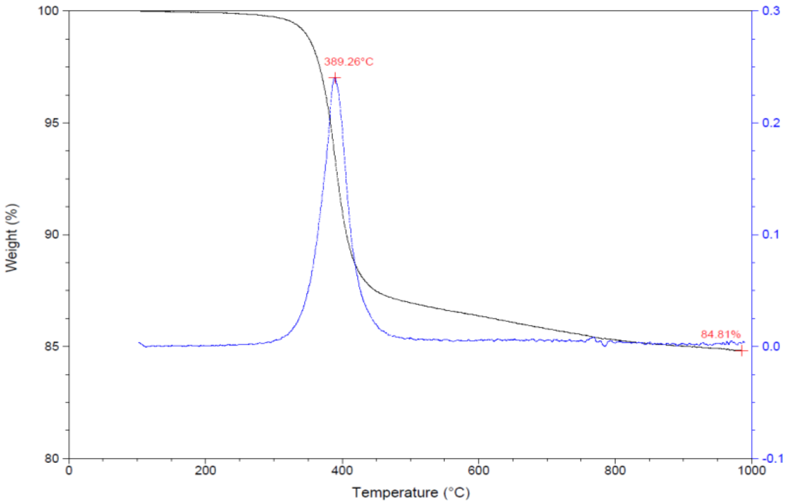

Figure 2.2: TGA result of the composite plate with 1wt% MWCNT after curing

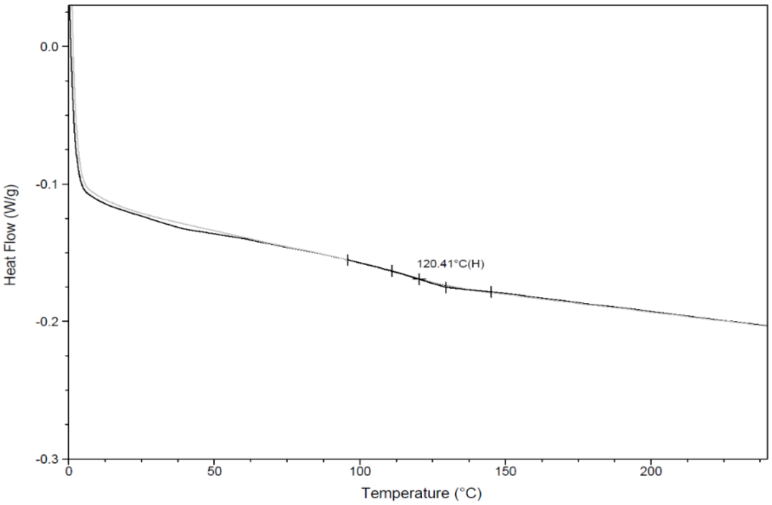

Figure 2.3: DSC result of the sample containing 1wt% MWCNT after curing

2.3.4 Electrical resistivity measurements

The electrical resistivity is an intrinsic property of the material that exhibits the ability of the material to resist an electrical current independent of its geometry. The electrical resistivity is reciprocal of the electrical conductivity and can be expressed using the unit of (Ohm-cm). The electrical resistivity can be measured using the following methods:

2.3.4.1 Two-probe method

To measure the electrical resistivity by the two-probe method, two probes are used to apply voltage and to measure electrical resistance of glass fiber/epoxy/CNT composite sample based on the corresponding current change as shown in Figure 2.4. The electrical resistivity can be calculated by:

$$\rho = R\frac{wt}{l} \tag{2.1}$$

Where ρ, w, t, l and R represent electrical resistivity, width of sample, thickness of sample, distance between electrodes and electrical resistance respectively.

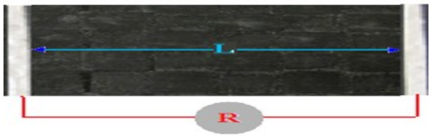

Figure 2.4: Two-probe method for measuring electrical resistivity of sample

2.3.4.2 Four-probe method:

To measure the electrical resistivity using the four-probe method, four probes are used. An outer pair of probes is utilized to apply electric current while an inner pair of probes is used to measure the electric potential of the glass fiber/epoxy/CNT composite sample as shown in Figure 2.5. The electrical resistivity can be measured based on ASTM D4496-04 by:

$$\rho = \frac{V}{I} \times \frac{wt}{l} \tag{2.2}$$

Where ρ, w, t, l, V and I represent electrical resistivity, width of sample, thickness of sample, distance between electric potential probes, electric potential difference and electric current respectively.

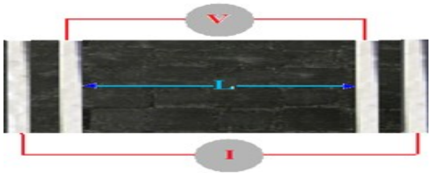

Figure 2.5: Four-probe method for measuring electrical resistivity of sample

2.3.4.3 Van der Pauw method

The van der Pauw method (resistivity /Hall effect measuring system) [77] is used to measure the electrical resistivity of the sample as shown in Figure 2.6. This method is similar to the four-probe method except that the four probes are placed on the corners of the sample as shown in Figure 2.6b. In this method, a current (I_{12}) is injected through two adjacent corners of (1 and 2) and the voltage drop (V_{34}) is measured at the other two corners (3 and 4) of the sample as shown in Figure 2.6b. The (I_{34}, I_{23} and I_{41}) and (V_{12}, V_{41} and V_{23}) are electrical current and the voltage drop respectively. The electrical resistivity which is reciprocal of the conductivity is calculated by the following equation:

$$\exp(-\pi . t . \sigma . R_A) + \exp(-\pi . t . \sigma . R_B) = 1 \tag{2.3}$$

Where t is the thickness of sample (cm), σ is the electrical conductivity (S/cm), and R_A and R_B are expressed by:

$$R_A = (\frac{V_{34}}{I_{12}} + \frac{V_{12}}{I_{34}})/2 \tag{2.4}$$

$$R_B = (\frac{V_{41}}{I_{23}} + \frac{V_{23}}{I_{41}})/2 \tag{2.5}$$

It should be mentioned that for square-shaped samples the correction factors are not needed when the ratio of thickness (t) to the lateral dimension (a) and the ratio of the contact size (δ) to the lateral dimension (a) are less than 0.5 and 0.1 respectively [78] . The ratio ($t/a = 0.013$) and ($\delta/a = 0.1$) were calculated for the samples. Therefore the correction factors are not required for the samples. The thicknesses of the samples were averaged over ten measurements. Keithley 6220 DC and Keithley 218A were used as current source and nanovoltmeter respectively. These machines were linked together to measure the electrical resistivity of glass fiber/epoxy/CNT composite sample as shown in Figure 2.6a.

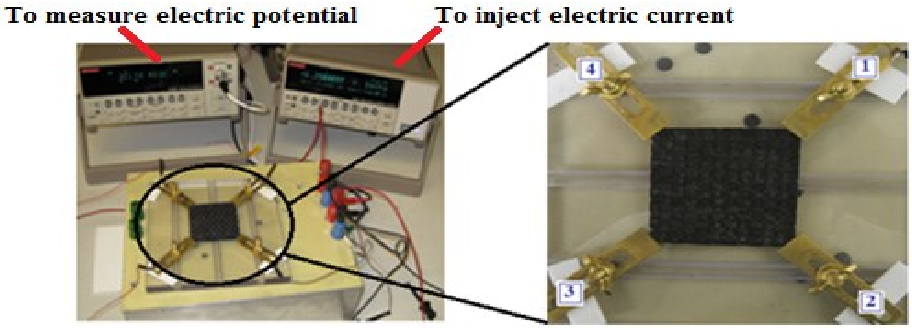

a) **b)**

Figure 2.6: Van der Pauw fixtures for measuring electrical resistivity by Keithley machines a) Experimental set-up b) Close-up view of sample

2.3.5 Variability of electrical resistivity

The electrical conductivity of the glass/epoxy/MWCNT composite samples is completely dominated by MWCNT while epoxy and glass fiber exhibit resistance preventing the electrons to flow through the sample. The dispersion of MWCNT in glass fiber/epoxy/MWCNT composite plates is evaluated by electrical resistivity measurements. Glass fabric/epoxy composite plates 1 and 2 containing 1wt% MWCNT and 0.3wt% MWCNT with the same size of 22×13 inch^2 were prepared. Plates 1 and 2 are labeled from 1 to 28 as shown in Figures 2.7a and 2.8a respectively. Each plate was cut into twenty eight 3×3 inch^2 samples. The state of dispersion of 1wt% MWCNT and 0.3wt% MWCNT in large plates 1 and 2 were assessed by volume resistivity measurements using Vander Pauw method. Sample configuration and experimental set-up to measure volume resistivity by Van der Pauw method are shown in Figure 2.6. Figures 2.7b and 2.8b show the locations and values of volume resistivity measured for smaller square samples cut out from plate 1 and plate 2 respectively. Coefficient of variation in percent as a measure of uniformity of electrical resistivity distribution is determined for plate 1 and plate 2 containing 1wt% MWCNT and 0.3wt% MWCNT as shown in Table 2.1. By comparing coefficient of variation in percent for plates 1 and 2 presented in Table 2.1, it is found that plate 1 containing 1wt% MWCNT indicates more uniformity in distribution of volume resistivity compared to that for plate 2 containing 0.3wt% MWCNT.

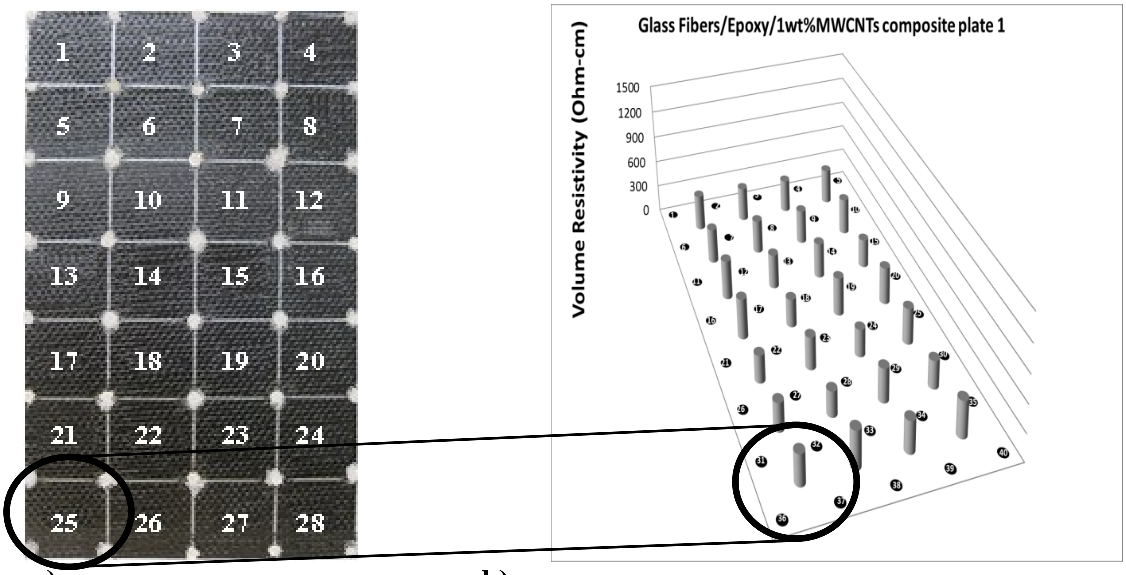

a) b)

Figure 2.7: a) Light transmission image of plate 1 containing 1wt% MWCNT b) Distribution of volume resistivity corresponding to twenty eight samples

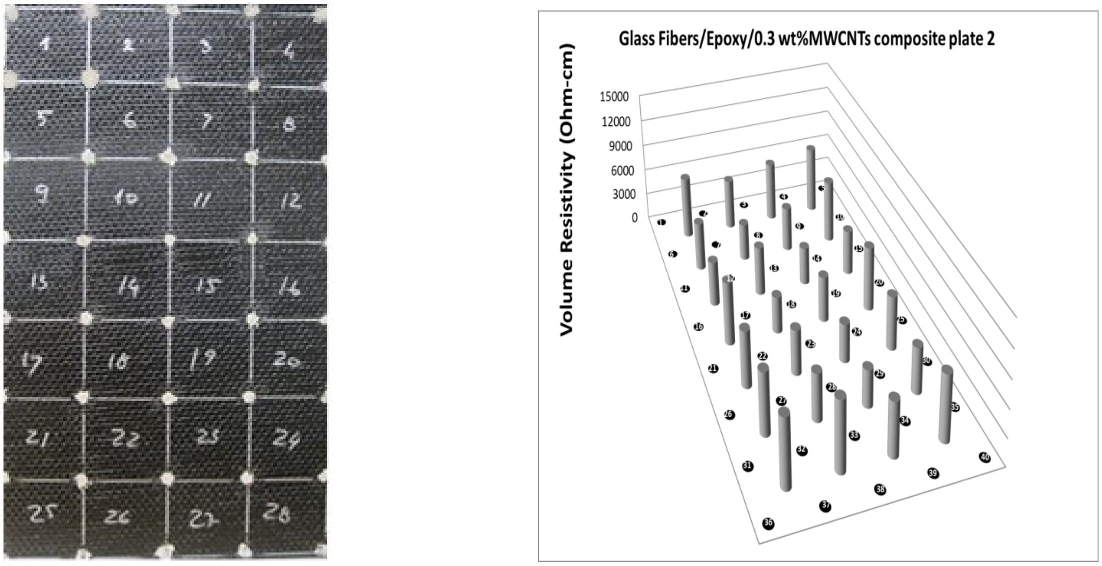

a) b)

Figure 2.8: a) Light transmission image of plate 2 containing 0.3wt% MWCNT b) Distribution of volume resistivity corresponding to twenty eight samples

Table 2.1: Comparing electrical resistivity, uniformity of MWCNT distribution for plates 1 and 2 containing 1w% and 0.3wt% MWCNT

Glass fiber/epoxy/MWCNT Composite	Plate 1 containing 1wt% MWCNT	Plate 2 containing 0.3wt% MWCNT
Average Volume Resistivity (AVR) (Ohm-cm)	370.2	5844.3
Standard Deviation (SD) (Ohm-cm)	44.43	1185.1
Coefficient of variation (%) = (SD/AER)×100	12	20.3

To compare the Vander Pauw method with the four-probe method, the same samples labeled from 1 to 8 cut out from plate 1 were chosen. These samples were cut into 1×3 $inch^2$ eight bars. Sample configuration for measuring volume resistivity by the four-probe method is shown in Figure 2.5. Figure 2.9a shows that the volume resistivity measured by the four-probe method is approximately the same as that measured by the Vander Pauw method. The state of MWCNT distribution on top and bottom sides of plate 1 is studied by measuring surface resistivity for both sides of 8 bar samples using two-probe method. The sample configuration is indicated in Figure 2.4. Figure 2.9b shows that almost the same MWCNT distribution is found for both sides of each bar.

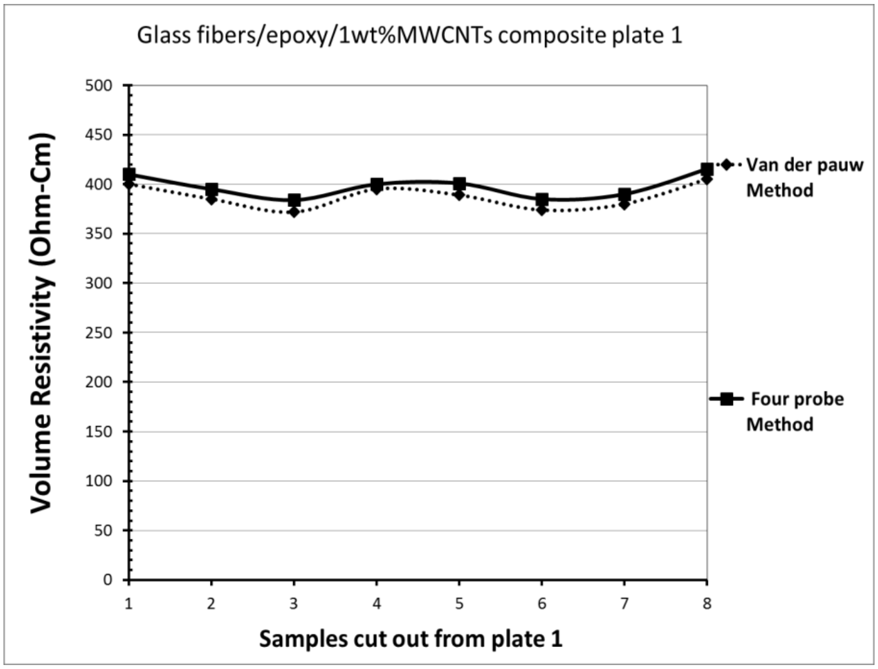

a)

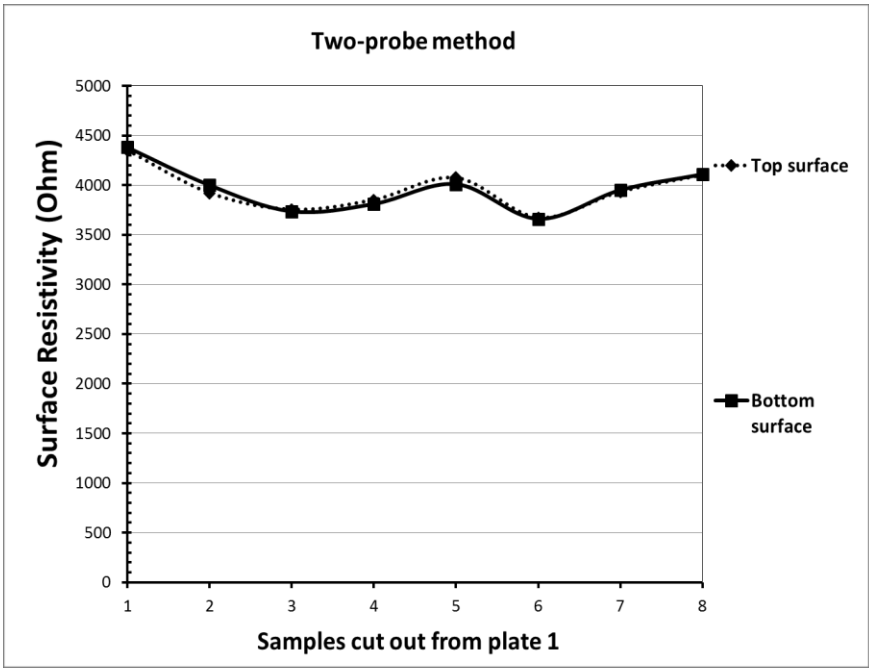

b)

Figure 2.9: Eight samples cut out from plate 1 containing 1wt% MWCNT a) Volume resistivity measured by the van der pauw and the four-probe methods b) Surface resistivity measured the by two-probe method on both sides

2.4 Investigation of grid points and grid lines

Two different types of electrical contact grid made from silver-epoxy paste are examined. One is grid points and the other is grid lines. Then, electrodes are prepared by attaching electrical wires to these grids for electrical resistance measurement (ERM).

2.4.1 Grid points

2.4.1.1 Composite plates 3, 4 and 5

Glass fabric/epoxy/1wt%MWCNT plates 3, 4 and 5 with the size of 4×5 inch^2 were prepared. Five contact-point electrodes are mounted on the surface of plates 3, 4 and 5 as shown in Figure 2.10.

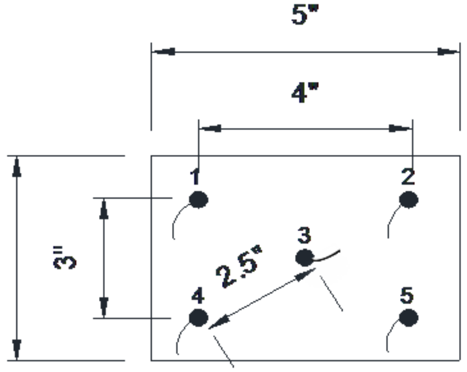

Figure 2.10: Plates 3, 4 and 5 specification. The wires attached to black dots, labeled from 1 to 5 are contact-point electrodes

2.4.1.2 Composite plate 6

Glass fabric /epoxy/1wt% MWCNT plate 6 with the size of 7×7 inch^2 was made. Nine contact-point electrodes spaced at 3 inch apart are deposited on the surface of plate 6 as illustrated in Figure 2.11.

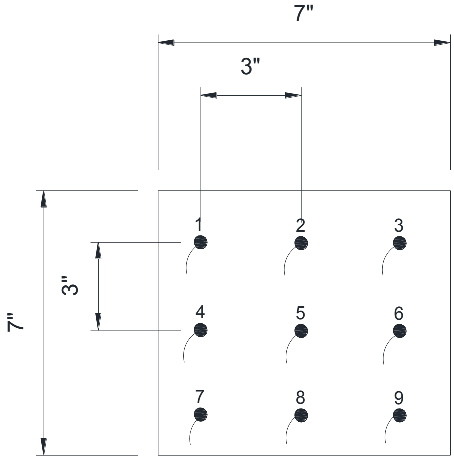

Figure 2.11: Specification of plate 6. The wires attached to black dots, labeled from 1 to 9 are contact-point electrodes

2.4.1.3 Composite plate 7

Glass fabric /epoxy/1wt% MWCNT plate 7 with the size of 13×13 inch^2 was prepared. Twenty five contact-point electrodes spaced at 3 inch apart are bonded on the surface of plate 7 as shown in Figure 2.12.

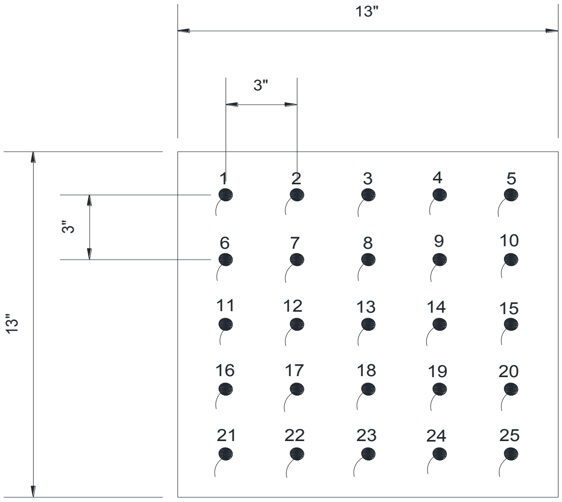

Figure 2.12: Plate 7 specification. The wires attached to black dots, labeled from 1 to 25 are contact-point electrodes

2.4.1.4 Composite plate 8

Glass fabric/epoxy/0.3wt% MWCNT plate 8 with the size of 22×13 inch^2 was fabricated. Forty contact points spaced at 3 inch apart are mounted on the surface of plate 8 as illustrated in Figure 2.13.

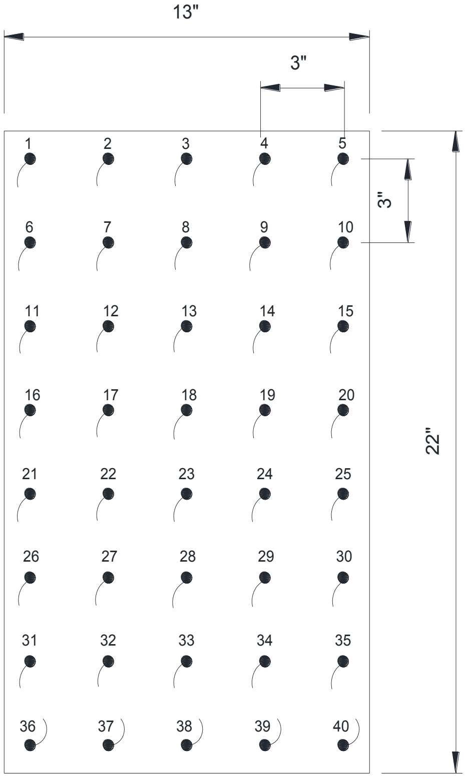

Figure 2.13: Plate 8 specification. The wires attached to black dots, labeled from 1 to 40 are contact-point electrodes

2.4.2 Grid lines

2.4.2.1 Composite plate 9

Glass fabric/epoxy/1wt% MWCNT plate 9 with the size of 8×14 inch^2 was prepared. Twenty eight parallel contact-line electrodes are attached on the surface of plate 9 as shown in Figure 2.14.

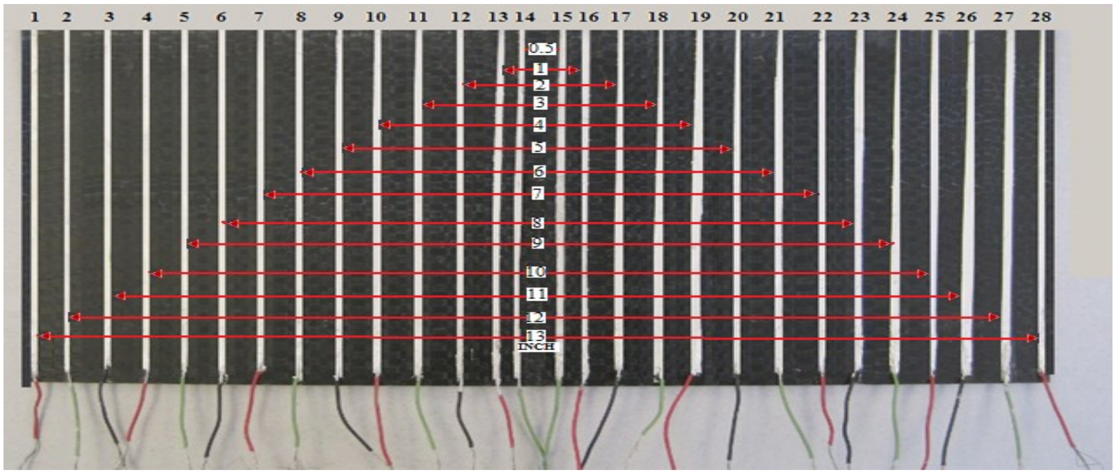

Figure 2.14: Plate 9 mounted with twenty eight contact-line electrodes with different spacing

2.4.2.2 Composite plate 10

Glass fabric/epoxy/1wt% MWCNT plate 10 with the size of 8×14 inch^2 was made. Five and three parallel contact-line electrodes spaced at 3 inch apart are mounted on the top and bottom surfaces of plate 10 respectively as illustrated in Figure 2.15.

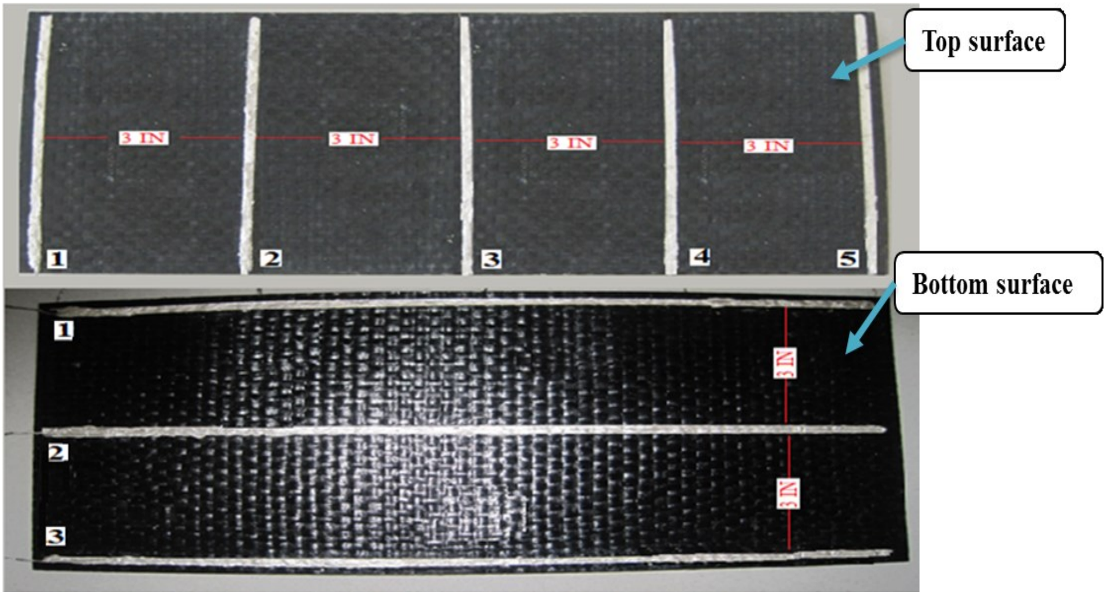

Figure 2.15: Plate 10 mounted with five and three contact-line electrodes on top and bottom surfaces respectively

2.4.2.3 Composite plate 11

Glass fabric/epoxy/0.3wt% MWCNT plate 11 with the size of 22×13 inch^2 was fabricated. Five vertical and eight horizontal parallel contact-line electrodes spaced at 3 inch apart are mounted on the surface of plate 11 as illustrated Figure 2.16. It should be noted that there is no connection between vertical and horizontal electrical contact lines at the cross over points.

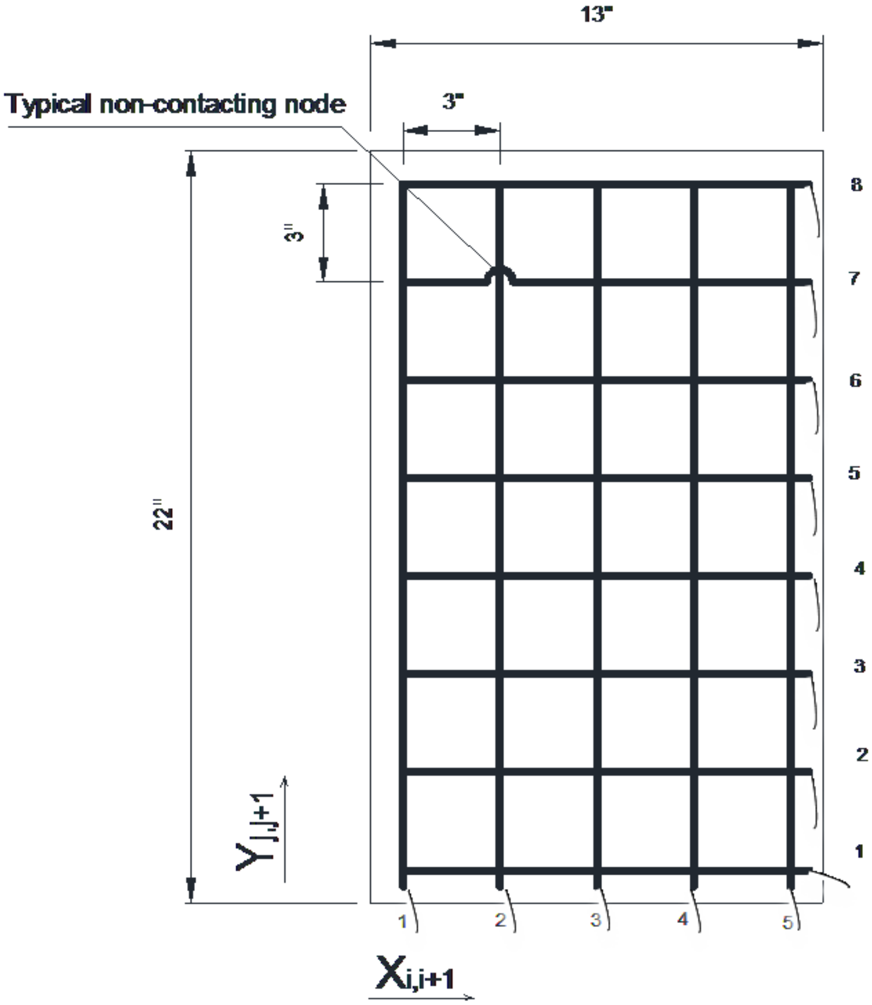

Figure 2.16: Specification of plate 11 .The wires attached to black lines labeled from 1 to 5 and 1 to 8 are vertical and horizontal contact-line electrodes respectively

2.5 Electrical resistance measurements

The electrical resistance measurement (ERM) is used to detect damage in non-conductive fiber (kevlar and glass fibers) reinforced epoxy composite structures containing CNT. The ERM adopts the electrically conductive CNTs enhanced epoxy themselves as sensors and it does not need expensive equipment. A constant source voltage was directly applied and the electrical current was measured to calculate the electrical resistance using the two-probe method. ERM is performed by grid points and grid lines that are presented as follows:

2.5.1 Grid points

The grid points are used for ERM. The electrical resistance change (ERC) is expressed by:

$$\Delta R(\%) = \frac{R_{f,i,j} - R_{I,i,j}}{R_{I,i,j}} \times 100 \tag{2.6}$$

Where

$R_{I,i,j}$: is the initial electrical resistance before damage between grid points i and j

$R_{f,i,j}$: is the final electrical resistance after damage between grid points i and j.

2.5.2 Grid lines

Grid lines are mounted to measure the electrical resistance. The average electrical resistance change (AERC) is expressed by:

Average electrical resistance change (%) $= \frac{\Delta X_{i,i+1} + \Delta Y_{j,j+1}}{2}$ **(2.7)**
in areas surrounded by i,i+1 and j,j+1

where $\Delta X_{i,i+1}$ and $\Delta Y_{j,j+1}$ are the electrical resistance change in percent between two consecutive vertical (X lines) and horizontal electrical contact lines (Y lines), respectively, which are defined in the following equations:

$$\Delta X_{i,i+1}\,(\%) = \frac{X_{i,i+1,F} - X_{i,i+1,I}}{X_{i,i+1,I}} \times 100 \tag{2.8}$$

$$\Delta Y_{j,j+1}\,(\%) = \frac{Y_{j,j+1,F} - Y_{j,j+1,I}}{Y_{j,j+1,I}} \times 100 \tag{2.9}$$

where

$X_{i,i+1,I}$ is the initial electrical resistance measured between two consecutive vertical electrical contact lines i and $i+1$ before damage.

$X_{i,i+1,F}$ is the final electrical resistance measured between two consecutive vertical electrical contact lines i and $i+1$ after damage.

$Y_{j,j+1,I}$ is the initial electrical resistance measured between two consecutive horizontal electrical contact lines j and $j+1$ before damage.

$Y_{j,j+1,F}$ is the final electrical resistance measured between two consecutive horizontal electrical contact lines lines j and $j+1$ after damage.

i is the vertical electrical contact line number.

j is the horizontal electrical contact line number.

2.6 Drilled Holes

Drilled holes of different sizes were introduced to simulate damage in plates. The specifications of plates and experimental conditions are presented in Table 2.2.

Table 2.2: Specifications and experimental conditions of the plates

Number of Glass fiber /epoxy/CNT Plates	Size (inch^2)	MWCNT wt%	Grid points	Grid lines	Spacing between electrodes (inch)	Damage type
Plate 1	22×13	1.00	-	-	-	-
Plate 2	22×13	0.30	-	-	-	-
Plate 3	4×5	1.00	✓	-	2.5,3,4	Drilled hole
Plate 4	4×5	1.00	✓	-	2.5,3,4	Drilled hole
Plate 5	4×5	1.00	✓	-	2.5,3,4	Drilled hole
Plate 6	7×7	1.00	✓	-	3	Drilled hole
Plate 7	13×13	1.00	✓	-	3	Drilled hole
Plate 8	22×13	0.30	✓	-	3	Drilled holes
Plate 9	8×14	1.00	-	✓	0.5,….,13	Drilled hole
Plate 10	8×14	1.00	-	✓	3	Drilled hole
Plate 11	22×13	0.30	-	✓	3	Drilled holes

2.7 Results and discussion

The effects of distance between pair of contact-point electrodes closest to damage, spacing between electrodes, proximity of pair of electrodes to damage, plate size and, damage severity on the ERC for damage detection, location and quantification are studied using grid points and grid lines and they are presented in the following:

2.7.1 Grid points:

2.7.1.1 Effect of distance between pair of contact-point electrodes closest to damage on ERC

To investigate the effect of distance between pair of contact-point electrodes closest to damage on ERC for damage detection, location and quantification, plates 3, 4 and 5 containing 1wt% MWCNT with the same size were drilled to make a hole of size (1/4) inch as shown in Figures 2.17a, 2.17c and 2.17e. The electrical resistances before and after drilling were measured by contact-point electrodes spaced at 2.5, 3 and 4 inch apart. ERC was calculated based on Eq. (2.6). Figures 2.17b, 2.17d and 2.17f show the locations and values of the changes in electrical resistance. In these figures, significant variation in distribution of ERC corresponds to the location of drilled hole. This indicates the capability of CNT networks for detecting and locating damage. Figure 2.17g show the change in electrical resistance measured by contact-point electrodes spaced at 2.5, 3 and 4 inch apart due to the introduction of a similar drilled hole. It is observed form Figure 2.17g that the change in electrical resistance decreases as distance between pair of contact-point electrodes closest to damage increases. Three inch is found as an effective distance between pair of contact-point electrodes that can provide significant change in electrical resistance while being suitable for practical implementation to avoid using extensively large number of contact-point electrodes for large structures.

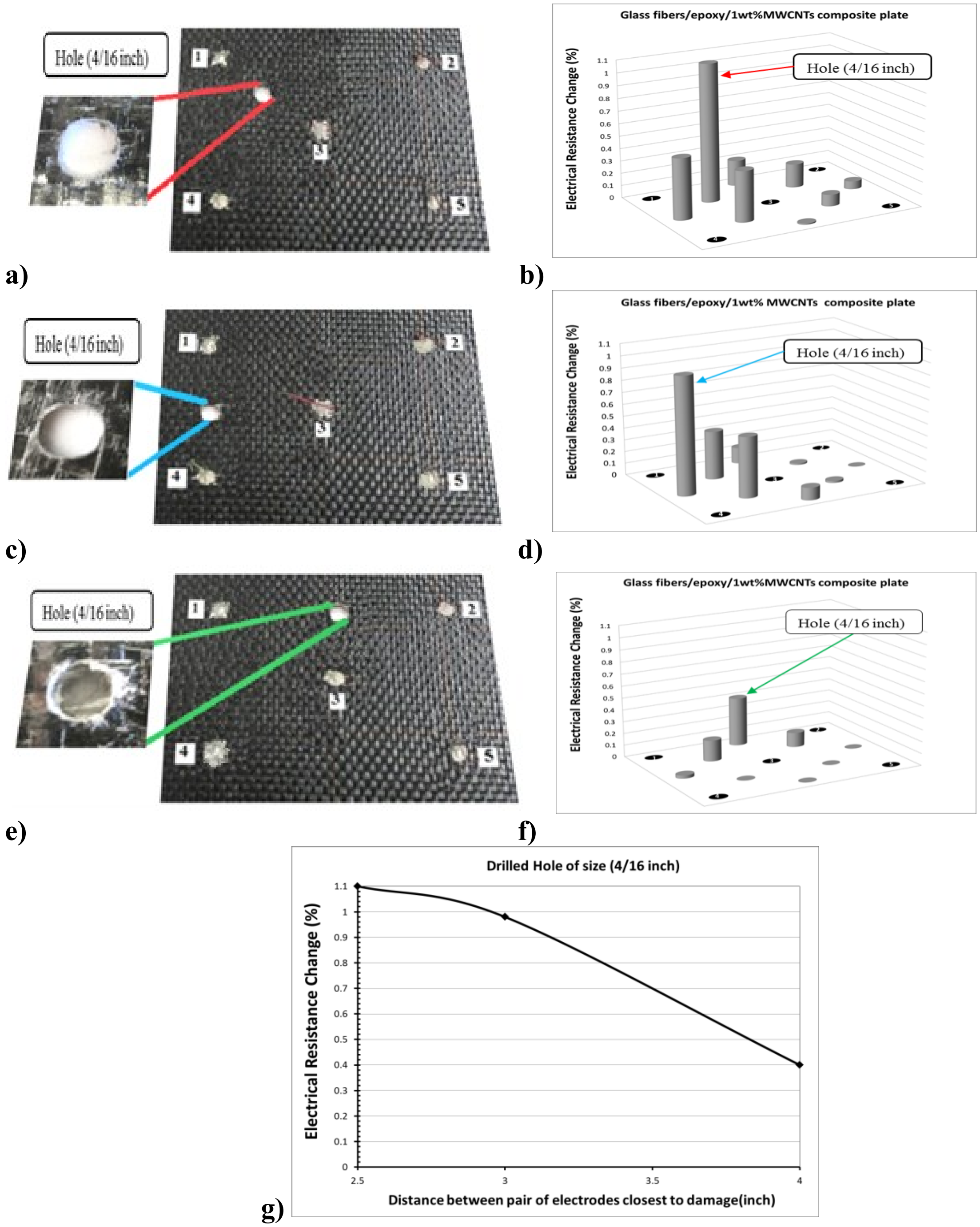

Figure 2.17: Plate 3 a) After hole of size (1/4 inch) is drilled b) ERC distribution, plate 4 c) After the hole is drilled d) ERC distribution, plate 5 e) After the hole is drilled f) ERC distribution, g) ERC versus distance between pair of electrodes closest to the hole location

2.7.1.2 Effect of proximity of contact-point electrodes pair to damage on ERC

The effect of proximity of pair of contact-point electrodes to hole location on ERC is studied when spacing between contact-point electrodes, drilled hole size and hole location are kept constant. A hole of size (4/16) inch was drilled in plate 6 as shown in Figure 2.18a. Figure 2.18b shows the location and value of the ERC. Comparing Figures 2.18a and 2.18b, it is clear that significant variation in distribution of ERC shows the location of drilled hole. It is observed from Figure 2.18c that the change in resistance decreases as the distance between drilled hole location and pair of electrodes spaced at 3 inch apart increases. In this figure, the distance is calculated between hole location and middle of each pair of electrodes.

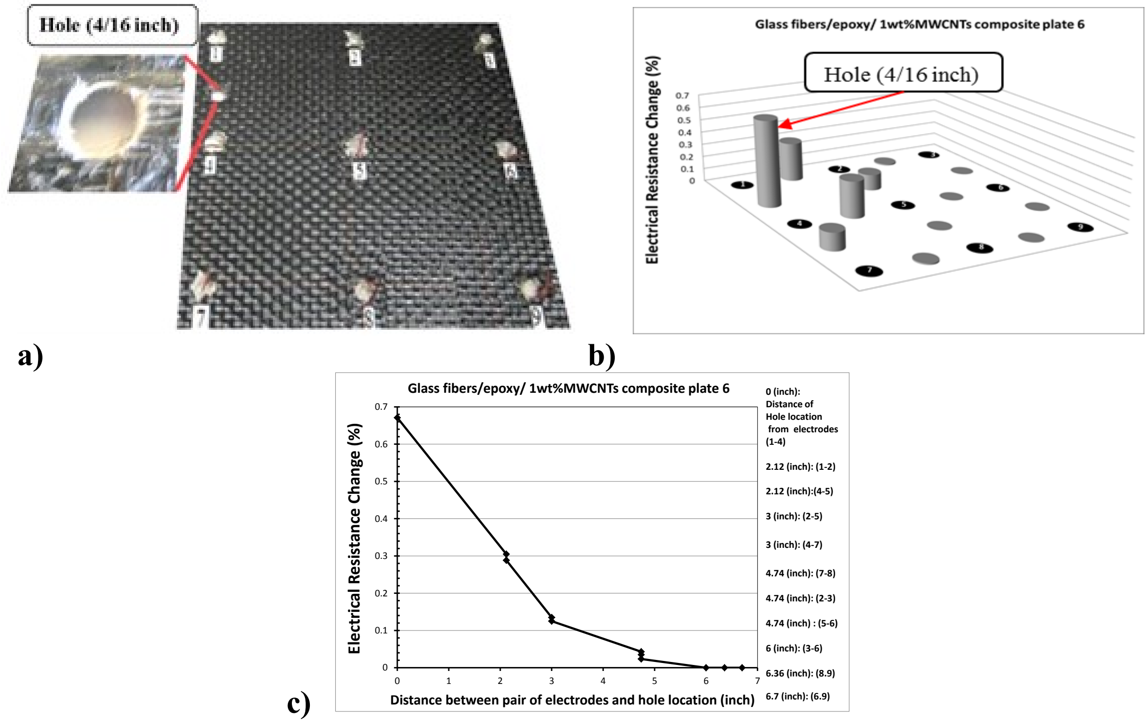

Figure 2.18: a) Plate 6 after hole of size (4/16) inch is drilled b) ERC distribution of plate 6 c) ERC versus distance between pair of electrodes and drilled hole (1/4) inch

2.7.1.3 Effect of plate size on ERC

To explore the effect of plate size on ERC for damage detection and location, the same experiments are performed on 13×13 (inch^2) plate 7 containing 1wt% MWCNT mounted with contact-point electrodes spaced at 3 inch and drilled hole size as well as hole location are fixed. A hole of size (4/16) inch was drilled in plate 7 as shown in Figure 2.19a. Observing Figures 2.19a and 2.19b, the hole is detected and located according to the sharp variation in distribution of ERC in plate 7. The value of the ERC measured by pair of electrodes spaced at 3 inch apart for plates 4, 6 and 7 containing 1wt% MWCNT with different sizes were determined to be 0.98%, 0.67% and 0.45% respectively due to the introduction of the same-sized hole. This reveals that the ERC does not decrease significantly when increasing plate size. This is because of an increase in current spreading (more alternative paths for the electrons to flow) with increasing plate size.

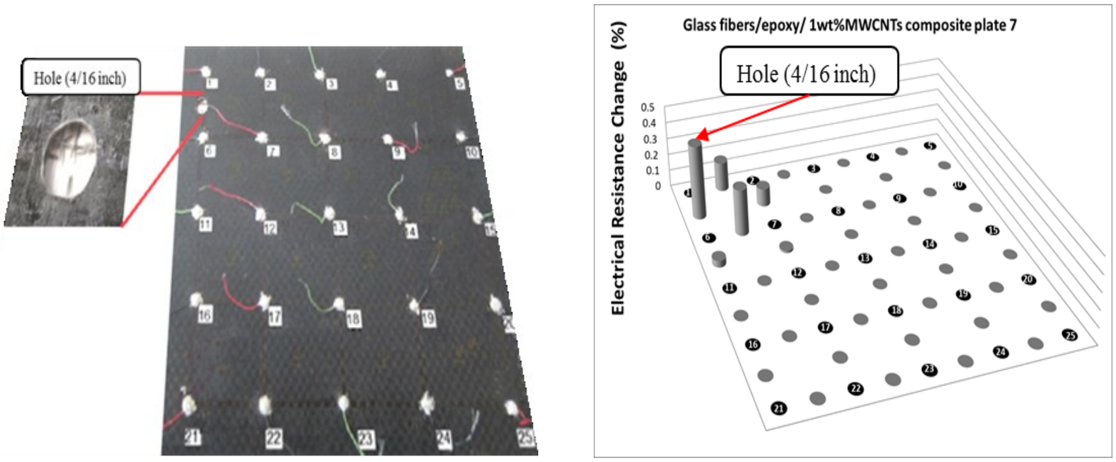

a) b)

Figure 2.19: a) Plate 7 after hole of size (4/16) inch is drilled, b) ERC distribution of the composite plate 8. The black dots, labeled from 1 to 25 are representation of contact points

2.7.1.4 Effect of damage severity on ERC

To study the effect of hole severity on ERC for the determination of hole quantification, plate 8 (22×13 inch^2) containing 0.30 wt% MWCNT is considered. Holes of sizes 1/16, 2/16, 3/16, 4/16, 5/16 and 6/16 inch respectively were drilled in plate 8 as shown in Figures 2.20a, 2.20c, 2.20e. Figures 2.20b, 2.20d and 2.20f show the locations and values of the change in electrical resistance due to the drilling of holes of sizes 1/16, 2/16, 3/16, 4/16, 5/16 and 6/16 inch respectively. From observing Figures 2.20a and 2.20b, hole 1 is detected and located based on the sharp local variations in distribution of the electrical resistance change. Good correspondence also is seen between Figures 2.20c and 2.20d to detect and locate holes 1 and 2 distinctly. By comparing Figures 2.20e and 2.20f, it is clear that the significant local variations in distribution of the electrical resistance change correspond exactly to the locations of holes of different sizes drilled at different locations in the plate. Figure 2.21 presents the influence of hole volume on the change in electrical resistance. In figures 2.21, the numbers below the curve represent the pairs of electrodes for the ERM. This pair of electrodes is closest to the hole or damage region. As it can be observed from Figure 2.21, there is a clear correlation between the hole volume and the change in electrical resistance proving that this technique can also be used to quantify the extent of damages, in addition to the detection and location capabilities.

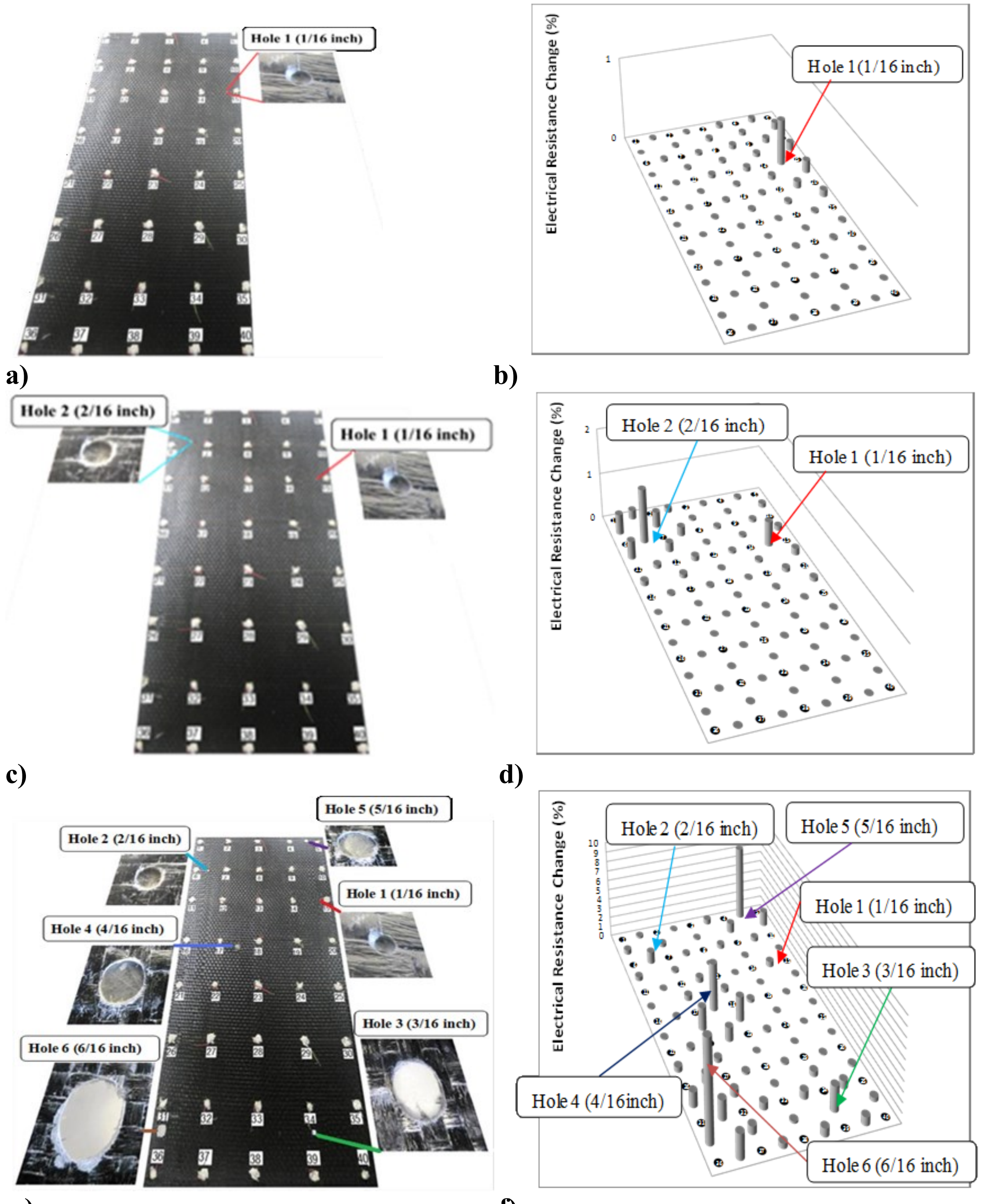

a) b) c) d) e) f)

Figure 2.20: a) Plate 8 after hole 1(1/16) inch is drilled b) ERC distribution c) Plate 8 after holes 1 and 2 (1/16 and 2/16) inch are drilled d) ERC distribution e) Plate 8 after holes 1, 2, 3, 4, 5 and 6 (1/16, 2/16, 3/16, 4/16, 5/16 and 6/16) inch are drilled f) ERC distribution

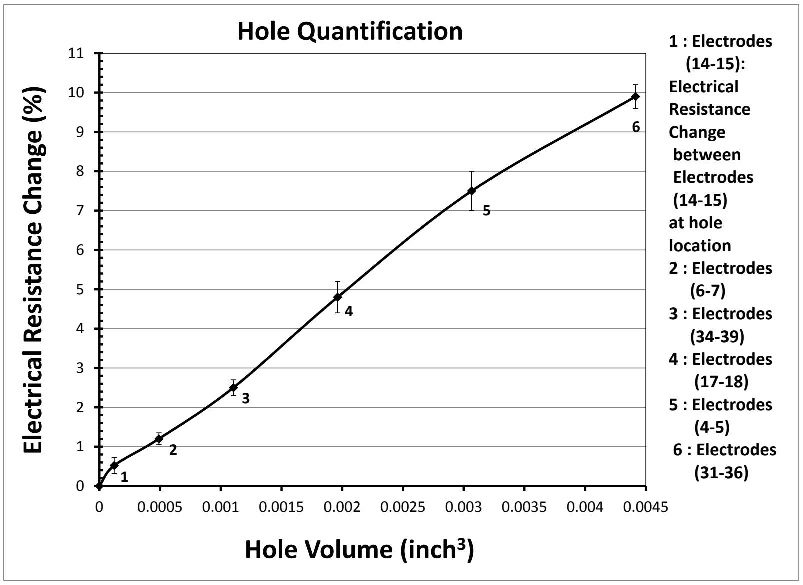

Figure 2.21: Effect of hole volume on ERC (Average electrical resistance: 276,000 ohms) (Data are presented as mean ± standard deviation (SD) from three experiments)

2.7.1.5 Effect of MWCNT concentrations on ERC

To explore the effect of MWCNT concentrations on the ERC for damage detection, location and quantification, plate 7 (13×13 inch^2) containing 1wt% MWCNT and plate 8 (22×13 inch^2) containing 0.3wt% MWCNT are compared when the contact-point electrodes spaced at 3 inch apart, the location and size of drilled hole are fixed. The ERC for plates 7 and 8 were measured to be 0.44% and 4.78% respectively due to introduction of the same hole of size (4/16) inch. Even though the size of plate 8 containing 0.3wt% MWCNT is larger than plate 7 containing 1wt%MWCNT, the ERC for plate 8 is larger than that measured for plate 7. This reveals that ERC increases significantly when the concentration of MWCNT is reduced from 1w% to 0.3wt% MWCNT.

2.7.2 Grid Lines

A variation of the technique using grid points is the technique using lines of contacts. In this technique, lines of conductive paint are drawn on the surface of plates 9, 10 and 11.

2.7.2.1 Effects of spacing between contact-line electrodes and hole severity

The effects of spacing between contact-line electrodes and hole severity on ERC are studied by drilling holes of 1/16, 2/16, 4/16, 6/16, 8/16 and 12/16 inch in plate 9 respectively as shown in Figure 2.22. The electrical resistances before and after drilling each hole were measured by contact-line electrodes with different spacing. Figure 2.23 shows ERC increases with increasing the holes size while the ERC linearly decreases with increasing the spacing between pairs of contact-line electrodes. It is observed from Figure 2.23 that the pair of electrodes spaced at 3 inch is effective for damage detection, location and quantification.

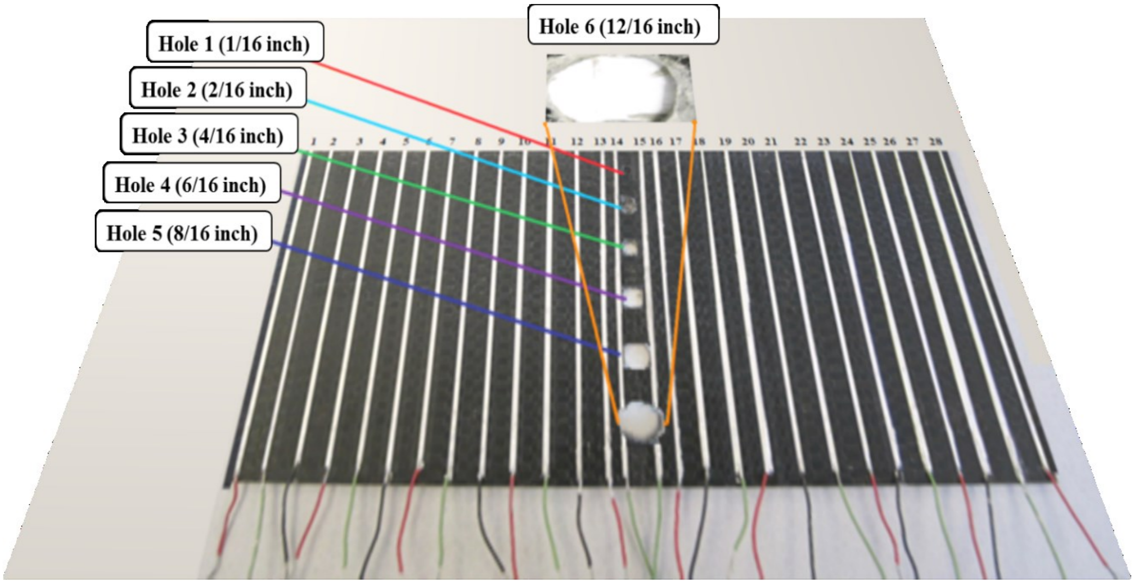

Figure 2.22: Plate 9 mounted with twenty eight contact-line electrodes after six holes of sizes (1/16, 2/16, 4/16, 6/16, 8/16 and 12/16) inch are drilled respectively

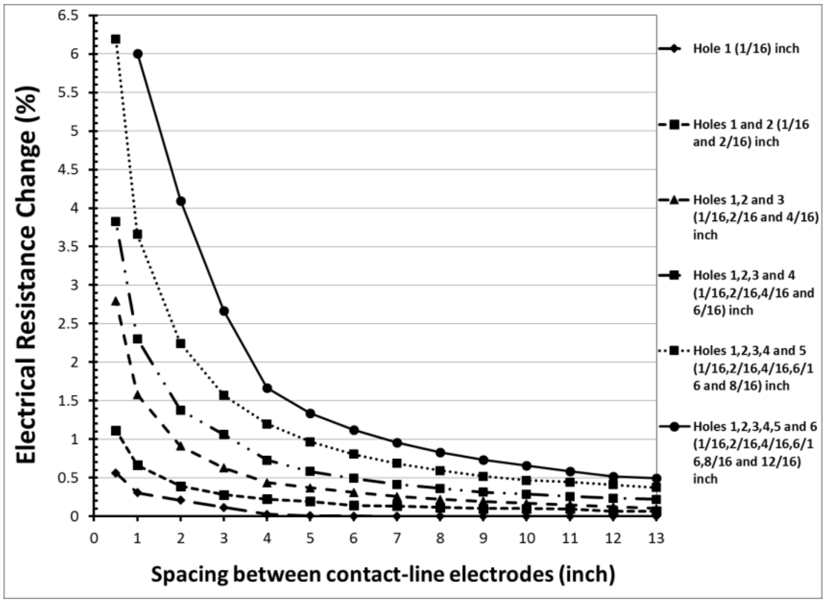

Figure 2.23: ERC versus spacing between contact-line electrodes for drilled holes of sizes 1/16, 2/16, 4/16, 6/16, 8/16 and 12/16 inch

2.7.2.2 Effect of placing contact-line electrodes on both sides of composite plate

The effect of using contact-line electrodes on both sides of plate for damage detection and location is investigated. Five vertical and three horizontal parallel contact-line electrodes spaced at 3 inch apart were mounted on the top and bottom surfaces of plate 10 respectively as shown in Figure 2.15. Plate 10 was drilled to make a hole of size (4/16) inch as indicated in Figure 2.24a. The electrical resistances were measured using pairs of vertical and horizontal contact-line electrodes mounted on both surfaces of plate 10. The average electrical resistance change (AERC) was calculated based on Eq. (2. 7). Figure 2.24b shows the location and value of the average change in electrical resistance due to the drilling of hole of size (4/16) inch. The hole drilled in plate10 is detected and located based on the sharp AERC which corresponds to segment H as illustrated in Figure 2.24b.

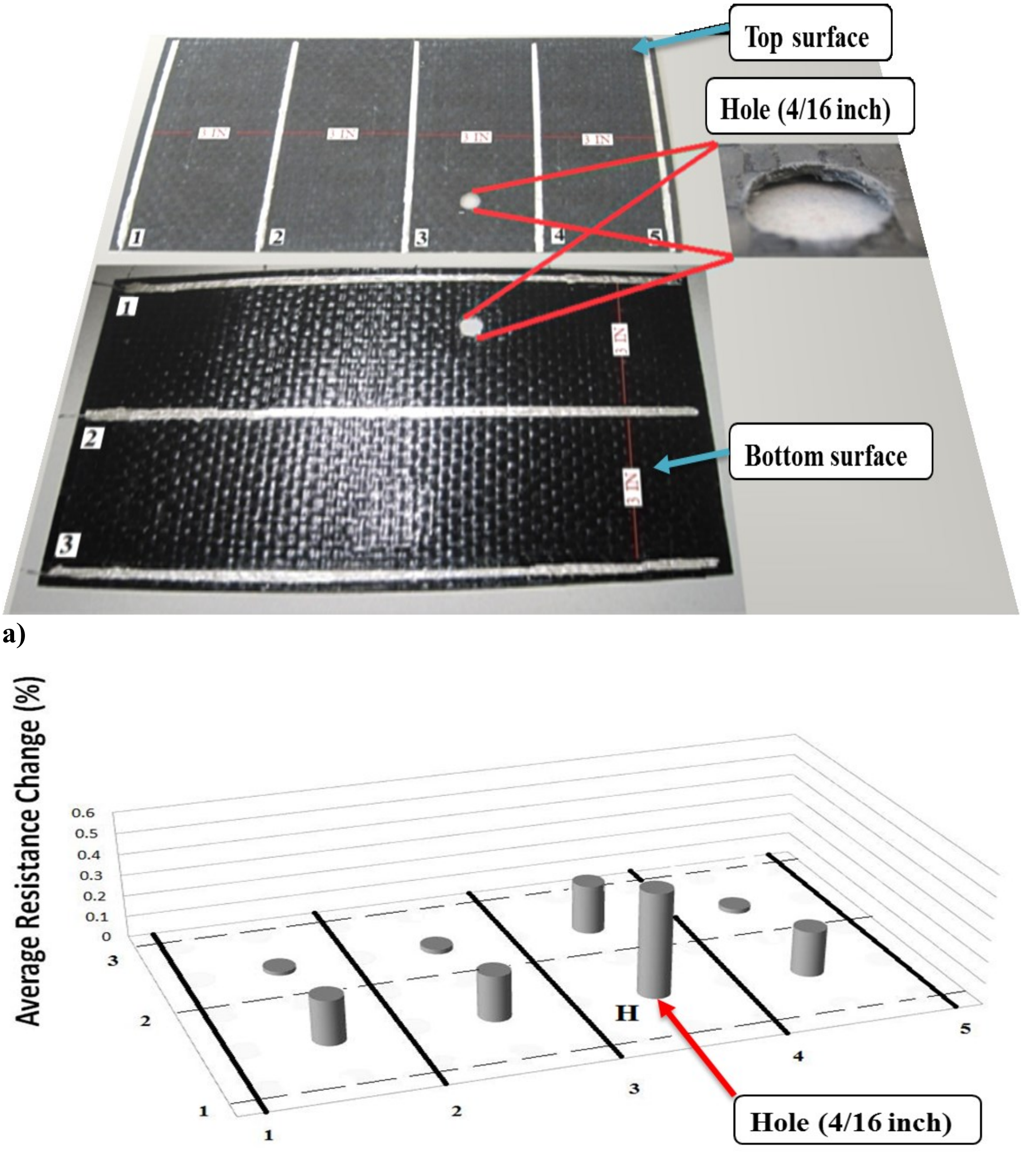

Figure 2.24: a) Plate 10 mounted with contact-line electrodes on both sides after hole of size (4/16) inch is drilled. b) AERC distribution after drilling of hole of size 1(4/16) inch. The vertical black lines, labeled from 1 to 5 and the horizontal dash lines, labeled from 1 to 3 are representation of electrical contact lines on top and bottom surfaces of plate 10 respectively

2.7.2.3 Effect of hole severity on ERC

To investigate the effect of hole severity on ERC for the determination of hole quantification using grid lines, plate 11 (22×13 inch^2) containing 0.30wt% MWCNT mounted with grid lines spaced 3 inch apart on its surface was prepared. Plate 11 was drilled to make holes of size 1/16, 2/16, 3/16, 4/16, 5/16 and 6/16 inch respectively as shown in Figures 2.25a, 2.25c and 2.25e. The electrical resistances of plates 11 were measured using five vertical and eight horizontal contact-line electrodes. The average changes in electrical resistance were calculated based on Eq. (2.7). Figures 2.25b, 2.25d and 2.25f show the average changes in electrical resistance when these holes were drilled in plate 11. The sharp increases in distribution of the AERC labeled A, B, C, D, E and F shown in Figures 2.25b, 2.25d and 2.25f respectively correspond to holes of 1/16, 2/16, 3/16, 4/16, 5/16 and 6/16 inch drilled in plate 11. It is observed from Figure 2.26 that the average change in electrical resistance measured between contact-line electrodes at hole locations increase with increasing hole volume. This reveals quantification capability of the technique using grid lines in addition to detection and location of damage.

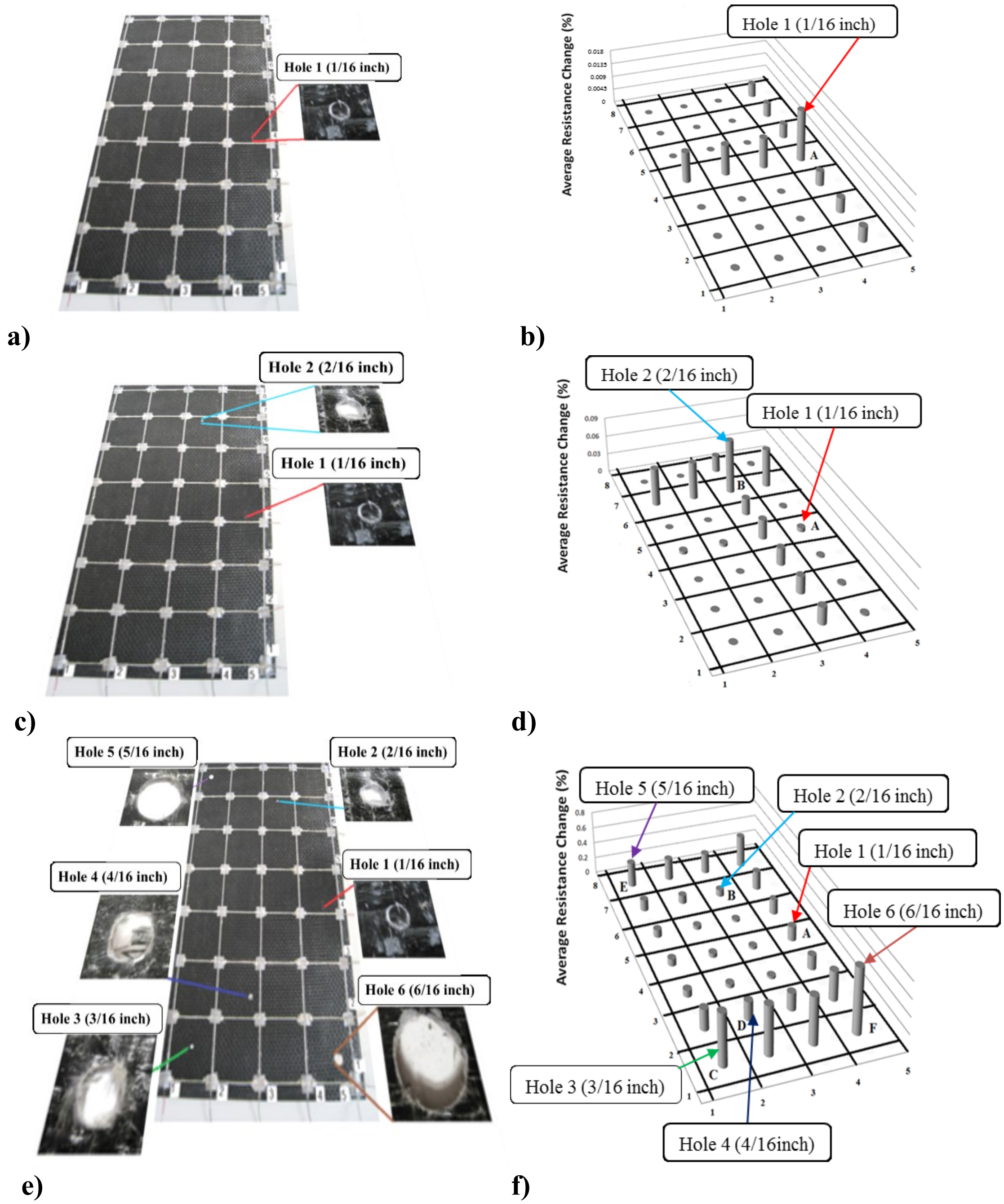

Figure 2.25: a) Plate 11 after hole 1(1/16) inch is drilled b) AERC distribution c) Plate 11 after holes 1 and 2 (1/16 and 2/16) inch are drilled d) AERC distribution e) Plate 11 after holes 1, 2, 3, 4, 5 and 6 (1/16, 2/16, 3/16, 4/16, 5/16 and 6/16) inch are drilled f) AERC distribution. The vertical black lines labeled from 1 to 5 and the horizontal black lines labeled from 1 to 8 are representation of contact lines

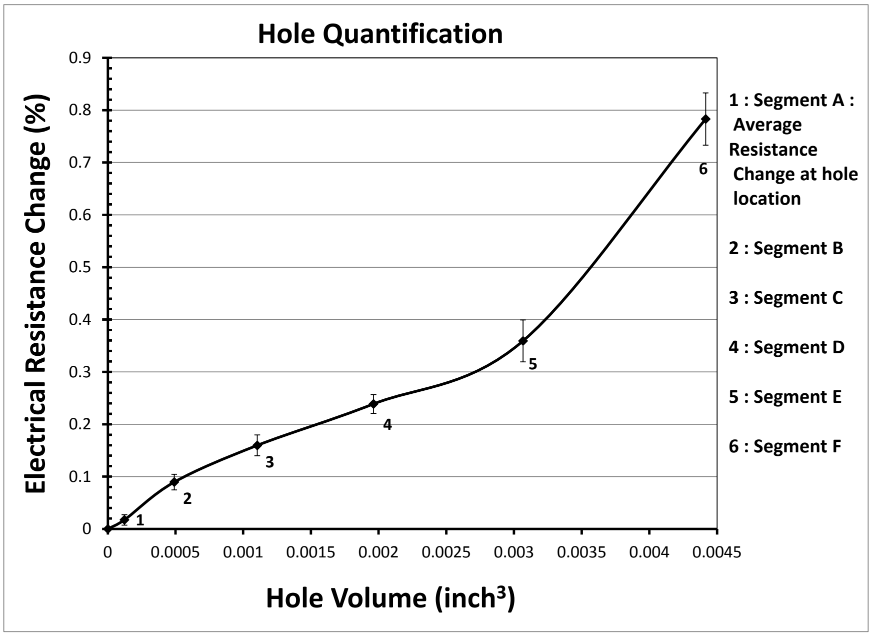

Figure 2.26: Effect of hole volume on AERC (Average of AER: 54,570 ohms) (Data are presented as mean ± SD from three experiments)

2.7.2.4 Effect of MWCNT concentration on ERC

To study the effect of MWCNT concentrations on the ERC, comparison between plate 10 (8×14 inch^2) containing 1wt% MWCNT and plate 11 (22×13 inch^2) containing 0.3wt% MWCNT is performed with the contact-line electrodes spaced 3 inch apart and the size of the drilled hole is fixed. The AERC for plates 10 and 11 were measured to be 0.49% and 0.238%. Even though the concentration of MWCNT in plate 11 is smaller than that for plate 10, the average change in resistance for plate 10 is larger than that for plate 11 due to the introduction of the same drilled hole of size (4/16) inch. This is due to the direct relation between plate size and the length of electrical contact lines drawn along the dimension of plate. As plate size is increased, larger electrical contact lines are required. The use of larger contact lines would cause a reduction in current density while reducing resolution for hole detection and location. As such, aspects of the material property (as a result of the MWCNT concentration) and length of electrical contact lines are intertwined to detect, locate and quantify damage using grid lines.

2.7.2.5 Comparison of grid points and grid lines:

Plates 8 and 11 containing 0.3wt% MWCNT with the same size mounted with grid points and grid lines spaced 3 inch apart respectively are compared. It is found that the grid points give a significant increase in electrical resistance compared to grid lines for the same-sized hole. Moreover, by comparing Figures 2.20b and 2.25b, 2.20d and 2.25d, and 2.20f and 2.25f, it is observed that the grid point strategy is much better at providing the location of the damage than the grid line strategy.

2.8 Conclusion

Experimental investigations were performed to study the influences of distance between pair of contact-point electrodes closest to damage, proximity of pair of electrodes to damage, plate size, damage severity, MWCNT concentration and electrical contact geometry on change in electrical resistance for damage detection, location and quantification. The knowledge obtained from experimental results can be highlighted as follows:

- ERC increases as spacing between electrodes decreases
- ERC increases as the distance between electrodes and hole location decreases
- ERC decreases as the size of plate (containing 1wt% MWCNT) increases
- ERC increases as size of damage increases

- ERC increases with decreasing MWCNT concentration from 1w% MWCNT to 0.30wt% MWCNT in glass fiber/epoxy/MWCNT composite plates
- Grid points provides greater ERC and spatial resolution as well as effectiveness for practical implementation to detect, locate and quantify damage in large polymer composite structures as compared to grid lines

Chapter 3

A technique for real-time detection, location and quantification of damages in large polymer composite structures made of electrically non-conductive fibers and carbon nanotube networks

In this chapter, a novel, practical and real-time structural health monitoring (SHM) technique is developed to detect, locate and quantify damages that occur at one or several locations in large polymer composite structures (LPCSs) made of electrically non-conductive fibers and carbon nanotube networks. This technique exploits the piezoresistive effect of multiwalled carbon nanotubes (MWCNT) in epoxy resin. The electrically conductive epoxy resin was used to prepare composite plates containing electrically non-conductive fibers such glass and Kevlar fibers. The plates were marked with grid points where electrically conductive silver-epoxy paste was deposited. The electrical resistances between the grid points were measured and used as a reference set. Two new concepts are introduced. One is uniformity of MWCNT distribution which gives rise to uniformity in electrical conductivity. The second is maximum sensitivity to change in electrical resistance due to the damage occurrence. These issues are demonstrated as criteria to determine the optimal quantity of MWCNT. This optimal quantity is used to assure damage detectability at any region in the large plates. Drilled holes and impact testing were conducted to simulate damage. The damage increases the electrical resistance between the contact points surrounding the damages. This increase is used to detect, locate and quantify the damage.

3.1 Experimental Methods

3.1.1 Materials

MWCNT purchased from Bayer Material Science (described in Chapter 2), and plain weave glass fabrics and Kevlar fabrics purchased from HL. plasto company were used as fillers and reinforcements respectively. Epon 862 and EPIKURE W were purchased from Miller-Stephenson chemical company.

3.1.2 Methods

3.1.2.1 Fabrication of composite plates

To fabricate electrically non-conductive fabric/epoxy/MWCNT composite plates, the epoxy resin and curing agent (26.4 wt%) were first mixed. Then various weight percentages (wt%) of MWCNT comprising 0.10, 0.20, 0.25, 0.30, 0.40 and 1.00wt% were added into the epoxy matrix. The mixture was processed on a three roll milling (EXAKT 80E, EXAKT Technologies Inc.) to disperse the MWCNT within the epoxy matrix. The modified epoxy matrix was heated up to 60^0C for 20 min in a vacuum oven to remove air bubbles. The modified epoxy matrix was dispersed between three layers of glass fabrics and six layers of kevlar fabrics to manufacture glass fabric/epoxy/MWCNT plates and Kevlar fabric/epoxy/MWCNT plates respectively by hand lay-up method. The plates were cured using an autoclave.

3.1.2.2 Dynamic viscosity measurements

Dynamic viscosity measurement is performed to determine the state of liquidity of the epoxy resin with and without MWCNT to make large polymer composite structures. The dynamic viscosity of the epoxy matrix unfilled and filled with 0.3wt% MWCNT at 25^0C and 60^0C were measured using a Viscometer (Brookfield, CAP 2000) as shown in Figure 3.1.

Figure 3.1: Viscometer for measuring dynamic viscosity

3.1.2.3 Plate specification and arrangement of electrical connections

To apply connections for electrical resistance measurement (ERM), a grid of forty conductive electrical contact points made from silver-epoxy paste spaced 3 inch apart was mounted on the surface of the 22×13 inch^2 plates. Electrical wires were attached to the contact points to make electrodes. Then the electrodes were connected to the data acquisition system (Vishay Micro-Measurements System 7000) for recording the signals.

The computer algorithm was written for real-time determination of detection, location and severity of damage in composite structures. The flowchart of the proposed technique and computer program are presented in Appendix A. Figure 3.2 shows a representation of the grid points made by conductive silver paste mounted on the surface of the 22×13 inch^2 plate. Each point serves as an electrical contact point. The spacing between the grid points is very important. If the spacing between the grid points is too large, the change in the resistance between the two grid points may not reflect the occurrence of damage that has occurred in the vicinity. If the spacing between the grid points is too small, there would require a huge number of grid points for structure of a certain size. Too many grid points render the technique impractical. The 3 inch spacing between the grid points was found to be more sensitive in electrical resistance change for detection and location of damage. For the rectangular grid array as shown in Figure 3.2, examples of electrical resistances between adjacent pair of grid points corresponding to the first cell are $R_{1,2}$, $R_{1,6}$, $R_{2,7}$, $R_{6,7}$ where R stands for electrical resistance between two points represented by the subscripts. The subscript numbers, separated by a space represent the associated grid points.

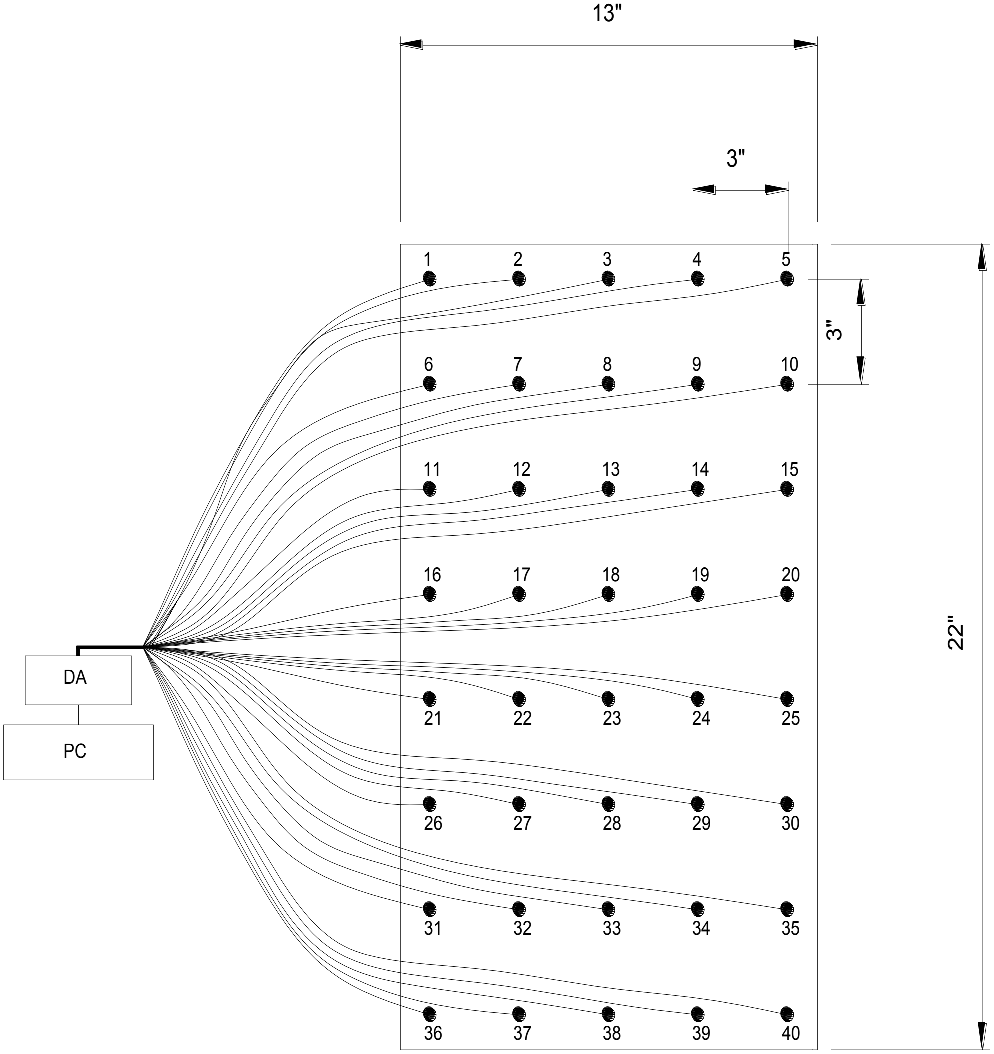

Figure 3.2: Schematic illustration of instrumented plate showing wires attached to the grid points connected to data acquisition (DA) system and computer with program

3.1.3 Electrical resistance measurements

The ERM was carried out by the two-probe method using a high resistance meter (Agilent 4339B), a multimeter (Agilent 34401A) and a data acquisition system. A constant source voltage was directly applied and the electrical current was measured to calculate resistance. Electrical resistance change (ERC) is calculated based on Eq. (2. 6)

3.2 Drilled holes and impact tests

Two types of damage were produced in the glass fabric/epoxy/MWCNT plates and the kevlar fabric/epoxy/MWCNT plates. The first type was performed by drilling holes of different sizes at different locations in the plates. The second type was carried out by impact caused by collision with high velocity projectiles and from drop weight on the plates. The high velocity projectile impact tests were done using a gas gun with an impact energy of 78J created by 318 mg aluminum particle travelling at 700 m/sec. The experimental set-up to detect and locate damage due to the high velocity impact test is shown in Figure 3.3. The low velocity impact tests were carried out by dropping weights on the clamped plates placed on electrically non-conductive rigid supports.

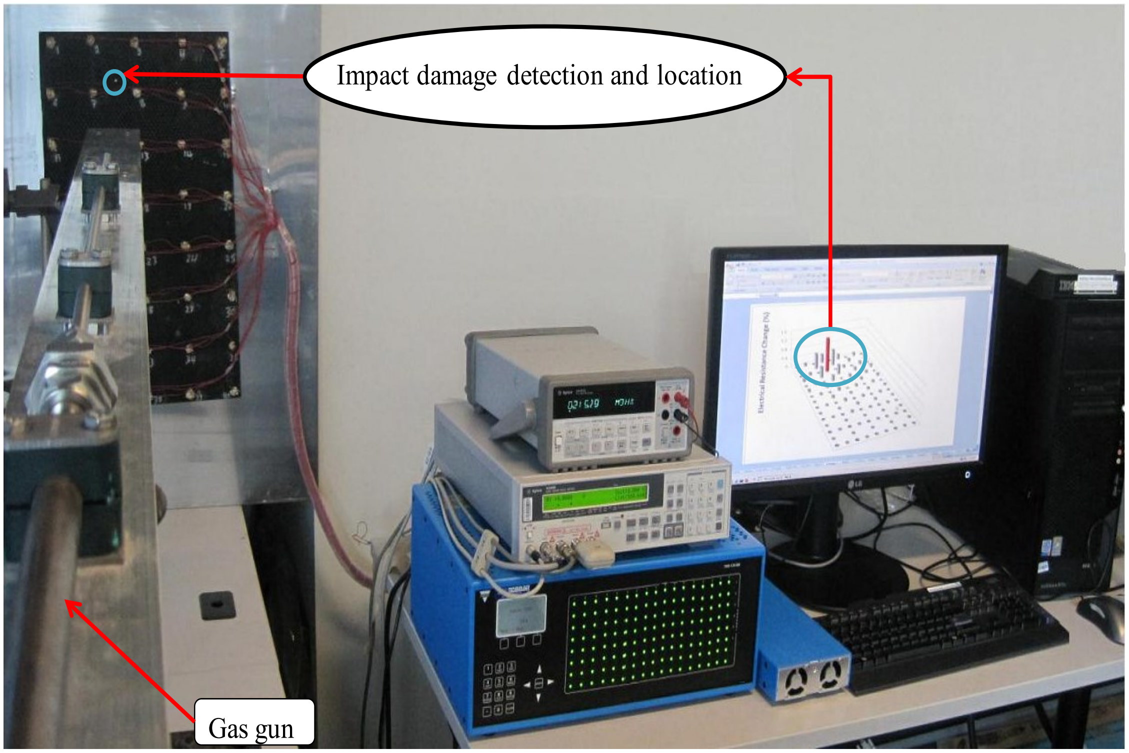

Figure 3.3: Experimental set-up to detect and locate damage due to high velocity impact test

The specifications of the large plates and experimental conditions are presented in Table 3.1.

Table 3.1: Specifications and experimental conditions of large plates

Number of Plates	**Materials**	**Plate Size (inch^2)**	**MWCNT wt%**	**A Grid of points spaced 3 inch apart**	**Damage types**
Plate 1	Glass fiber/epoxy/MWCNT composites	22×13	0.10	40	-
Plate 2	Glass fiber/epoxy/MWCNT composites	22×13	0.20	40	-
Plate 3	Glass fiber/epoxy/MWCNT composites	22×13	0.25	40	-
Plate 4	Glass fiber/epoxy/MWCNT composites	22×13	0.30	40	Drilled hole
Plate 5	Glass fiber/epoxy/MWCNT composites	22×13	0.40	40	Drilled hole
Plate 6	Glass fiber/epoxy/MWCNT composites	22×13	1.00	40	Drilled hole
Plate 7	Glass fiber/epoxy/MWCNT composites	22×13	0.30	40	Impacted
Plate 8	Glass fiber/epoxy/MWCNT composites	22×13	0.30	40	Impacted
Plate 9	Kevlar fiber/epoxy/MWCNT composites	22×13	0.30	40	Drilled holes
Plate 10	Kevlar fiber/epoxy/MWCNT composites	22×13	0.30	40	Impacted
Plate 11	Kevlar fiber/epoxy/MWCNT composites	22×13	0.30	40	Impacted

3.3 Results and discussion

3.3.1 Glass fabric /epoxy/ MWCNT composite plates

3.3.1.1 Uniformity of MWCNT distribution in large composite plates

The electrical resistances between adjacent electrodes for the plates 1 , 2, 3, 4, 5 and 6 containing 0.10, 0.20, 0.25, 0.30, 0.40 and 1.00wt% of MWCNT were measured. Plate 1 containing 0.10wt% MWCNT does not behave as a conductive material but more like an insulator (Table 3.2). This reveals that too small a quantity of MWCNT will not provide a good electrical conductivity, even though this may be more than the percolation threshold found for small samples [75]. This does not provide stability of the results for the plate.

Table 3.2: Comparing electrical resistance, uniformity of MWCNT distribution and sensitivity to resistance change for plates containing different MWCNT concentrations

MWCNT Concentrations (wt%)	0.10	0.20	0.25	0.30	0.40	1.00
Average electrical resistance (AER) (Ohms)	▨	0.95×10^{12}	24.4×10^{6}	276.6×10^{3}	64.8×10^{3}	2.5×10^{3}
Standard Deviation (SD) (Ohms)	▨	→ 2.35×10^{12}	32×10^{6}	79.67×10^{3}	18.1×10^{3}	0.44×10^{3}
Coefficient of variation(%) = (SD/AER)×100	▨	247.4 →	131.1	28.8	27.9	17.6
Sensitivity to ERC (%)due to hole (1/4") drilled	▨	▨	▨	4.8	1.9	0.38 ←

Light transmission images of plates 1, 2, 3, 4, 5 and 6 containing 0.10, 0.20, 0.25, 0.30, 0.40 and 1.00wt% of MWCNT respectively are shown in Figures 3.4, 3.5a to 3.8a. By comparing Figures 3.4 and 3.5a to 3.8a, it is observed that the dispersed MWCNT in large plates 1, 2, 3, 4 are becoming more uniform while the matrix-rich regions and glass fibers (transparent regions) are reduced as MWCNT concentrations increases. Figures 3.5b to 3.8b and 3.9a present the distribution of the electrical resistances between grid points in the plates 2, 3, 4, 5 and 6 containing 0.20, 0.25, 0.30, 0.40 and 1.00wt% of MWCNT respectively. The coefficient of variation in percent, as a measure of uniformity, calculated for different plates (Table 3.2) shows that the uniformity of MWCNT distribution increases as the MWCNT concentration increases. Observing Figures 3.5b and 3.6b, the distribution of the electrical resistance between the grid points is not uniform over the surface of plates 2 and 3 containing 0.20wt% MWCNT and 0.25wt% MWCNT. This indicates that a quantity of MWCNT of just more than percolation threshold for a small sample (the percolation threshold of the MWCNT in epoxy was determined experimentally to be 0.1883wt% [75]) will tend to give spatial non-uniformity in the electrical conductivity over the surface of the plates. Non-uniform distribution does not provide good results. For these plates, there are regions of high conductivity and regions of low conductivity, the electric current will follow along the path of high conductivity and avoid the path of low conductivity. When there is a defect in the region of low conductivity, the technique cannot sense it due to the lack of current flow. In other words, larger samples give rise to non-uniformity in the MWCNT distribution. This non-uniformity produces noise that blurs the detection and location of damage.

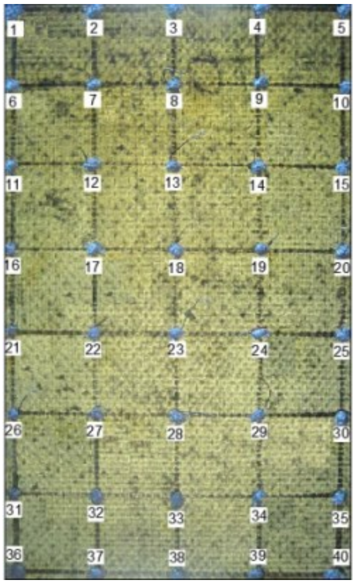

Figure 3.4: Light transmission image of glass fiber/epoxy/0.10wt% MWCNT plate 1 mounted with 40 contact points on its surface showing transparent (glass fibers and resin) regions as compared to dark (dispersed MWCNTs) regions

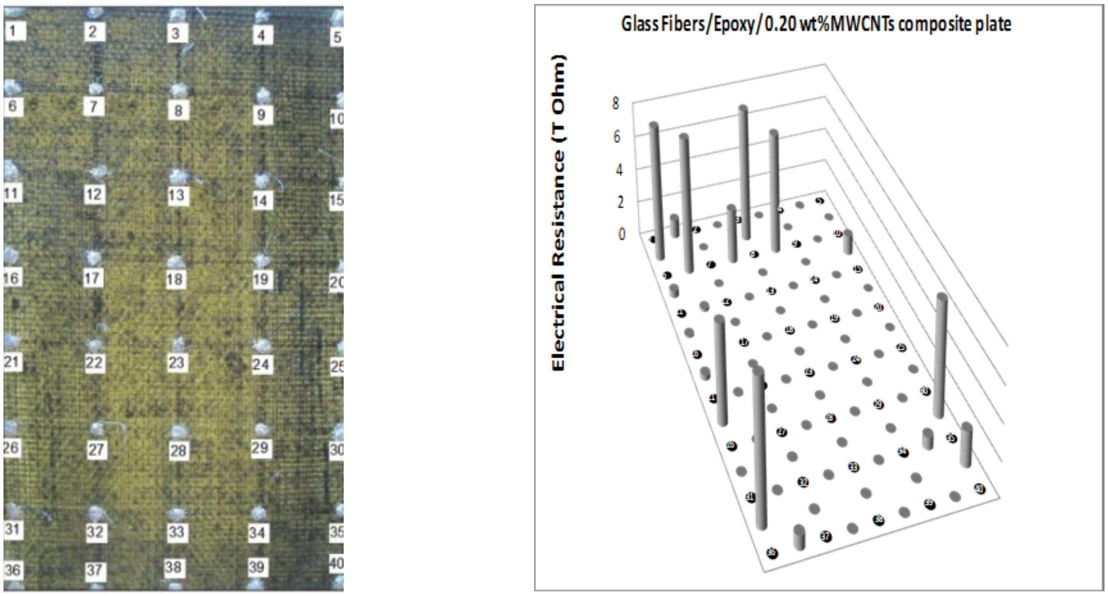

a) **b)**

Figure 3.5: a) Light transmission image of glass fiber/epoxy/0.20wt% MWCNT plate 2 showing transparent (glass fibers and resin) regions as compared to dark (dispersed MWCNTs) regions b) Distribution of electrical resistance

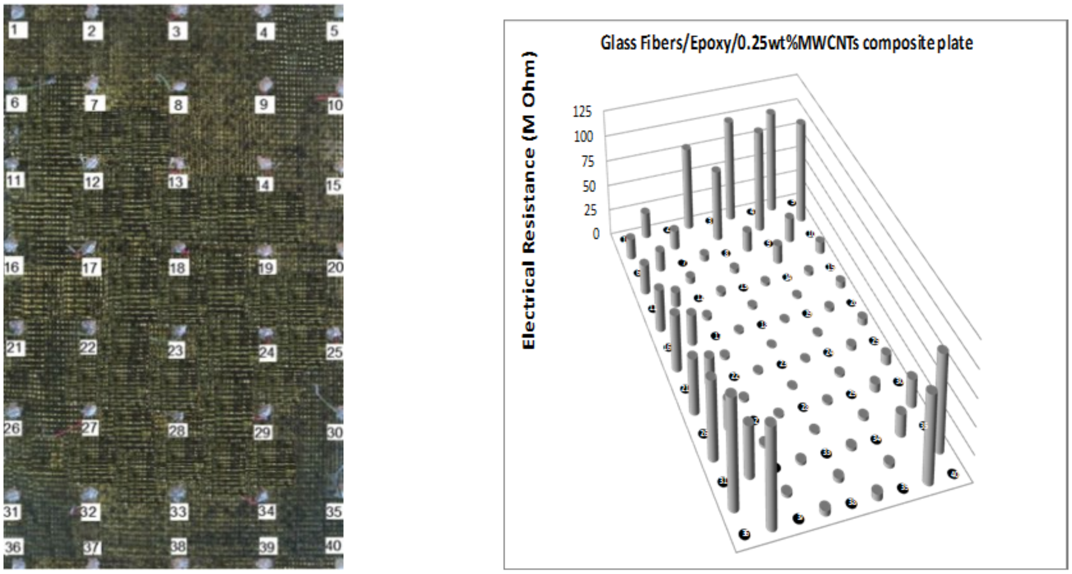

a) b)

Figure 3.6: a) Light transmission image of glass fiber/epoxy/0.25wt% MWCNT plate 3 showing transparent (glass fibers and resin) regions as compared to dark (dispersed MWCNTs) regions b) Distribution of electrical resistance

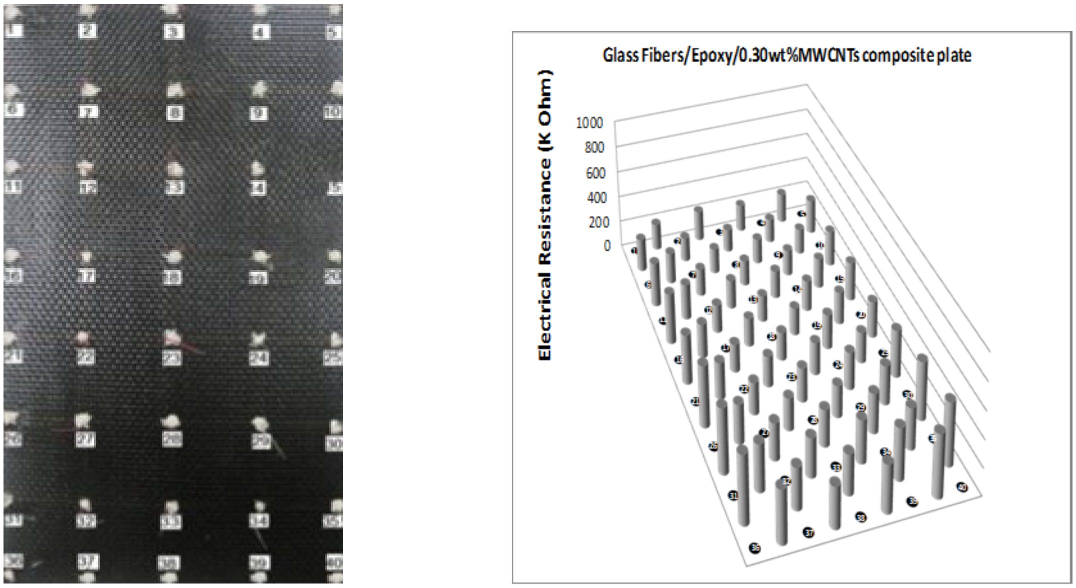

a) b)

Figure 3.7: a) Light transmission image of glass fiber/epoxy /0.30wt% MWCNT plate 4 showing dark (dispersed MWCNTs) regions b) Distribution of resistance

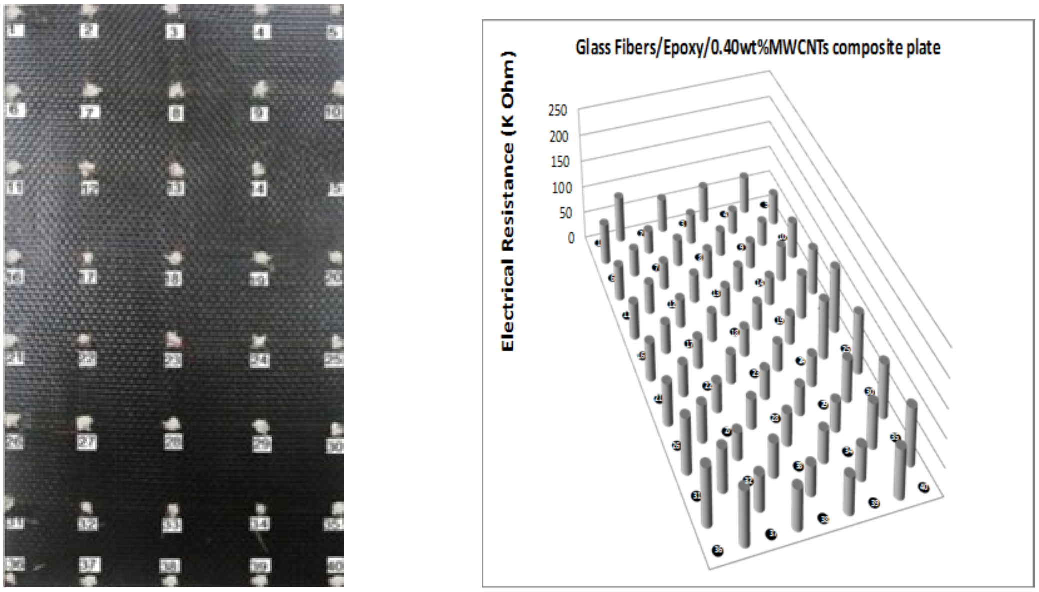

a) b)

Figure 3.8: a) Light transmission image of glass fiber/epoxy/0.40wt% MWCNT plate 5 showing dark (dispersed MWCNTs) regions b) Distribution of resistance

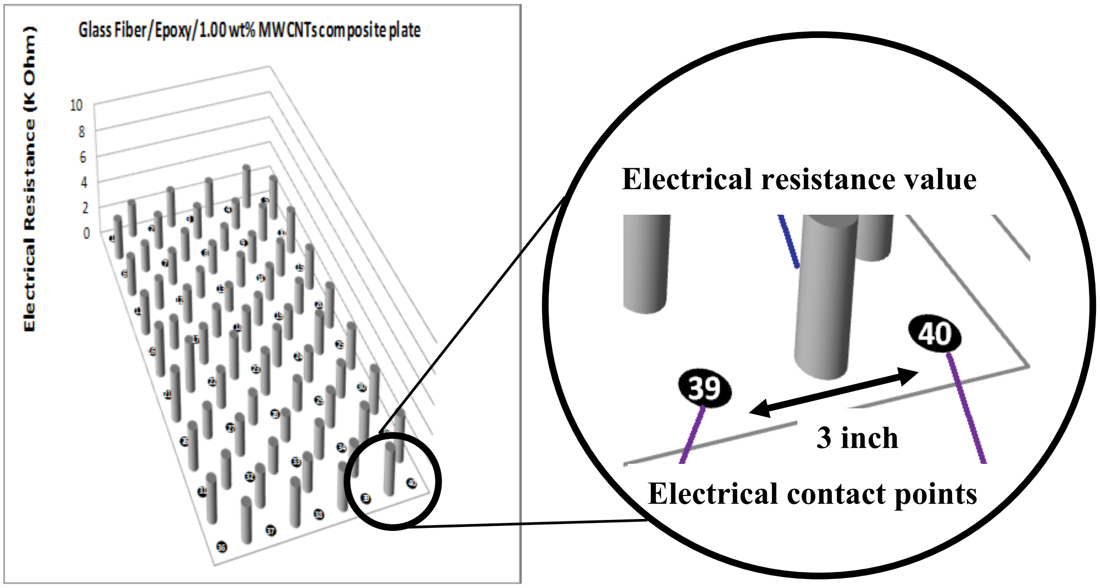

a) b)

Figure 3.9: a) Distribution of electrical resistance for glass fiber/epoxy composite plate 6 containing 1.00wt% MWCNT b) Close up view of electrical contact points

It has become clear that the issue of uniformity of CNT distribution is very important for detecting, locating and quantifying damage in large structures. This issue is found by the measurement of electrical resistance distribution. For further investigation, optical images are taken to study this phenomenon.

3.3.1.1.1 Non-uniformity due to re-agglomeration of MWCNTs during curing

Light transmission optical micrographs at low magnification (4x) are used to cover a large area. This allows the observation of the gradual formation of a complex MWCNT networks and the global uniformity of MWCNT distribution in epoxy samples containing MWCNT. The liquid epoxy resins containing 0.10, 0.20, 0.25, 0.30, 0.40 and 1.00wt% of MWCNT before subjecting them to a curing temperature were assessed under an optical microscope. Observing Figures 3.10a to 3.15a, it is clear that the uniform dispersion of MWCNT in epoxy is seen right after using three roll milling for all uncured samples. Figures 3.10b to 3.15b show images of cured samples. By comparing optical images of uncured and cured samples, reagglomeration of MWCNTs in epoxy is observed. Figures 3.10b to 3.15b show the state of MWCNTs dispersion in epoxy for all cured samples that exhibit the changes with MWCNT concentrations. It is found that the uniformity of MWCNT (above the percolation threshold) in cured samples increases as the MWCNT concentration increases. The dispersed MWCNTs were agglomerated due to the curing at elevated temperature while the matrix-rich regions (transparent regions) were shown to be less pronounced as MWCNT concentrations increases. As a consequence, MWCNTs reagglomeration is found in cured samples.

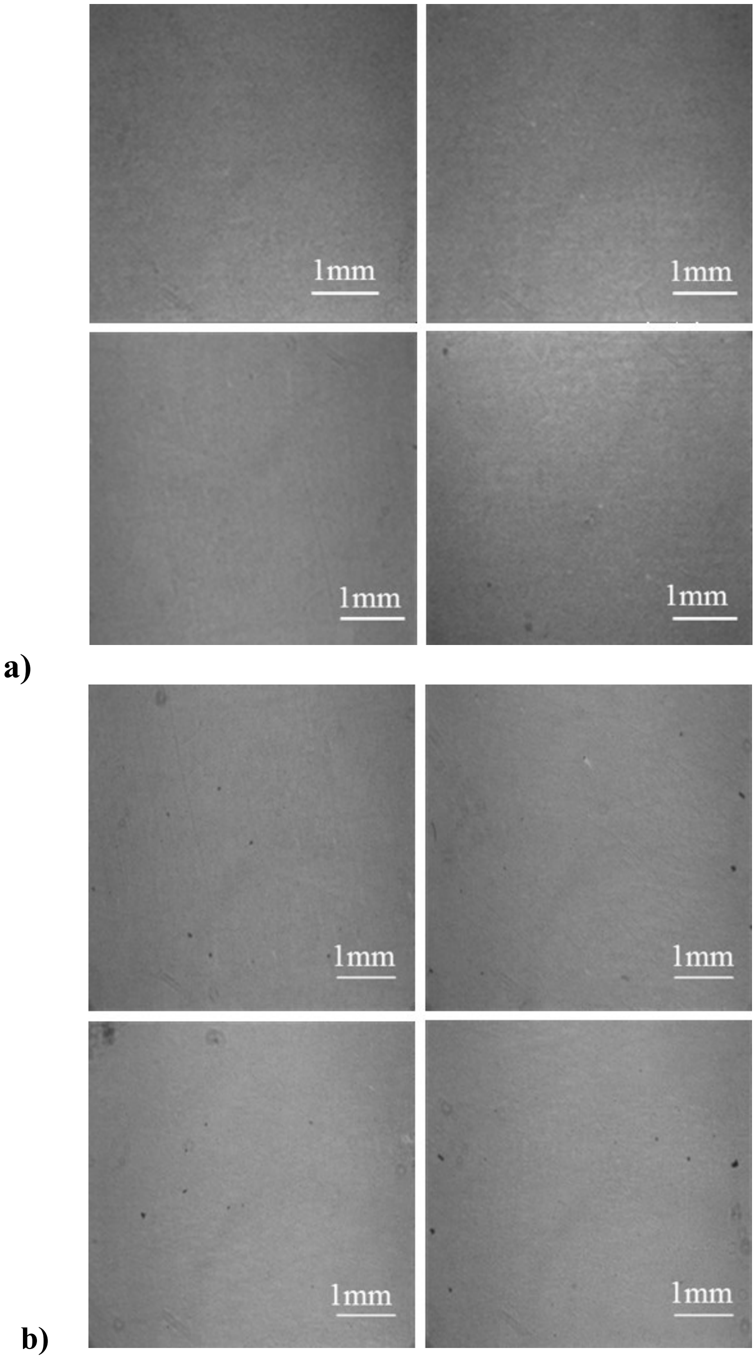

Figure 3.10: Light transmission optical micrographs of an epoxy composite containing 0.1wt% MWCNT with magnification (4x) a) Liquid uncured sample b) Cured sample. Reagglomeration of MWCNTs is observed by comparing uncured sample with cured sample

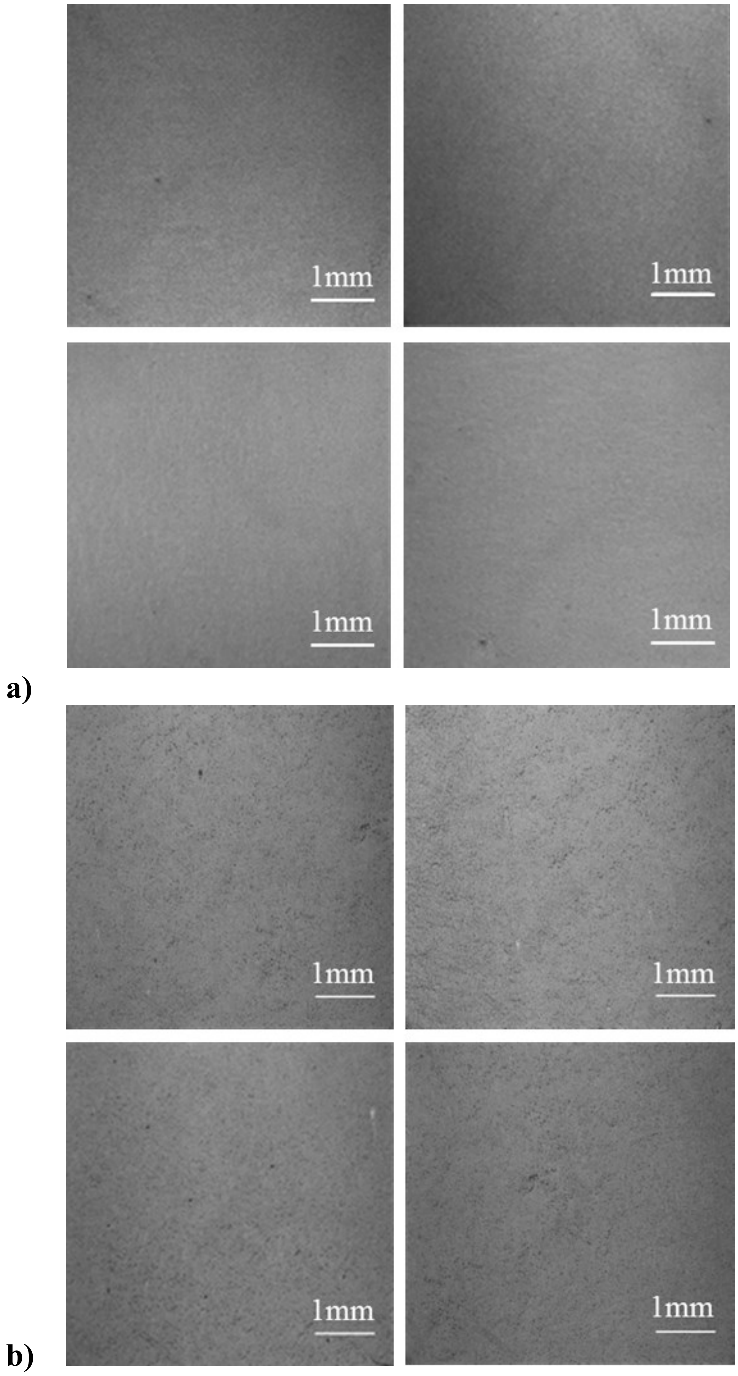

Figure 3.11: Light transmission optical micrographs of an epoxy composite containing 0.2wt% MWCNT with magnification (4x) a) Liquid uncured sample b) Cured sample. Reagglomeration of MWCNTs is observed by comparing uncured sample with cured sample

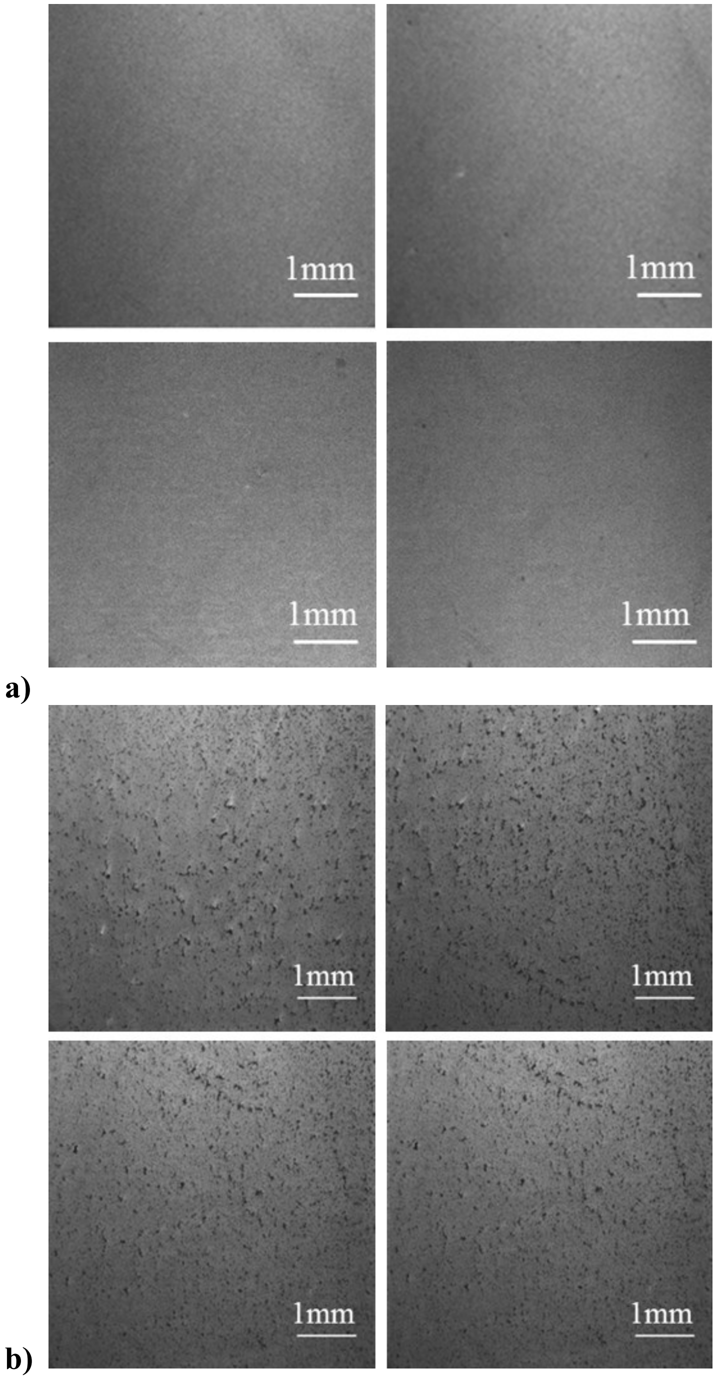

Figure 3.12: Light transmission optical micrographs of an epoxy composite containing 0.25wt% MWCNT with magnification (4x) a) Liquid uncured sample b) Cured sample. Reagglomeration of MWCNTs is observed by comparing uncured sample with cured sample

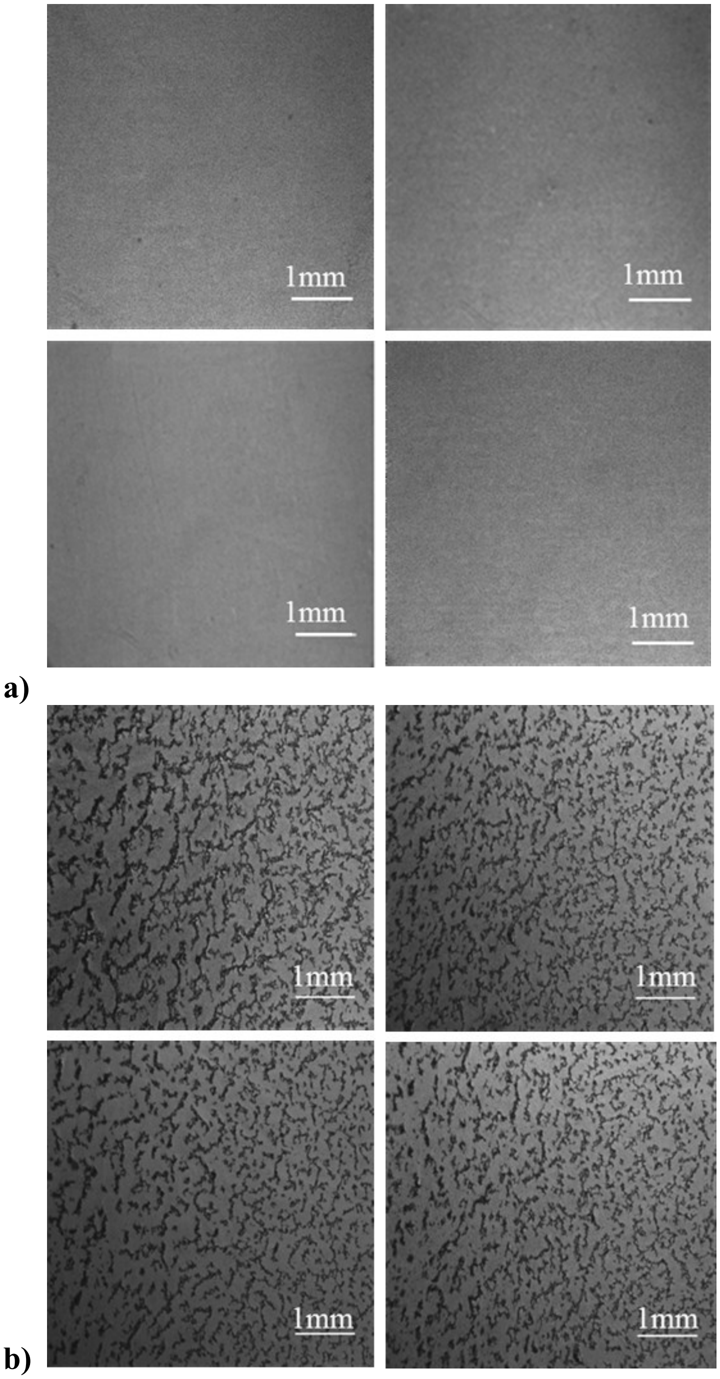

Figure 3.13: Light transmission optical micrographs of an epoxy composite containing 0.3wt% MWCNT with magnification (4x) a) Liquid uncured sample b) Cured sample. Reagglomeration of MWCNTs is observed by comparing uncured sample with cured sample

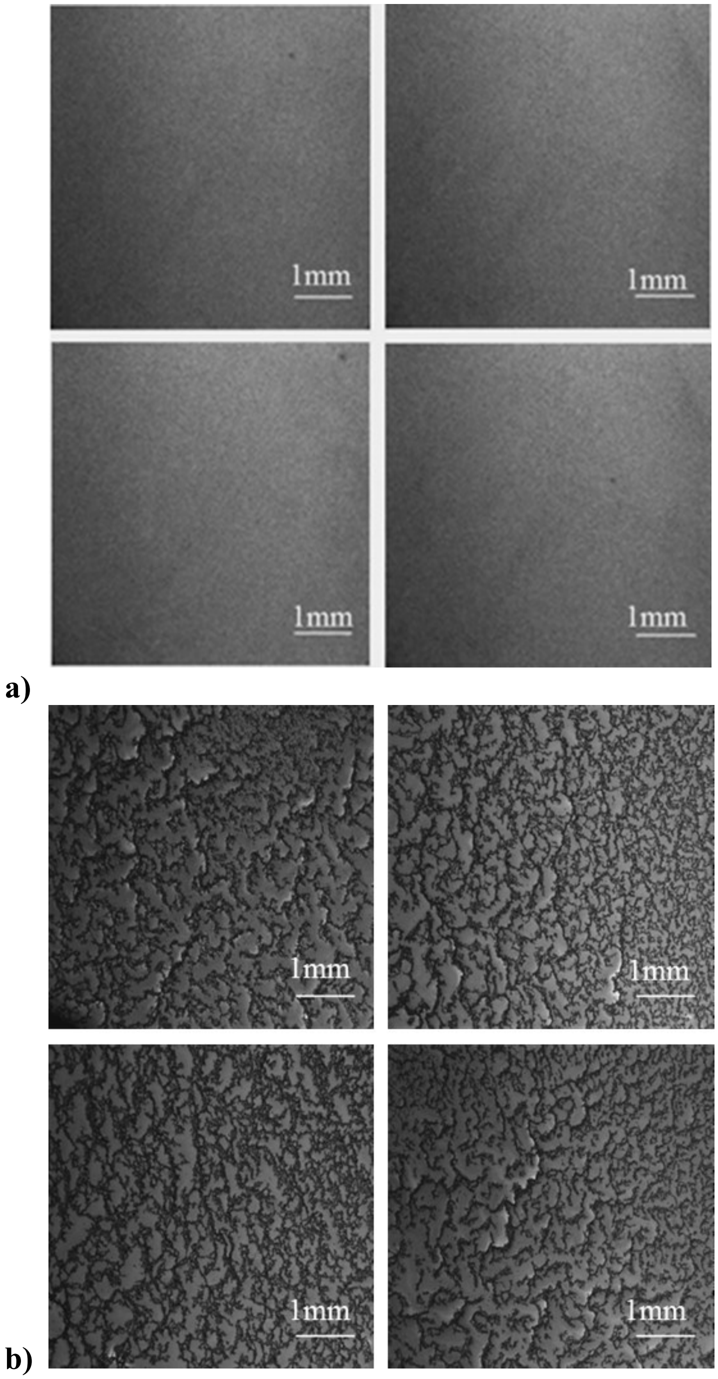

Figure 3.14: Light transmission optical micrographs of an epoxy composite containing 0.4wt% MWCNT with magnification (4x) a) Liquid uncured sample b) Cured sample. Reagglomeration of MWCNTs is observed by comparing uncured sample with cured sample

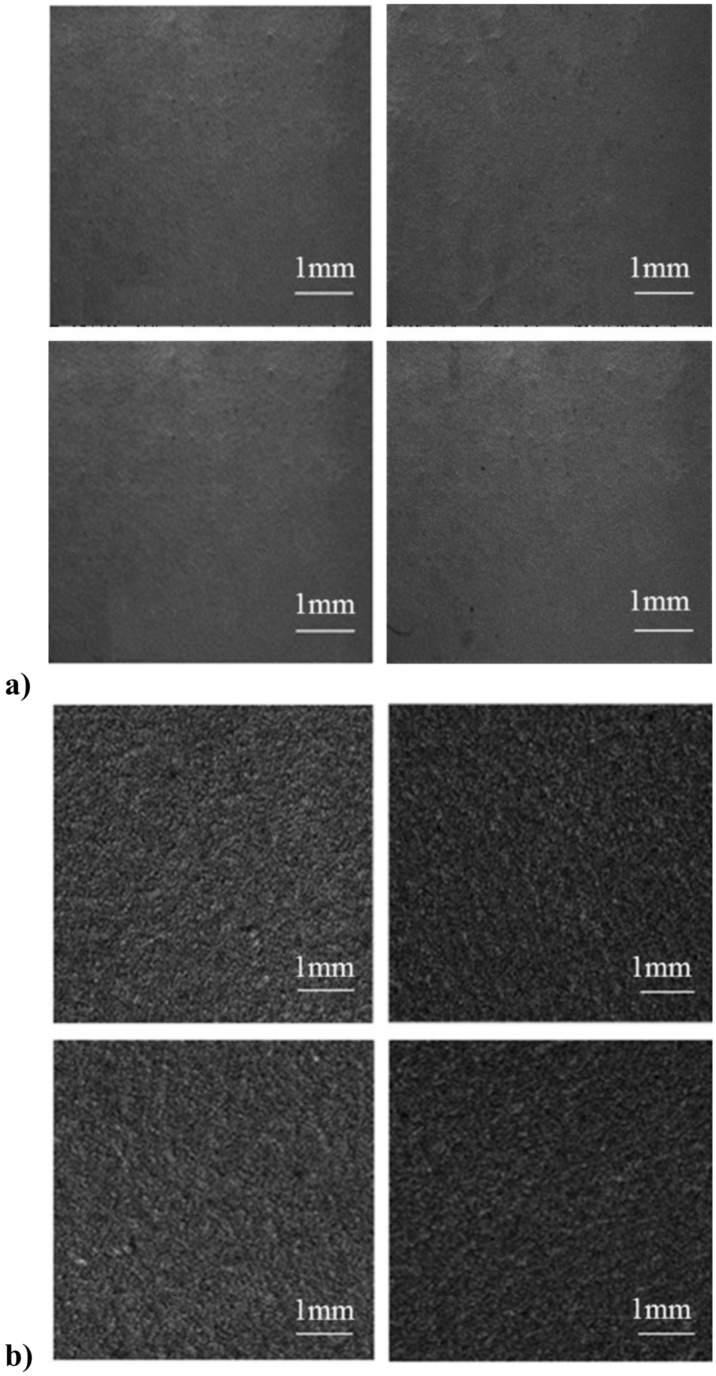

Figure 3.15: Light transmission optical micrographs of an epoxy composite containing 1wt% MWCNT with magnification (4x) a) Liquid uncured sample b) Cured sample. Reagglomeration of MWCNTs is observed by comparing uncured sample with cured sample

When using elevated temperatures for curing, initially the viscosity of the resin is significantly reduced. This reduction in viscosity causes MWCNTs reagglomeration due to their tendency to attract each other by van der Waals forces to form larger clusters [75]. The new concept of uniformity of distribution of MWCNT in large plates was found by measuring electrical resistance distribution. From experimental results for distribution of electrical resistivity presented in Chapter 2, electrical resistance and optical images, it can be concluded that the uniformity of distribution of MWCNT in large plate increases as MWCNT concentrations increases.

3.3.1.2 Sensitivity to change in electrical resistance

To investigate plate sensitivity to change in electrical resistance, plates 4, 5 and 6 containing 0.30 wt%, 0.40 wt% and 1.00wt% of MWCNT were drilled. Table 3.2 shows that for plates containing a large enough quantity of MWCNT, sensitivity to the change in the electrical resistance decreases as the MWCNT concentration increases on the introduction of the same-sized hole (4/16) inch. It is observed from Table 3.2 that too small a quantity of MWCNT does not allow conductivity, even if uniformity is obtained. Also too large a quantity of MWCNT will allow conductivity as well as uniformity of MWCNT distribution but may not allow sensitivity to the change in the electrical resistance. As such, uniformity of electrical conductivity and maximum sensitivity to change in electrical resistance are two key practical issues. These two new issues did not exist for the case of small samples, while they are very important for the case of large samples. We propose criteria based on these issues for the determination of the optimal quantity of CNT that allows the detection, location and quantification of damages in the

LPCSs. We have found that 0.3wt% of MWCNT is the optimal quantity that can provide damage detectability at any region in the large plates. Putting it in terms of electrical resistance, the range of resistance is between 10^3 to 10^6 ohms.

From a practical point of view, it is desirable to have a low viscosity of modified epoxy to make the LPCS. This is because addition of a large quantity of CNT in the resin creates high viscosity which renders subsequent incorporation of continuous fibers difficult. Figures 3.16a and 3.16b indicate the dynamic viscosity of the epoxy matrix unfilled, and filled with 0.30 wt% MWCNT at 25^0C and 60^0C respectively. It is found from figures 3.16a and 3.16b that the dynamic viscosity remains low even after adding 0.30wt% MWCNT in the epoxy matrix which allows the modified epoxy to penetrate into the tows of fibers.

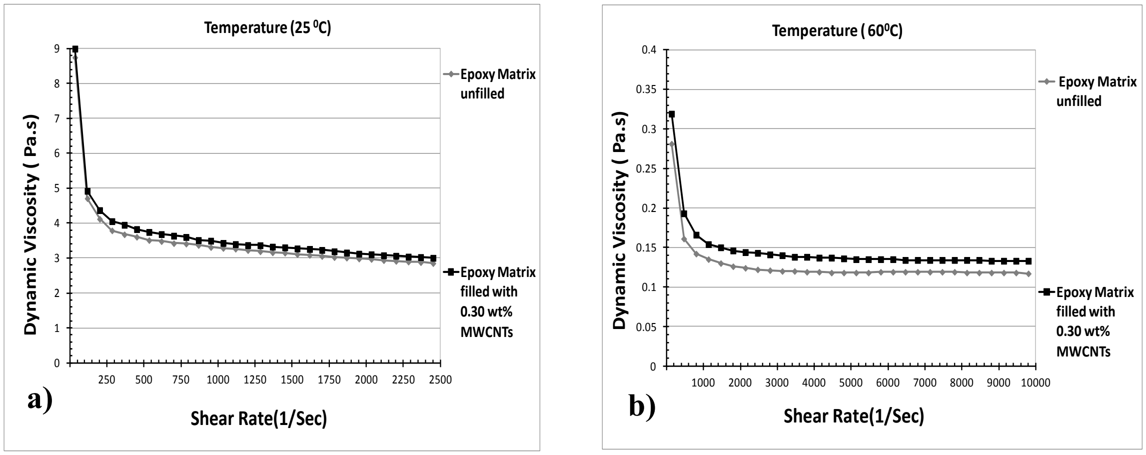

Figure 3.16: Dynamic viscosity-shear rate curves of epoxy matrix unfilled and filled with 0.30 wt% MWCNT at a) 25^0C and b) 60^0C

In addition to the experimental results presented in Chapter 2 to demonstrate the capabilities of the technique to detect, locate and quantify drilled holes of different sizes, two glass fabric/epoxy plates 7 and 8 with the dimensions of 22×13 inch^2 containing

0.30wt% MWCNT were impacted. Figures 3.17a and 3.17b show the locations and values of the changes in electrical resistance due to the collision with high velocity projectiles (78J each) in plate 7. By comparing Figures 3.17b and 3.17c, it is seen that impact damages 1 and 2 are detected and located according to the sharp local variations in distribution of the electrical resistance change.

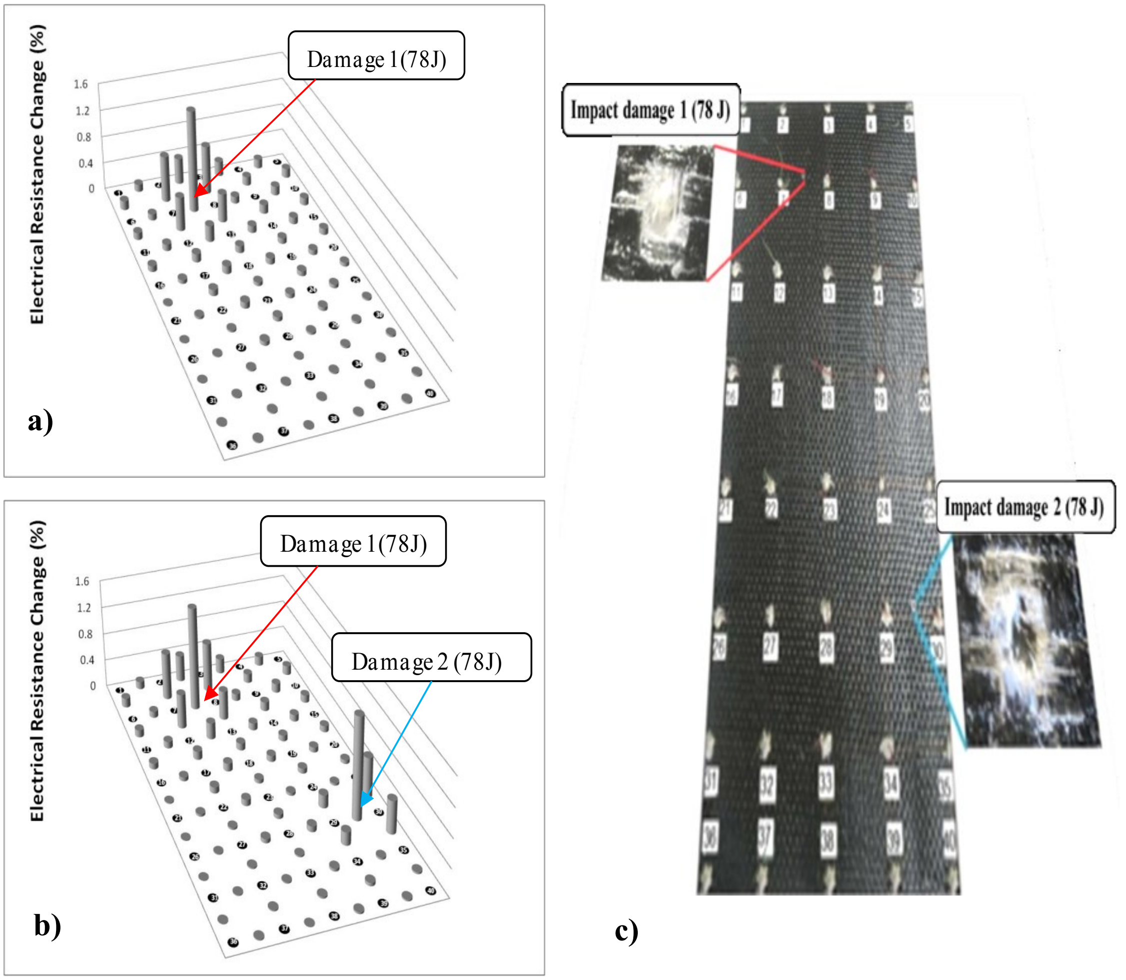

Figure 3.17: ERC distribution of glass/epoxy/MWCNT plate 7 after a) Impact damage 1 (78J) , b) Impact damages 1 and 2 (78J each) and c) Plate 7 after impact damages 1 and 2

Figures 3.18a to 3.18c display the locations and values of the changes in electrical resistance due to the collision with low velocity projectiles in plate 8. The energy levels vary from 1J to 10J as produced by drop weight impact tests.

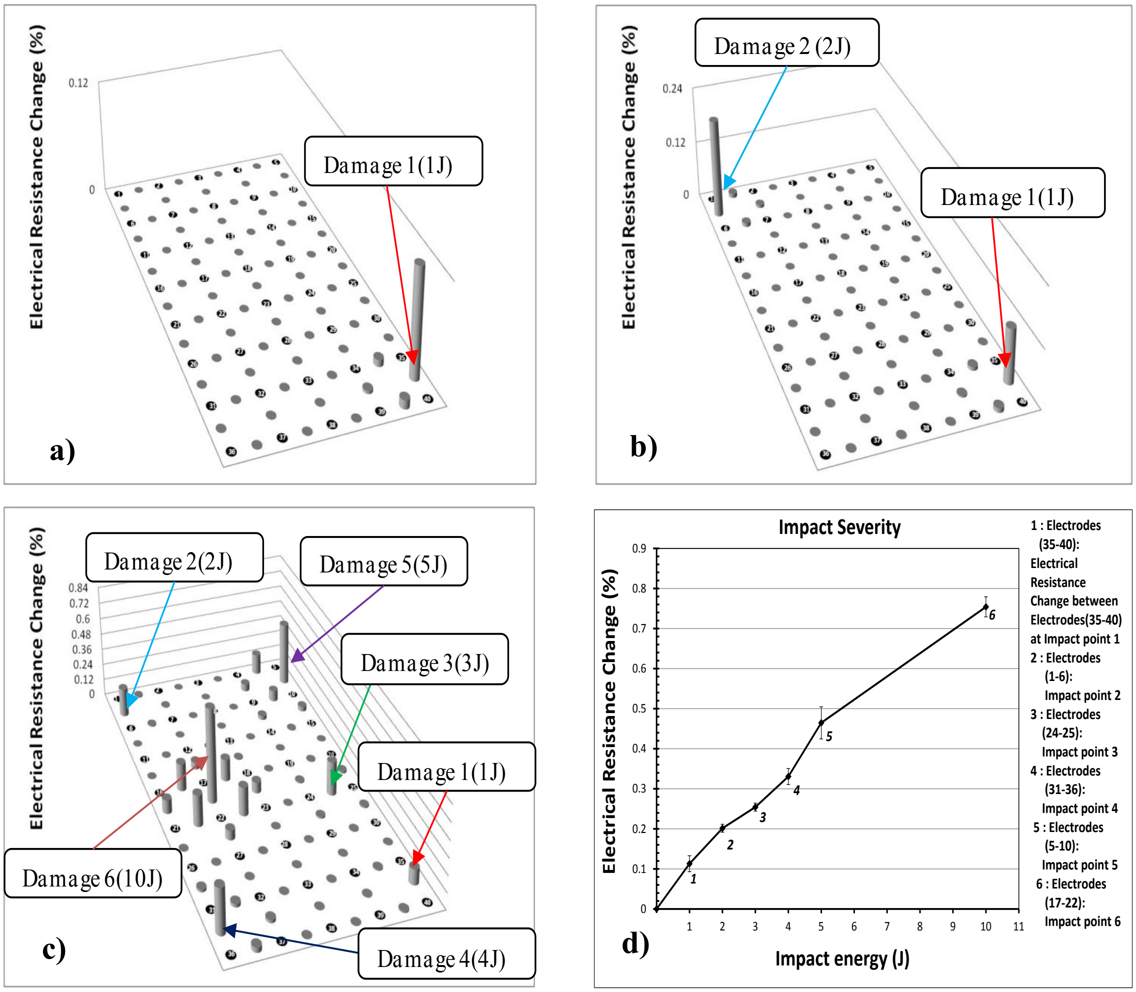

Figure 3.18: ERC distribution of glass/epoxy/MWCNT plate 8 after , a) BVI damage 1 (1J), b) BVI damages 1 and 2 (1J and 2J) , c) Impact damages 1, 2,3,4,5 and 6 (1J, 2J, 3J, 4J, 5J and 10J) and d) Effect of energy level on the change in electrical resistance (Data are presented as mean ± SD from three experiments)

Plate 8 impacted at six regions is schematically illustrated in Figure 3.19. Some of the damage at the lower energy levels (1J to 4J) is barely visible by the naked eye. These locations correspond exactly to the location of the damage created and barely visible damage zones. It is clear from figures 3.18c that the six impacts created with different energy levels at different locations in plate 8 are detected and located distinctly based on the significant local variations in distribution of the electrical resistance change. Figure 3.18d and Table 3.3 show the relation between the change in resistance and the energy level which indicates impact severity.

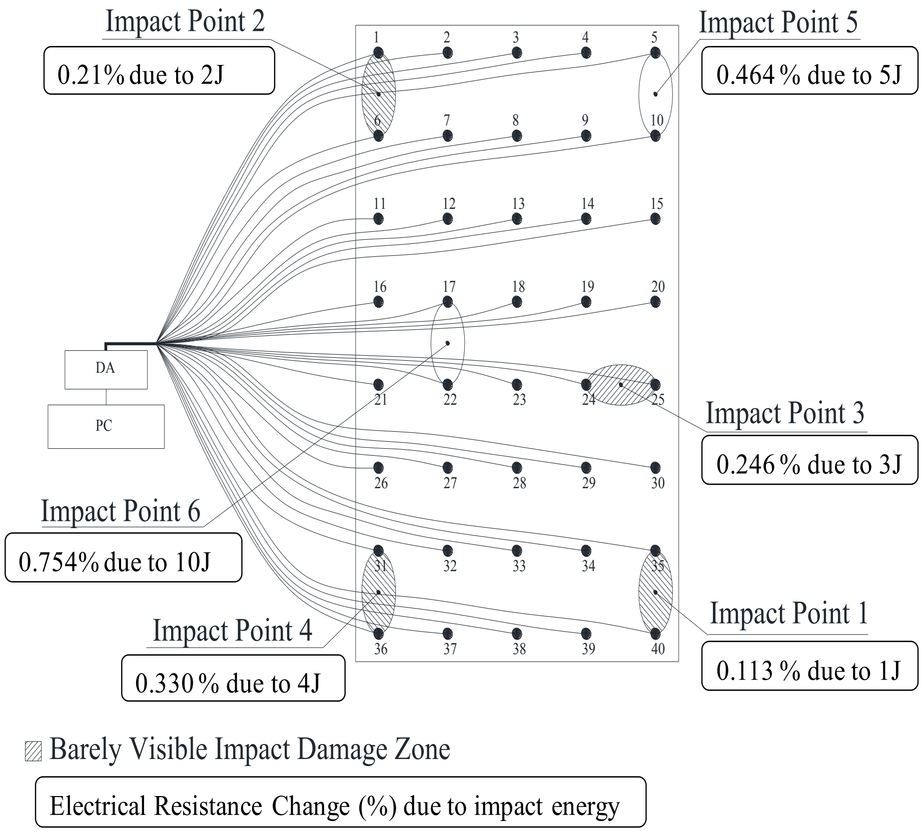

Figure 3.19: Schematic illustration of 22×13 inch^2 glass fiber/epoxy/0.30wt% MWCNT (plate 8) impacted at six regions using drop weights with impact energies of 1J, 2J, 3J, 4J, 5J and 10J respectively

Table 3.3: The importance of electrical resistance change (ERC) in relation to the severity of damage introduced by impact with different energy levels in plate 8

Impact energy levels	$R_{\text{Initial (Ohms)}}$	$R_{\text{Final (Ohms)}}$	ERC (%)
1J	370510	370930	0.113
2J	363220	363980	0.21
3J	354160	355030	0.246
4J	332750	333850	0.330
5J	293060	294420	0.464
10J	303520	305810	0.754

3.3.2 Kevlar fiber/epoxy/MWCNT composite plates

The new technique is demonstrated by showing examples for Kevlar fiber/epoxy composite plates. Three kevlar fiber/epoxy/0.30wt% MWCNT composite plates 9, 10 and 11 with 22×13 inch^2 were prepared. Plate 9 was drilled to make holes of sizes 1/16, 2/16, 3/16, 4/16, 5/16 and 6/16 inch respectively. The location and value of the change in resistance due to drilled hole 1 is shown in Figure 3.20a. It is seen from Figure 3.20b that holes 1 and 2 are detected and located distinctly based on the significant local variations in ERC distribution. Observing Figures 3.20c and 3.20d, it is found that holes of sizes 1/16, 2/16, 3/16, 4/16, 5/16 and 6/16 inch respectively drilled at different locations of plate 9 are detected and located distinctly according to the sharp local changes in distribution of the ERC. The effect of hole volume on the ERC is indicated in Figure 3.20e. A clear correlation is observed between the hole volume and the change in resistance. This reveals that the new technique is capable of quantifying the extent of damages.

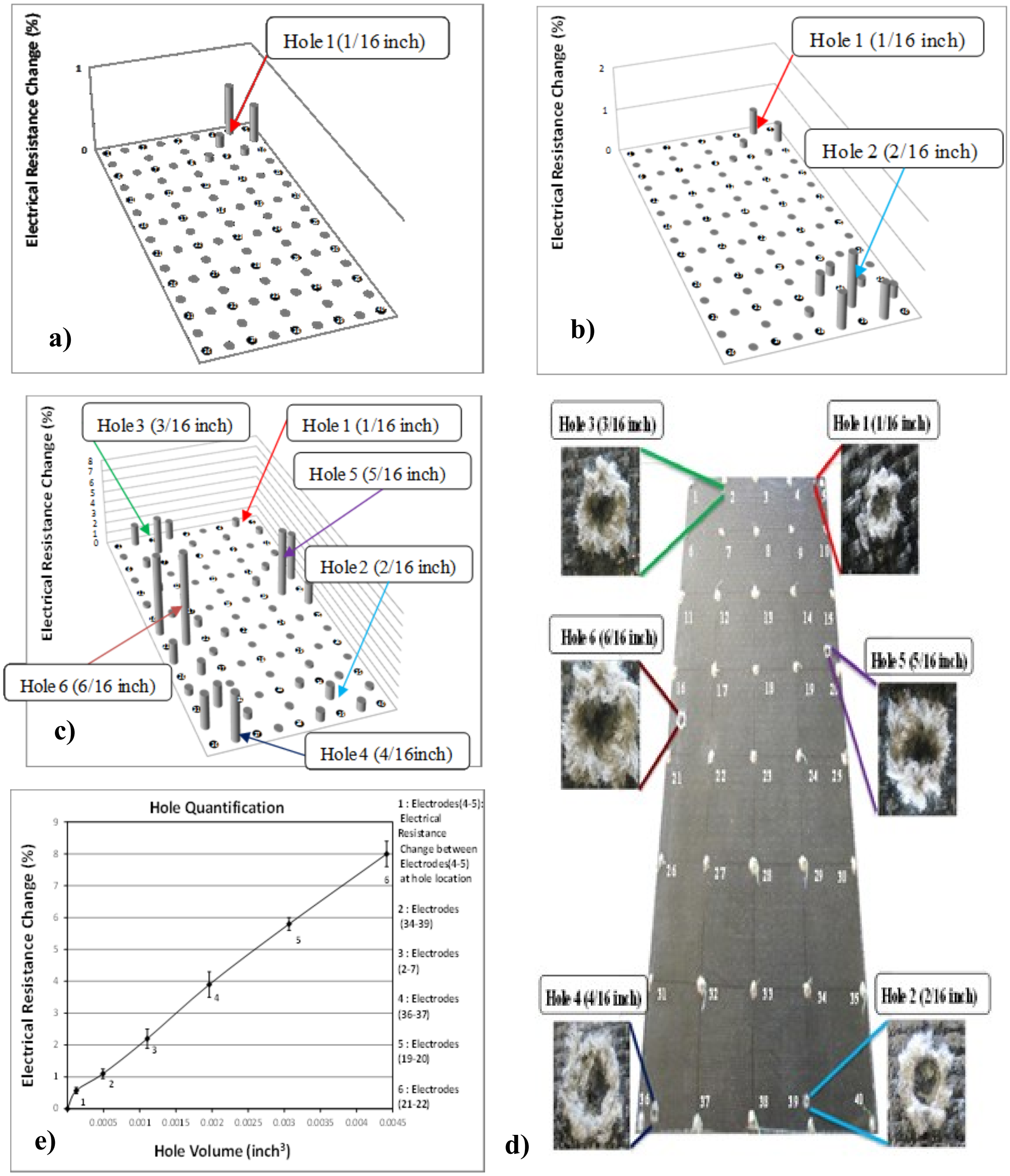

Figure 3.20: ERC distribution for Kevlar fiber/epoxy/0.3wt%MWCNT plate 9 after drilling of a) Hole1 (1/16 inch) b) Holes1 and 2 (1/16 and 2/16 inch), c) Holes1, 2, 3, 4, 5 and 6 (1/16, 2/16, 3/16, 4/16, 5/16 and 6/16 inch) d) Plate 9 after six drilled holes e) Effect of hole volume on the ERC (Data are presented as mean ± SD from three experiments)

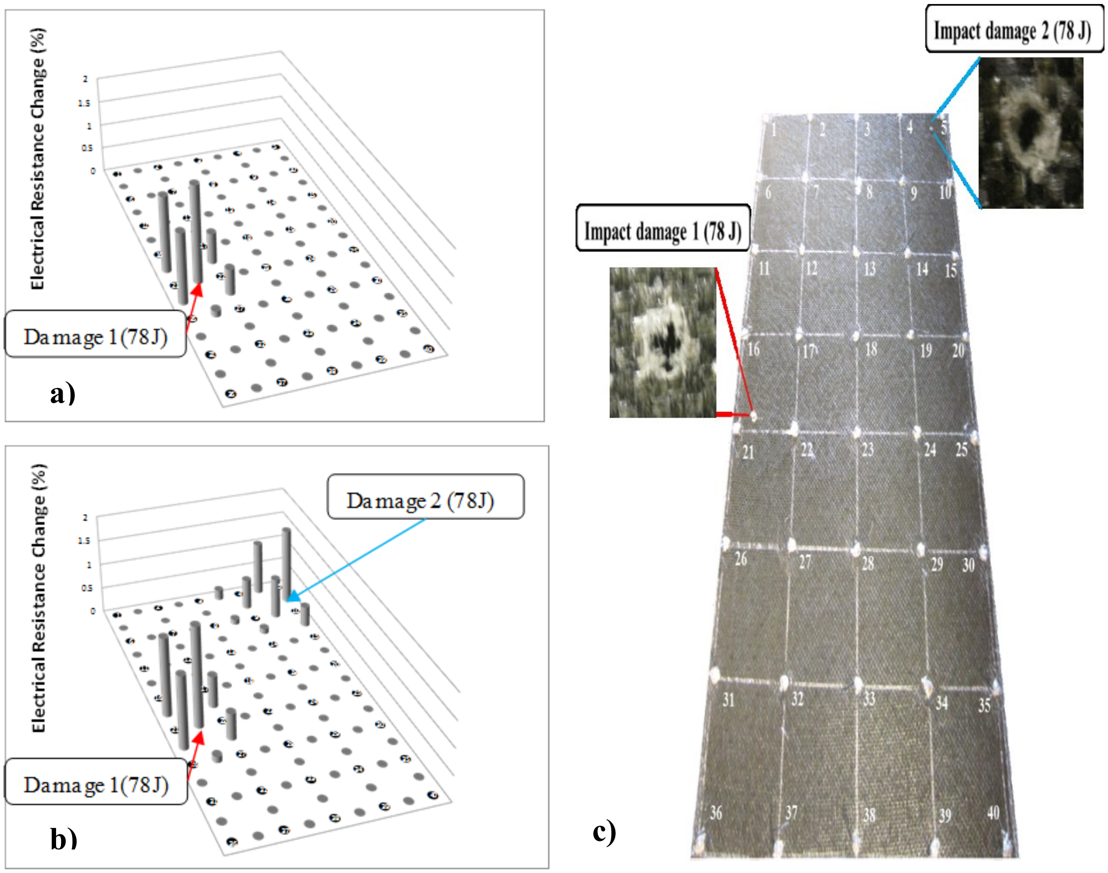

Figure 3.21: ERC distribution of kevlar fiber/epoxy/0.30wt% MWCNT plate 10 after a) Impact damage 1 (78J), b) Impact damages 1 and 2 (78J each) and c) Plate 10 after two impact damages 1 and 2

Figures 3.21a and 3.22b show the locations and values of the changes in electrical resistance due to the collision with high velocity projectiles (78J each) in plate 10. Comparing Figures 3.21b and 3.21c, good correspondence is observed between the locations of impact damages 1 and 2 and significant local variations in ERC distribution. Plate 11 is impacted at six different locations as shown in Figure 3.22. The locations and values of the changes in resistance due to low velocity impact tests in plate 11 are shown in Figures 3.23a to 3.23c. The different energy levels ranging from 1J to 10J were produced by drop weight impact tests. Some of the damages at the lower energy levels are barely visible impact damage (BVID) and cannot be detected by visual observation. As it can be seen in Figure 3.23d, the good relation is found between the change in electrical resistance and the energy level which reveals impact severity.

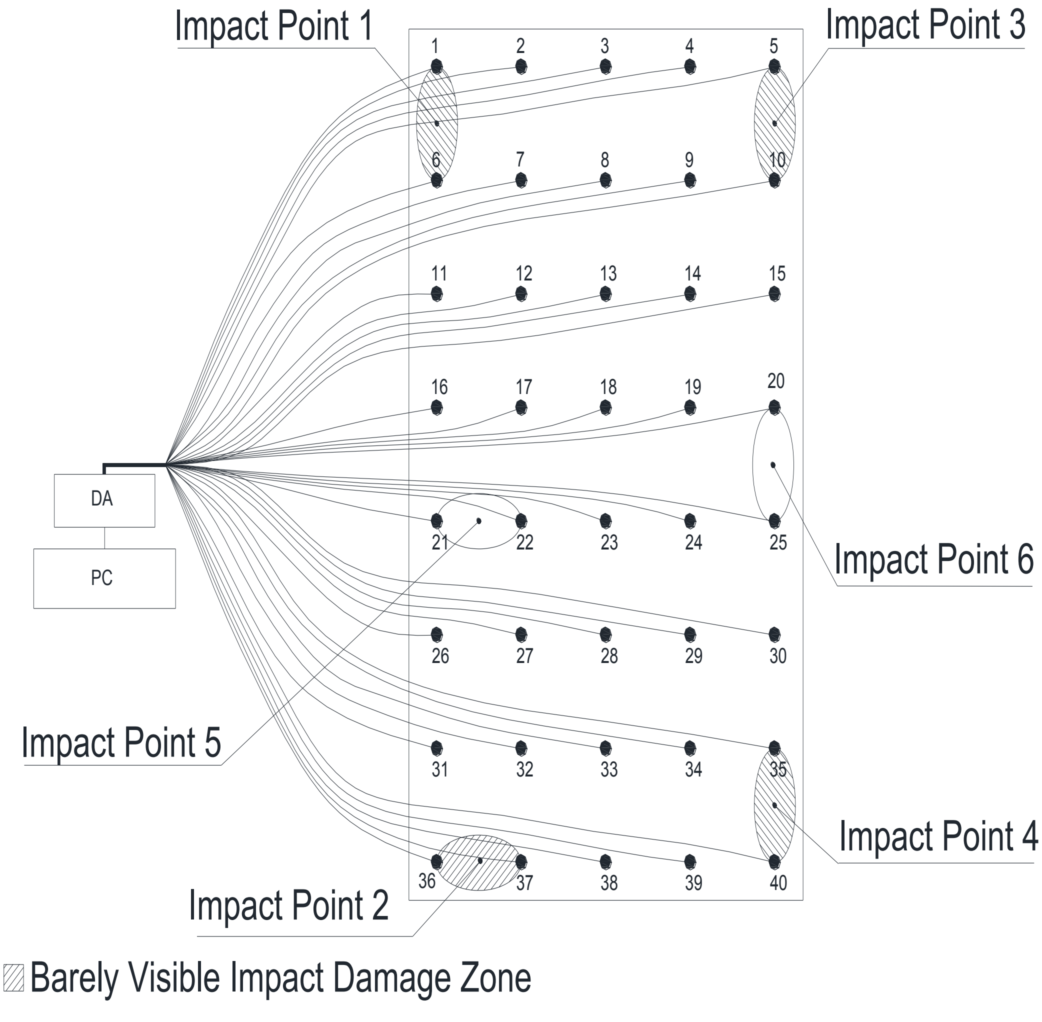

Figure 3.22: Schematic illustration of 22×13 inch^2 kevlar fiber/epoxy/0.30wt% MWCNT (plate 11) impacted at six regions using drop weights with impact energies of 1J, 2J, 3J, 4J, 5J and 10J respectively

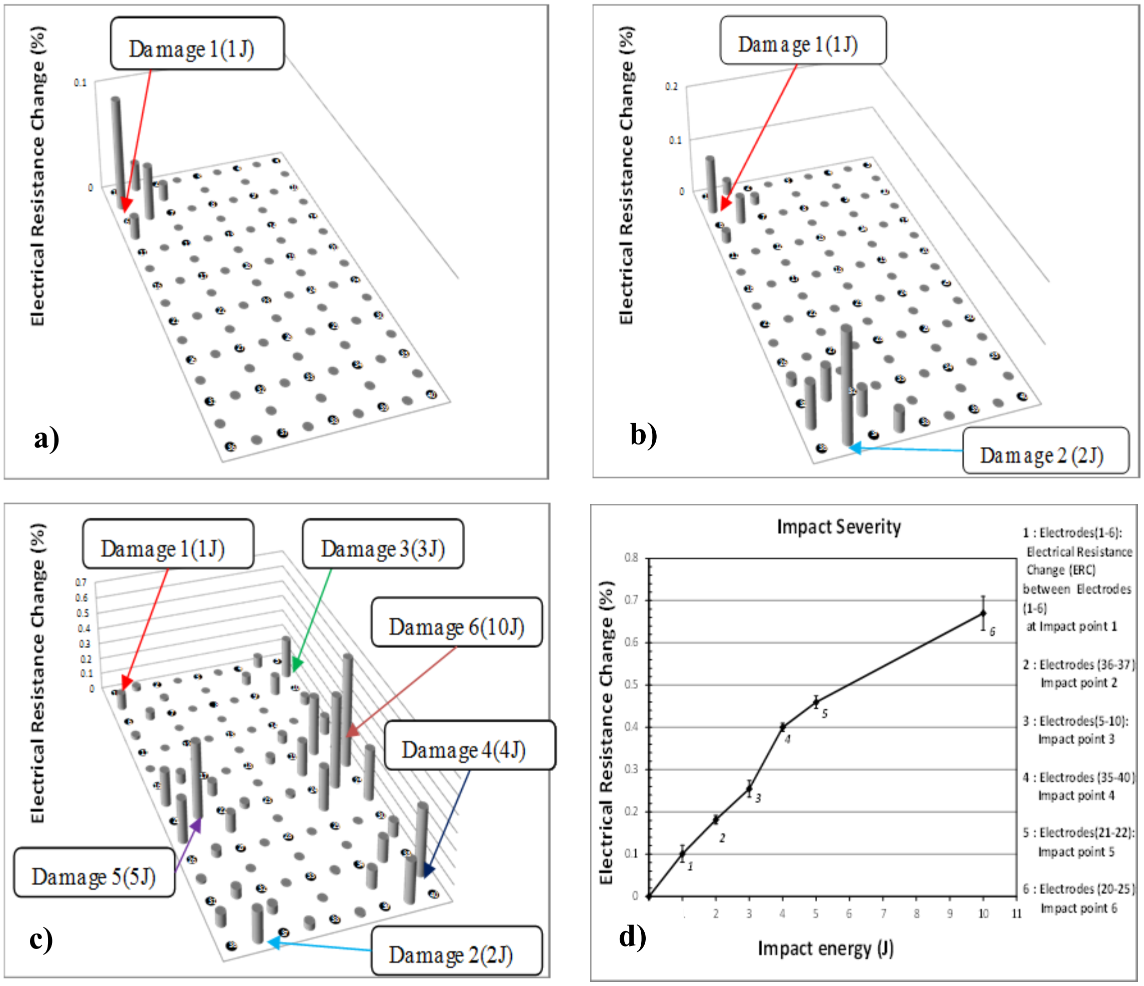

Figure 3.23: ERC distribution of plate 11 after a) BVI damage 1 (1J), b) BVI damages 1 and 2 (1J and 2J) c) Impact damages 1, 2,3,4,5 and 6 (1J, 2J, 3J, 4J, 5J and 10J) d) Effect of energy level on the change in electrical resistance (Data are presented as mean ± SD from three experiments)

3.4 Conclusions

In summary, a new SHM technique has been developed that enables real-time detection, location and quantification of damage in the LPCSs. This technique is based on real-time monitoring of electrical resistance distribution over the surface of large plates to sense sharp changes in electrical resistance distribution as an indication of detection, location and quantification of damage. Drilled holes, impact damage and barely visible impact damage were detected and located in the large plates. Drilled holes and impact damage made with different sizes and different energy levels respectively were quantified in the plates. The success of the technique strongly depends on the use of an optimal quantity of MWCNT to assure damage detectability at any region in large plates. We demonstrated the criteria for the determination of the optimal quantity of MWCNT. The first criterion consists of uniformity of MWCNT distribution which results in uniformity in electrical conductivity. The second criterion is sensitivity to change in electrical resistance for detection, location and quantification of damage in the large plates. These practical issues render the large structure to be self-sensing. As such sensing can be carried out globally, and locally.

Chapter 4

A technique for real-time detecting, locating and quantifying damage in large polymer composite structures made of carbon fibers and carbon nanotube networks

A significant safety concern preventing extensive use of composite materials for large polymer composite structure (LPCS) is the ability to detect, locate and quantify damages that occur at one or several locations in LPCS. Real-time health monitoring of LPCS improves their performance, durability, reliability while minimizing life cycle cost of LPCS. In this chapter, a new, practical and real-time SHM technique is presented for detecting, locating and quantifying damages in LPCS made of carbon fibers and CNT networks. In this technique, electrically conductive epoxy resin was prepared by dispersing multiwalled carbon nanotubes into the epoxy matrix. This modified epoxy matrix was then incorporated with long carbon fibers to make large composite plates. Two sets of grid points made from silver-epoxy paints were mounted on the surface of the large plates. The first set was used to apply the constant electric current and the second set was utilized to measure the electric potential. The electric potentials across the second set of grid points on the undamaged plate were measured and used as a reference set. Different damage was created by drilling holes and by applying impact loading on the large plates. It is found that the electric potential between the contact points surrounding the damage changes. The significant change in electric potential corresponds to the damage location in the plates. As such, drilled holes, impact damage and barely visible impact damage are detected, located and quantified.

4.1 Introduction

Carbon fiber reinforced polymer composites (CFRPCs) have received attention in many industrial applications due to their high strength-to-weight and stiffness-to-weight ratios. One of the critical challenges in the practical use of CFRPC is to monitor the health of CFRPC structures in real-time due to their susceptibility to different types of damages [10]. The long term use of the composites depends a lot on the ability to detect and locate the damages in the structures. Various non-destructive evaluation (NDE) techniques such as X-ray tomography [11, 30], ultrasonic C-scanning [11, 12], liquid penetrant [11, 70], acoustic emission [11, 12, 26], piezoelectric active sensors [11, 71], fiber optics [11, 12, 37] and measuring electrical conductivity along the direction of carbon fibers [11, 41] have been used for health monitoring of CFRPC structures. Techniques such as liquid penetrant, ultrasound scanning, X-Ray tomography, Shearography can detect damages in composites but these techniques can only work in a laboratory setting. They cannot be used on real composite structures during the operation of the engineering component. Techniques such as Acoustic emission can detect the occurrence of damage in composite structures. However it is very difficult for this technique to locate the damage due to confusion created by extraneous sources. Techniques such as the use of fiber optical sensors can measure strains in the composite structures. The optical fibers may pick up the change in strains due to the occurrence of defects. However the size of the optical fibers is usually large (52 micrometers). When the optical fibers are incorporated within the composite structures, they create stress concentration which can degrade the mechanical properties of the composite structures. Besides, the optical fibers are fragile and they tend to break fairly easily. Over the past few years, measuring electrical conductivity of the carbon fibers was used as a technique to indicate the presence of damage by many researchers [41, 47, 79-90]. Since carbon fibers are electrically conductive along the fiber direction, by applying an electric current over two probes at two points along the direction of the fibers, the change in electric potential can be taken as an indication of damage in CFRPC structures. Schulte and Baron [80] first proposed electrical resistance change measurement (ERCM) for structural health monitoring, which can be used to monitor internal damage of CFRPC. Chung et al. [86, 87] showed that electric potential change measurement (EPCM) is more sensitive than ERCM to detect internal damage in CFRPC plates where the electric potential probes are close to the electric current probes (current input locations). The problem with this technique is that since the resin is not conductive, one cannot use the technique to detect resin cracks. The majority of damage at the relatively low loads is due to matrix cracking and delamination, rather than to fiber breakage. As such, the usefulness of this technique is limited. The recent advent of polymer nanocomposites where carbon nanotubes (CNTs) are added in polymers has provided the impetus for scientists and researchers to produce functionally tailored matrix and fibers. This is because CNTs possess outstanding properties including structural, mechanical, electrical, and thermal properties [72]. The outstanding properties of CNTs combined with their small size offer them not only for the modification of polymers but also a method for detecting both strain and subsequently failure in polymer matrix composites (PMCs). Adding CNTs at small concentrations in a polymer matrix to form electrically conductive networks distributed around the structural fiber reinforcement displays piezoresistive behavior. The piezoresistive behavior of the CNT networks enables their use as highly responsive sensors to monitor initiation and detection of matrix cracks in the structures [4, 91, 92]. Zhang et al. [19] embedded CNTs in graphite fiber/epoxy laminates to improve their electrical conductivity in the thickness direction due to the continuous electrical conduction pathways made by CNTs in between graphite fibers. This approach was used to detect delamination created by inserting a Teflon film in the laminates. They found that there is a good correspondence between the delamination length and changes in through-thickness electrical resistance. Kostopoulos et al. [69] dispersed CNTs in carbon fiber/epoxy composite not only for improving the electrical conductivity of the composite in the transverse direction but also for detecting matrix cracks in the composite. They found that the addition of CNTs in the composites acts as direct sensors with high damage sensitivity to detect matrix damage accumulation during monotonic and cyclic tensile loading. The above works illustrate very interesting and innovative attempts to monitor damage in CFRPC coupons with small size using CNT networks. No technique has existed to detect and locate damage in LPCSs made of carbon fibers and CNT networks. Here, a new SHM technique is developed to detect, locate and quantify damage in large carbon fiber/epoxy/CNT composite plates.

4.2 Experimental methods

4.2.1 Materials

MWCNT (described in Chapter 2) and woven carbon fibers (5.7 oz/yd2) with thickness of 0.01 inch were purchased from Bayer Material Science and US Composites, Inc. respectively. The epoxy resin Epon 862 and the curing agent EPIKURE W were produced by Miller-Stephenson Chemical Company.

4.2.2 Methods

4.2.2.1 Fabrication of composite plates

To manufacture the carbon fiber/epoxy/ MWCNT composite plates, 0.3wt% MWCNT (as the optimal quantity of MWCNT) [91] were dispersed into epoxy resin mixed with curing agent (26.4wt%) using three roll milling (EXAKT 80E, EXAKT Technologies Inc.). The mixture was heated up to 60^0C for 20 min in a vacuum oven to remove air bubbles. The modified epoxy matrix was dispersed in six layers of plain weave carbon fabric by hand lay-up. The composite plates were cured using an autoclave.

4.2.2.2 Electrical measurement strategy

Electrical measurements can be performed by two methods for detecting damage in composite structures. One is the two-probe method and the other is the four-probe method. In the two-probe method, two electrical contacts are used to apply constant electric voltage and to determine electrical resistance based on the measured electric current. In the four-probe method, four electrical contacts are used. One pair of electrical contacts is utilized to apply constant electric current between the two probes while the other pair of electrical contacts is used to measure electric potential over two points in the vicinity of the first two points. Contact resistance exists between the probes and the plate. In situations where the intrinsic resistance of the material is much larger than the contact resistance at the probes (such as glass fiber/epoxy composites containing CNT), the effect of the contact resistance is small and two-probe method can be used effectively. However in situations where the intrinsic resistance of the material is small compared to the contact resistance at the probes (such as the case of carbon fiber/epoxy composites containing CNT), contact resistance is more dominant and the two-probe method is not suitable. For this case, the four-probe method is more suitable since electric potential does not depend on the contact resistance at the probes. Wang and Chung [88] demonstrated that the four-probe method is very effective and accurate compared to the two-probe method for detecting damage in CFRPC structures. As such in this work, the four-probe method is used to minimize contact resistance. Another issue in using the electrical method for damage detection in a two-dimensional plate is current spreading which reduces damage sensitivity. High sensitivity for detection of minor damage in the structures can be achieved where current input location is close to the electric potential line [86, 87]. This close distance between electric current line and electric potential line provides high current density while minimizing current spreading. A new strategy of electric potential measurement (EPM) is proposed to overcome the aforementioned issues for in-situ damage monitoring in LPCSs made of carbon fibers and CNT networks. The EPM strategy is described in Figure 4.1. In this figure, two sets of grid points are applied to avoid the contact resistance issue. The first set is used to inject constant electric current by pairs of $I_{1I,2I}$, $I_{1I,3I}$, $I_{2I,4I}$, $I_{3I,4I}$, $I_{2I,3I}$ and $I_{1I,4I}$ (not shown for clarity). The second set is used to measure electric potentials between adjacent pairs of $V_{1v,2v}$, $V_{1v,3v}$, $V_{2v,4v}$, $V_{3v,4v}$, $V_{2v,3v}$ and $V_{1v,4v}$ (not shown for clarity) where I and V stand for electric current and potential. The subscript numbers, separated by a space represent the associated first and second sets of grid points respectively.

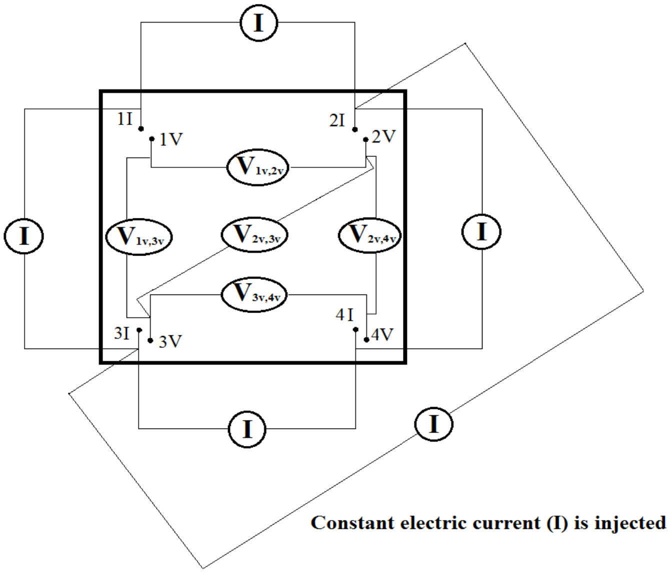

Figure 4.1: Schematic illustrating strategy for EPM using the four-probe method

4.2.2.3 Plate specification and electrical measurement strategy

The specification of the composite plate and a new strategy of EPM for in-situ damage monitoring are schematically illustrated in Figure 4.2. In this figure, two sets of grid points were mounted on the surface of the plate. Each set consists of 40 electrical contact points. Each contact point was made from electrically conductive silver-epoxy paste. The first set of grid points labeled from 1I to 40I spaced 3 inches apart was used to apply a constant electric current to the CFRPC structures. The second set of grid points labeled from 1V to 40V spaced 3 inches apart was diagonally shifted by 0.2 inch with respect to the first set to measure electric potentials. Electrical wires were attached to the two grid points to make electrodes. Then the electrodes were connected to the data acquisition system. The flowchart of the proposed technique and the computer program are shown in Appendix B.

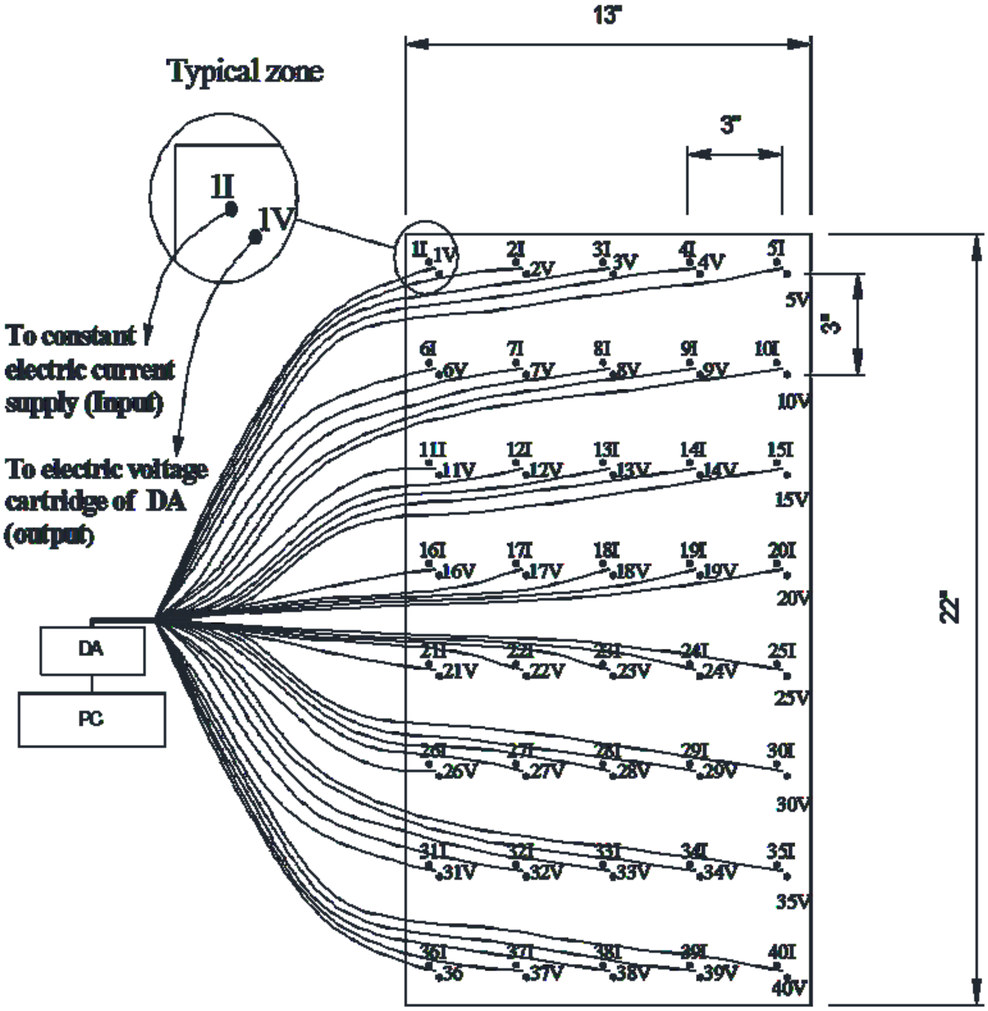

Figure 4.2: Schematic illustration of plate specification and strategy of EPM

The EPM strategy corresponding to nearest points to 13I and 13V is described in Figure 4.3. In this figure, pairs of the first set of grid points corresponding to point 13I identified by solid red lines to inject constant current are $I_{13I,7I}$, $I_{13I,8I}$, $I_{13I,9I}$, $I_{13I,12I}$, $I_{13I,14I}$, $I_{13I,17I}$, $I_{13I,18I}$ and $I_{13I,19I}$ while the pairs of second set of grid points corresponding to point 13V identified by dashed blue lines to measure electric potentials are $V_{13v,7v}$, $V_{13v,8v}$, $V_{13v,9v}$, $V_{13v,12v}$, $V_{13v,14v}$, $V_{13v,17v}$, $V_{13v,18v}$ and $V_{13v,19v}$.

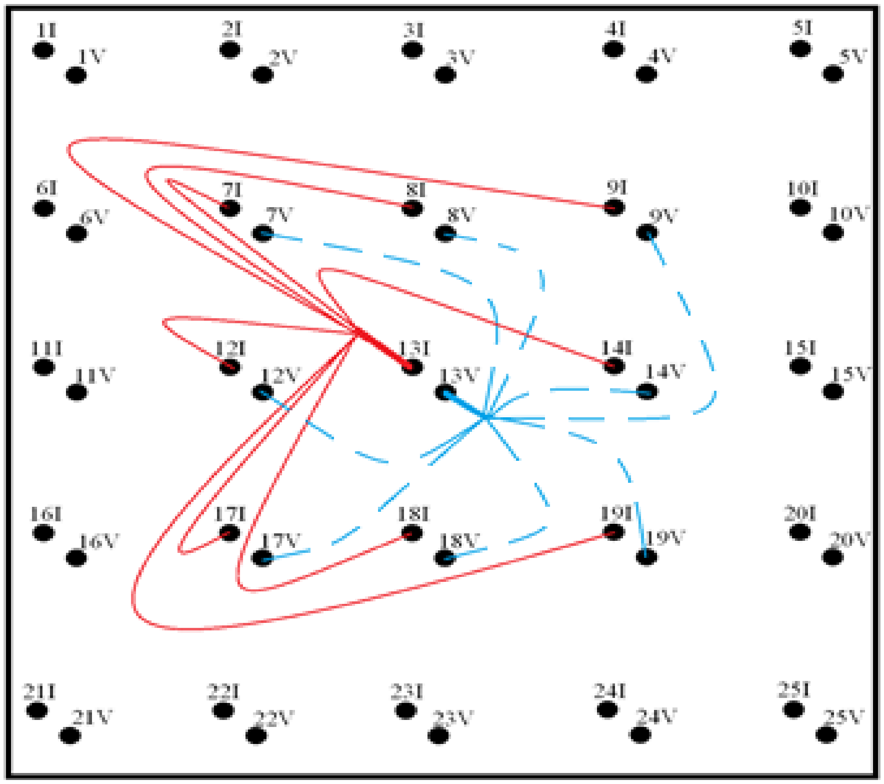

Figure 4.3: Schematic illustration for describing pairs of electrical contacts corresponding to points 13I and 13V to inject constant electric current (solid red lines) and to measure electric potentials (dashed blue lines) respectively

The current input location to measure electric potential between one point and its nearest neighbors (for example for points 13I and 13V) are presented in Table 4.1. In this Table, for example constant electric current is injected between points 13-7 ($I_{13I,7I}$) while electric potential is measured between points 13-7 ($V_{13V,7V}$).

Table 4.1: The pairs of electrical contacts nearest to points 13 I and 13 V

Pair of electrical contacts	Constant current input location	Measured electric potential
13-7	$I_{13I,7I}$	$V_{13v,7v}$
13-8	$I_{13I,8I}$	$V_{13v,8v}$
13-9	$I_{13I,9I}$	$V_{13v,9v}$
13-12	$I_{13I,12I}$	$V_{13v,12v}$
13-14	$I_{13I,14I}$	$V_{13v,14v}$
13-17	$I_{13I,17I}$	$V_{13v,17v}$
13-18	$I_{13I,18I}$	$V_{13v,18v}$
13-19	$I_{13I,19I}$	$V_{13v,19v}$

4.2.3 Electric potential measurements

The EPM is used to detect damage in carbon fiber/epoxy/MWCNT composite plates. The EPM adopts the electrically conductive carbon fibers and CNTs themselves as self-sensing materials. The EPM was performed by the four-probe method using a Keithley 6220 DC, Keithley 218A and Vishay Micro-Measurements System 7000. A constant current (100 mA) was directly applied to the mounted first grid points through the plate using a Keithley 6220 DC. Then the electric potential across the second grid points was measured using a Keithley 218A. Electric potential change (EPC) is expressed by:

$$\Delta V(\%) = \frac{V_{f,iv,jv} - V_{I,iv,jv}}{V_{I,iv,jv}} \times 100 \quad \textbf{(4.1)}$$

Where $V_{I,iv,jv}$ and $V_{f,iv,jv}$ represent the initial and final electric potential values between grid points iv and jv respectively.

4.3 Drilled holes and impact tests

Two damage types were introduced in carbon fiber/epoxy/MWCNT composite plates. One was drilled holes of different sizes at different locations in the plates. The other was impact loading caused by collision with high velocity projectiles and drop weights on the plates. The plates were subjected to high velocity impacts with energy of 78J produced by a 318 mg aluminum particle travelling at 700 m/sec using a gas gun. The details of high velocity impact test set-up to detect and locate damage are shown in Figure 4.4. The drop weights were applied on the clamped plates placed on electrically non-conductive rigid supports to create the low velocity impacts.

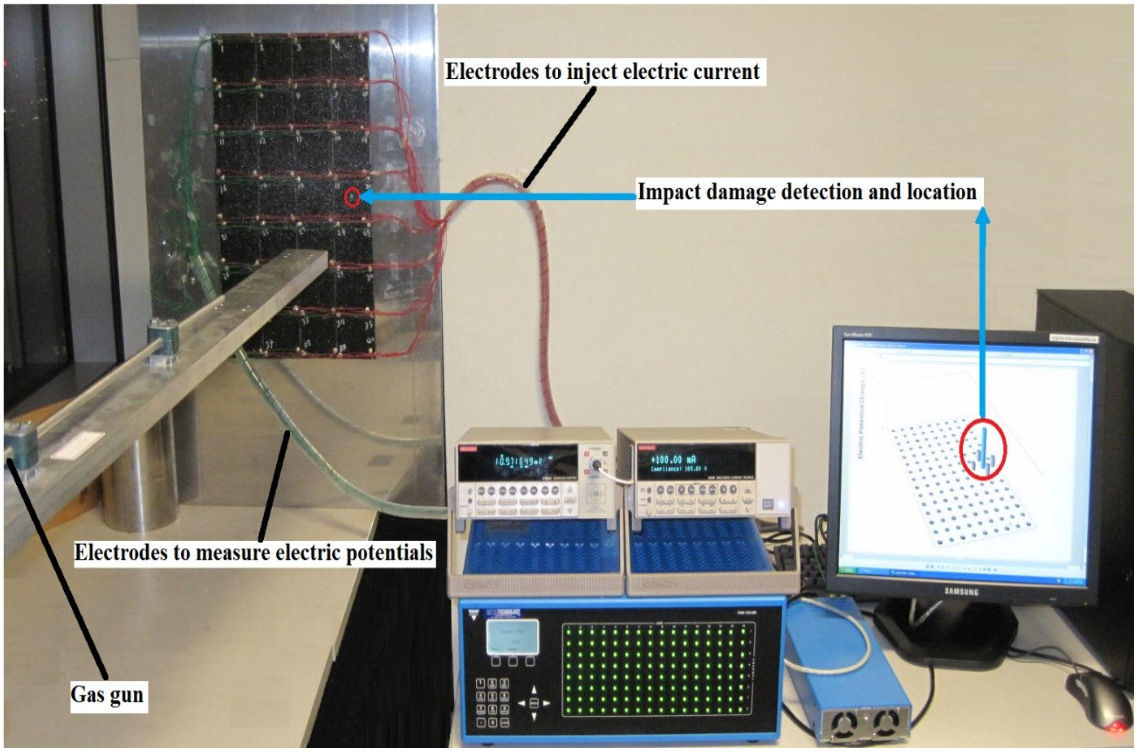

Figure 4.4: Experimental set-up to detect and locate damage due to high velocity impact test

4.4 Result and discussion

The electric potentials between pairs of the second set of grid points spaced 3 inch apart before damage for 22 ×13 inch^2 carbon fiber/epoxy/0.3wt% MWCNT plate 1 were measured and used as reference values. The electric potential distribution of plate 1 is shown in Figure 4.5. Coefficient of variation in percent (100×Standard deviation divided by Average electric potential) as a measure of uniformity of electric potential distribution for undamaged plate 1 was determined to be 14 %.

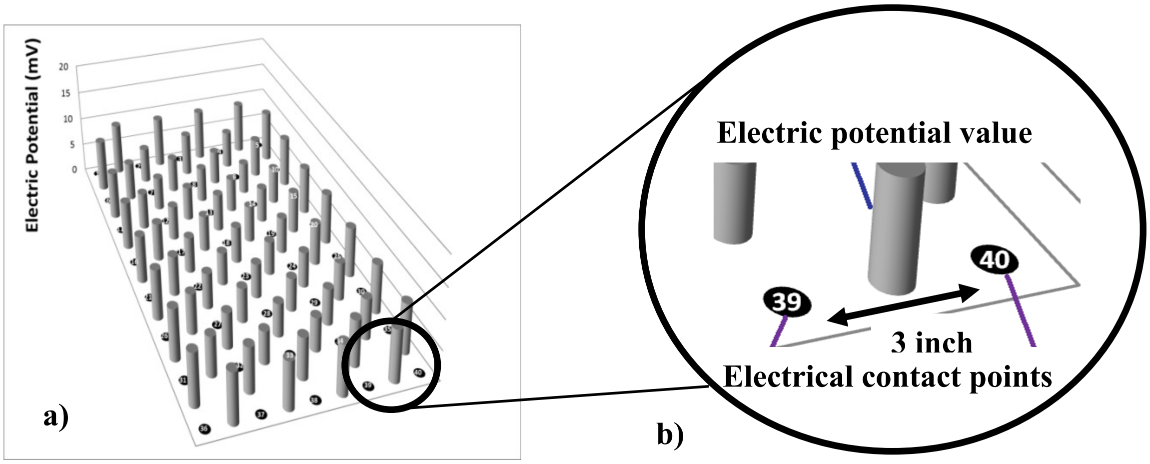

Figure 4.5: a) Distribution of electric potential of plate 1. The black dots, labeled 1,., 40 are representations of potential contacts b) Close up view of electrical contact points

4.4.1 Drilled holes and impacted areas

A hole of size 1/16 inch was drilled in plate 1. The values of electric potentials were measured after the hole is drilled. These values were compared against the reference values. The difference between the values of the electric potentials and the reference values is calculated based on Eq. (4. 1). The hole is detected and located based on the significant local variations in distribution of the EPC as shown in Figure 4.6a.

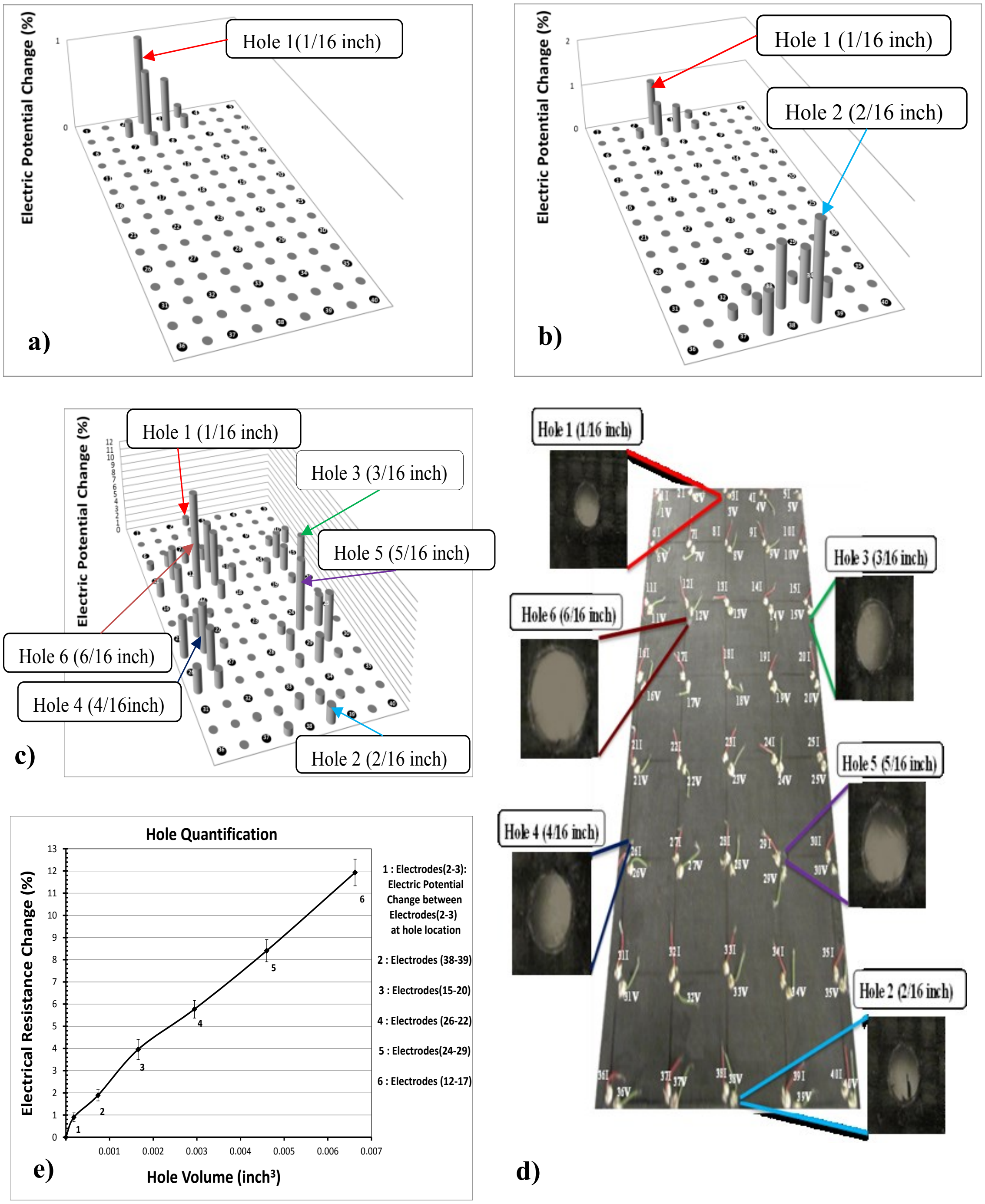

Figure 4.6: EPC distribution of plate 1 after drilling a) Hole 1 (1/16 in), b) Holes 1 and 2 (1/16 and 2/16 in), c) Holes 1, 2, 3, 4, 5 and 6 (1/16, 2/16, 3/16, 4/16, 5/16, d) plate 1 after six drilled holes and e) Effect of hole volume on the change in electric potential (Data are presented as mean ± SD from three experiments)

Subsequently another hole of size 2/16 inch was drilled. It is observed from Figure 4.6b that the significant local variations in distribution of the EPC reveal the locations of holes of sizes 1/16 and 2/16 inch drilled in plate 1. Other holes were then introduced. Observing Figures 4.6c and 4.6d, good correspondence is found between the significant local variations in distribution of the EPC and holes of sizes 1/16, 2/16, 3/16, 4/16, 5/16 and 6/16 inch respectively in plate 1. Figure 4.6e shows the effect of hole volume on the EPC. In this figure, the numbers below the curve represent the pairs of electric potential probes. This pair of probes is closest to the hole. A clear relationship between hole volume and change in electric potential is observed in Figure 4.6e. This reveals the capability of the technique to determine severity of the damages.

High velocity projectiles were impacted using a gas gun at two different locations of plate 2. Figures 4.7a and 4.7b show the locations and values of the changes in electric potential due to the collision with high velocity projectiles (78J each). Plate 2 impacted at 2 different locations is shown in Figure 4.7c. By comparing Figures 4.7b and 4.7c, it is clear that impact damages 1 and 2 are detected and located according to the sharp local variations in distribution of the EPC. This indicates that the technique is capable of detecting and locating of impact damages.

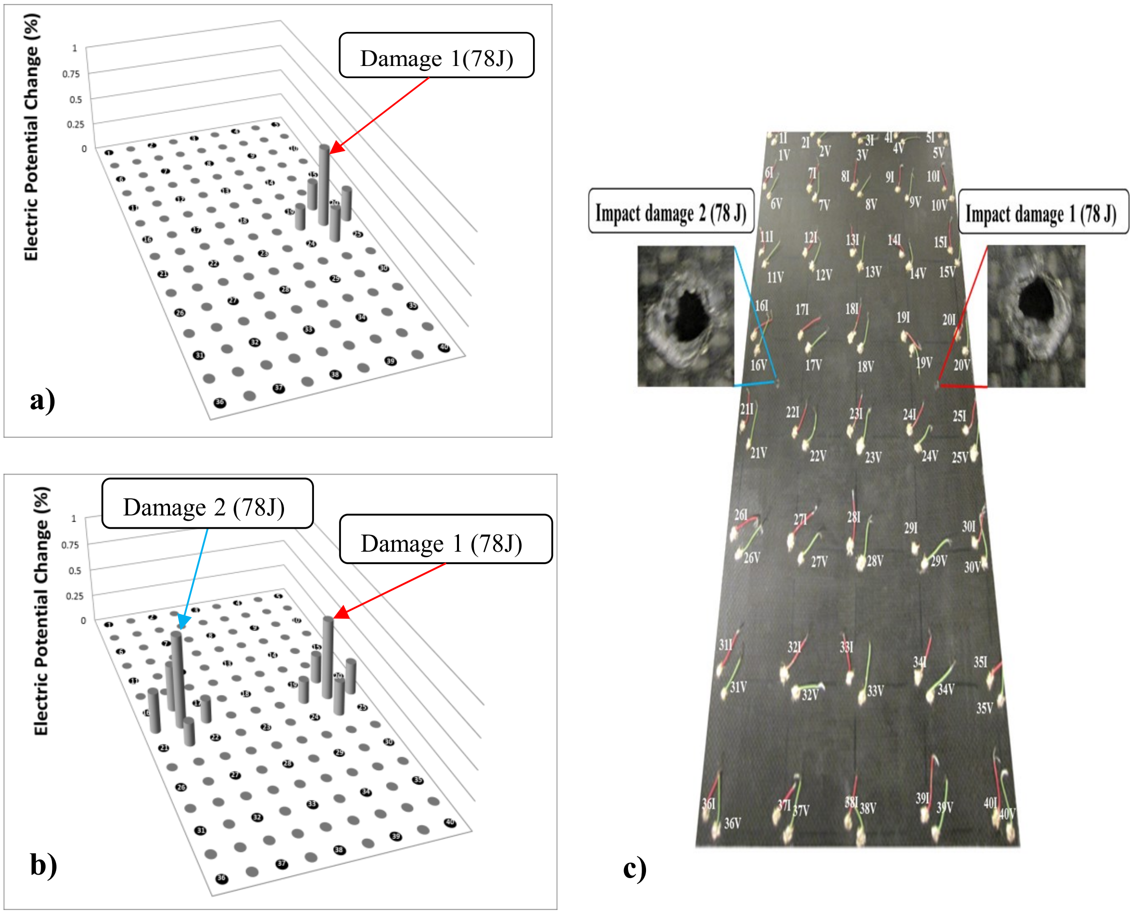

Figure 4.7: Electric potential change distribution of plate 2 after a) Impact damage 1 (78J) and b) Impact damages 1 and 2 (78J each) c) Plate 2 after two impact damages

To explain the experimental results, from Ohm's law, the electrical resistance R is defined by:

$$R = \frac{V}{I} \tag{4.2}$$

Where R , V and I are electric resistance, electric potential, electric current, respectively. The relationship between electrical resistivity as a material property and electrical resistance is expressed as:

$$R = \frac{\rho l}{wt} \tag{4.3}$$

Where ρ , w, t, l and R represent electrical resistivity, width of sample, thickness of sample, the distance over which the electrical resistance is determined and electrical resistance respectively. Substituting Eq. (4. 2) into Eq. (4. 3) is given as:

$$I = \frac{V}{\rho \frac{l}{wt}} \tag{4.4}$$

In the case of electric potential in the plate measured using the four-probe method, constant electric current is injected. The electric current flowing through the plate before damage (I_1) and after damage (I_2) was kept constant. Eq. (4. 4) can be written as:

$$\frac{V_2}{V_1} = \frac{\rho_2 \frac{l_2}{w_2 t_2}}{\rho_1 \frac{l_1}{w_1 t_1}} \tag{4.5}$$

Where subscript numbers 1 and 2 represent before and after damage respectively.

If the resistivity, the distance over which the electric potential is measured and thickness of plate do not change, Eq. (4. 5) can be given as:

$$\frac{V_2}{V_1} = \frac{w_1}{w_2} \tag{4.6}$$

If hole (broken fibers and matrix) is made in plate, this hole would result in a reduction in width ($w_2 < w_1$). This reduction would cause an increase in electric potential ($V_2 > V_1$) according to Eq. (4. 6). The fraction of the change in electric potential is given as:

$$\frac{\Delta V}{V_1} = \frac{V_2 - V_1}{V_1} = \frac{w_1 - w_2}{w_2} \tag{4.7}$$

Where w_2 is smaller than w_1 due to hole.

From physical point of view, as the amount of electric charge flowing at given time (electric current) is constant, the energy to push the same amount of electric charge flowing through the plate (electric potential) is increased due to the hole. As such any discontinuity such as a hole in the plate would cause an increase in change in electric potentials.

4.4.2 Barely visible impact damage (BVID)

Plate 3 was tested under low velocity impact performed using drop weights with different energy levels ranging from 1J to 3J. These energy levels were applied to create barely visible impact damage (BVID) which cannot be detected by visual observations. Plate 3 impacted at three different locations with different energy level is schematically illustrated in Figure 4.8a. Figures 4.8b and 4.8c show the locations and values of the changes in electric potential for plate 3 due to low velocity impact tests. Comparing Figures 4.8a and 4.8c, good correspondence is found between the significant local variations in absolute electric potential change distribution and barely visible damage zones. This reveals that BVI damages 1, 2 and 3 produced by different energy levels at different locations in plate 3 are detected and located distinctly.

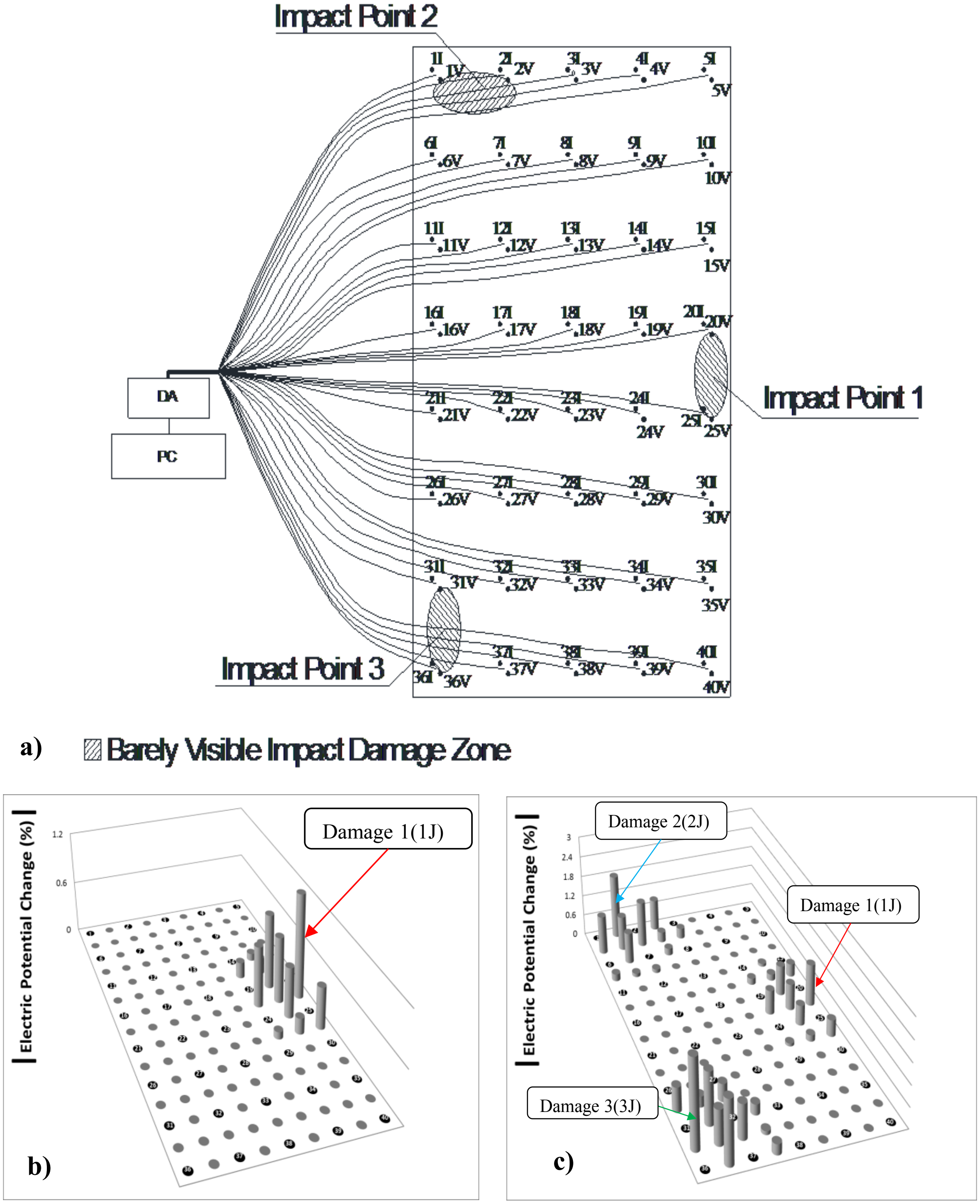

Figure 4.8: a) Schematic illustration of 22×13 inch^2 plate 3 impacted at three regions using drop weights with impact energies of 1, 2 and 3J. Absolute EPC distribution of plate 3 after b) BVI damage 1 (1J), c) BVI damages 1, 2 and 3 (1, 2 and 3J)

From impact damage detection and location points of view, significant change in electric potential can be taken as an indication of impact damage detection and location in the large structures. However, complex electrical responses due to low velocity impact damage were observed by many researchers for CFRPC structures [46, 83-90, 93]. It was shown that an impact causes electric current path distortion which results in a reduction in electric potential in the plane of CFRPC plate [86-88]. Another explanation is that impact test may cause partial reduction in thickness direction of the laminates. This may result in fiber-fiber contacts at the interlaminar interface and minimizing contact resistance which may cause a reduction in electric potential and increasing current flow in interlaminar carbon fibers laminates. As such conductivity of the laminates increases with permanent local deformation of resin caused by impact [46, 89, 90, 93].

4.5 Conclusion

A new, practical and real-time SHM technique was developed to detect, locate and quantify damages in the large polymer composite plates made of carbon fibers and CNT networks. In this technique, electric current was applied through the large plate and electric potentials were measured. This electric potential distribution in the undamaged plate was used as a reference map. Real-time monitoring of electric potential distribution over the surface of the plate was performed to provide an actual map of electric potential distribution. This map was compared against a reference map to identify significant changes in electric potential. These significant changes provide the ability for detection, location and quantification of damages and barely visible impact damages in the large plates.

Chapter 5

Electrical model of composite plates: Theory and Simulation

In this chapter, an electrical model is proposed for conductive composite plates with different electrical conductivities. The current paths between two electrodes are modeled by considering a network of resistors whose configuration depends on the electrical conductivity level of the material. Composite plates with relatively high and low electrical conductivities are modeled by fine and coarse grids of resistors respectively. By using Ohm's and Kirchhoff's laws the total resistance of the plate viewed from the electrodes is obtained and its sensitivity with respect to damages is studied. Numerical simulations are given to demonstrate the effect of the material's electrical conductivity, damage severity, spacing between electrodes, the proximity of pair of electrodes to the damage location, and electrical contact geometry on the sensitivity of the electrical resistance with respect to damage. The simulation results are compared with experimental results presented in Chapters 2 and 3.

5.1 Basic definition for electrical conduction

5.1.1 Ohm's law

Ohm's law states the relation between electric current and voltage (see Eq. (4. 2)).

5.1.2 Kirchhoff's Laws

Kirchhoff's current law (KCL) and Kirchhoff's voltage law (KVL) are fundamental laws in electrical engineering to analyze electric circuits. The integral of the normal component of the current density J over a closed surface S is assumed to be zero because as electric current must flow into a volume as it leaves [94]. This is KCL for a finite region which is defined as:

$$\oint_S J.dS = 0 \tag{5.1}$$

KCL states that the sum of the current flowing into a junction point at any instant is equal to the sum of the current flowing out of that. In a circuit, two or more circuit elements at a junction point are joined together (independent node) [94]. KCL is expressed as:

$$\sum_{j=1}^{k} I_j = 0 \tag{5.2}$$

where k is the number of independent nodes.

KVL states that the sum of voltages in a closed circuit is zero. KVL is expressed as:

$$\sum_{j=1}^{k} V_j = 0 \tag{5.3}$$

where Vj represents the voltage drop in the j_{th} element in any given closed circuit having k elements.

5.1.3 Current density

The current density for current distributed uniformly over a wire cross-section is defined as:

$$J = \frac{I}{A} \tag{5.4}$$

Where J, I and A are current density, current and cross sectional area respectively.

5.2 Theoretical modeling

Epoxy resins containing CNT have a range of electrical conductivity which depends on the quantity of CNT. At a very small concentration of CNT (0.1wt%CNT), the material is not conductive. When the percolation threshold is reached (0.18wt% MWCNT [75]), conductivity increases drastically and the material can be considered as conductive. However at the percolation level, if mixing cannot disperse the CNT uniformly in large structures, non-uniform conductivity over the domain of the large structure may occur. As such the CNT concentration needs to be higher than the percolation threshold to assure uniform conductivity over the large structure. As the concentration of CNT increases, uniformity improves. However if the CNT concentration is too high (for example about 5%), high viscosity of the resulting resin may prevent uniform dispersion of CNT and non-uniform conductivity may occur again. As such there is a window of concentration of CNT that can assure uniform electrical conductivity. In this thesis, the large quantity of CNT is not considered, not only from the difficulty in mixing, but also the high cost. Rather, the range of CNT concentration considered here is between percolation threshold (0.18%) and 1wt%MWCNT as shown in Figure 5.1.

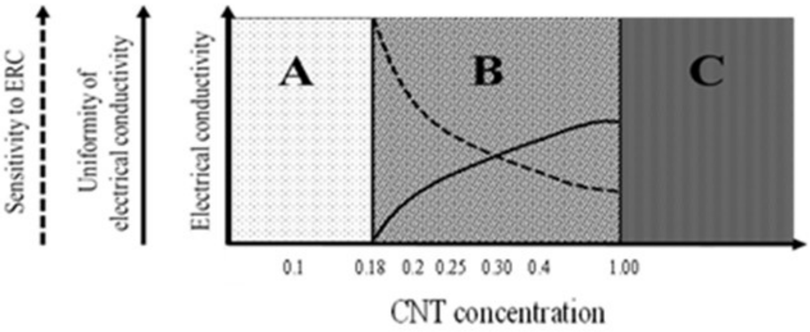

Figure 5.1: Window (segment B) that can provide sensitivity to ERC and uniformity of electrical conductivity for damage detection, location and quantification

Once the issue of uniformity is addressed, there remains the sensitivity to resistance change due to the occurrence of damage. If the material is highly conductive, the electrical resistance between grid points in the structure may not be sensitive to the occurrence of damage. Take for example, the case of an aluminum plate as shown in Figure 5.2. One injects a current I at A and conducts it away at B. The voltage between points A and B in the plate may not change much without or with the presence of damage (such as a hole) between the two points. This is because there are many paths that the current can take to go from A to B. The difference in the length of the paths may not be significant to cause a significant change in the voltage.

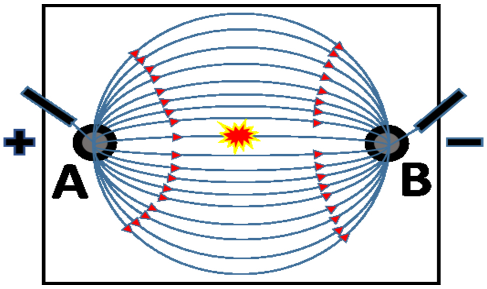

Figure 5.2: Example of how damage can cut off a conductive path in aluminum plate. Conduction continues with many conductive paths

It is found that the case of epoxies (or other type of polymers) containing CNT represent a different type of conductive materials. They are conductive but not continuously conductive as the case of metals. In metals, conductivity is continuous down to the atomic level. In polymer nanocomposites such as that of epoxy/CNT, the continuity is on a coarser level. One may call this as “aggregately conductive”. If a large quantity of CNT can be uniformly dispersed in the epoxy, then there exist many paths for the current to flow from point A to point B in a structure. If the quantity of CNT is smaller (but more than the percolation threshold), the number of conductive paths is reduced. Figure 5.3 shows an example of how damage may cut off a conductive path in an epoxy/CNT sample. If the number of conductive paths between two point is limited, the occurrence of damage between the two points will give rise to increase electrical resistance between the two points (see Figure 5.3a). However if there are a large number of conductive paths (see Figure 5.3b), the electrical resistance is not significantly affected. The number of conductive paths depends on the CNT concentration. Higher concentration gives rise to higher number of paths. Higher number of paths would represent less sensitivity to the detection of damage. The dashed line in Figure 5.1 represents this behavior. As such, within the window of uniform conductivity, one needs to find an optimal value of the CNT concentration so that one can have uniform conductivity within a large structure, and at the same time high sensitivity for the detection of damage. For the epoxy/CNT system studied in this thesis, the optimal quantity was found experimentally to be 0.30wt%MWCNT. The value may vary depending on the material system (combination of type of epoxy and nanotubes).

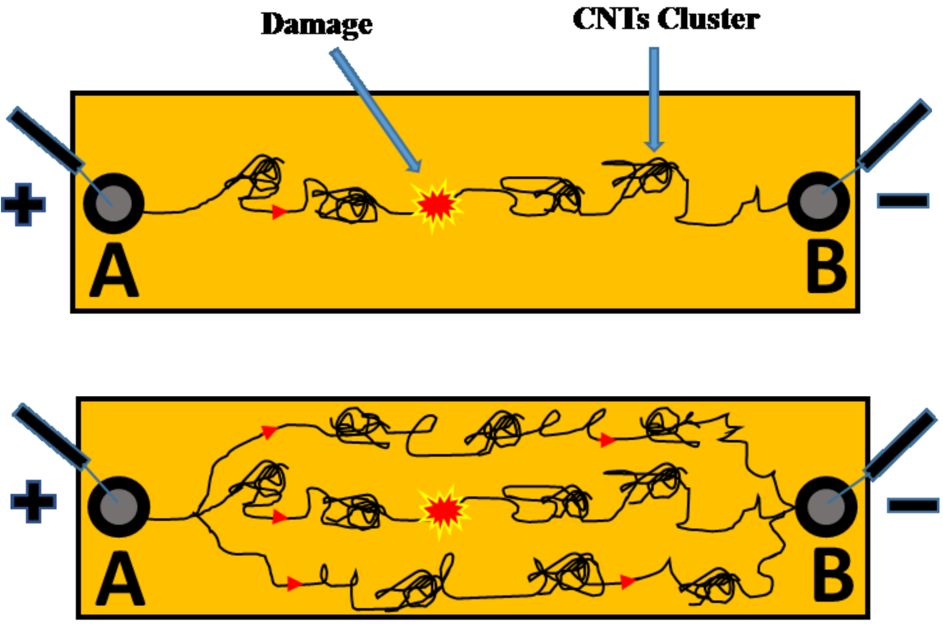

a)

b)

Figure 5.3: Schematic illustration of CNT clusters dispersed in polymer representing example of how damage can cut off a conductive path in epoxy containing relatively a) Small CNT concentration and b) Large CNT concentration

The change in sensitivity with the CNT concentration is illustrated using the model of grids of resistors. Figure 5.4 shows two grids of resistors representing two samples of epoxy/CNT composite. Coarse grid (see Figure 5.4a) represents a material with smaller quantity of CNT and as such with higher equivalent electrical resistance (Req) between two points A and B. Fine grid (see Figure 5.4b) represents a material with larger quantity of CNT and as such a smaller Req between points A and B. If one resistor is removed, there are more alternative paths for the current to flow from A to B in fine grid due to the large network of interconnected elements compared to that in coarse grid. This indicates lower sensitivity in fine grid compared to that in coarse grid due to removed resistor.

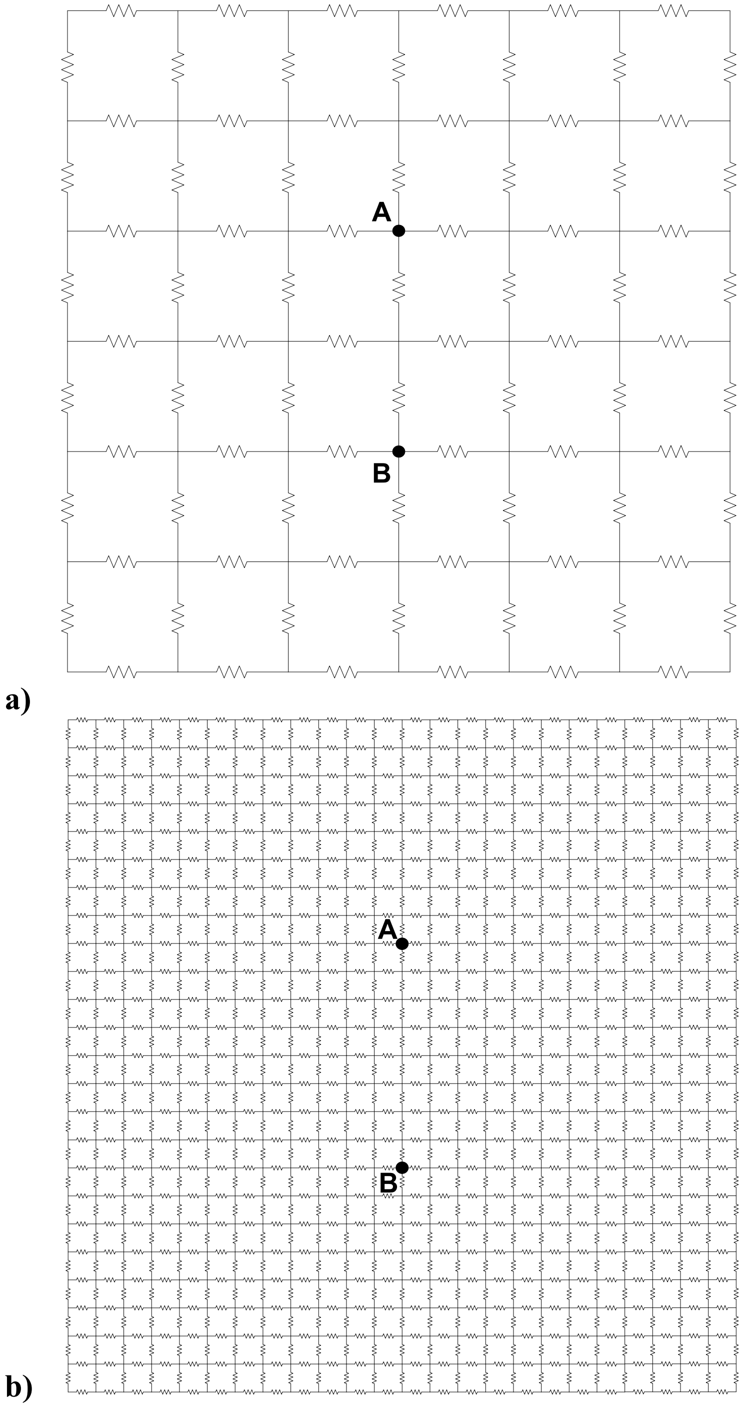

Figure 5.4: An electrical model of network of resistors, representing a) Plate 1 with relatively low conductivity (coarse grid) b) Plate 2 with relatively high conductivity (fine grid) with multiple current paths

The electrical resistance between A and B in the coarse grid is taken to be 100,000 ohms (10^5) while that in fine grid is 1000 ohms (10^3). A change of two orders of magnitude is reasonable considering the large change in electrical conductivity over a small change in CNT concentration as shown in Figure 5.5.

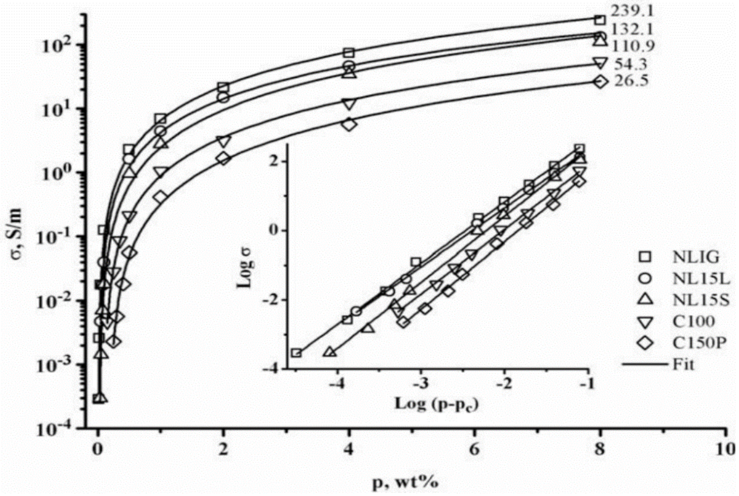

Figure 5.5: Effect of CNT concentration(wt%) on electrical conductivity [75]

Plate 1 and plate 2 are modeled with coarse and fine grids of resistors of resistances R_1 and R_2 respectively. M represents the number of resistors in the electrical model along the length (vertical direction) and width (horizontal direction) of the plate that depends on the level of the material's electrical conductivity. The distinct number of conductive paths (M) increases as the conductivity of a composite plate increases. Values of (M=6×6) and (M=24×24) are assumed for modeling of composite plates 1 and 2 with relatively low and high electrical conductivity as shown in Figures 5.4a and 5.4b respectively where plate size and the spacing between electrodes are fixed. As plate 2 is more conductive compared to plate 1, one can give $Req_{(AB)2}$ smaller than $Req_{(AB)1}$ which offers R_1 (resistance of each resistor in coarse grid) to be larger than R_2.(resistance of each resistor in fine grid). Electrical resistance change (ERC) is calculated based on Eq. (2. 6).

To simplify an electrical model of a network of resistors for analyzing the effect of partial failure in the network on the sensitivity to ERC, equivalent resistance (Req) is replaced by n parallel resistors of the same resistance R (for simplicity of presentation) as shown in Figure 5.6.

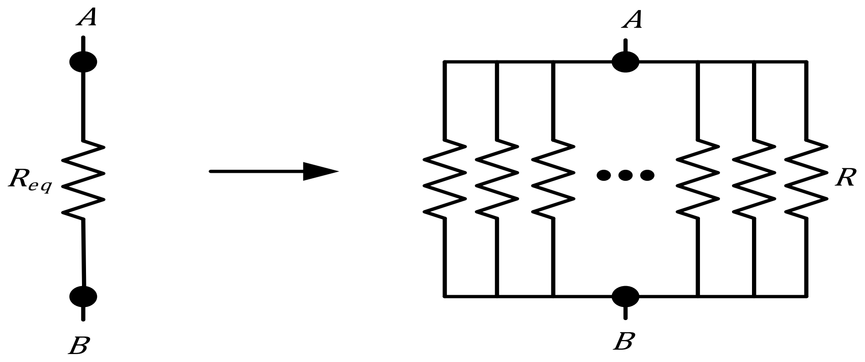

Figure 5.6: A network of resistors, showing equivalent resistance of parallel resistances

The equivalent resistance (Req) for parallel resistors of the same resistance R is expressed by

$$R_{eq} = \frac{1}{n} \times R \tag{5.5}$$

where n represents the number of parallel resistors of equal resistance R.

The modeling of partial failure in the network of parallel resistors can be simulated by removing some (not all) of the parallel resistors. For instance, Req due to removing only one of the parallel resistors is calculated as

$$R'_{eq} = \frac{1}{n-1} \times R \tag{5.6}$$

The change in the equivalent resistance is calculated based on Eq. (2.6) as:

$$(R'_{eq} - R_{eq} / R_{eq})(\%) = \frac{1}{n-1} \times 100 \qquad \textbf{(5.7)}$$

Eq. (5. 7) implies that independent of the value of R, by changing n, the sensitivity to ERC varies. Therefore, in this model, the value of n is the only effective factor which plays a profound role in determining the sensitivity to ERC. If each resistor is represented as a conductive path from A to B, then n is the total number of distinct conductive paths. Obviously, as electrical conductivity of the composite plate increases, the number of conductive paths between any two electrodes increases and the network offers less electrical resistance to the flow of electric current between two electrodes. The sensitivity to ERC is affected by the material's electrical conductivity, the proximity of pair of electrodes to the removed resistor (Damage), the number of removed resistors (Damage severity), the spacing between electrodes and the electrode geometry. From the physical point of view, in first case for the effect of the material's electrical conductivity, one can show that an increase in electrical conductivity would offer more conducting pathways resulting in an increase in n. This increase would result in a reduction of sensitivity of the ERC based on Eq. (5. 7). Higher Req is obtained when n is reduced according to Eq. (5. 5). This reduction in n causes an increase in the sensitivity of the ERC according to Eq. (5. 7). In second case, where the material's electrical conductivity is constant and damage location is fixed, one can assume that two different spacings between electrodes are used. If the number of the removed resistors (damage size) does not change, then a smaller spacing between electrodes gives more ERC compared to a larger spacing. In third case, one can remove different number of resistors as a representative of damage size. If the spacing between electrodes is fixed, then a larger number of removed resistors (bigger damage size) indicates higher ERC compared to a smaller number of removed resistors. It can be observed that the fixed spacing between electrodes with bigger damage size is equal to fixed damage size with smaller spacing between electrodes. In fourth case, when the material's electrical conductivity, damage size and spacing between electrodes are fixed, as the removed resistors (damage) in the network becomes closer to location of electrodes, the ERC increases. This can be related to the electric current density distribution in the network of resistors. Assume the equivalent resistance between points A and B is R_{eq} and n = 11. R_{eq} is modeled by 11 parallel resistors with different resistances labeled from R_1 to R_{11} as shown in Figure 5.7. In a simple model one may assign weights to the resistors based on the distance from the line connecting A to B (representing strong and weak links between A and B). As the electric current tends to pass from the shortest distance between electrodes, the electrical resistances of the resistors close to electrodes are expected to be smaller. The values of resistances are presented based on the electric current density distribution between electrodes A and B as follows: $R_1 > R_2 > R_3 > R_4 > R_5 > R_6 < R_7 < R_8 < R_9 < R_{10} < R_{11}$.

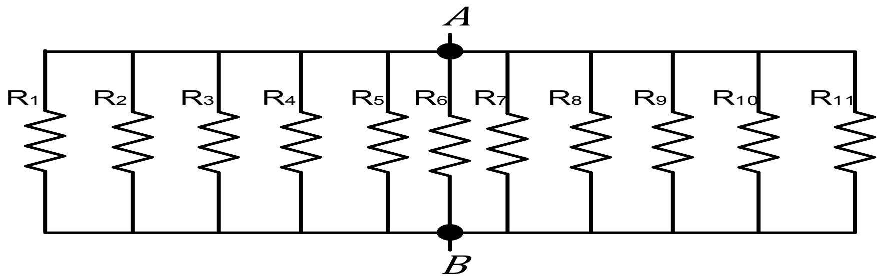

Figure 5.7: A network of resistors, equivalent resistance of parallel resistances

Removing R_1 or R_6 with the largest and smallest amount of resistance from the parallel resistors model has a different influence in determining ERC. Removing the smallest resistance (R_6) gives higher ERC compared to removing the largest resistance (R_1).

5.3 Numerical Study

5.3.1 Theoretical formulation of numerical simulation

The starting point of analyzing any electric circuit is based on the KCL and KVL. The parametric study is presented to illustrate the theoretical formulation of the numerical simulation. For instance, a network of resistors (M=3×2) is assumed for a large plate as shown in Figure 5.8. In this figure, the connection points labeled 1 to 12 are called nodes. The KCL holds at these nodes in which the electric current entering the node equals the current leaving the node in the network.

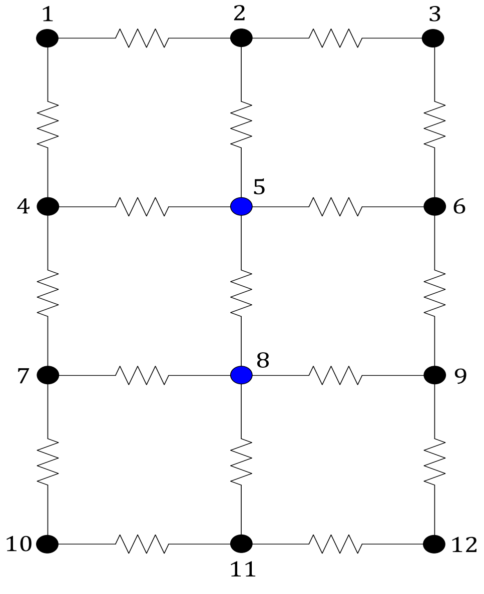

Figure 5.8: A representative resistors network of conductive plate to illustrate formulation

To find the equivalent resistance R_{eq} between nodes 5 and 8, current $I = 1A$ is injected into node 5 and sucked from node 8. The potential difference V between nodes 5 and 8 is computed. Then, the equivalent resistance between nodes 5 and 8 is calculated based on Ohm's law as:

$$R_{eq} = \frac{V}{I} = \frac{V}{1} \tag{5.8}$$

Where V and I are the potential difference between nodes 5 and 8 and the current $(1A)$ injected.

To determine the potential difference between nodes 5 and 8, KCL is written for each node labeled 1 to 12 in the network as shown in Figure 5.8.

KCL for node 1 can be written as:

$$\frac{V_1 - V_2}{R} + \frac{V_1 - V_4}{R} = 0 \tag{5.9}$$

KCL for node 2 can be given as:

$$\frac{V_2 - V_1}{R} + \frac{V_2 - V_3}{R} + \frac{V_2 - V_5}{R} = 0 \tag{5.10}$$

KCL for node 3 can be expressed as:

$$\frac{V_3 - V_2}{R} + \frac{V_3 - V_6}{R} = 0 \tag{5.11}$$

KCL for node 4 can be given as:

$$\frac{V_4 - V_1}{R} + \frac{V_4 - V_5}{R} + \frac{V_4 - V_7}{R} = 0 \tag{5.12}$$

KCL for node 5 can be written as:

$$\frac{V_5 - V_2}{R} + \frac{V_5 - V_4}{R} + \frac{V_5 - V_6}{R} + \frac{V_5 - V_8}{R} = 1 \tag{5.13}$$

KCL for node 6 can be expressed as:

$$\frac{V_6 - V_3}{R} + \frac{V_6 - V_5}{R} + \frac{V_6 - V_9}{R} = 0 \tag{5.14}$$

KCL for node 7 can be given as:

$$\frac{V_7 - V_4}{R} + \frac{V_7 - V_8}{R} + \frac{V_7 - V_{10}}{R} = 0 \tag{5.15}$$

KCL for node 8 can be written as:

$$\frac{V_8 - V_5}{R} + \frac{V_8 - V_7}{R} + \frac{V_8 - V_9}{R} + \frac{V_8 - V_{11}}{R} = -1 \tag{5.16}$$

KCL for node 9 can be expressed as:

$$\frac{V_9 - V_6}{R} + \frac{V_9 - V_8}{R} + \frac{V_9 - V_{12}}{R} = 0 \tag{5.17}$$

KCL for node 10 can be written as:

$$\frac{V_{10} - V_7}{R} + \frac{V_{10} - V_{11}}{R} = 0 \tag{5.18}$$

KCL for node 11 can be given as:

$$\frac{V_{11} - V_8}{R} + \frac{V_{11} - V_{10}}{R} + \frac{V_{11} - V_{12}}{R} = 0 \tag{5.19}$$

KCL for node 12 can be expressed as:

$$\frac{V_{12} - V_9}{R} + \frac{V_{12} - V_{11}}{R} = 0 \tag{5.20}$$

The equations (5. 9) to (5. 20) can be given as a system of linear equations in the matrix form:

$$A\mathrm{x} = \mathrm{b} \tag{5.21}$$

where

$$A=\begin{bmatrix} 2 & -1 & 0 & -1 & 0 & 0 & 0 & 0 & 0 & 0 & 0 & 0 \\ -1 & 3 & -1 & 0 & -1 & 0 & 0 & 0 & 0 & 0 & 0 & 0 \\ 0 & -1 & 2 & 0 & 0 & -1 & 0 & 0 & 0 & 0 & 0 & 0 \\ -1 & 0 & 0 & 3 & -1 & 0 & -1 & 0 & 0 & 0 & 0 & 0 \\ 0 & -1 & 0 & 0 & 4 & -1 & 0 & -1 & 0 & 0 & 0 & 0 \\ 0 & 0 & -1 & 0 & -1 & 3 & 0 & 0 & -1 & 0 & 0 & 0 \\ 0 & 0 & 0 & -1 & 0 & 0 & 3 & -1 & 0 & -1 & 0 & 0 \\ 0 & 0 & 0 & 0 & -1 & 0 & -1 & 4 & -1 & 0 & -1 & 0 \\ 0 & 0 & 0 & 0 & 0 & -1 & 0 & -1 & 3 & 0 & 0 & -1 \\ 0 & 0 & 0 & 0 & 0 & 0 & -1 & 0 & 0 & 2 & -1 & 0 \\ 0 & 0 & 0 & 0 & 0 & 0 & 0 & -1 & 0 & -1 & 3 & -1 \\ 0 & 0 & 0 & 0 & 0 & 0 & 0 & 0 & -1 & 0 & -1 & 2 \end{bmatrix}, \text{b=}\begin{bmatrix} 0 \\ 0 \\ 0 \\ 0 \\ 1 \\ 0 \\ 0 \\ -1 \\ 0 \\ 0 \\ 0 \\ 0 \end{bmatrix}, \quad \text{x}=\frac{1}{R}\begin{bmatrix} V_1 \\ V_2 \\ V_3 \\ V_4 \\ V_5 \\ V_6 \\ V_7 \\ V_8 \\ V_9 \\ V_{10} \\ V_{11} \\ V_{12} \end{bmatrix}$$

$$\mathrm{A}^{-1}=\begin{bmatrix} 1.50 & 1.21 & 1.21 & 0.80 & 1.00 & 1.04 & 0.89 & 0.96 & 0.99 & 0.92 & 0.95 & 0.97 \\ 1.00 & 1.42 & 1.25 & 0.60 & 1.00 & 1.07 & 0.78 & 0.91 & 0.97 & 0.84 & 0.90 & 0.93 \\ 0.88 & 1.21 & 1.74 & 056 & 1.00 & 1.27 & 0.80 & 0.96 & 1.08 & 0.87 & 0.95 & 1.01 \\ 1.00 & 1.00 & 1.00 & 1.00 & 1.00 & 1.00 & 1.00 & 1.00 & 1.00 & 1.00 & 1.00 & 1.00 \\ 0.63 & 0.83 & 0.87 & 0.43 & 1.00 & 0.91 & 0.66 & 0.83 & 0.85 & 0.73 & 0.79 & 0.82 \\ 0.76 & 1.00 & 1.24 & 0.52 & 1.00 & 1.48 & 0.81 & 1.00 & 1.19 & 0.90 & 1.00 & 1.10 \\ 0.86 & 0.96 & 1.01 & 0.77 & 1.00 & 1.06 & 1.45 & 1.22 & 1.16 & 1.35 & 1.26 & 1.21 \\ 0.76 & 0.92 & 1.00 & 0.61 & 1.00 & 1.08 & 1.05 & 1.39 & 1.24 & 1.16 & 1.27 & 1.26 \\ 0.77 & 0.96 & 1.10 & 0.58 & 1.00 & 1.25 & 0.97 & 1.22 & 1.64 & 1.12 & 1.26 & 1.45 \\ 0.83 & 0.95 & 1.02 & 0.71 & 1.00 & 1.09 & 1.29 & 1.26 & 1.24 & 1.90 & 1.51 & 1.38 \\ 0.79 & 0.94 & 1.03 & 0.64 & 1.00 & 1.12 & 1.13 & 1.30 & 1.32 & 1.45 & 1.77 & 1.54 \\ 0.78 & 0.95 & 1.06 & 0.61 & 1.00 & 1.18 & 1.05 & 1.26 & 1.48 & 1.28 & 1.51 & 2.00 \end{bmatrix},$$

x = A^{-1}b; gives the solution as follows:

$$\text{x}=\frac{1}{R}\begin{bmatrix} V_1 \\ V_2 \\ V_3 \\ V_4 \\ V_5 \\ V_6 \\ V_7 \\ V_8 \\ V_9 \\ V_{10} \\ V_{11} \\ V_{12} \end{bmatrix}=\begin{bmatrix} 0.04 \\ 0.09 \\ 0.04 \\ 0 \\ 0.17 \\ 0 \\ -0.22 \\ -0.39 \\ -0.22 \\ -0.26 \\ -0.30 \\ -0.26 \end{bmatrix}$$

Then equivalent resistance can be calculated as $R_{eq}=V_5-V_8=0.56\,R$.

5.3.2 Numerical simulation

The numerical simulations are conducted to study the effect of the material's electrical conductivity, number of removed resistors (damage severity), spacing between electrodes, the proximity of pair of electrodes to the damage location and electrode geometry on the sensitivity to electrical resistance. Plate 1 and plate 2 with relatively low and high electrical conductivity were modeled by coarse and fine grids of resistors as shown in Figures 5.4a and 5.4b respectively. These grids of resistors are analyzed based on the KCL and KVL using Matlab Simulink.

5.3.2.1 Fibers reinforced epoxy composites containing CNT

Damage modeling is an important parameter in analyzing the electrical model. Damage modes in fiber/polymer composite materials consist of fiber breakage, matrix cracking, delamination and fiber-matrix debonding [10]. From electrical point of view, the effects of electrically non-conductive and conductive fiber reinforced epoxy composites containing CNT are required to be taken into account for damage modeling in an electric circuit. In fiber/epoxy composites containing CNT where electrically non-conductive fiber is used, the occurrence of damage in the composite can be simulated as a removed resistor or increasing resistance of resistor in an electric circuit. In fibers/epoxy composites containing CNT where electrically conductive fiber is used, modeling of damage in the composites is much more complicated. This is due to the fact that there are two electrical networks made from conductive fibers and conductive CNTs in the composites that cause a complicated electrical current paths and strong electrical anisotropy. The breakages of carbon fibers and CNT networks cause an increase in electrical resistance while impact damage may indicate an increase or decrease in electrical resistance. Although there have been extensive studies on detecting damages in carbon fibers reinforced plastic (CFRP) using electrical measurements, very limited electric circuit analysis was conducted for damage detection in the composites. This is because of the complex electrical responses of CFRP composites due to damage. Damage in CFRP may cause either increase or decrease in electrical resistance [82, 84-89, 95]. Todoroki [90] studied the electrical behavior of CFRP samples due to damage using an electrical circuit as illustrated in Figure 5.9. They impacted CFRP samples and found the increase and decrease in electrical resistance due to damage. These increase and decrease are related to disconnection and connection (new path) of resistor in electric circuit respectively as shown in Figures 5.9b and 5.9c.

It is shown that an impact test may cause partial reduction in the thickness direction of the composite. This may result in fiber-fiber contacts at the interlaminar interface and minimizing contact resistance which may cause a reduction in electrical resistance or adding new paths in electric circuit as shown in Figure 5.9c. As such, conductivity increases with permanent local deformation of resin caused by impact [89, 90].

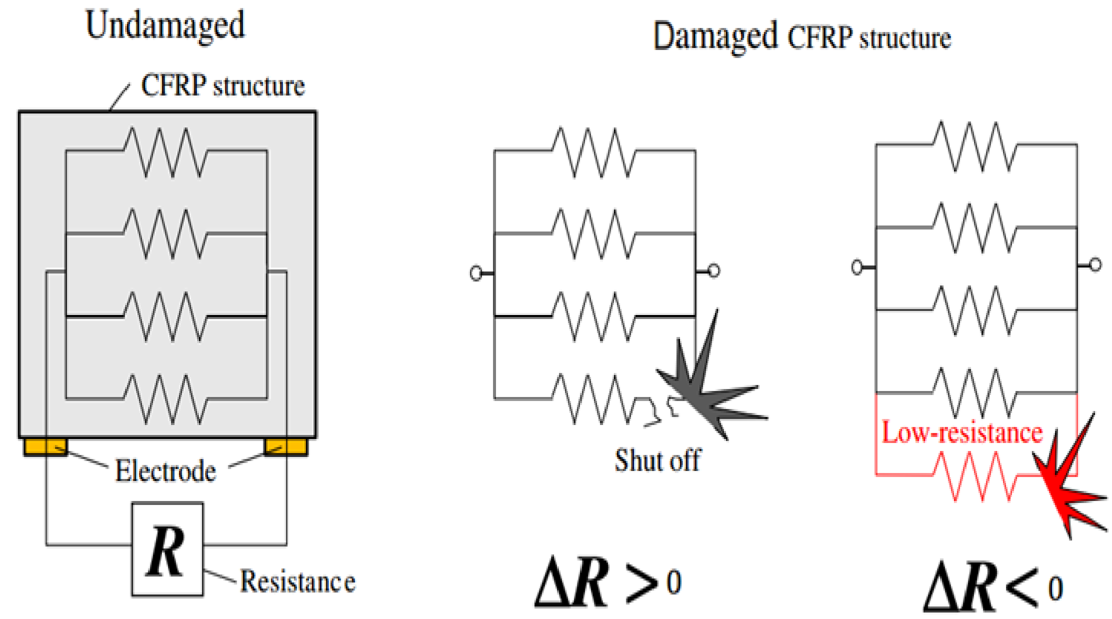

a) b) c)

Figure 5.9: Schematic circuit representing the electrical network in a) Undamaged CFRP structure and damaged CFRP structure b) Increase in resistance change and c) Decrease in resistance change [90]

The simulations were conducted for fiber/epoxy composites containing different concentration of CNT where damage was simulated by removing resistor which results in an increase in electrical resistance as shown in the following:

5.3.2.2 Effect of electrical conductivity

In order to study the effect of different electrical conductivities on the sensitivity to change in electrical resistance due to damage, two plates with relatively low and high electrical conductivity are simulated and analyzed using Matlab Simulink. Figure 5.10 shows simulation of plate 1 with relatively low conductivity modeled by a 6×6 coarse grid of resistors.

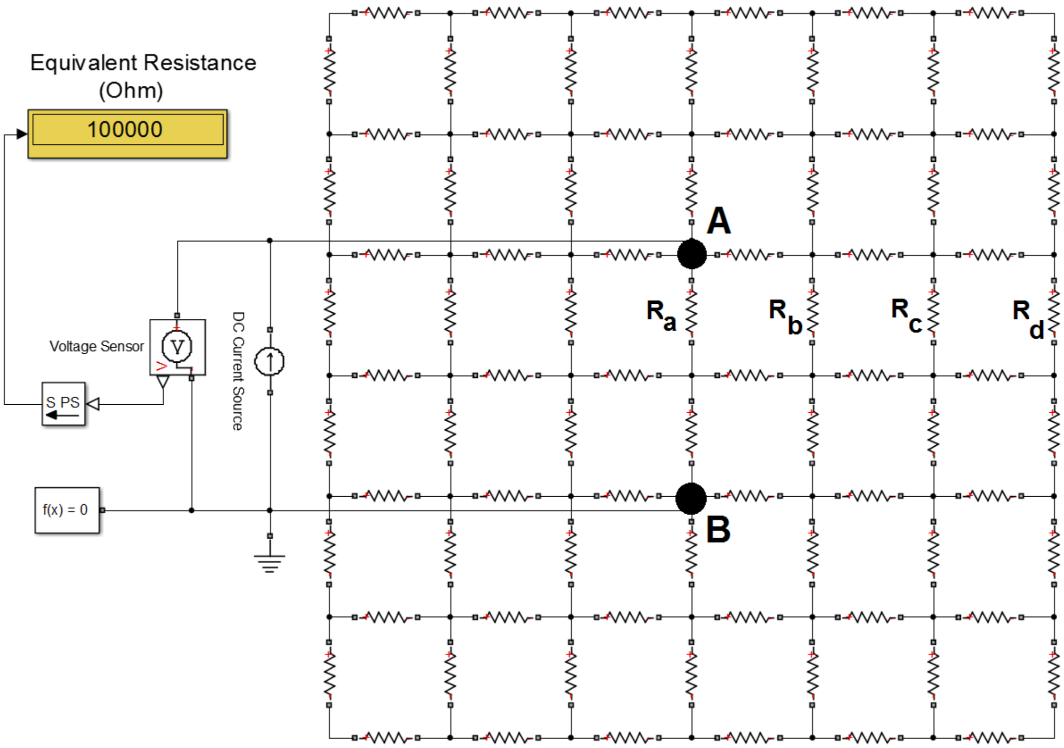

Figure 5.10: Network of resistors each of resistance (R=129,491Ohm), representing plate 1 with low conductivity modeled by a 6×6 network of resistors with contact-point electrodes

The simulation of plate 2 with relatively high conductivity modeled by a 24×24 fine grid of resistors is shown in Figure 5.11. Damage in plate 1 and 2 is simulated by removing resistors from the network of resistors. Electrical resistances before and after removing resistors (R_a) as a representative of damage in the electrical models of plate 1 and plate 2 are compared where spacing between electrodes is fixed. ERC is calculated based on Eq. (2. 6).

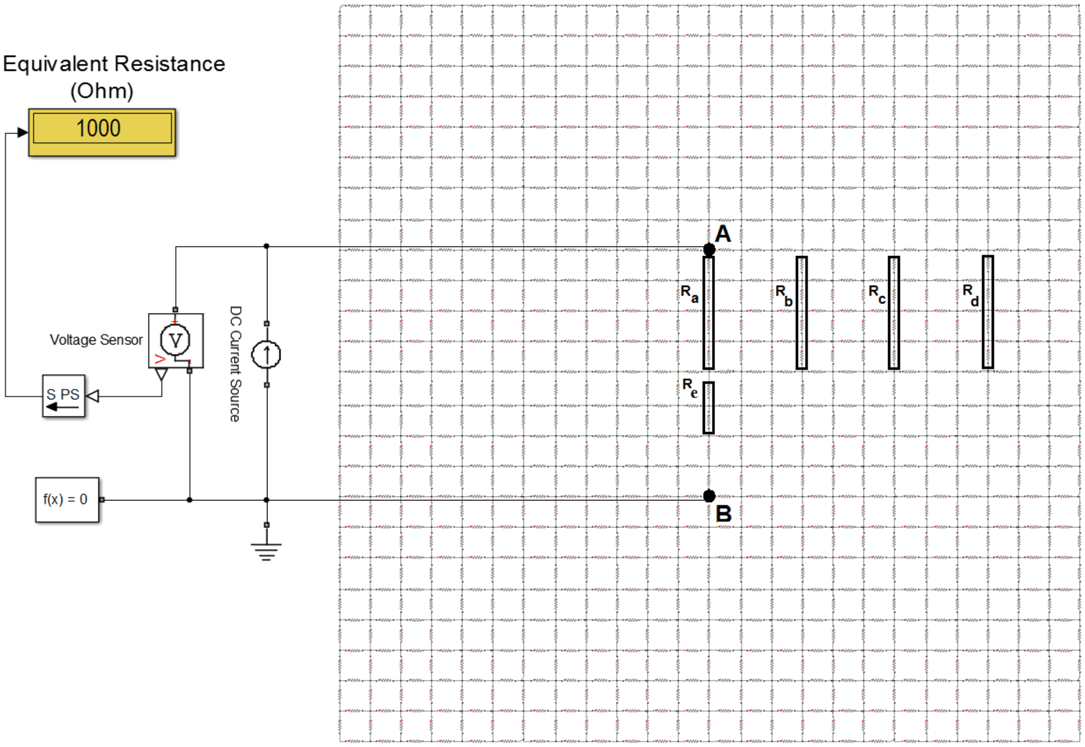

Figure 5.11: Network of resistors each of resistance (R=812 Ohm), showing plate 2 with high conductivity modeled by a 24×24 resistors network with contact-point electrodes

The numerical results are presented in Table 5.1. It is observed from Table 5.1 that plate 1 with relatively low conductivity shows greater sensitivity to change in electrical resistance than plate 2 due to removed resistors (R_a). This reveals that the plate's sensitivity to change in electrical resistance decreases as the material's electrical conductivity increases. This is because when a resistor (R_a) is broken, there are more alternative conductive paths for electric current to flow in plate 2 with relatively high conductivity compared to that in plate 1 with relatively low conductivity.

Table 5.1: Numerical results for comparing the effect of material's electrical conductivity on the electrical resistance change (ERC)

Plate with different conductivity	Removed resistors (Damage)	R $_{\text{Initial (Ohms)}}$	R $_{\text{Final (Ohms)}}$	ERC (%)
Plate 1 (lower conductivity)	R_a	100000	139541	39.54
Plate 2 (higher conductivity)	R_a	1000	1146	14.6

5.3.2.3 Effect of proximity of pair of electrodes to removed resistor (Damage)

The influence of removed resistors labeled R_a, R_b, R_c and R_d having different distances with respect to fixed electrodes (A and B) respectively on the change in resistance is investigated as illustrated in Figure 5.11. The numerical results for plate 2 with relatively high conductivity are presented in Table 5.2. It is found that the ERC increases as the distance between the electrodes and the removed resistors decreases. The closest distance between the removed resistors (R_a) and electrodes provides the highest ERC.

Table 5.2: Numerical results for comparing the effect of the proximity of pair of electrodes to removed resistors on the change in electrical resistance for plate 2

Removed resistors	Distance between removed resistors and electrodes	R $_{\text{Initial (Ohms)}}$	R $_{\text{Final (Ohms)}}$	ERC (%)
R_a	0	1000	1146	14.6
R_b	3	1000	1010	1
R_c	6	1000	1003	0.3
R_d	9	1000	1001	0.1

5.3.2.4 Effect of number of removed resistors (Damage severity)

The effect of number of removed resistors as an indication of damage size on the ERC is studied where the material's electrical conductivity and spacing between two electrodes are fixed. The numerical simulation was done by removing R_a and R_e that include 4 and 2 resistors respectively as shown in Figure 5.11. The numerical results for plate 2 are indicated in Table 5.3. It is observed that the ERC increases with the increase in number of removed resistors which indicates damage severity.

Table 5.3: Numerical results for comparing the effect of the number of removed resistors (damage size) on the change in electrical resistance for plate 2.

Removed resistors	Spacing between Contact-point electrodes	$R_{\text{Initial (Ohms)}}$	$R_{\text{Final (Ohms)}}$	ERC (%)
R_a (4 resistors)	8 resistors	1000	1146	14.6
R_e (2 resistors)	8 resistors	1000	1023	2.3

5.3.2.5 Effect of spacing between electrodes

The effect of spacing between electrodes on the ERC is investigated where the material's electrical conductivity and removed resistors (R_a) are fixed. Two different spacings between electrodes for plate 2 are considered. One is 8 resistors between electrodes (A and B) as shown in Figure 5.11. The other is 12 resistors between electrodes (A and B) as illustrated in Figure 5.12. The simulation was carried out for plate 2 with 8 and 12 resistors spacing between electrodes where R_a was cut. Table 5.4 shows numerical results for plate 2 with relatively high conductivity mounted with 2 different spacings between electrodes. It is clear from Table 5.4 that the ERC increases as spacing between electrodes reduces. By comparing Table 5.3 and Table 5.4, it is found that fixed spacing between electrodes (8 resistors) with smaller damage size (removed R_e including 2 resistors) approximately equals to fixed damage size (removed R_a including 4 resistors) with larger spacing.

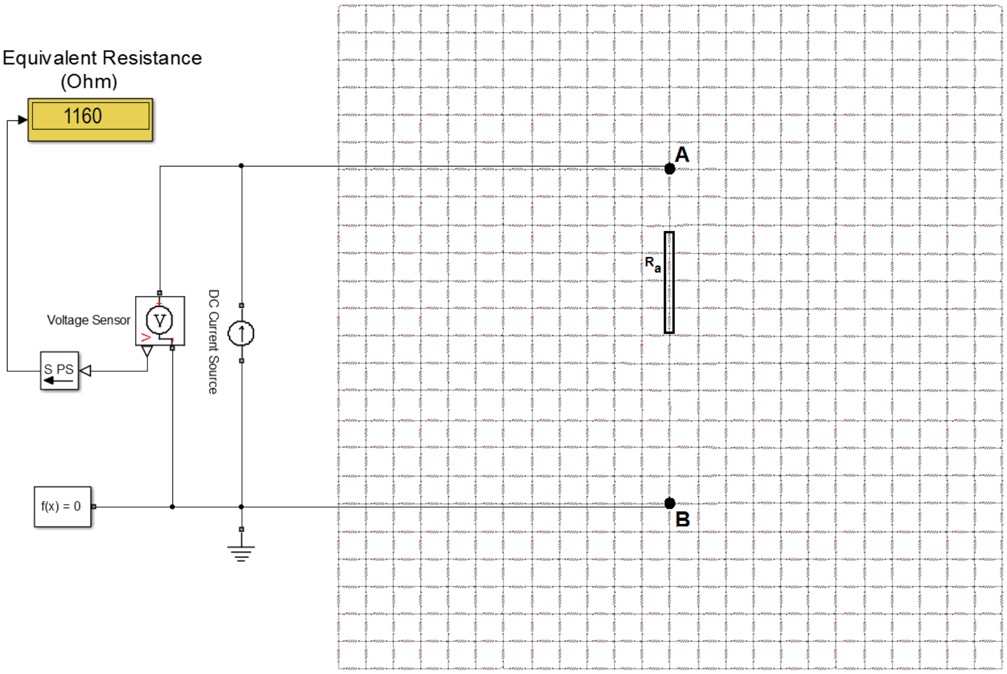

Figure 5.12: Network of resistors each of resistance (R=812 Ohm), showing plate 2 modeled by a 24×24 resistors network with contact-point electrodes

Table 5.4: Numerical results for comparing the effect of spacing between electrodes on the change in electrical resistance for plate 2 with relatively high conductivity

Spacing between Contact-point electrodes	Removed resistors (Damage)	$R_{\text{Initial (Ohms)}}$	$R_{\text{Final (Ohms)}}$	ERC (%)
8 resistors	R_a	1000	1146	14.6
12 resistors	R_a	1160	1186	2.24

5.3.2.6 Effects of contact-point electrodes and contact-line electrodes

The effect of electrode geometry on the sensitivity to electrical resistance is investigated while the material's electrical conductivity, spacing between electrodes and removed resistors (R_a) are fixed. Two different types of contact for electrodes on plate 2 are applied. One is contact-point electrodes and the other is contact-line electrodes as shown in Figures 5.11 and 5.13 respectively.

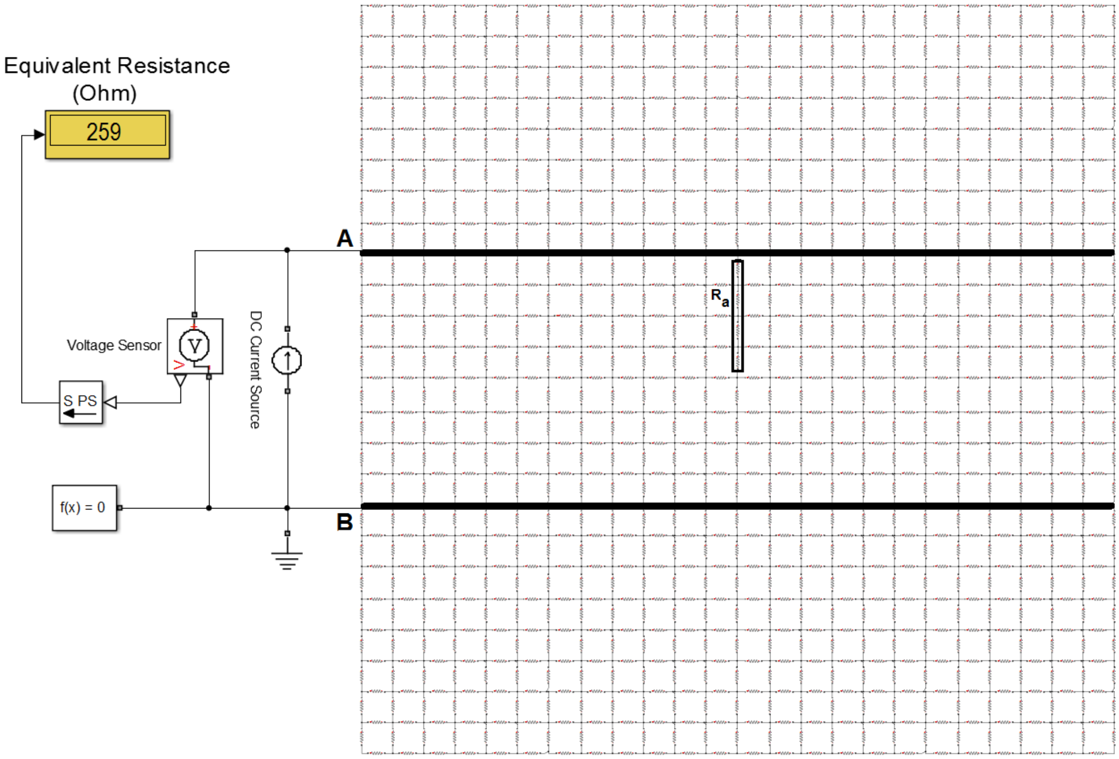

Figure 5.13: Network of resistors each of resistance (R=812 Ohm), showing plate 2 with high conductivity modeled by a 24×24 network of resistors with contact-line electrodes

The numerical analyses for plate 2 mounted with contact-point and contact-line electrodes with the same spacing were performed where R_a was removed. Comparing initial electrical resistance shown in Figures 5.11 and 5.13, it is found that even though electrical conductivity (plate 2) and spacing between electrodes are kept constant, the initial resistance measured via contact-point electrodes indicates higher resistance compared to that measured via contact-line electrodes. Table 5.5 shows numerical results for plate 2 to study the effect of contact-point electrodes and contact-line electrodes on the ERC. It can be seen that higher change in electrical resistance is obtained where contact-point electrodes are used.

Table 5.5: Numerical results for comparing the effect of electrode geometry on the change in electrical resistance for plate 2 with relatively high conductivity

Electrode geometry	Spacing between electrodes	$R_{\text{Initial (Ohms)}}$	$R_{\text{Final (Ohms)}}$	ERC (%)
Contact-point electrodes	8resistors	1000	1146	14.6
Contact-line electrodes	8resistors	259	266	2.7

5.4 Comparing simulation results with experimental results

Comparison between experimental results presented in Chapters 2 and 3 and simulation results is performed to study the effect of adding different concentration of MWCNT on the sensitivity to change in electrical resistance in glass fiber/epoxy/ MWCNT plates due to introduction of damage. A model of a resistor network has been proposed for composite plates containing CNT. The experimental measurements are employed to verify the numerical simulations. The simulation results indicate good agreements qualitatively with the obtained experimental results presented in Chapters 2 and 3. Both simulation and experimental results show that the higher sensitivity to ERC is obtained for the plate containing lower concentration of MWCNT (above the percolation threshold) that gives rise to lower electrical conductivity.

5.5 Conclusions

An electrical model has been proposed for epoxy composite plates containing CNT. Simulations were conducted based on Ohm's law, KCL and KVL using Matlab Simulink. The simulation results demonstrate that ERC depends on the level of material's conductivity, the spacing between electrodes, damage size, the proximity of pair of electrodes to damage, and the electrode geometry. A careful investigation of the electrical resistance of composite plates reveals the following:

- Sensitivity to ERC increases as the concentration of MWCNT in plate decreases while being above the percolation threshold
- The sensitivity to ERC was investigated experimentally and theoretically. Good correspondence was found.
- ERC increases as distance between the electrodes and damage location decreases
- ERC increases by decreasing the spacing between the electrodes.
- ERC increases with increasing damage size
- Contact-point electrodes leads to higher ERC compared to contact-line electrodes

Chapter 6

Relationship between through-thickness strain and electrical resistance in glass fiber/epoxy composite laminates containing carbon nanotube

6.1 In situ monitoring of through-thickness strain in glass fiber/epoxy composite laminates using carbon nanotube sensors

The intention of the work presented in this chapter was to find a way to measure the through-thickness strain (TTS) in composite laminates. The reason for this was because there did not seem to be any effective technique for the measurement of the TTS, particularly for locations away from the free edge. In the present work, Multiwalled carbon nanotubes (MWCNTs) were added into epoxy resin to make the resin electrically conductive. The modified resin was then incorporated with long glass fibers to make glass fiber/epoxy/CNT laminates. The laminate was subjected to a uniaxial load, while the electrical resistances across the thickness of the laminate were measured. Two different types of uniaxial loads were applied. One was along the length of the sample and the other across the thickness of the sample. For the case where lengthwise load was applied, classical lamination theory (CLT) was used to calculate the average TTS

(ATTS), and to find the stacking sequences that can provide the largest ATTS for a certain load. A strain gauge was mounted on the edge of the laminate in order to provide another means to measure the ATTS. It was found that the electrical resistance across the laminate thickness is sensitive to the axial load along the length of the sample. The magnitude of the change in electrical resistance across the laminate thickness is proportional to the strain measured by strain gauge. However, while the strain measured by strain gauge shows negative strain, there was an increase in the through-thickness electrical resistance (TTER). For the case of thicknesswise load, the strain is negative and the TTER shows a decrease. For the thicknesswise load, the change in TTER can be related to the ATTS. For the lengthwise load, even though the magnitude of the change in TTER is proportional to the ATTS, the change in TTER may not be completely due to the ATTS.

6.1.1 Introduction

Fiber reinforced polymer composites (FRPC) are widely used in many industrial applications due to their high strength-to-weight and stiffness-to-weight ratios [10]. When composite laminates are subjected to loading, apart from in plane strains and stresses, through-thickness strains (TTSs) and stresses also exist. The TTSs occur due to Poisson coupling effect. Around free edges these give rise to interlaminar stresses which can cause delamination failure. Significant amount of work on interlaminar (IL) strains and stresses took place in the 1970 [96] and 1980 [97] where analytical and numerical analyses were used to calculate the values of the IL strains and stresses. Experimental method to measure IL strain is required. Small strain gauges may be used to measure TTS at free edges. However it is not possible to determine the TTS at locations away from the free edges. Fiber optics may be used to measure in-plane strains. Recently attempts have also been made to use fiber optics to measure TTS [98]. However due to the large diameters and the small values of the TTS, the interference due to the insertion of the optical fiber may not give accurate strain values. The advent of polymer nanocomposites where carbon nanotubes (CNTs) are added into the epoxy resin making the matrix electrically conductive gives rise to the potential of using this technique to measure the TTSs. CNTs are inherently multifunctional materials, they can be used to make sensors due to their small size, high aspect ratios (length to diameter ratio), exceptional electrical conductivity [1], thermal conductivity [2], physical and mechanical properties [3]. Currently many studies have focused on embedding CNT in polymers to make them behave like strain sensors. Subsequently failure in polymer matrix composites (PMCs) can be detected using electrical resistance measurement (ERM) [72]. Fiedler et al. [99] first reported the ability of CNTs as conductive additives for damage sensing in composites. Böger et al [8] added CNTs and carbon blacks in the glass/epoxy composites and found that there is correspondence between the change in in-plane strain and the change in TTER. Thostenson et al. [4, 5] dispersed CNTs into epoxy to make glass/epoxy/CNT composite samples and showed that cracking in tensile samples corresponds with the increase in in-plane electrical resistance. Nofar et al. [9] incorporated MWCNTs into epoxy to fabricate glass/epoxy/ MWCNT composite samples and found that damage in the samples is detected by significant change in in-plane electrical resistance during tensile and fatigue testing. They also reported that electrical resistance change (ERC) is more sensitive than strain gauge measurements for damage monitoring. Gao et al [60] deposited CNT onto glass fiber surfaces and showed that epoxy composites made using this fiber system may be used for in-situ sensing of strain and damage. Alexopoulos et al [74] developed fibers consisting of CNTs in a sheath of polymer matrix. These fibers are then embedded inside the glass /polymer structure for detecting mechanical deformation using the change in electrical resistance of the special fiber. Hena-Zamal and Hoa [64] embedded MWCNTs in the glass/epoxy composite and indicated that there is correspondence between the change in TTER and damage accumulation during fatigue testing. The above works illustrate very interesting attempts to monitor in-plane strain and damage in composite materials using CNT networks. The problem of through-thickness stresses and strains and subsequent effect of delamination was first investigated rigorously in the 1980s. Pipes et al [96, 100] carried out numerical calculations for laminates subjected to uniaxial displacement and showed that interlaminar strains and stresses exist at the free edges of the laminate. A review on the interlaminar stresses in composites was given by Salamon [97]. Murthy and Chamis [101] showed that free edge delamination depends not only on the lay-up sequence but also on the size of the component, and the loading conditions. Moire interferometry was used to measure the TTS at the edge of the laminates [102-104]. Even though optical fibers were used to detect the transverse strain in laminates [98], the diameter of the fiber is still large (52 micrometers, which is more than 6 times the diameter of a carbon fiber, and about half the thickness of ply). Moire interferometry can be used to measure the TTS at the edge of the laminate, but it cannot be used to determine the TTS at locations away from the laminate edge. Here, we attempted to find a new method for in-situ monitoring of the average through-thickness strain (ATTS). This is done by incorporating MWCNT in glass fiber/epoxy composites.

6.1.2 Experimental characterization and materials

6.1.2.1 Materials

MWCNTs produced by Bayer Material Science, Unidirectional S-glass fibers purchased from ACP Composites Company with thickness of 0.127 mm, and the epoxy Epon 862 and the curing agent EPIKURE W produced by Miller-Stephenson Chemical Company were utilized.

6.1.2.2 Fabrication of composite laminates

The epoxy resin and curing agent (26.4 wt%) were first mixed. Then 0.3wt% MWCNT were added into epoxy matrix (the percolation threshold of the MWCNTs in epoxy was determined experimentally to be 0.1883 wt% [75]). A concentration more than the percolation threshold (0.3wt%) was used to assure consistency in the electrical resistance. The mixture was processed on three roll mill (EXAKT 80E, EXAKT Technologies Inc.) to disperse the MWCNTs within the epoxy matrix. The neat epoxy matrix and modified epoxy matrix were heated up to 70^0C for 20 min in a vacuum oven to remove air bubbles. Unidirectional glass fibers were wetted with the neat and modified epoxy matrix by hand lay-up on the aluminum mould to make glass/epoxy plates and glass/epoxy/0.3wt% MWCNT plates. The composite plates were cured using an autoclave.

6.1.2.3 In-plane strain measurements

Conventional metallic strain gauges (Vishay micro measurements C2A-06-125LT-350) purchased from Intertechnology were used to measure in-plane strain.

6.1.2.4 Mechanical characterization

The tensile and shear properties for glass fiber/epoxy composite laminates unfilled and filled with 0.3wt%MWCNT were experimentally measured in both longitudinal and transverse directions in accordance with ASTM D 3039 M-07 and ASTM D3518M respectively. The mechanical tests were performed with the standard head displacement rate of 1.27 mm/min at room temperature. Five samples were tested to determine each mechanical property and the average value was made over five measurements. The experimental set-up and typical transverse failure for glass fiber/epoxy laminates unfilled and filled with 0.3wt% MWCNT are shown in Figures 6.1a and 6.1b respectively.

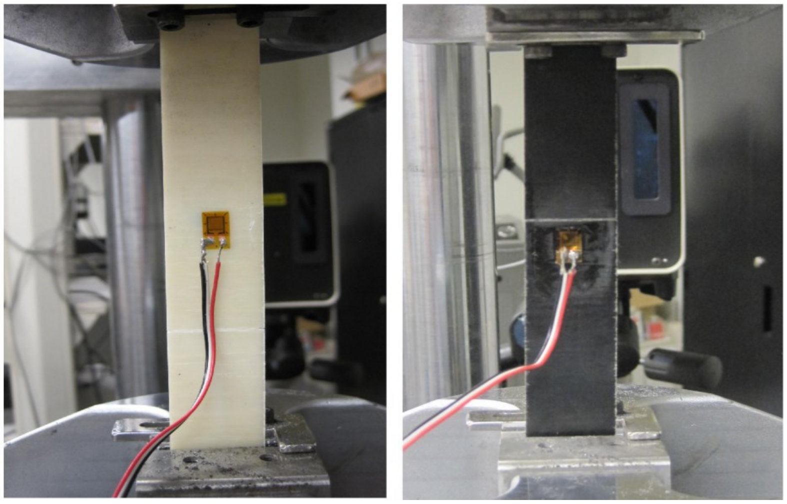

a) b)

Figure 6.1: Experimental set-up for tensile testing of coupons showing typical transverse (90^0) failure for samples a) Unfilled and b) Filled with 0.3wt% MWCNT

The measured properties for both composites (without and with MWCNT) with 60% fiber volume fraction (V_f) are shown in Table 6.1. From the experimental results, it is observed that the mechanical properties of glass/epoxy composite are enhanced a little (but not significantly) by adding 0.3wt%MWCNT.

Table 6.1: Measured mechanical properties of both glass fiber/epoxy composites without and with 0.3wt% MWCNT with 60% fiber volume fraction based on ASTM D 3039 M-07 and ASTM D3518M

Material Type	Measured properties	Number of sample	Average	STD of sample	CV(%) of sample
Glass fiber /epoxy composite	E_1 (GPa)	5	47.2	0.8	1.69
	X_1^T (MPa)	5	1391.1	62.81	4.51
	E_2 (GPa)	5	11.72	0.75	6.4
	X_2^T (MPa)	5	38.3	1.65	4.31
	ϑ_{12}	5	0.28	0.01	3.57
	G_{12} (GPa)	5	4.1	0.2	4.88
	S_6 (MPa)	5	91.7	2.05	2.24
Glass fiber/ epoxy/ 0.3w% CNT composite	E_1 (GPa)	5	49.4	1.1	2.23
	X_L^T (MPa)	5	1444.4	71.39	4.94
	E_2 (GPa)	5	12.4	1.08	8.71
	X_2^T (MPa)	5	40.1	2.27	5.66
	ϑ_{12}	5	0.28	0.01	3.57
	G_{12} (GPa)	5	4.22	0.33	7.81
	S_6 (MPa)	5	97.2	4.44	4.56

6.1.3 Analysis

When a composite laminate is subjected to uniaxial tension, its thickness changes due to Poisson coupling. This gives rise to the TTS. The magnitude of the TTS depends on the stacking sequence. It was desirable to have the largest TTS for a certain uniaxial stress. For this, classical laminate theory (CLT) [105] was used to determine the laminate stacking sequence that gives rise to maximum TTS.

6.1.3.1 Formulation of ATTS for symmetric laminate subjected to in-plane loads

When a composite laminate is subjected to in-plane loads, plane stress assumption in CLT states that the stresses $\sigma_3, \tau_{13}, \tau_{23}$ in the principal material coordinate system are small and negligible. Therefore, the three-dimensional stress-strain relation in plane stress condition for a ply is simplified to the following:

$$\begin{Bmatrix} \varepsilon_1 \\ \varepsilon_2 \\ \varepsilon_3 \\ \gamma_{23} \\ \gamma_{13} \\ \gamma_{12} \end{Bmatrix} = \begin{bmatrix} S_{11} & S_{12} & S_{13} & 0 & 0 & 0 \\ S_{12} & S_{22} & S_{23} & 0 & 0 & 0 \\ S_{13} & S_{23} & S_{33} & 0 & 0 & 0 \\ 0 & 0 & 0 & S_{44} & 0 & 0 \\ 0 & 0 & 0 & 0 & S_{55} & 0 \\ 0 & 0 & 0 & 0 & 0 & S_{66} \end{bmatrix} \begin{Bmatrix} \sigma_1 \\ \sigma_2 \\ 0 \\ 0 \\ 0 \\ \tau_{12} \end{Bmatrix} \tag{6.1}$$

From Eq. (6. 1), through-thickness strains $\varepsilon_3, \gamma_{13}, \gamma_{23}$ are given by

$$\varepsilon_3 = S_{13}\sigma_1 + S_{23}\sigma_2, \ \gamma_{13} = 0, \ \gamma_{23} = 0 \tag{6.2}$$

Eq. (6. 2) shows that the extensional strain is not zero and can be computed directly from the in-plane stresses σ_1 and σ_2 and the compliances S_{13} and S_{23}. Because ε_3 is not zero, a layer in a state of plane stress experiences a change in thickness, Δh, which is expressed by:

$$\Delta h = \varepsilon_3 h \tag{6.3}$$

h is the thickness of the layer. Eqs. (6. 2) and (6. 3) for ε_3 and Δh are independent of whether the layer is within a laminate or is isolated by itself. In fact, in order to indicate that the above expressions for ε_3 and Δh are valid for any layer, specifically the kth layer, the expressions can be rewritten as:

$$\varepsilon_{3k} = S_{13}\sigma_{1k} + S_{23}\sigma_{2k} \ , \Delta h_k = \varepsilon_{3k} h_k \tag{6.4}$$

Hence, by computing the thickness change of each layer, the total change in laminate thickness can be calculated by summing the various layer thickness changes. Therefore, the total thickness change of an N-layer laminate (ΔH) is expressed by:

$$\Delta H = \sum_{k=1}^{N} \Delta h_k \tag{6.5}$$

ATTS for an N-layer laminate $\bar{\varepsilon}_z$ can be calculated by summing the change in the thicknesses of the individual layers divided by the original laminate thickness of the (H) as:

$$\bar{\varepsilon}_z = \frac{\Delta H}{H} = \frac{1}{H}\sum_{k=1}^{N}(S_{13}\sigma_{1k} + S_{23}\sigma_{2k}) \ h_k \tag{6.6}$$

Where

$$H = \sum_{k=1}^{N} h_k \tag{6.7}$$

From Eq. (6. 4), it is necessary to have the on-axis stresses on each layer to calculate ATTS. The laminate constitutive relations for a symmetric laminate subjected to only in-plane loads N_x, N_y, N_{xy}, in the absence of thermal and moisture effects can be written as:

$$\begin{Bmatrix} N_x \\ N_y \\ N_{xy} \end{Bmatrix} = [A] \begin{Bmatrix} \overset{\circ}{\varepsilon}_x \\ \overset{\circ}{\varepsilon}_y \\ \overset{\circ}{\gamma}_{xy} \end{Bmatrix} \tag{6.8}$$

Off-axis strains are achieved by the following equation:

$$\begin{Bmatrix} \overset{\circ}{\varepsilon}_x \\ \overset{\circ}{\varepsilon}_y \\ \overset{\circ}{\gamma}_{xy} \end{Bmatrix} = [a] \begin{Bmatrix} N_x \\ N_y \\ N_{xy} \end{Bmatrix} \tag{6.9}$$

Where $[a] = [A]^{-1}$ and [A] is the laminate stiffness and A_{ij}'s are defined as:

$$A_{ij} = \sum_{k=1}^{N} \bar{Q}_{ij} (z_k - z_{k-1}) \tag{6.10}$$

Where $\bar{Q}_{ij}$ refers to off-axis reduced stiffness. By obtaining the mid-plane off-axis strains from Eq. (6. 9), the off-axis stresses of each layer are calculated as:

$$\begin{Bmatrix} \sigma_x \\ \sigma_y \\ \tau_{xy} \end{Bmatrix} = \begin{bmatrix} \bar{Q}_{11} & \bar{Q}_{12} & \bar{Q}_{16} \\ \bar{Q}_{12} & \bar{Q}_{22} & \bar{Q}_{26} \\ \bar{Q}_{16} & \bar{Q}_{26} & \bar{Q}_{66} \end{bmatrix} \begin{Bmatrix} \overset{\circ}{\varepsilon}_x \\ \overset{\circ}{\varepsilon}_y \\ \overset{\circ}{\gamma}_{xy} \end{Bmatrix} \tag{6.11}$$

The on-axis stresses or stresses in the principal material coordinate system can be obtained by a transformation on off-axis stresses Eq. (6. 11):

$$\begin{Bmatrix} \sigma_1 \\ \sigma_2 \\ \tau_{12} \end{Bmatrix} = \begin{bmatrix} m^2 & n^2 & 2mn \\ n^2 & m^2 & -2mn \\ -mn & mn & m^2 - n^2 \end{bmatrix} \begin{Bmatrix} \sigma_x \\ \sigma_y \\ \tau_{xy} \end{Bmatrix} \tag{6.12}$$

Where $m = \cos\theta$ and $n = \sin\theta$, finally the ATTS is calculated by substituting the obtained on-axis stresses for each layer from Eq. (6. 12) into Eq. (6. 6).

6.1.3.2 Determination of the lay-up sequence with large theoretical ATTS

In order to select a laminate that exhibits large ATTS when it is subjected to in-plane loads for experimentation, using values from Table 6.1, the above formulation was used.

The thickness of each layer of the laminate is measured to be 0.12 mm for the analysis. A computer program was written to calculate ATTS. It should be noted that ϑ_{23}=0.428 and G_{23}=3.28 (GPa) [105] are assumed for the analysis. Figure 6.2 shows variations of ATTS for the $[0_5,\theta_{n\ (n=6,\ldots,10)},\ 0_5]$ composite laminate with fiber orientations (θ) ranging from 0^0 to 90^0. Note that the selected laminate should be sufficiently thick so that strain gauge can be placed on its edge to measure TTS. It is observed from Figure 6.2 that the magnitude of ATTS increases gradually with increase in the degree of fiber orientations (θ). Also the magnitude of ATTS decreases as the number of layers in the composite laminate increases. The largest ATTS is achieved with $\theta = 90^0$. The $[0_5,\ 90_8,0_5]$ composite laminate was selected since it can give large ATTS and at the same time has adequate thickness for strain gauge application.

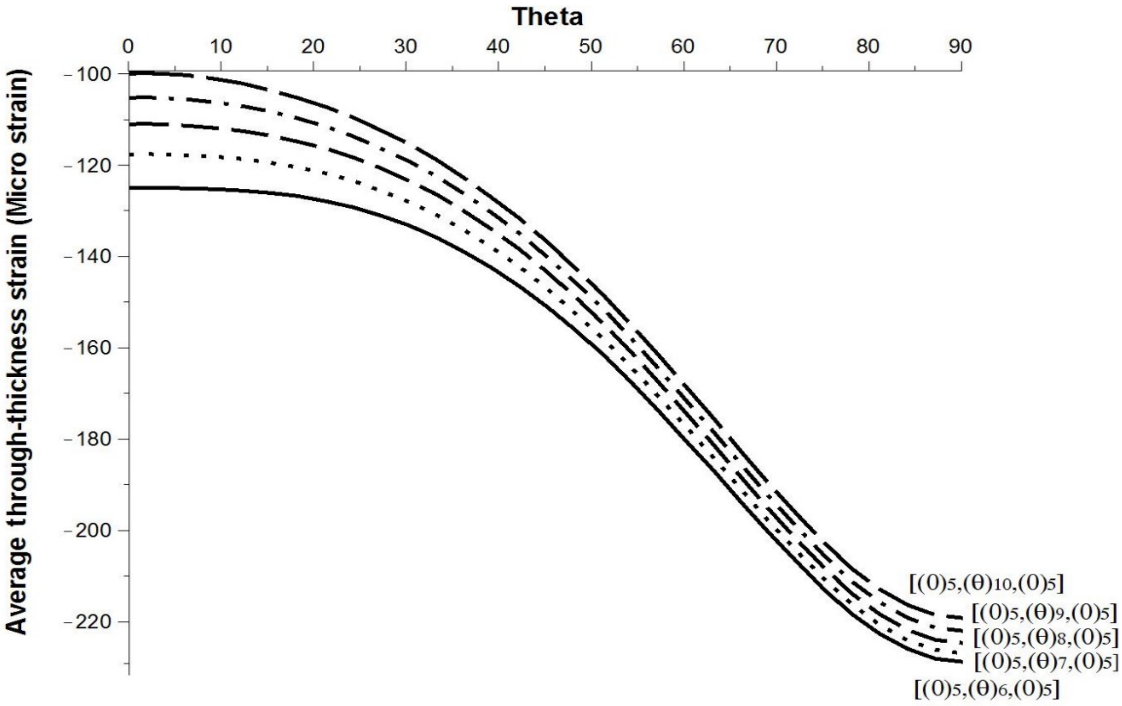

Figure 6.2: Analysis results for $[0_5,\ \theta_{n\ (n=6,\ldots,10)},0_5]$ laminate under N_x= 43.307 KN

6.1.4 Experimental methods

6.1.4.1 Fabrication of the [0_5, 90_8, 0_5] laminate

Two plates were made. Fiber volume fractions of plate 1 and 2 are calculated to be about 60% and 66% respectively. ASTM standard D 3039 M-07 was used. Average thickness of samples cut from plates 1 and 2 are shown in Table 6.2. The average thickness of samples is determined by making an average over fifteen measurements for each sample.

Table 6.2: Average thickness of samples

Plate Number	V_f	Samples	Average thickness (mm)
[0_5, 90_8, 0_5] plate 1	$V_f = 60\%$	Sample 1	2.16 ± 0.045
		Sample 2	2.09 ± 0.081
		Sample 3	2.12 ± 0.064
[0_5, 90_8, 0_5] plate 2	$V_f = 66\%$	Sample A	2.02 ± 0.041
		Sample B	1.98 ± 0.077
		Sample C	1.96 ± 0.053

6.1.4.2 Quality controls

Quality controls of the samples were carried out using Hitachi S-4700 Scanning electron microscopy (SEM). Figure 6.3 shows a sample SEM of the edge of the laminate. The SEM image is taken at the location where the strain gauge was mounted. Figure 6.3 indicates that no crack exists which reveals high quality laminate.

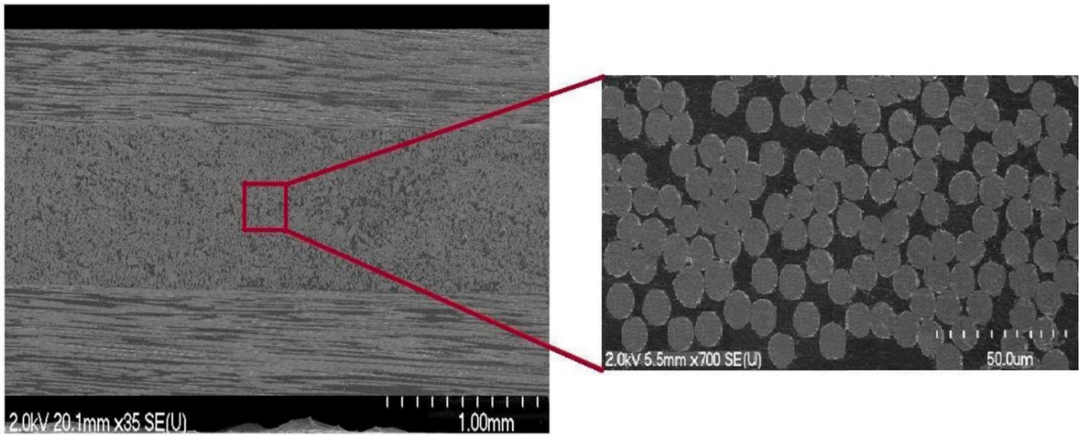

Figure 6.3: SEM of laminate section

6.1.4.3 Sample specification, arrangement of electrical connections and strain gauge

Tabs were bonded at both ends of the tensile sample to prevent the gripping damage and slipping while performing the tensile test. Six conductive electrical contact points made from silver-epoxy paste were mounted on the top (T) and bottom (B) surfaces of the tensile sample. Then electrical wires were attached to silver-epoxy paste on both surfaces of the sample to make electrodes for electrical resistance measurement. For measuring ATTS, a small strain gauge (1.9 mm long) was bonded on the thickness section of the sample. The dimensions and arrangements of electrical connections and bonded strain gauge on the tensile sample are shown in Figure 6.4.

6.1.4.4 Electrical resistance measurements

TTER measurements were carried out by the two-probe method using Agilent digital Multimeter (34401A). Electrical resistance change (ERC) is calculated according to Eq. (2. 6).

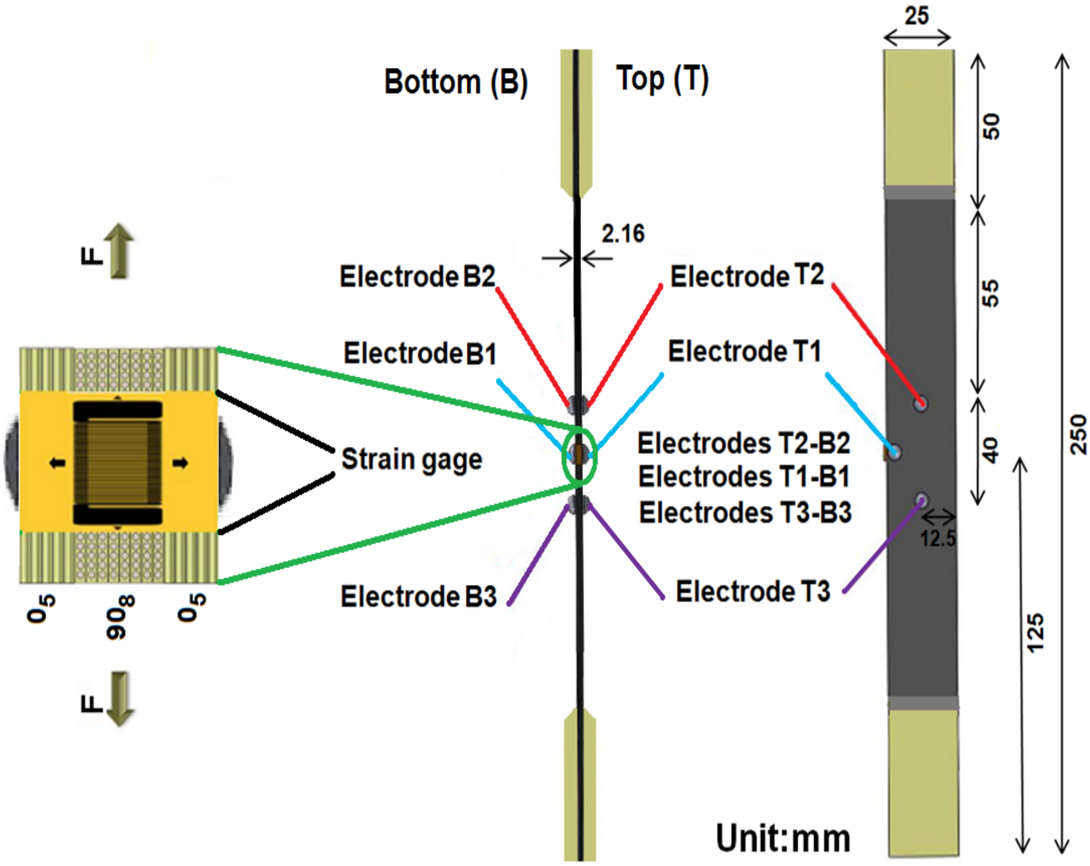

Figure 6.4: Schematic illustration of dimensions and locations of strain gauge and electrical contact points

6.1.4.5 Average through-thickness strain (ATTS) measurement

ATTS measurement was performed using conventional metallic strain gauge (L1E-350K-PC06-LE) from MFL Company [106]. The length of the copper wire in the strain gauge is 0.74 mm. However there is a backing required for bonding with the substrate. The length of the backing is 1.9 mm (the thickness of the sample was about 2.16 mm, which is adequate). The accuracy of these gages is 3%, as provided from the manufacturer. As such the strain gauge only measures the strain over the 90° layers (which is about 0.96 mm thick), and not over the whole thickness of the composite sample (see Figure 6.4).

6.1.5 Tensile tests along x direction

The tensile sample was mounted in the grips of a 100 KN-MTS mechanical testing machine and monotonically loaded in tension, to a maximum value of 1100N. Tensile tests were performed for six samples with a rate of 0.127 mm/min while monitoring TTERs and ATTS simultaneously. Figure 6.5 shows the arrangement for the measurement of TTER and ATTS by strain gauge.

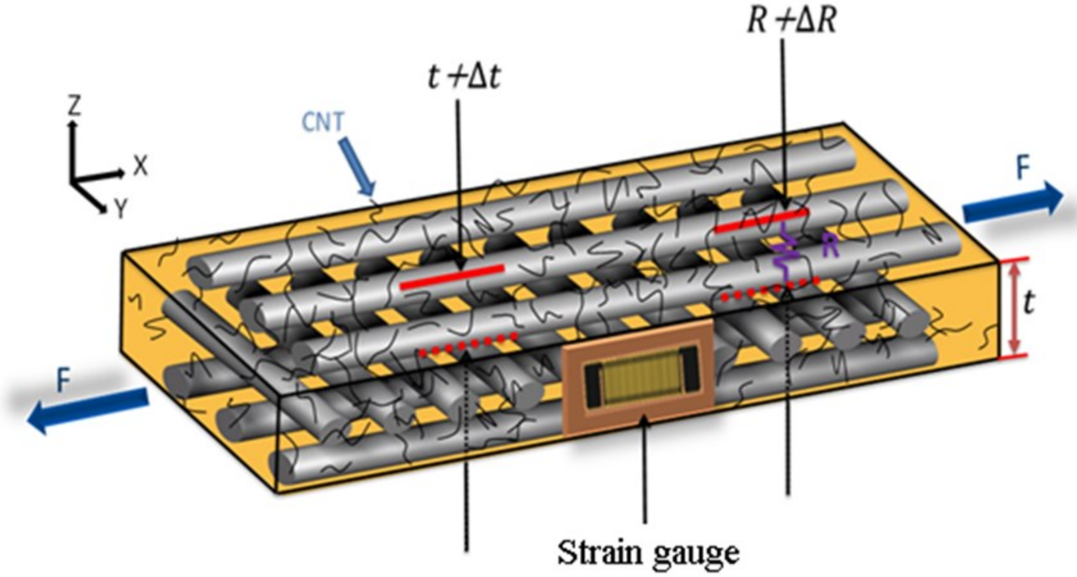

Figure 6.5: Schematic illustration of cross ply glass fiber/epoxy/CNT composite laminate showing out-of-plane deformation and change in through-thickness electrical resistance while it is loaded

The applied loads, measured strain and electrical resistance in real-time are simultaneously recorded using MTS machine, strain gauge conditioner (2120A), power supply (2111) and Agilent machine (34401A) respectively as shown in Figure 6.6.

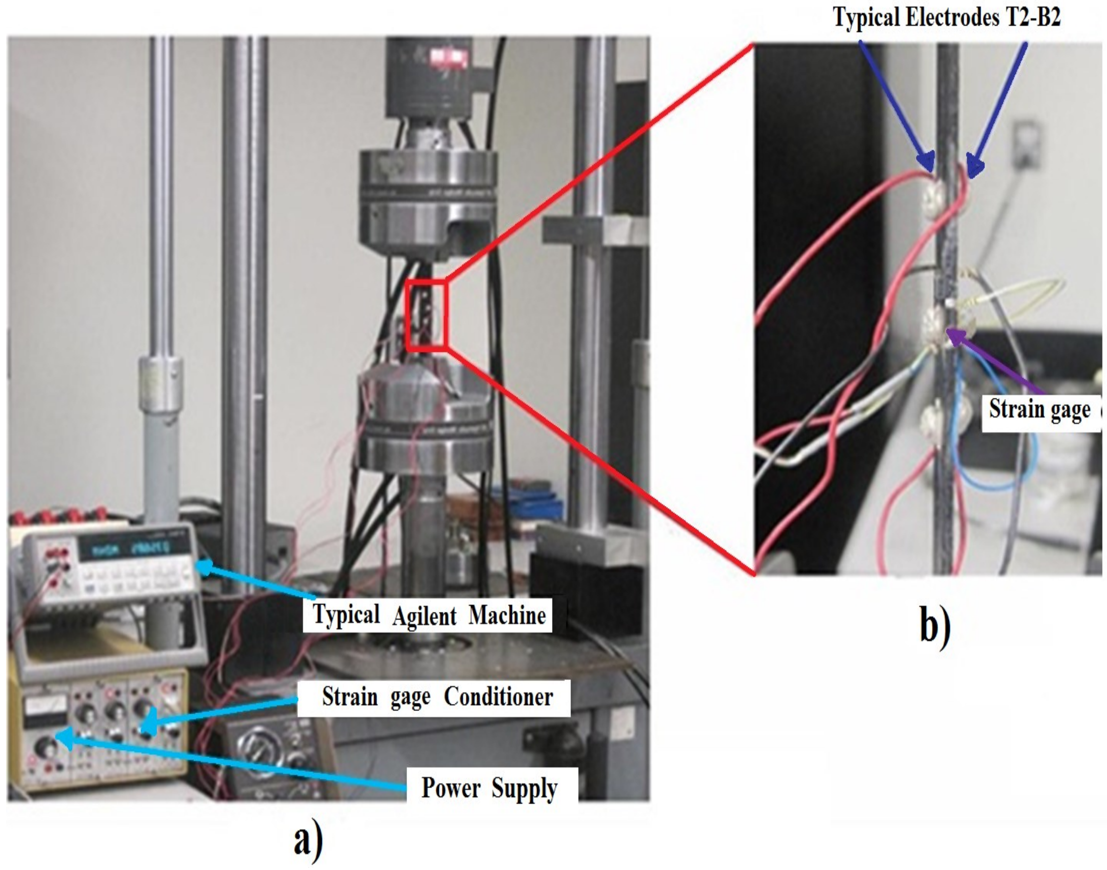

Figure 6.6: Experimental set-up for tensile test: a) Sample mounted on MTS machine and measurements system. b) Close-up view of strain gauge and electrodes bonded to sample through-thickness

6.1.5.1 Results and discussion for tensile loading (x direction) while measuring strain and resistance (z direction)

TTERs and ATTS of the $[0_5, 90_8, 0_5]$ sample with dimensions (250 mm × 25 mm × 2.16 mm) and ($V_f = 60\%$) were measured simultaneously while tensile load was applied. The ATTS over 90^0 layers localized at the center of the laminate was measured using strain gauge and was calculated from analysis based on CLT [105]. These are plotted in Figure 6.7. Good correspondence is obtained.

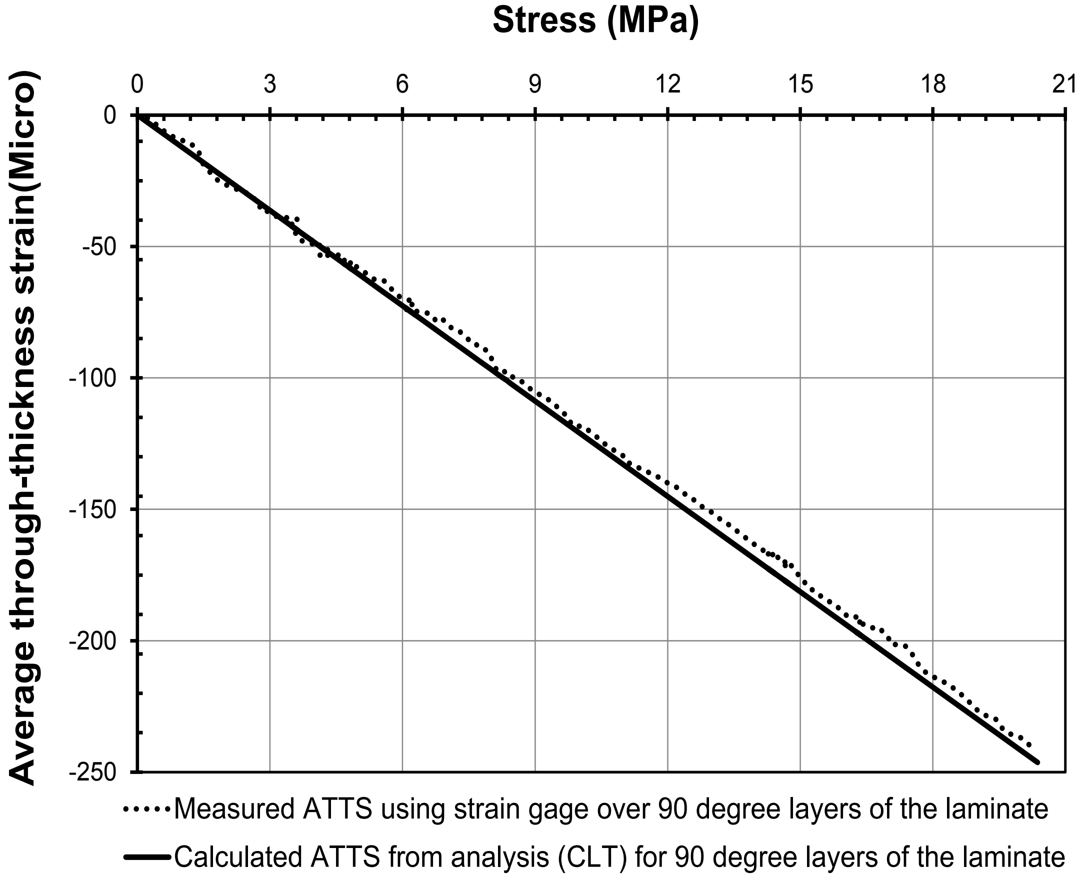

Figure 6.7: Tensile result, showing ATTS over 90^0 layers of $[0_5, 90_8, 0_5]$ versus stress

Since the strain gauge is not able to measure ATTS of the whole thickness of the laminate edge due to its gauge length limitation while the TTER measurement is performed over the whole thickness of laminate, analysis was carried out to calculate ATTS for the total thickness based on CLT. The change in electrical resistance was calculated based on Eq. (2.6). It can be seen from Figure 6.8 that the magnitude of ATTS obtained from analysis and ERC measured for the entire laminate thickness increase as stress increases. However their signs are different. Strains are negative while electrical resistance changes are positive. The negative sign of ATTS is to be expected due to the Poisson coupling effect.

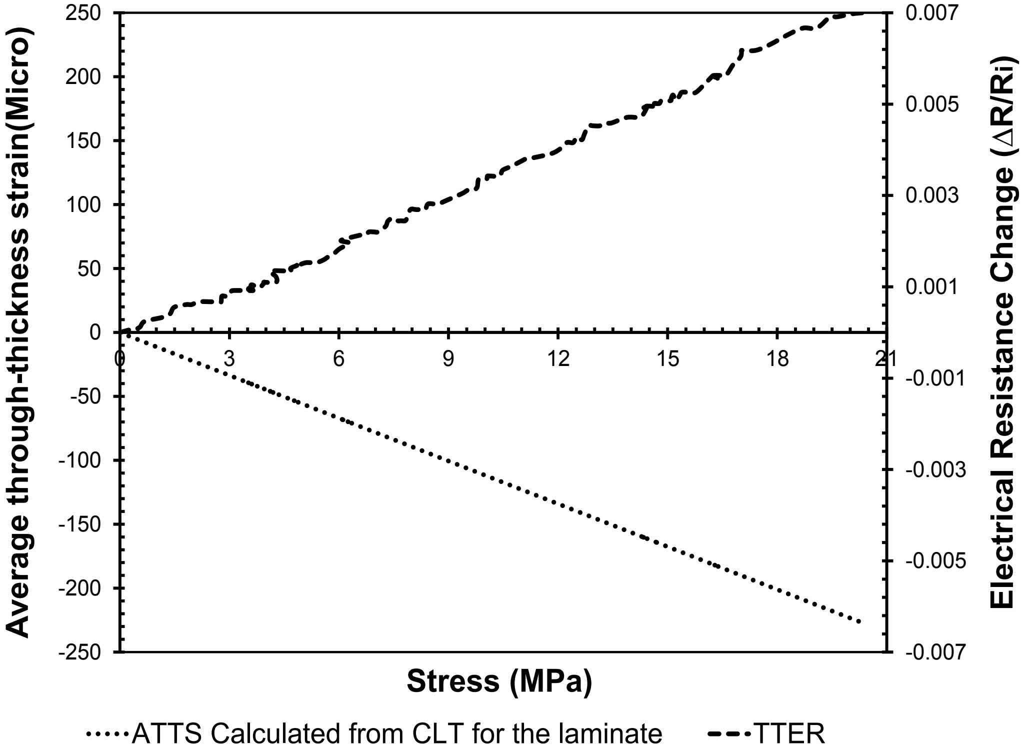

Figure 6.8: Variation of ATTS calculated from CLT for the laminate and TTER versus tensile stress along axial direction (initial electrical resistance at the electrodes T1-B1: 165,510 ohms)

When the laminate is subjected to tensile stress, the laminate thickness is expected to reduce due to Poisson coupling effect. This is reflected in the negative strains. Normally, one would expect that as the thickness is reduced it would result in smaller electrical resistance (or negative change in electrical resistance). However this is not what is observed. A closer examination is necessary.

From Ohm's law, the electrical resistance *R* is given by the equation:

$$R = \rho \frac{L}{A} \quad \textbf{(6.13)}$$

Where ρ is electrical resistivity, L is the distance over which the electrical resistance is determined and *A* is the cross sectional area.

In the case of electrical resistance across the thickness of the laminate, *L* is thickness *t*. One can assume that the cross section *A* does not change during tensile loading in the plane of the sample. If the resistivity does not change, then a reduction in *t* would result in a reduction in R. The fraction of the change in electrical resistance is given as:

$$\frac{\Delta R}{R} = \frac{R_2 - R_1}{R_1} = \frac{t_2 - t_1}{t_1} = \varepsilon \tag{6.14}$$

Where ε is the ATTS.

Figure 6.8 shows the ATTS of about -227 με (-2.27×10^{-4}) at a stress of 20.37 (MPa). At the same time, the ratio of the change in electrical resistance (ΔR/R) at 20.37 (MPa) in Figure 6.8 is about +0.007 (7×10^{-3}). The ratio between the TTER change and ATTS is – 30.8. This indicates that TTER is more sensitive than ATTS. However, the sign of the ratio is negative which means that TTER increases while the thickness decreases. As such TTER change may not be due only to the reduction in thickness. In order to examine the effect of transverse compression in thickness direction on TTER, further thicknesswise compression test was performed.

6.1.6 Compression test across the thickness of sample

In order to check to see if the reduction in sample thickness may give rise to the change in electrical resistance, an experiment was carried out to investigate the effect of compressive load across the laminate thickness on TTER. The details of the experimental set up are schematically illustrated in Figure 6.9. An L-shaped piece made of electrically non-conducting glass fiber/epoxy composite was used to support and to insulate the electrically conductive laminate from metallic grip and also to prevent bending of the laminate.

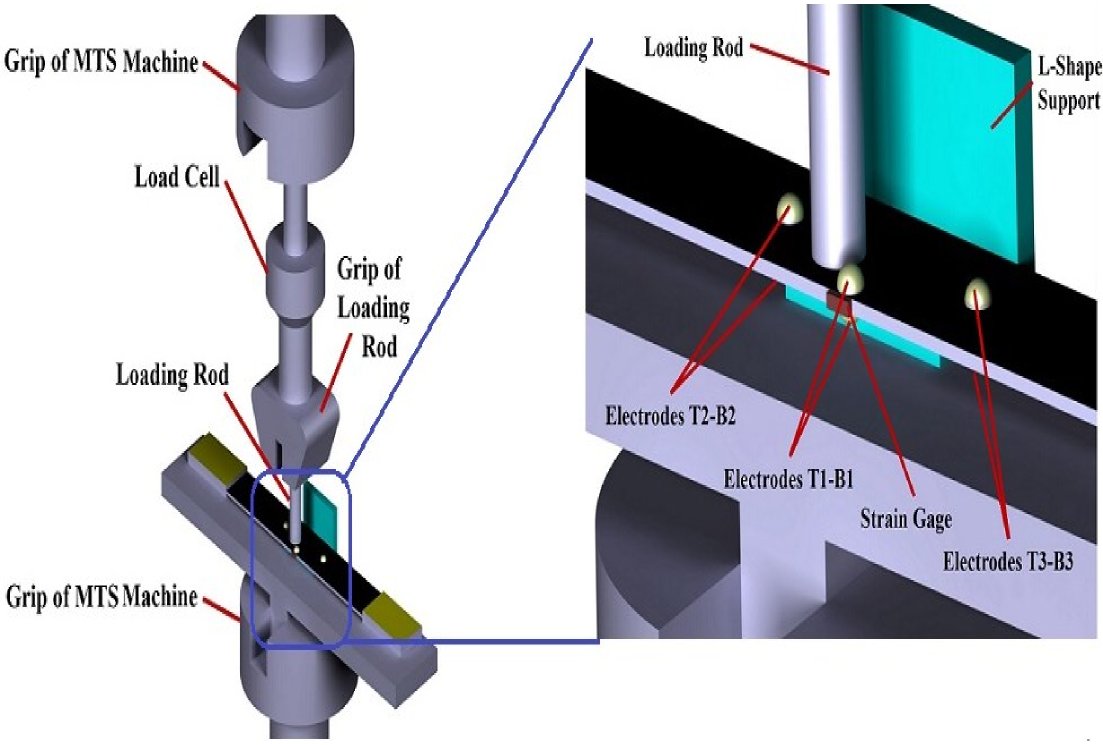

a) **b)**

Figure 6.9: Thicknesswise compression test setup a) Sample placed on MTS machine with load cell to apply compressive load. b) Close-up view of L-shaped support, electrodes and strain gauge bonded to sample and location of loading rod with diameter of 12.7mm

6.1.6.1 Results and discussion for thicknesswise compression tests (z direction) while monitoring resistances and strain (z direction)

Figure 6.10 indicates relation between TTER and ATTS measured by strain gauge versus stress. It is observed that compressive stress in the thickness direction produces negative strains and negative change TTERs. The above indicates that a reduction in thickness of the sample results in reduction in through-thickness electrical resistance (TTER). At the same time, a tensile stress along the x direction results in an increase in TTER.

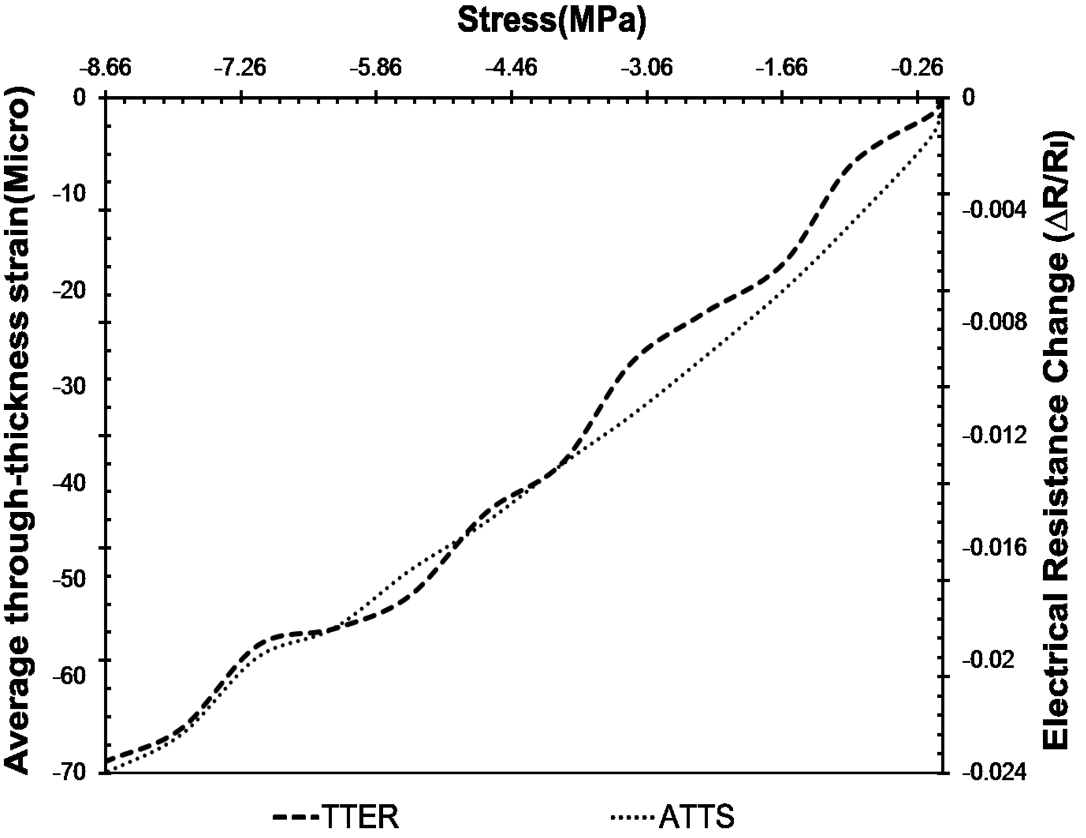

Figure 6.10: Thicknesswise compressive load result showing ATTS and TTER versus stress (initial electrical resistance at the electrodes T1-B1:169,100 ohms))

Figure 6.11a illustrates the hypothesis that the application of a tensile load along the x direction would produce a reduction in the thickness (z direction) due to Poisson coupling. This reduction in thickness gives rise to negative average through-thickness strain (ATTS). This reduction in thickness was thought to reduce the distance between the crossing CNTs. This in turn would reduce the tunneling resistance between the crossing CNTs and should reduce the through-thickness electrical resistance (TTER). However an increase in TTER was observed. One explanation for this increase in TTER can be the separation of the CNTs due to lengthwise load as shown in Figure 6.11b.

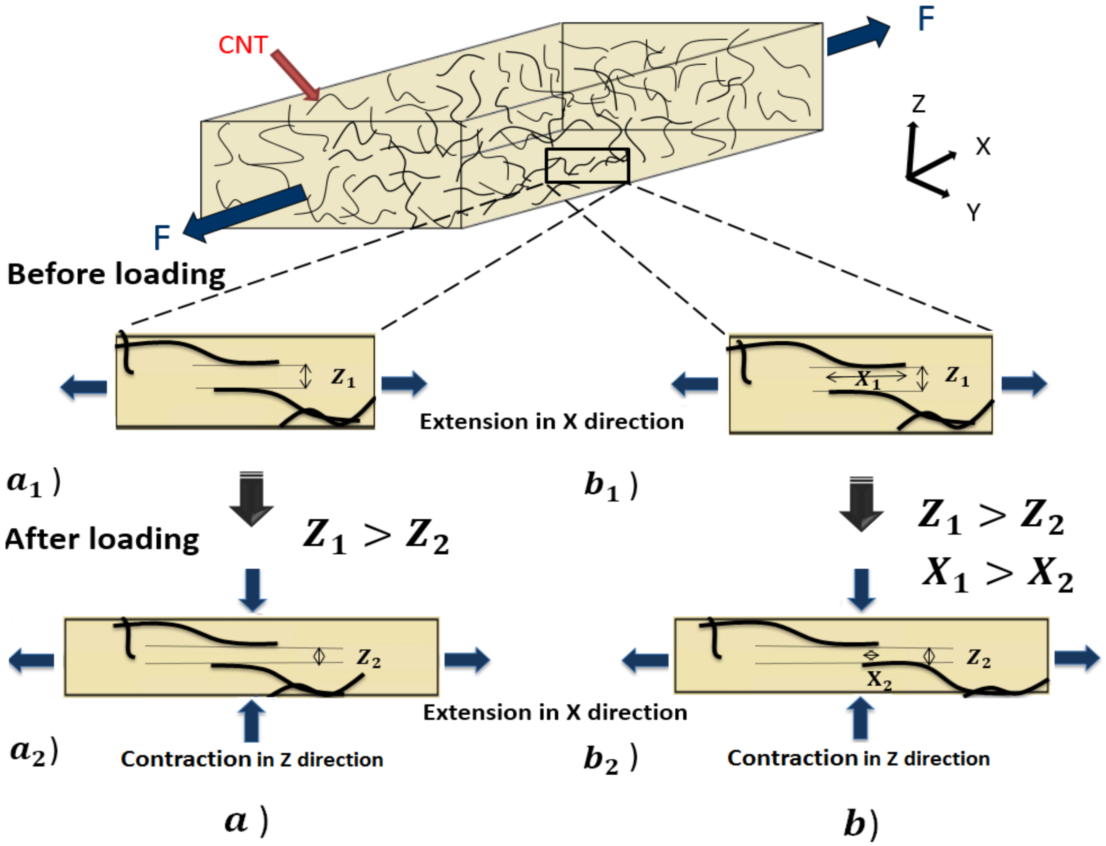

Figure 6.11: Poisson coupling reduces the laminate thickness. Schematic illustrating a) Reduction of the tunneling distance between crossing CNTs (a_1 and a_2 before and after loading), b) One possible explanation for the increase in TTER (b_1 and b_2 before and after loading)

6.1.7 Conclusions

In this work, a new method was attempted for in situ monitoring of ATTS in glass fiber/epoxy composite laminates using MWCNT. It was observed that the TTER are proportional to the change in ATTS. As such, the addition of CNTs in glass fiber/epoxy composite laminates and measuring the TTER may be used as a new method for the measurement of the TTSs, particularly at locations away from the free edges of the sample. However the reduction in the TTER due to lengthwise loads requires more work to explain. It was expected that with the application of a uniaxial stress along the x direction, a reduction in thickness (compressive strain along the thickness direction) causes the change in resistance along the thickness direction to be negative (meaning reduction in resistance). The reason for this expectation is that a reduction in the thickness direction would bring the CNTs closer, thus would increase in the number of electrical contacts and/or reduce the tunneling gaps. However the opposite is observed (resistance along the thickness direction actually increases). Further work was carried out to investigate this phenomenon.

6.2 Electrical resistance behavior of Glass fiber/Epoxy/CNTs composite laminates subjected to multi-directional deformation

An interesting behavior is observed on the electrical resistance across the thickness of glass fiber/epoxy/CNT laminate when the laminate is subjected to uniaxial stress along its length. The electrical conductivity of the laminate containing CNT relies on two mechanisms: One is the conductivity along the connecting networks of CNTs by electron transfer. The other is the electron tunneling conductivity by the jumping of electrons across the gap (made of polymeric material) from one nanotube to the adjacent nanotube when these gaps are small enough [107]. If the gap between the nanotubes is smaller, it is expected that the electrons jumping would be easier, thus facilitating tunneling conduction and this can result in lower electrical resistance. For a glass/epoxy/CNT laminate subjected to a uniaxial tensile load along the x direction, Poisson coupling between the x and z direction would result in a reduction in thickness (z direction). One would expect that this would translate into shorter tube-to-tube gap distance and this may result in lower electrical resistance along the thickness direction. However this is not the case and actually the opposite was observed. Additional experimentations were performed where loadings along different directions were imposed on the laminate and electrical resistances were measured. An explanation is provided for this behavior. The results from these simple experiments and the proposed explanation can provide insight into the effect of the motion of the nanostructure on the macro electrical resistance behavior of laminate containing CNT when the laminate is subjected to multi-directional deformation.

6.2.1 Experiments

Uniaxial compression along the x direction and four-point bending loads were applied while ATTS and TTER of samples were measured simultaneously.

6.2.1.1 Compression test along the x direction

The lay-up sequence $[0_5/90_8/0_5]$ for glass fiber/epoxy/CNT composite was found to give the largest ATTS using classical lamination theory. This laminate has 18 layers (2.16 mm) that is sufficiently thick to allow the application of a small strain gauge to measure strain along the thickness direction [92]. ASTM standard D3410 was employed to prepare sample for lengthwise compression test. Tabs were attached at both ends of the

$[0_5, 90_8, 0_5]$ sample with dimensions (142.5 mm × 25 mm × 2.16 mm). Four conductive electrical contact points made from silver-epoxy paste were bonded on the top (T) and bottom (B) surfaces of the sample. Then wires were attached to silver-epoxy paste on both surfaces of the sample to make electrodes for electrical resistance measurements. A strain gauge was attached to the edge of the sample. The details of the sample are schematically shown in Figure 6.12. The experimental set-up of compression test along the length of sample is schematically illustrated in Figure 6.13. In this experiment, a fixture was employed to align the sample placed in the wedge grips which were inserted in the fixture as shown in Figure 6.13.

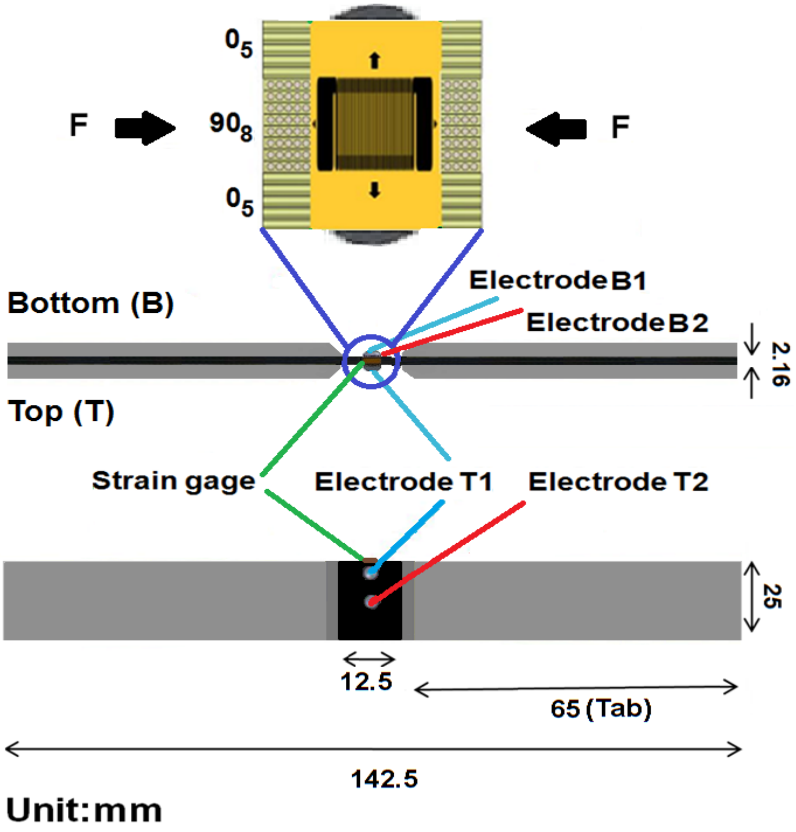

Figure 6.12: Schematic illustration of compressive sample details

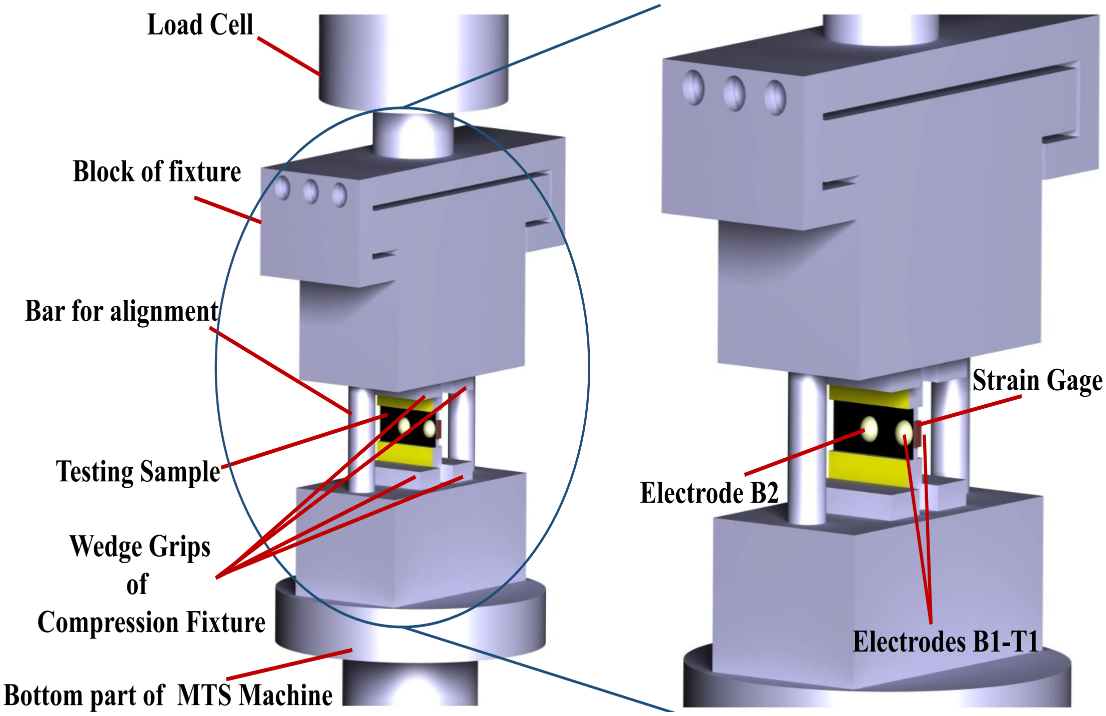

a) **b)**

Figure 6.13: Lengthwise compression test set-up a) Sample placed on MTS machine with compression fixture b) Close-up view of the fixture, electrodes and strain gauge bonded to sample

6.2.1.1.1 Results and discussion for lengthwise compressive loading (x direction) while monitoring electrical resistance and strain (z direction)

The sample was subjected to lengthwise compressive load while ATTS and TTER of the sample were measured simultaneously. Figure 6.14 shows the relation between TTER, and ATTS versus compressive stress. As the magnitude of the stress increases, the ATTS increases. This is to be expected since the thickness is expected to increase due to Poisson coupling effect. However, the change in TTER is becoming more and more negative, which means that the TTER is decreasing.

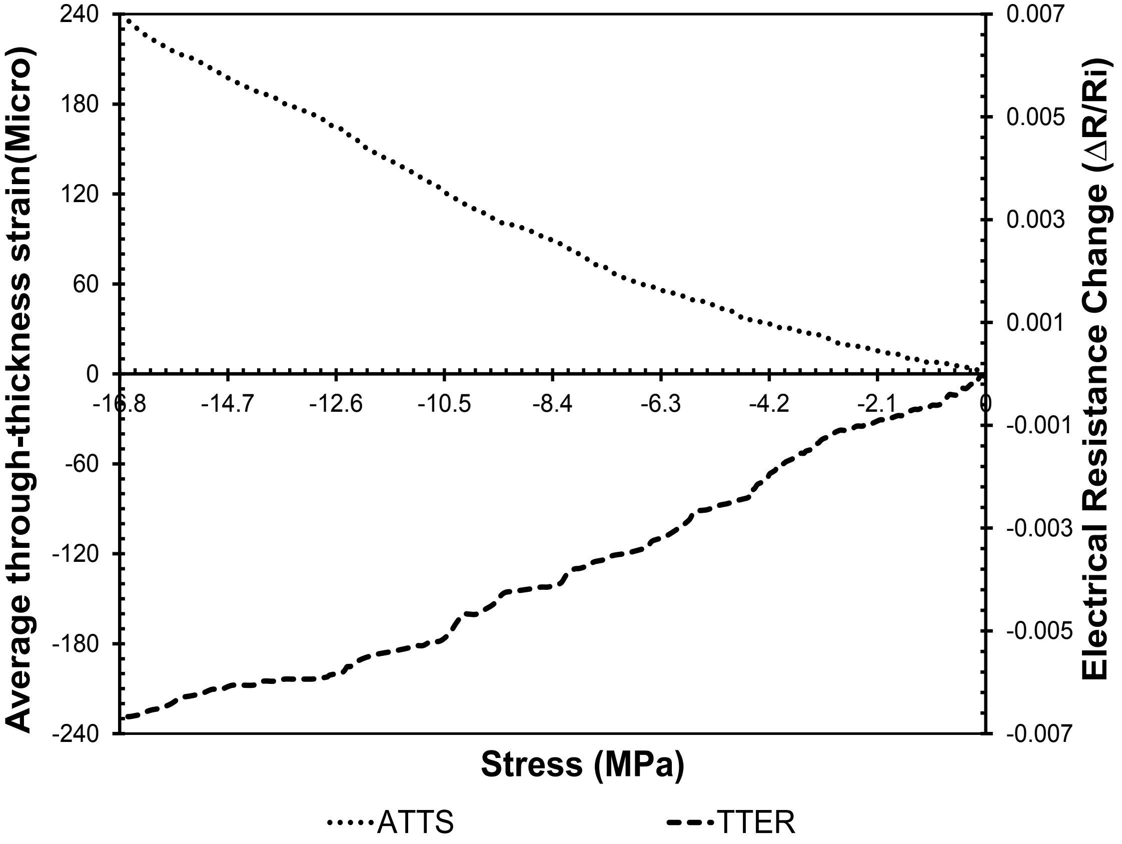

Figure 6.14: ATTS and TTER versus compressive stress along axial direction (initial electrical resistance at the electrodes T1-B1: 167,200 ohms)

6.2.1.2 Four-point bending test

Four-point bending tests were performed in accordance with ASTM standard D7264 M-07. A schematic of the four-point bending set-up and experimental details are illustrated schematically in Figure 6.15. Maximum allowable load that can provide linear (elastic) reign in Load-displacement curve is required. The sample was subjected to four-point bending while in-plane electrical resistances at top and bottom surfaces of the sample and also TTER were measured simultaneously.

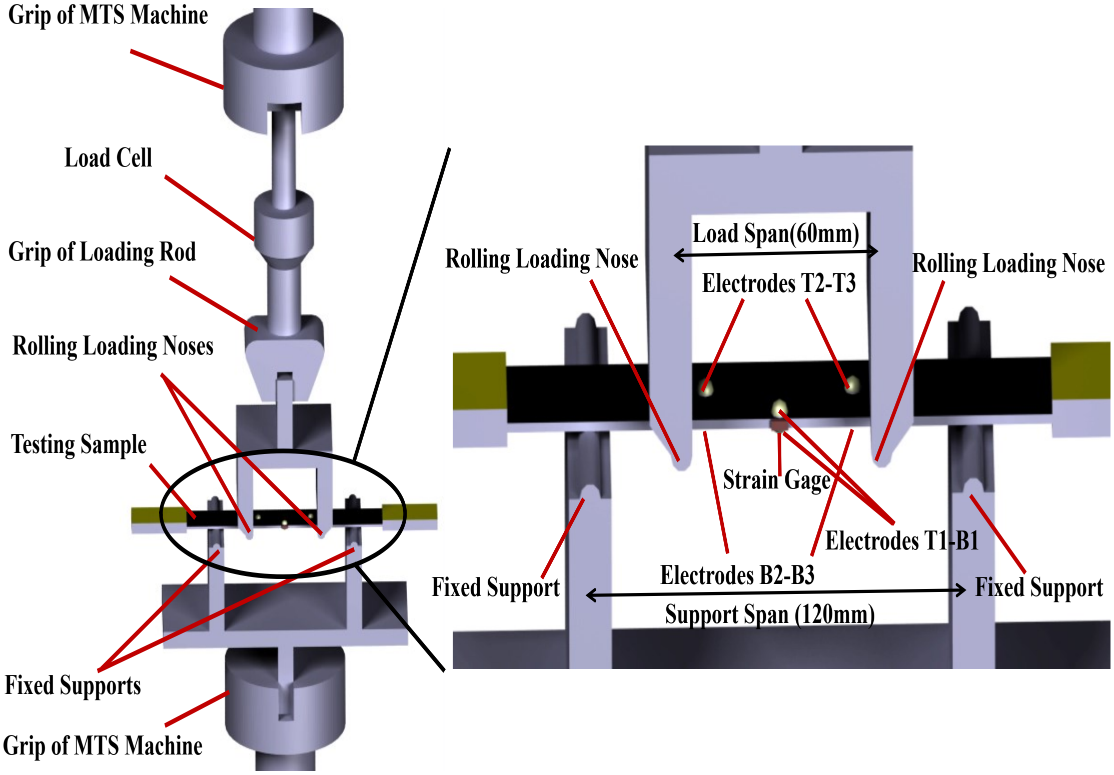

a) b)

Figure 6.15: Four-point bending test set-up a) Sample placed on MTS machine with load cell under four-point bending. b) Close-up view of Load span, support span, electrodes and strain gauge bonded to sample

6.2.1.2.1 Four-point bending test while monitoring displacement and electrical resistance (z direction)

Four-point bending load and change in TTER measured at the edge of the sample versus displacement curves are shown in Figure 6.16. As it can be observed from Figure 6.16, the load and change in TTER increase linearly as displacement increases. A maximum load of 500 N was experimentally determined for the $[0_5/90_8/0_5]$ sample in order to work in the elastic reign.

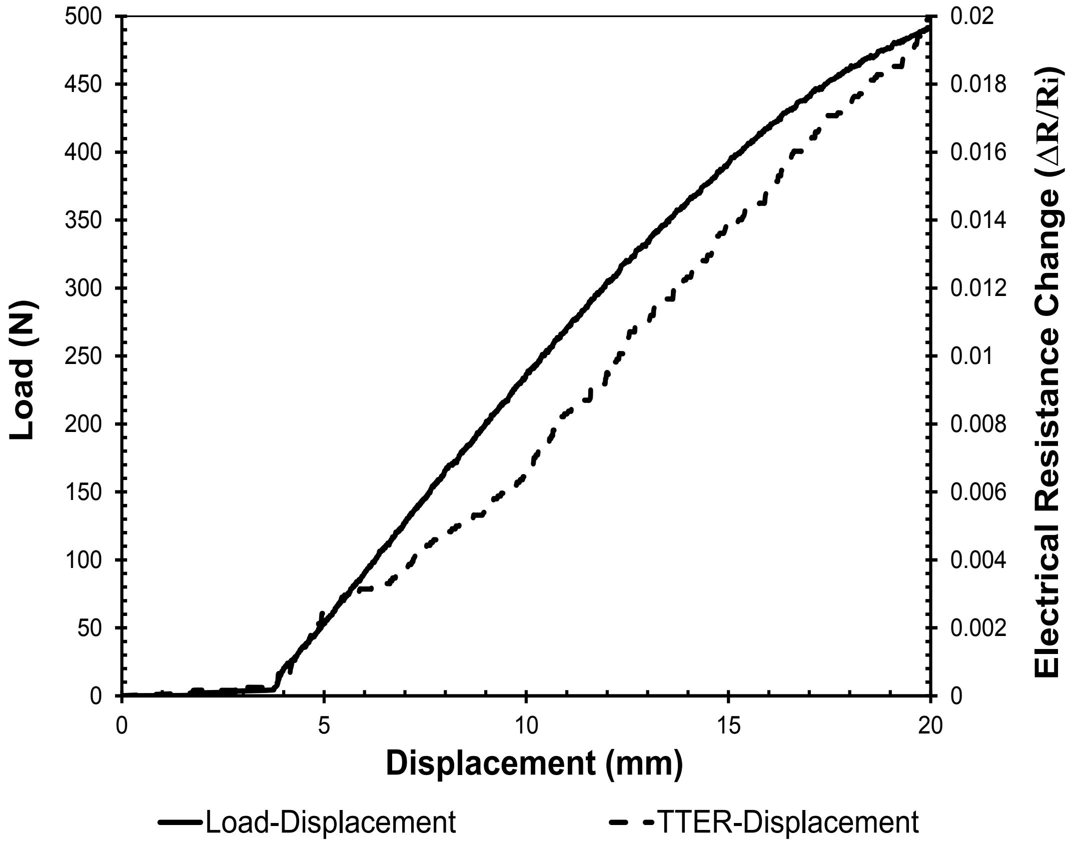

Figure 6.16: Four-point bending test results showing load and change in TTER at the electrodes T1-B1versus displacement curves for the specimen

6.2.1.2.2 Four-point bending test while monitoring in-plane resistances (compression side)

It is clear from Figure 6.17 that the change in in-plane electrical resistance measured on compression side of the sample decreases as the stress increases. This indicates that CNT networks are contracted due to compression. This contraction produces negative change in in-plane electrical resistance.

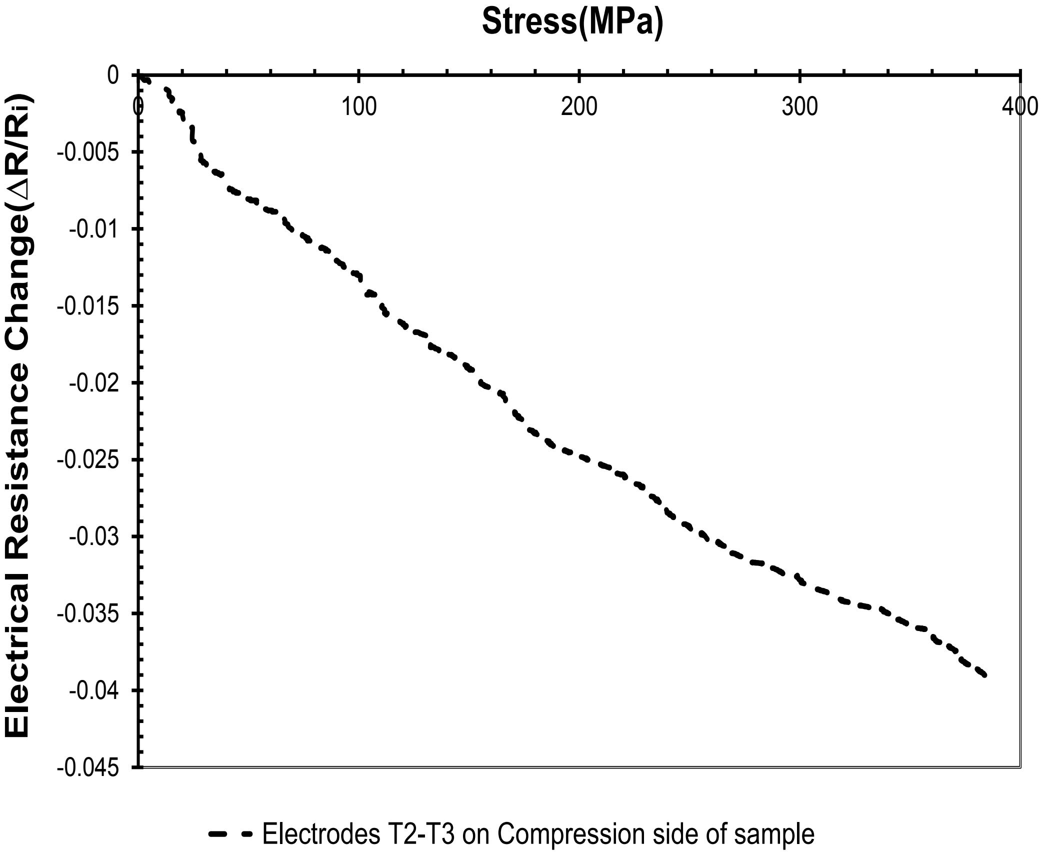

Figure 6.17: Four-point bending test results showing change in in-plane electrical resistance at the electrodes T2-T3 measured on compression side of the sample versus stress

6.2.1.2.3 Four-point bending test while monitoring in-plane resistances (tension side)

Figure 6.18 shows that the change in in-plane electrical resistance measured on tension side of the sample increases as the stress increases. This reveals that CNT networks are extended due to tension. This extension produces positive change in in-plane electrical resistance.

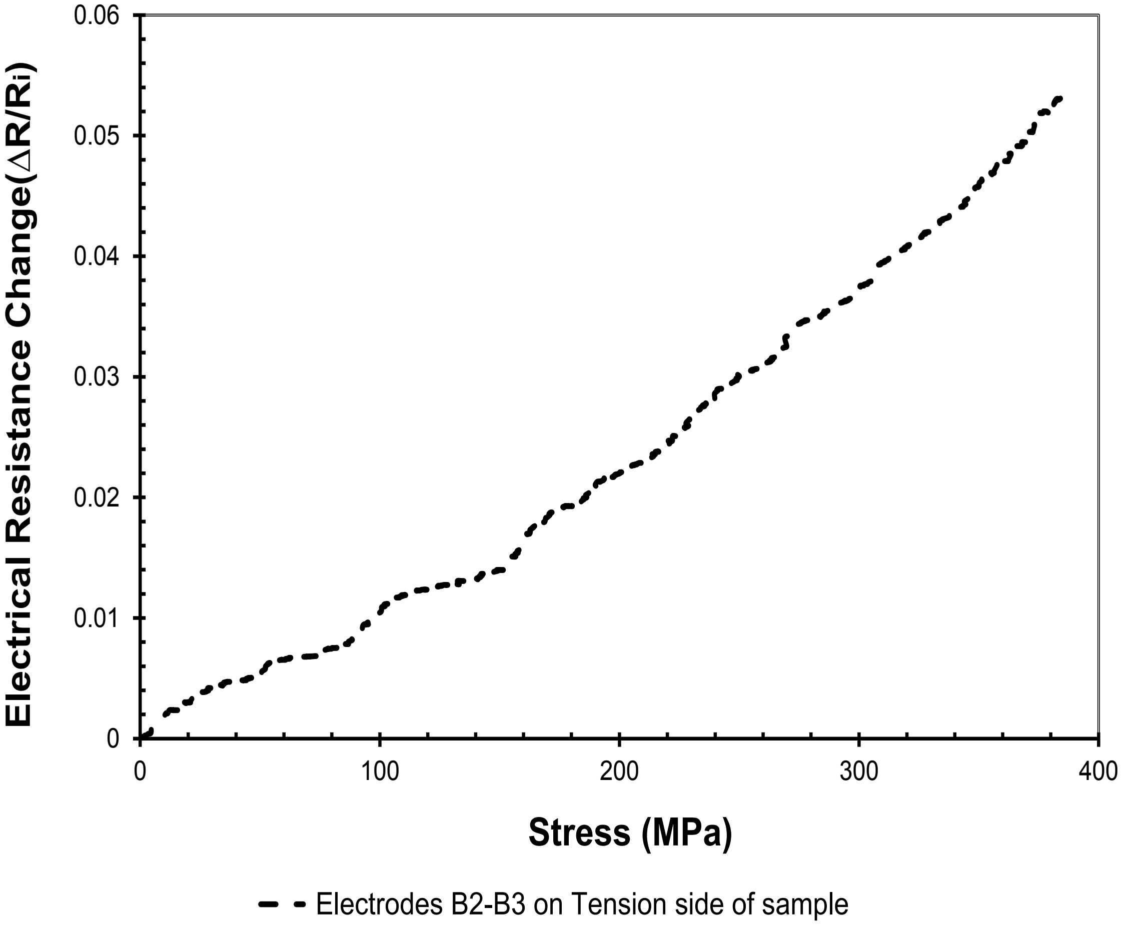

Figure 6.18: Four-point bending test results showing change in in-plane electrical resistance at the electrodes B2-B3 measured on tension side of the sample versus stress

6.2.2 Explanation for the obtained experimental results

Incorporating small amount of MWCNT into epoxy in glass fiber/epoxy/MWCNT composite allows creating the formation of in-situ sensors. The formation of MWCNT networks play significant role in determining the electrical resistance of the laminated glass fiber/epoxy/MWCNT composite. Even though glass fiber and epoxy resin are electrically insulating materials, the MWCNT is incorporated to increase the electrical conductivity of the non-conducing epoxy enough that the electrical resistance of the MWCNT enhanced epoxy can be easily measured. As such, the sensor is the MWCNT-enhanced epoxy. Electrical resistance of the composite laminate comes from intrinsic electrical resistance of MWCNT, resistance of MWCNT-MWCNT contacts and contact resistance created by thin insulating polymer formed between crossing nanotubes. The experimental results in electrical resistance behavior obtained from the three different tests show one expected result and two unexpected results. Normally one would expect that an elongation along a certain direction would take the CNTs further apart and this would increase the electrical resistance of the sample, and the opposite would be the case if the sample is shortened. This may be true when the deformation is unidirectional. When a uniaxial stress is applied, the deformation is not unidirectional, but rather multi-directional. In addition to a deformation along the direction of the load, there is also deformation in directions transverse to the load. The combination of the effect of deformations along all directions needs to be taken into account to explain the behavior of the electrical resistance in this case.

The arrangement of the CNT networks in the epoxy resin is very complicated. In an attempt to explain the above behavior, a very simplified arrangement is proposed. This is intended to illustrate the concept. Consider as a start a pair of two straight nanotubes as shown in Figure 6.19. Assuming that before loading (see Figure 6.19a), there is an overlap length of x_1 along the x direction, and the distance between the tubes is z_1 along the z direction. When tensile stress is applied (see Figure 6.19b), the tubes move further apart along the x direction (x_2), but closer in the z direction (z_2). Since z_2 is less than z_1, if there is no motion along the x direction, it would be expected that the resistance between the two tubes would decrease. However, the motion along the x direction eliminates (or reduces) the overlap length between the tubes, this would increase the electrical resistance. When a compressive stress along the x direction is applied as illustrated in Figure 6.19c, similar explanation can be used except that the directions are reversed in this case.

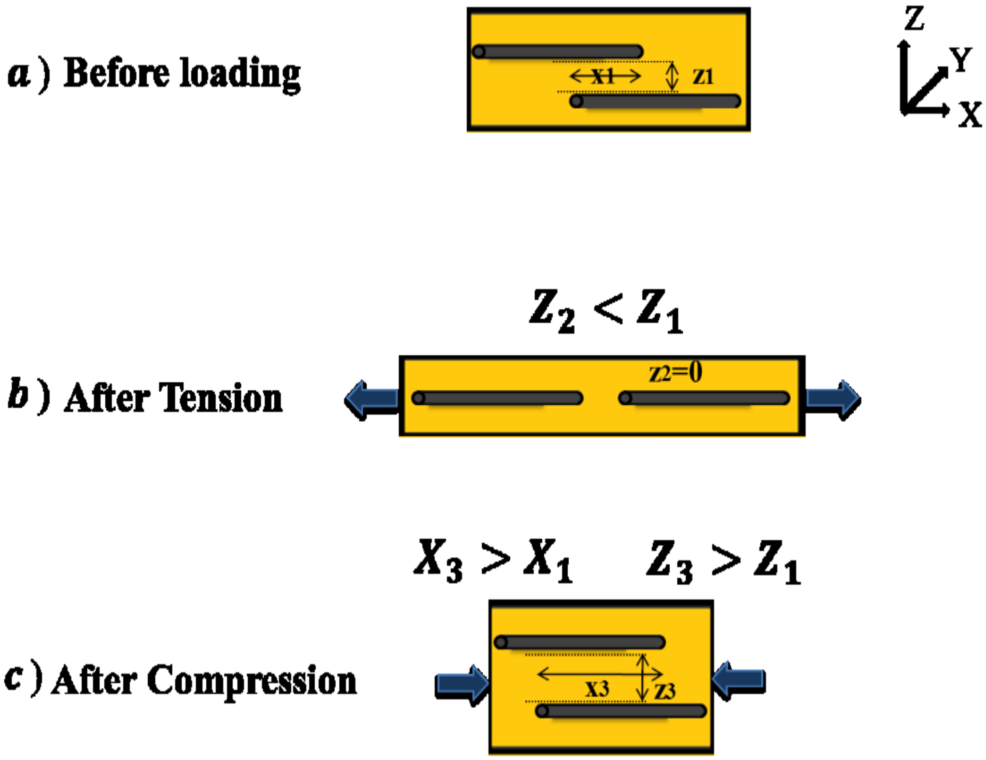

Figure 6.19: Simplified representation of the relative motion between a pair of straight CNTs

A more complicated arrangement involving large number of CNTs to explain this behavior is given in Figures 6.20 and 6.21. In figure 6.20a, a random configuration of the nanotube inside a piece of epoxy containing CNT taken from glass fiber/epoxy/CNT laminate is represented. At the center of Figure 6.20b, a unit cell consisting of two pairs of CNT is shown. Two tubes are in contact and there is a distance between the two pairs. It is assumed that the different spatial arrangements consist of 7 different configurations, and these can be generated by the rotation of one pair of nanotubes around the center point of the cell, with respect to the other pair. It is found from Figure 6.8 that the application of lengthwise uniaxial tensile stress creates negative strain along the z direction. Normally this reduction in thickness is expected to decrease in tube-to-tube distance which would translate into a reduction in TTER. However, the TTER increases as the uniaxial stress is increased (Figure 6.8). The fact that TTER increases indicates that apart from the reduction in thickness due to Poisson coupling, there are other factors that influence the change in TTER. The relation between ATTS versus stress is linear and so is the relation between TTER and stress. These relations may be expressed as: ATTS/σ = a and TTER/σ = b. One may be tempted to establish a relation:

$$\mathrm{TTER}/\mathrm{ATTS} = b/a = c \tag{6.15}$$

which indicates that there may be a coupling effect between TTER and ATTS. However one needs to be careful about attaching some physical meaning to this relation. This is because the TTER increases while it is expected to decrease. The reason for this behavior is because the spacing between the nanotubes depends not only on the deformation along the z direction, but it is also dependent on the deformation along the x direction, when the laminate is subjected to uniaxial stress along the x direction. When the laminate is subjected to multi-directional deformations (even though loading is only unidirectional), the spacing between nanotubes depends more on the deformation that is more dominant.

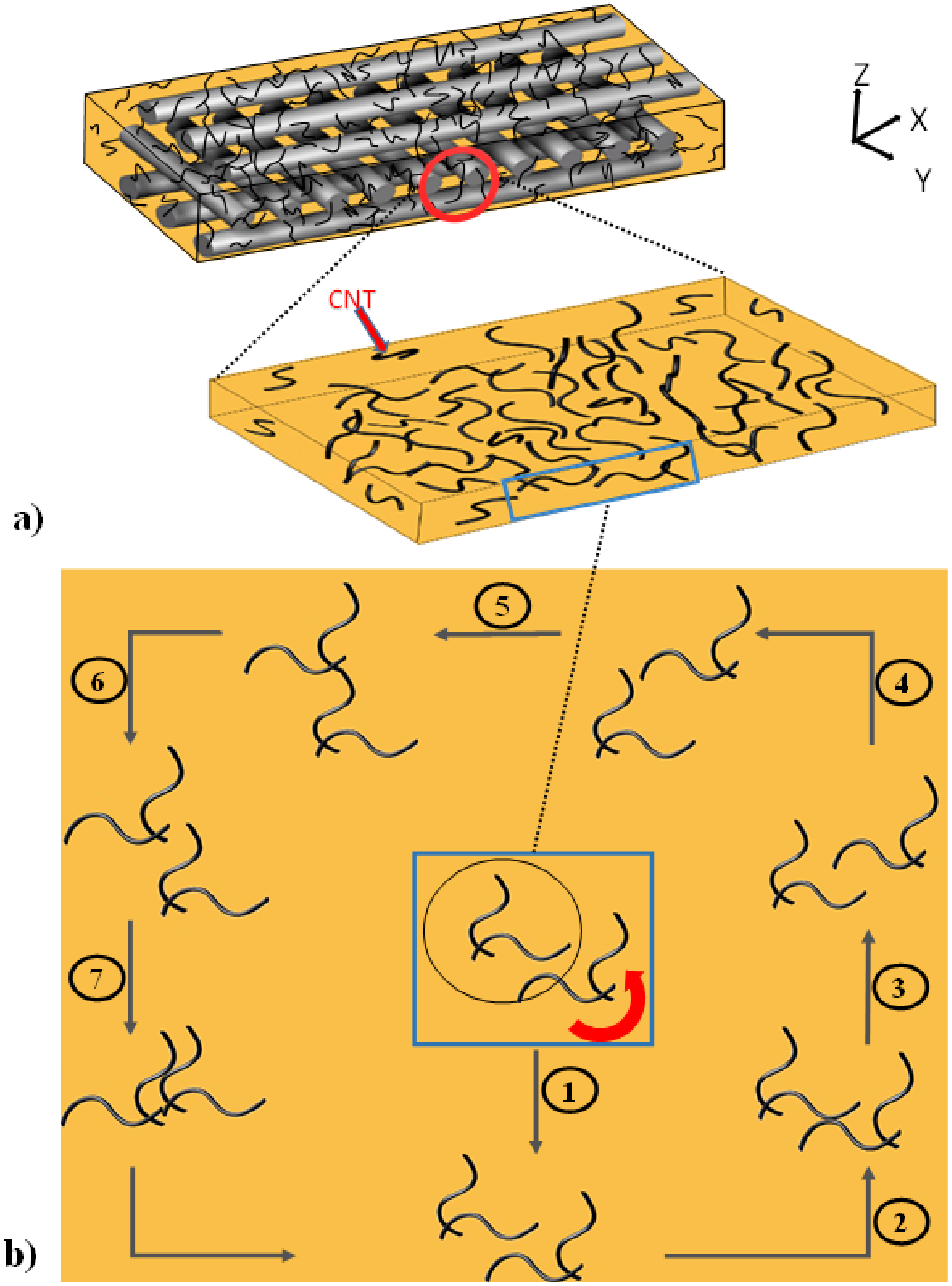

Figure 6.20: Schematic illustration showing a) Cross ply glass fiber/epoxy/CNT composite laminate b) Systematic creation of CNT-CNT contact configurations by rotating one CNT pair with respect to other one

In figure 6.21, the second column (from left) shows the 7 configurations before any loading is applied, and the third column shows the 7 configurations after uniaxial tensile loading is applied. In configuration 1 as shown in Figure 6.21a, elongation along the x direction makes $x_2 > x_1$, while reduction in the thickness direction gives $z_2 < z_1$. It can also be observed that the shortest distance between the two tubes increases, thus an increase in electrical resistance between the two tubes. In the remaining configurations (2 to 7) as illustrated in Figures 6.21b to 6.21g, $x_2 > x_1$, $z_2 < z_1$ and the resistance after loading is more than the resistance before loading.

The above explanation is confirmed by the observation on the behavior of TTER due to the application of compressive stress along the x direction. Figure 6.14 shows the relation between TTER, and ATTS versus lengthwise compressive stress. As the magnitude of the stress increases, the ATTS increases. This is to be expected since the thickness is expected to increase due to Poisson coupling effect. However, the change in TTER is becoming more and more negative, which means that the TTER is decreasing. The explanation for this behavior is again indicated in Figure 6.21. Column 4 shows the deformation after lengthwise compressive stress. In configuration 1 (see Figures 6.21a), $x_3 < x_1$ which indicates that the electrical resistance decreases, even though $z_3 > z_1$. In the remaining configurations (2 to 7) (see Figures 6.21b to 6.21g), $x_3 < x_1$, $z_3 > z_1$ and the resistance after deformation is less than the resistance before deformation.

Further confirmation of the explanation for the change in TTER due to multi-directional deformation was done by observing the change in TTER due to compressive stress along the z direction. Figure 6.10 indicates this behavior.

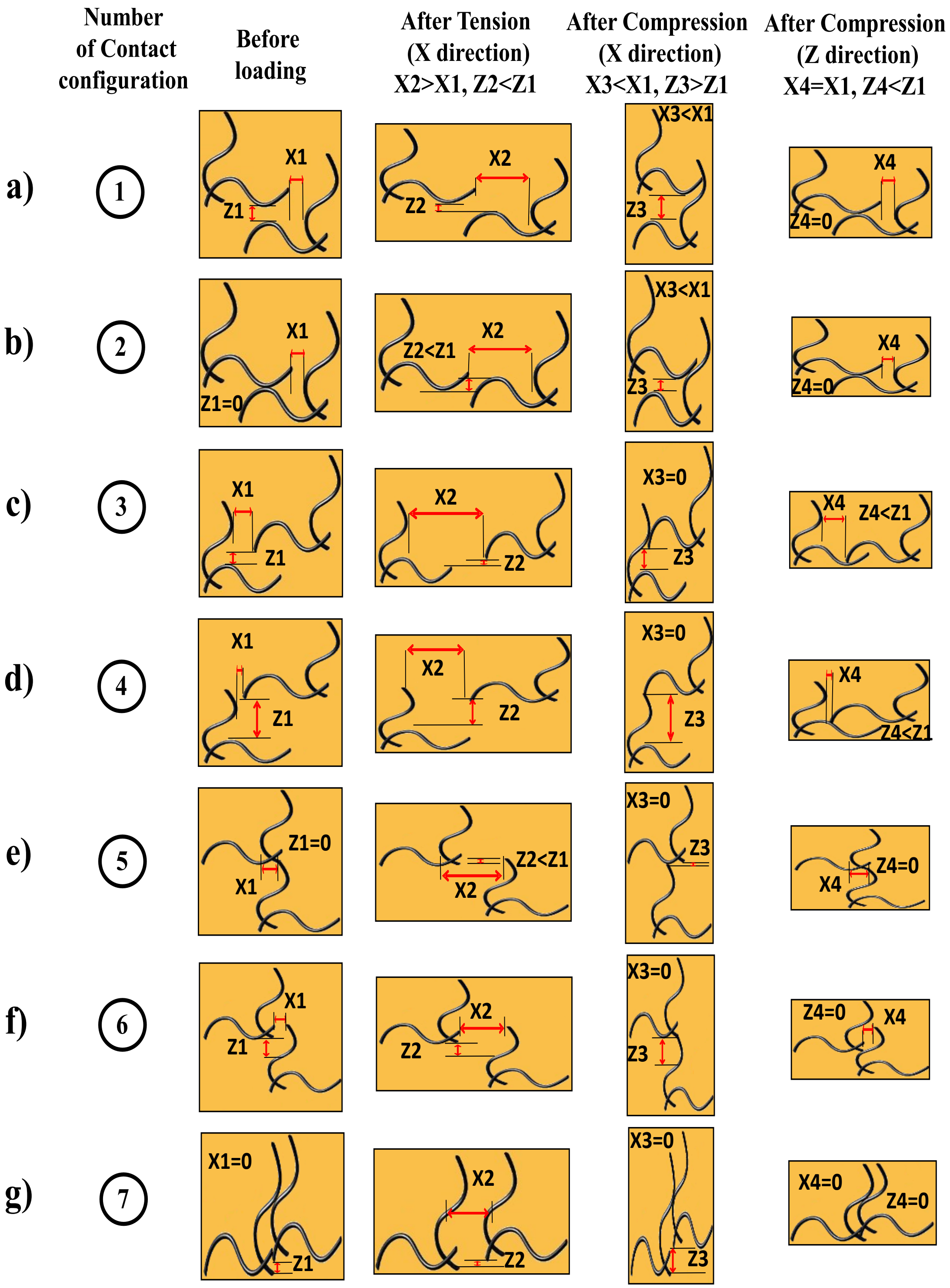

Figure 6.21: Schematic illustration showing seven CNT-CNT contact configurations (a to g) before loading and after lengthwise and thicknesswise loadings

When the stress is increased in magnitude, both the ATTS and change in TTER become more and more negative. This is to be expected since the thicknesswise compressive stress would reduce the thickness and this in turn would decrease the tube-to-tube distance, which in turn would reduce the electrical resistance. This is again explained as shown in Figure 6.21. Column 5 shows that the distances x_4 and x_1 are the same while distance z_4 is smaller than the distance z_1, which in turn makes the tube-to-tube distances to be smaller, thus facilitating tunneling conduction, due to the application of the compressive stress. This in turn makes the resistance after deformation to be less than the resistance before deformation. It is observed from four-point bending test results that the change in in-plane electrical resistance measured on compression side and tension side of the sample indicate negative and positive as shown in Figures 6.20 and 6.21 respectively. These behaviors are again described using the model in Figure 6.21. Column 4 shows the deformation on compression side while Column 2 indicates the deformation on tension side of sample.

6.2.3 Conclusions

It is concluded that the change in TTER of composite laminates containing carbon nanotubes dispersed in epoxy resin matrix depends on the competing deformation along the different directions. For laminates subjected to uniaxial lengthwise tension, lengthwise deformation tends to move the tubes further apart while Poisson coupling may want to push the tubes closer together. Since the lengthwise deformation is more dominant (Poisson ratio is only about 0.3) [92], the tubes are further apart and the net result is an increase in TTER. For laminates subjected to lengthwise uniaxial compression, lengthwise deformation tends to push the tubes closer together, while Poisson coupling along the thickness direction tends to separate the tubes further apart. Again due to the dominance of the lengthwise deformation, the net effect is a decrease in TTER. When thicknesswise compressive stress is applied, the thickness is reduced and this results in a decrease in TTER. The knowledge obtained from this behavior can be stated as follows: For laminates subjected to multi-directional deformation, the largest deformation may dictate the change in electrical resistance along all directions.

Chapter 7

Conclusions, contributions and future works

7.1 Conclusions

Regarding the first part of the thesis, Chapters 2, 3, 4 and 5, the following conclusions are made:

The effects of distance between pair of electrodes closest to damage, proximity of pair of electrodes to the damage, plate size, electrical contact geometry, spacing between electrodes, damage severity and MWCNT concentration on the change in electrical resistance were experimentally investigated in Chapter 2. From experimental results, it was shown that change in electrical resistance increases with reducing distance between pair of electrodes closest to damage, the spacing between electrodes, distance between pair of electrodes and damage location, plate size and MWCNT concentration. Likewise, grid points gives more change in electrical resistance as well as greater spatial resolution for detection, location and quantification of damage compared to grid lines.

A novel, practical and real-time SHM technique was developed for real-time detection, location and quantification of damage in large polymer composites structures made of electrically non-conductive fibers and MWCNT networks in Chapter 3. The technique was demonstrated for large glass fiber/epoxy/MWCNT composite plates and kevlar fiber/epoxy/MWCNT composite plates. Drilled holes, impact damages and barely visible impact damages were detected, located and quantified in the large plates based on the significant local variations in distribution of electrical resistance change. Two new concepts were introduced for the determination of the optimal concentration of MWCNT to assure damage detectability at any region in large plates. One was uniformity of MWCNT distribution which results in uniformity in electrical conductivity. The other was sensitivity to change in electrical resistance due to damage occurrence for detection, location and quantification of damages in the large plates.

A new, practical and real-time SHM technique to detect, locate and quantify damages in the large polymer composite plates made of carbon fibers and MWCNT networks was presented in Chapter 4. In this technique, new strategy of electric potential measurement was proposed. The electric potential distribution was monitored while constant electric current was applied. It was shown that drilled holes, impact damages and barely visible impact damages cause significant change in electric potential between contact points in the vicinity of the damage. This significant change is used for detecting, locating and quantifying damage in the large plates.

An electrical model was proposed for composite plates containing MWCNT in Chapter 5. Numerical simulations were performed according to Ohm’s law, KCL and KVL using Matlab Simulink. It was shown from simulations results that the sensitivity to change in electrical resistance increases as the concentration of MWCNT decreases while being above the percolation threshold. Moreover, it was concluded from simulation results that ERC increases with reducing spacing between the electrodes, decreasing distance between pair of electrodes and damage location, increasing damage size and using contact-point electrodes compared to contact-line electrodes. Good correspondence was observed between simulation results presented in Chapter 5 and experimental results presented in Chapters 2 and 3.

Regarding the second part of the thesis, Chapter 6, conclusions are summarized as follows:

It was shown that the application of a uniaxial stress along the x direction produces electrical resistance change along the z direction that is proportional to the strain along the z direction. This offers that in situ monitoring of through-thickness electrical resistance (TTER) in glass fiber/epoxy laminates containing MWCNT may be used as a new method for the measurement of the through-thickness strains, particularly at locations away from the free edges of the sample.

Likewise, the behavior of electrical resistance along the thickness direction for laminates containing CNT that were subjected to uniaxial stresses along different directions was investigated and an explanation was presented. It was found that the change in TTER for glass/epoxy laminates containing MWCNT is dependent on the competing deformation along the different directions. As such, for laminates subjected to multi-directional deformation, the largest deformation may dictate the change in electrical resistance along all directions.

7.2 Contributions

This thesis presents some studies on the use of carbon nanotubes dispersed into epoxy matrix to develop SHM technique for large polymer composite structures and also to investigate the effect of multi-directional deformation on through-thickness electrical resistance. The contribution of the thesis can be highlighted as follows:

In chapter 2

1. The effects of distance between pair of electrodes closest to damage, proximity of pair of electrodes to the damage, plate size, electrical contact geometry (grid points and grid lines), spacing between electrodes, damage severity and MWCNT concentration on the change in electrical resistance with respect to damage have been studied experimentally.

In chapter 3

1. Two new concepts have been introduced for the determination of optimal quantity of carbon nanotubes to detect, locate and quantify damage in large polymer composite structures. One is uniformity of CNT dispersion which gives rise to uniformity in electrical conductivity. The second is sensitivity to change in electrical resistance due to damage occurrence. These two new concepts did not exist for the case of small samples, while they are very important for the case of large samples.
2. Development of a new, practical and real-time SHM technique to detect, locate and quantify damage in large polymer composite structures made of electrically

non-conductive fiber and CNT networks and also a SHM program has been written for this purpose as shown in Appendix A.

In chapter 4

1. A new strategy of electric potential measurements has been proposed for the detection, location and quantification of damage in large polymer composite structures made of electrically conductive fiber and MWCNT networks.
2. Development of a new, practical and real-time SHM technique to detect, locate and quantify damage in large polymer composite structures made of electrically conductive fiber and MWCNT networks and also a SHM program has been made for this purpose as presented in Appendix B.

In chapter 5

1. A new two-dimensional electrical model of network of resistors has been proposed for composite plates containing MWCNT and the simulations have been performed to investigate the effects of sensitivity to change in electrical resistance, electrical contact's geometry, the proximity of pair of electrodes to the damage, damage severity and spacing between electrodes on the ERC.

In chapter 6

1. An explanation has been provided to describe the electrical resistance behavior of glass fiber/epoxy composite laminates containing MWCNT under multi-directional deformation.

7.3 Future works

According to this work, some future work can be recommended as follows:

1. To design printed thin films of grid points for monitoring electrical properties of large structures
2. To study the effects of temperature and moisture on large composite plates for detection and location of damage
3. To investigate the effects of applying tensile and fatigue loads on large composite plates to detect and locate damage in real-time
4. To study the effect of curing process on the uniformity of CNT distribution in large structures
5. Producing prepreg containing electrically conductive polymer matrix with self-sensing capabilities
6. To investigate the effect of glass fiber/epoxy/CNT laminates with different stacking sequence on change in through-thickness electrical resistance

7.4 List of Publications

1. Ali Naghashpour, Suong Van Hoa "*A technique for real-time detection, location and quantification of damages in large polymer composite structures made of electrically non-conductive fibers and carbon nanotube networks*" Journal of Nanotechnology, 24, 455502, 2013.

2. Ali Naghashpour, Suong Van Hoa " *In-situ monitoring of through-thickness strain in composite laminates using carbon nanotube sensors*" Journal of Composite Science and Technology, 78, 41-47, 2013.
3. Ali Naghashpour, Suong Van Hoa "*A technique for real-time detecting, locating and quantifying damage in large polymer composite structures made of carbon fibers and carbon nanotube networks*" submitted to Journal of Structural Health Monitoring, 2014.
4. Ali Naghashpour, Suong Van Hoa "*Electrical resistance behavior of glass fiber/epoxy/carbon nanotubes composite laminates subjected to multidirectional deformation*" To be submitted.
5. Ali Naghashpour, Suong Van Hoa "*Effects of uniformity of carbon nanotube distribution and sensitivity to change in electrical resistance for in-situ damage detection, location and quantification in large polymer composite structures*" To be submitted.
6. Ali Naghashpour, Suong Van Hoa "*Theoretical and experimental investigations for in-situ damage detection, location and quantification in large polymer composite structures using carbon nanotube networks*" To be submitted.
7. Ali Naghashpour, Suong Van Hoa "*Effects of distance between pair of electrodes, plate size, and damage severity on change in electrical resistance for in-situ damage detection, location and quantification in glass fiber/epoxy plates containing carbon nanotube*" 10th Canada-Japan Workshop on Composites, Vancouver, Canada, 2014.

8. Ali Naghashpour, Suong Van Hoa "*Enhancing electrical sensing capabilities of large epoxy composite structures using carbon nanotube networks*" Thermoset Resin Formulators Association (TRFA), 5th Annual Excellence in Thermoset Polymer Research, USA, 2014.
9. Ali Naghashpour, Suong Van Hoa "*A nondestructive evaluation technique for detecting, locating and quantifying damage in large polymer composite structures made of electrically non-conductive fibers and carbon nanotube networks*" The American Society for Nondestructive Testing Annual Conference, USA, 2014.
10. Ali Naghashpour, Suong Van Hoa "*Comparison between grid points and grid lines for detecting, locating and quantifying damage in large polymer composite structures made of electrically non-conductive fibers and carbon nanotube networks*" American Society for Composites 29th Technical Conference 16th US-Japan Conference, USA, 2014.
11. Ali Naghashpour, Suong Van Hoa "*Technique for in-situ health monitoring of large polymer composite structures made of carbon fiber and carbon nanotube networks*" European Conference on Composite Materials (ECCM-16), 2014.
12. Ali Naghashpour, Suong Van Hoa "*Method for real-time health monitoring of large polymer composite structures using carbon nanotube networks*" 9th International workshop on structural health monitoring, Stanford University, USA, Sep 2013.

13. Ali Naghashpour, Suong Van Hoa "*Through-thickness electrical resistance in glass/epoxy/CNT composite laminates subjected to mechanical loading*" 19th International Conference on Composite Materials (ICCM 19), Montreal, Canada, 2013.
14. A. Naghashpour, S. V. Hoa "*Determination of through-thickness strain in composite laminates*" American Society for Composites 27th Technical Conference 15th US-Japan Conference, Arlington, Texas, USA, OCT 3, 2012.

7.5 Patent

Suong. Van. Hoa, Ali Naghashpour "*Method and system for detecting and locating damages in composite structures*" International Patent application Number: WO2013086626A1, Date of publication: Jun. 20, 2013.

Appendix A

Flowchart of proposed technique presented in Chapter 3

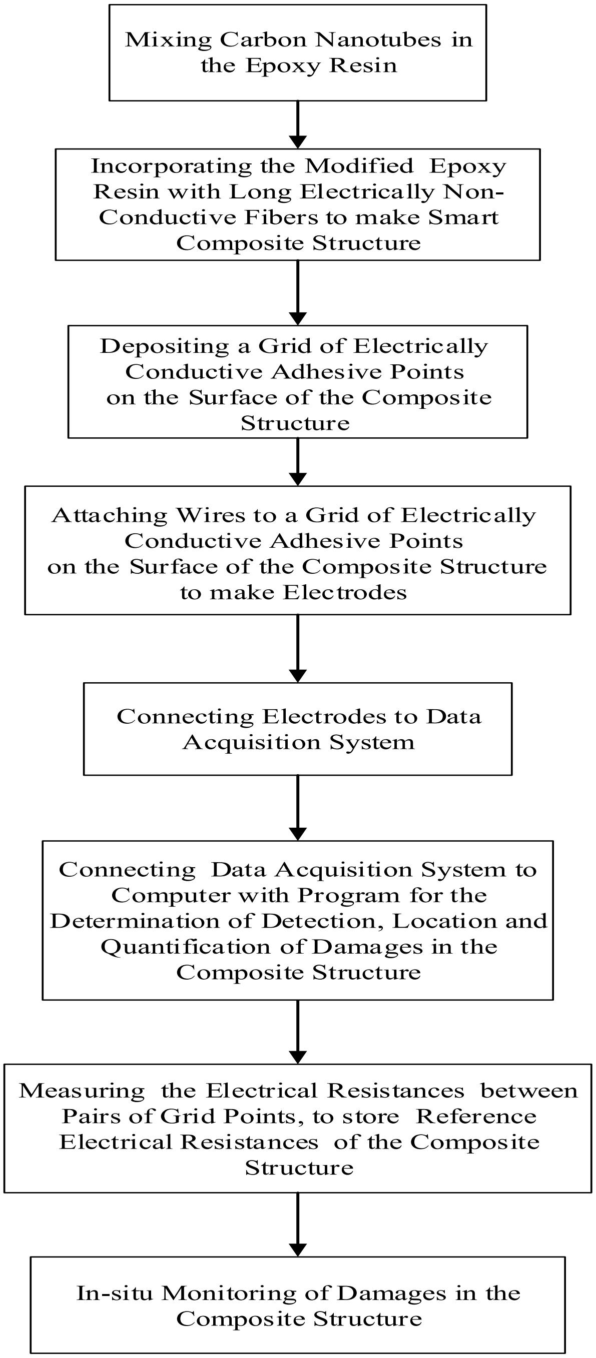

Structural health monitoring program for electrically non-conductive fiber/epoxy composite structures containing CNT

The computer program is written for electrically non-conductive fiber/epoxy composite structures containing CNT. It should be emphasized that electric resistances are used as in-put values for electrically non-conductive fibers such as kevlar and glass fiber/epoxy composite structures containing CNT in the algorithm program. In general, L, W and N are representation of Length, Width and number of electrical contact points of structural composites, respectively. These are used to determine the number of rows and columns of the contact points, depending on the space between the contact points. Let R_i and R_f be the initial and final electrical resistances between the grid points, respectively. The real-time health monitoring system of a composite plate with L=22 inch, W=13 inch and N= 40 is schematically shown in Figure 3.2. The flowchart of computer program is illustrated in Figure A.1. The algorithm of this program is presented in the following:

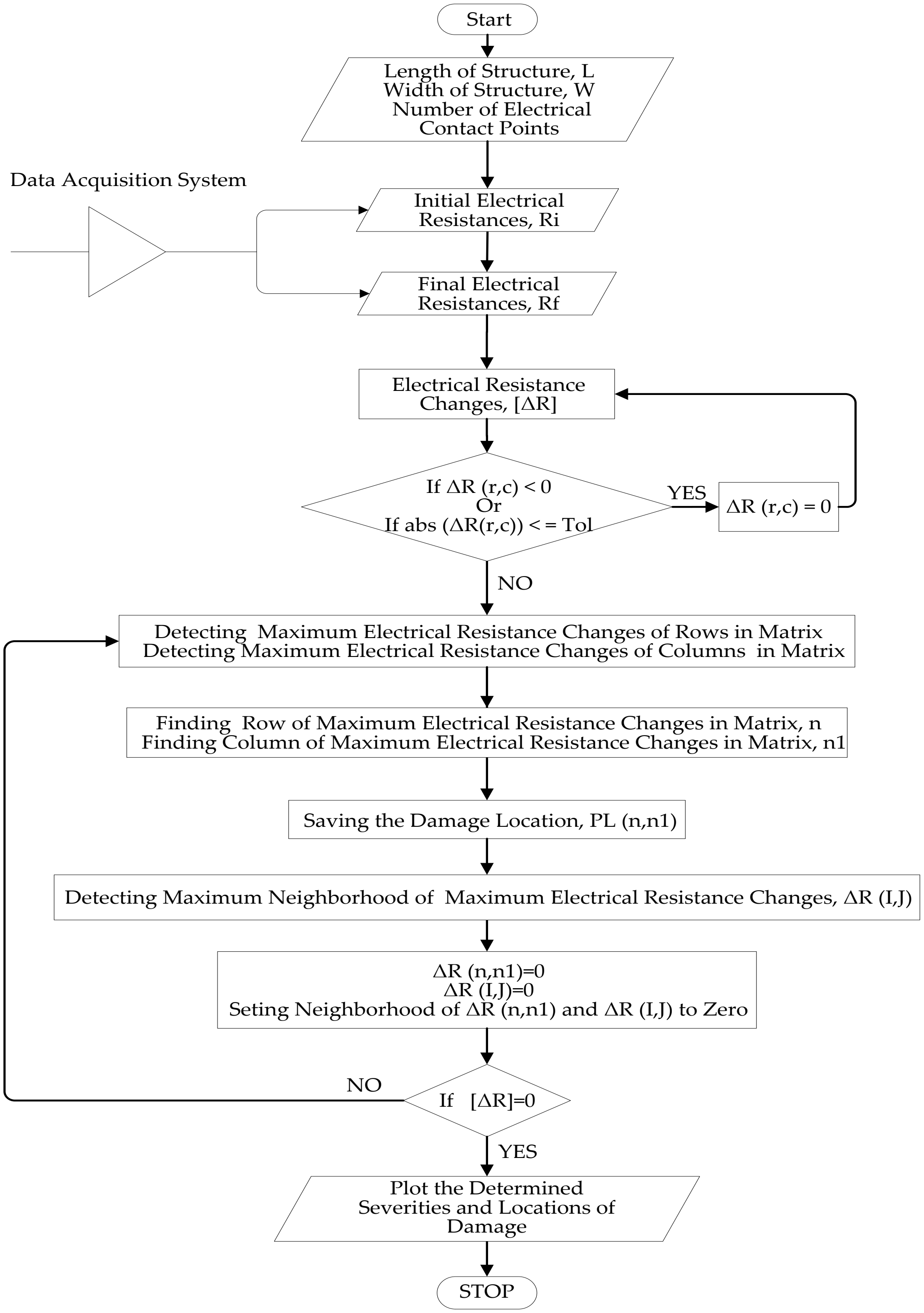

Figure A.1: Flowchart of SHM program for electrically non-conductive fibers reinforced polymer composite structures containing CNTs

Algorithm A:

MERC means Maximum Electrical Resistance Change

Let L and W be the length and width of structure, respectively.

Let N be the number of electrical contact points.

Let Tolerance (δ) be 0.0001

Let electrical resistance change (ΔR)

Main: **Read** $[R_i]_{(r\times c)}$ and $[R_f]_{(r\times c)}$ as the set of initial and final electrical resistances, respectively.

```
    For $\mathrm{j} = 1\,\mathrm{to}\,\mathrm{c}$
        For $\mathrm{i} = 1\,\mathrm{to}\,\mathrm{r}$
        If $R_f(r,c) = 0$ then $\Delta R(r,c) = 0$
            Else
                $\Delta R = \frac{(1-\delta)R_f - (1+\delta)R_i}{(1+\delta)R_i} \times 100$
            End
        End
    End
    Replace $\Delta R(r,c) = \Delta R$
Omit those electrical resistance changes which less than tolerance

For $\mathrm{tt} = 1\,\mathrm{to}\,20$
```

```
For $i = 1 to r$
    For $j = 1 to c$
  If $\Delta R(r,c) < 0$ then $\Delta R(r,c) = 0$
      End
      If $|\Delta R(r,c)| =< \delta$ then $\Delta R(r,c) = 0$
      End
End
End
```

Detecting MERC of Columns in matrix

$$[m1, n1] = Max(Max[\Delta R])$$

Detecting MERC of Rows in matrix

$$[m, n] = Max(Max\Delta R(:, n1))$$

Setting MERC to Zero

$$\Delta R(n, n1) = 0$$

Finding Row and Column of MERC in matrix

$$row(tt) = n$$

$$column(tt) = n1$$

Saving the place of Damage Location

$$PL(n, n1) = 1$$

Finding coordinates of damage on the structure

$$x1 = (n - 1) \times 1.5 + 0.5$$

$$x = 0.5 + 1.5 \times (15 - n1)$$

Applying Boundary Conditions:

Detecting Maximum Neighborhood of MERC and Setting it and its neighbor and MERC and its neighborhood to Zero

```
If $n = 1 \text{ And } n1 = 1$ then $[G] = [\Delta R(n, n1+1), \Delta R(n+1, n1), \Delta R(n+1, n1+1)] = 0$
        $B = \max[G]$
        $[I, J] = \text{find}(\Delta R = B)$
    If $\Delta R(n, n1) \times (0.5) - B < 0.1$
      If $I \sim= 1 \text{ And } J \sim= 1$
            $\Delta R(I-1, J-1) = 0, \Delta R(I-1, J) = 0, \Delta R(I-1, J+1) = 0,$
            $\Delta R(I, J-1) = 0, \Delta R(I, J) = 0, \Delta R(I, J+1) = 0,$
            $\Delta R(I+1, J-1) = 0, \Delta R(I+1, J) = 0, \Delta R(I+1, J+1) = 0,$
            $\Delta R(n, n1) = 0, \Delta R(n, n1+1) = 0, \Delta R(n+1, n1) = 0,$
            $\Delta R(n+1, n1+1) = 0,$
        End
      End
  End
```

Detecting Maximum Neighborhood of MERC and Setting it and its neighbor and MERC and its neighborhood to Zero

```
If $(n = 1) \text{ And } (n1 = c)$ then $G = [\Delta R(n+1, n1), \Delta R(n, n1-1), \Delta R(n+1, n1-1)]$
        $B = \max(G)$
        $[I, J] = \text{find}(\Delta R = B)$
```

```
        If $\Delta R(n,n1)\times(0.5) - B < 0.1$
            If $I \sim= 1$ And $J \sim= c$
                        $\Delta R(I-1,J-1)=0, \Delta R(I-1,J)=0, \Delta R(I-1,J+1)=0,$
                        $\Delta R(I,J-1)=0, \Delta R(I,J)=0, \Delta R(I,J+1)=0,$
                        $\Delta R(I+1,J-1)=0, \Delta R(I+1,J)=0,$
                        $\Delta R(I+1,J+1)=0, \Delta R(n,n1)=0,$
                        $\Delta R(n+1,n1)=0, \Delta R(n,n1-1)=0,$
                        $\Delta R(n+1,n1-1)=0,$
            End
        End
    End
```

Detecting Maximum Neighborhood of MERC and Setting it and its neighbor and MERC and its neighborhood to Zero

```
    If $(n=1)$ And $(n1=c)$ then $G=[\ \Delta R(n,n1+1), \Delta R(n-1,n1), \Delta R(n-1,n1+1)]$
            $B=\max[G]$
            $[I,J]=\text{find}(\Delta R=B)$
        If $\Delta R(n,n1)\times(0.5) - B < 0.1$
        If $I \sim= R$ And $J \sim= 1$
                $\Delta R(I-1,J-1)=0, \Delta R(I-1,J)=0, \Delta R(I-1,J+1)=0,$
                $\Delta R(I,J-1)=0, \Delta R(I,J)=0, \Delta R(I,J+1)=0,$
                $\Delta R(I+1,J-1)=0, \Delta R(I+1,J)=0,$
                $\Delta R(I+1,J+1)=0, \Delta R(n,n1)=0,$
                $\Delta R(n,n1+1)=0,\ \Delta R(n-1,n1)=0,$
                $\Delta R(n-1,n1+1)=0,$
            End
            End
```

```
End
Detecting Maximum Neighborhood of MERC and Setting it and its neighbor and MERC and its neighborhood to Zero

If $(n = r)$ And $(n1 = c)$ then $G = [\ \Delta R(n, n1 - 1), \Delta R(n - 1, n1), \Delta R(n - 1, n1 - 1)]$
            $B = \max[G]$
                $[I, J] = \mathrm{find}(\Delta R = B)$
    If $\Delta R(n, n1) \times (0.5) - B < 0.1$
        If $I \sim= r$ And $J \sim= c$
                $\Delta R(I - 1, J - 1) = 0, \Delta R(I - 1, J) = 0, \Delta R(I - 1, J + 1) = 0,$
                $\Delta R(I, J - 1) = 0, \Delta R(I, J) = 0, \Delta R(I, J + 1) = 0,$
                $\Delta R(I + 1, J - 1) = 0, \Delta R(I + 1, J) = 0,$
                $\Delta R(I + 1, J + 1) = 0, \Delta R(n, n1) = 0,$
                $\Delta R(n - 1, n1) = 0, \Delta R(n, n1 - 1) = 0,$
                $\Delta R(n - 1, n1 - 1) = 0,$
        End
    End
End
Detecting Maximum Neighborhood of MERC and Setting it and its neighbor and MERC and its neighborhood to Zero

  If $(n > 1 \| n < r)$ And $(n1 > 1 \| n1 < c)$
     If $n \sim= 1$ Or $n \sim= r$
        If $n1 \sim= 1$ Or $n1 \sim= c$ then
        $G = [\ \Delta R(n + 1, n1), \Delta R(n, n1 + 1), \Delta R(n + 1, n1 + 1), \Delta R(n, n1 - 1), \Delta R(n + 1, n1 - 1),$
        $\Delta R(n - 1, n1 - 1), \Delta R(n - 1, n1), \Delta R(n - 1, n1 + 1)]$
```

```
$B = \max[G]$
$[I, J] = \mathrm{find}(\Delta R = B)$
    If $\Delta R(n, n1) \times (0.5) - B < 0.1$
        If $I = 1$
            $\Delta R(I, J-1) = 0, \Delta R(I, J) = 0, \Delta R(I, J+1) = 0,$
            $\Delta R(I+1, J-1) = 0, \Delta R(I+1, J) = 0, \Delta R(I+1, J+1) = 0,$
            $\Delta R(n, n1) = 0, \Delta R(n+1, n1) = 0, \Delta R(n, n1+1) = 0,$
            $\Delta R(n+1, n1+1) = 0, \Delta R(n, n1-1) = 0, \Delta R(n+1, n1-1) = 0,$
            $\Delta R(n-1, n1-1) = 0, \Delta R(n-1, n1) = 0, \Delta R(n-1, n1+1) = 0,$
        ElseIf $I = r$
            $\Delta R(I-1, J-1) = 0, \Delta R(I-1, J) = 0, \Delta R(I-1, J+1) = 0,$
            $\Delta R(I, J-1) = 0, \Delta R(I, J) = 0, \Delta R(I, J+1) = 0,$
            $\Delta R(n, n1) = 0, \Delta R(n+1, n1) = 0, \Delta R(n, n1+1) = 0,$
            $\Delta R(n+1, n1+1) = 0, \Delta R(n, n1-1) = 0,$
            $\Delta R(n+1, n1-1) = 0, \Delta R(n-1, n1-1) = 0,$
            $\Delta R(n-1, n1) = 0, \Delta R(n-1, n1+1) = 0,$
        ElseIf $J = 1$
            $\Delta R(I-1, J) = 0, \Delta R(I-1, J+1) = 0, \Delta R(I, J) = 0,$
            $\Delta R(I, J+1) = 0, \Delta R(I+1, J) = 0, \Delta R(I+1, J+1) = 0,$
            $\Delta R(n, n1) = 0, \Delta R(n+1, n1) = 0, \Delta R(n, n1+1) = 0,$
            $\Delta R(n+1, n1+1) = 0, \Delta R(n, n1-1) = 0,$
            $\Delta R(n+1, n1-1) = 0, \Delta R(n-1, n1-1) = 0,$
            $\Delta R(n-1, n1) = 0, \Delta R(n-1, n1+1) = 0,$
        ElseIf $J = c$
```

```
$\Delta R(I-1,J-1)=0, \Delta R(I-1,J)=0, \Delta R(I,J-1)=0,$
$\Delta R(I,J)=0, \Delta R(I+1,J-1)=0, \Delta R(I+1,J)=0,$
$\Delta R(n,n1)=0, \Delta R(n+1,n1)=0, \Delta R(n,n1+1)=0,$
$\Delta R(n+1,n1+1)=0, \Delta R(n,n1-1)=0, \Delta R(n+1,n1-1)=0,$
$\Delta R(n-1,n1-1)=0, \Delta R(n-1,n1)=0, \Delta R(n-1,n1+1)=0,$
            Else
                $\Delta R(I-1,J-1)=0, \Delta R(I-1,J)=0, \Delta R(I-1,J+1)=0,$
                $\Delta R(I,J-1)=0, \Delta R(I,J)=0, \Delta R(I,J+1)=0,$
                $\Delta R(I+1,J-1)=0, \Delta R(I+1,J)=0, \Delta R(I+1,J+1)=0,$
                $\Delta R(n,n1)=0, \Delta R(n+1,n1)=0, \Delta R(n,n1+1)=0,$
                $\Delta R(n+1,n1+1)=0, \Delta R(n,n1-1)=0, \Delta R(n+1,n1-1)=0,$
                $\Delta R(n-1,n1-1)=0, \Delta R(n-1,n1)=0, \Delta R(n-1,n1+1)=0$
          End
        End
      End
    End
  End
```

Detecting Maximum Neighborhood of MERC and Setting it and its neighbor and MERC and its neighborhood to Zero

```
  If $(n=1)$ And $(n1>1 \| n1<c)$
    If $n1 \sim= 1$ Or $n1 \sim= c$ then
          $G=[\Delta R(n+1,n1), \Delta R(n,n1+1), \Delta R(n+1,n1+1),$
          $\Delta R(n,n1-1), \Delta R(n+1,n1-1)]$
      $B=\max[G]$
      $[I,J]=\mathrm{find}(\Delta R=B)$
            If $\Delta R(n,n1)\times(0.5)-B<0.1$
```

```
        If $I = 1$
                    $\Delta R(I,J-1) = 0, \Delta R(I,J) = 0, \Delta R(I,J+1) = 0, \Delta R(I+1,J-1) = 0,$
                    $\Delta R(I+1,J) = 0, \Delta R(I+1,J+1) = 0, \Delta R(n,n1) = 0, \Delta R(n+1,n1) = 0,$
                    $\Delta R(n,n1+1) = 0, \Delta R(n+1,n1+1) = 0, \Delta R(n,n1-1) = 0,$
                    $\Delta R(n+1,n1-1) = 0, \Delta R(n-1,n1-1) = 0, \Delta R(n-1,n1) = 0,$
                    $\Delta R(n-1,n1+1) = 0,$

        ElseIf $J = 1$

$\Delta R(I-1,J) = 0, \Delta R(I-1,J+1) = 0, \Delta R(I,J) = 0; \Delta R(I,J+1) = 0,$
$\Delta R(I+1,J) = 0, \Delta R(I+1,J+1) = 0, \Delta R(n,n1) = 0, \Delta R(n+1,n1) = 0,$
$\Delta R(n,n1+1) = 0, \Delta R(n+1,n1+1) = 0, \Delta R(n,n1-1) = 0, \Delta R(n+1,n1-1) = 0,$
$\Delta R(n-1,n1-1) = 0, \Delta R(n-1,n1) = 0, \Delta R(n-1,n1+1) = 0,$

        ElseIf $J = c$

$\Delta R(I-1,J-1) = 0, \Delta R(I-1,J) = 0, \Delta R(I,J-1) = 0, \Delta R(I,J) = 0,$
$\Delta R(I+1,J-1) = 0, \Delta R(I+1,J) = 0, \Delta R(n,n1) = 0, \Delta R(n+1,n1) = 0,$
$\Delta R(n,n1+1) = 0, \Delta R(n+1,n1+1) = 0, \Delta R(n,n1-1) = 0, \Delta R(n+1,n1-1) = 0,$
$\Delta R(n-1,n1-1) = 0, \Delta R(n-1,n1) = 0, \Delta R(n-1,n1+1) = 0,$

        Else

$\Delta R(I-1,J-1) = 0, \Delta R(I-1,J) = 0, \Delta R(I-1,J+1) = 0,$
$\Delta R(I,J-1) = 0, \Delta R(I,J) = 0, \Delta R(I,J+1) = 0, \Delta R(I+1,J-1) = 0,$
$\Delta R(I+1,J) = 0, \Delta R(I+1,J+1) = 0, \Delta R(n,n1) = 0, \Delta R(n+1,n1) = 0,$
$\Delta R(n,n1+1) = 0, \Delta R(n+1,n1+1) = 0, \Delta R(n,n1-1) = 0, \Delta R(n+1,n1-1) = 0,$
$\Delta R(n-1,n1-1) = 0, \Delta R(n-1,n1) = 0, \Delta R(n-1,n1+1) = 0,$

                End
            End
        End
  End
```

Detecting Maximum Neighborhood of MERC and Setting it and its neighbor and MERC and its neighborhood to Zero

```
If $(n = r)\ \text{And}\ (n1 > 1 \| n1 < c)$
  If $n1 \sim= 1$ Or $n1 \sim= c$ then
$G = [\ \Delta R(n, n1+1), \Delta R(n, n1-1), \Delta R(n-1, n1-1), \Delta R(n-1, n), \Delta R(n-1, n1+1)]$
    $B = \max[G]$
    $[I, J] = \text{find}(\Delta R = B)$
     If $\Delta R(n, n1) \times (0.5) - B < 0.1$
       If $I = r$
$\Delta R(I-1, J-1) = 0, \Delta R(I-1, J) = 0, \Delta R(I-1, J+1) = 0, \Delta R(I, J-1) = 0,$
$\Delta R(I, J) = 0, \Delta R(I, J+1) = 0, \Delta R(n, n1) = 0, \Delta R(n+1, n1) = 0,$
$\Delta R(n, n1+1) = 0, \Delta R(n+1, n1+1) = 0, \Delta R(n, n1-1) = 0,$
$\Delta R(n+1, n1-1) = 0, \Delta R(n-1, n1-1) = 0, \Delta R(n-1, n1) = 0,$
$\Delta R(n-1, n1+1) = 0,$
       ElseIf $J = 1$
$\Delta R(I-1, J) = 0, \Delta R(I-1, J+1) = 0, \Delta R(I, J) = 0, \Delta R(I, J+1) = 0,$
$\Delta R(I+1, J) = 0, \Delta R(I+1, J+1) = 0, \Delta R(n, n1) = 0, \Delta R(n+1, n1) = 0,$
$\Delta R(n, n1+1) = 0, \Delta R(n+1, n1+1) = 0, \Delta R(n, n1-1) = 0,$
$\Delta R(n+1, n1-1) = 0, \Delta R(n-1, n1-1) = 0, \Delta R(n-1, n1) = 0,$
$\Delta R(n-1, n1+1) = 0,$
       ElseIf $J = c$
```

```
$\Delta R(I-1,J-1) = 0, \Delta R(I-1,J) = 0, \Delta R(I,J-1) = 0, \Delta R(I,J) = 0,$
$\Delta R(I+1,J-1) = 0, \Delta R(I+1,J) = 0, \Delta R(n,n1) = 0, \Delta R(n+1,n1) = 0,$
$\Delta R(n,n1+1) = 0, \Delta R(n+1,n1+1) = 0, \Delta R(n,n1-1) = 0,$
$\Delta R(n+1,n1-1) = 0, \Delta R(n-1,n1-1) = 0, \Delta R(n-1,n1) = 0,$
$\Delta R(n-1,n1+1) = 0,$
          Else
$\Delta R(I-1,J-1) = 0, \Delta R(I-1,J) = 0, \Delta R(I-1,J+1) = 0, \Delta R(I,J-1) = 0,$
$\Delta R(I,J) = 0, \Delta R(I,J+1) = 0, \Delta R(I+1,J-1) = 0, \Delta R(I+1,J) = 0,$
$\Delta R(I+1,J+1) = 0, \Delta R(n,n1) = 0, \Delta R(n+1,n1) = 0,$
$\Delta R(n,n1+1) = 0, \Delta R(n+1,n1+1) = 0, \Delta R(n,n1-1) = 0,$
$\Delta R(n+1,n1-1) = 0, \Delta R(n-1,n1-1) = 0,$
$\Delta R(n-1,n1) = 0, \Delta R(n-1,n1+1) = 0,$
          End
               End
          End
 End
```

Detecting Maximum Neighborhood of MERC and Setting it and its neighbor and MERC and its neighborhood to Zero

```
 If $(n > 1 \| n < r)$ And $(n1 = 1)$
    If $n \sim= 1$ Or $n \sim= r$ then
          $G = [\Delta R(n+1,n1), \Delta R(n,n1+1), \Delta R(n+1,n1+1), \Delta R(n-1,n1),$
          $\Delta R(n-1,n1+1)]$
    $B = \max[G]$
    $[I,J] = \mathrm{find}(\Delta R = B)$
       If $\Delta R(n,n1) \times (0.5) - B < 0.1$
```

```
        If $J = 1$
    $\Delta R(I-1,J) = 0, \Delta R(I-1,J+1) = 0, \Delta R(I,J) = 0, \Delta R(I,J+1) = 0,$
    $\Delta R(I+1,J) = 0, \Delta R(I+1,J+1) = 0, \Delta R(n,n1) = 0, \Delta R(n+1,n1) = 0,$
    $\Delta R(n,n1+1) = 0, \Delta R(n+1,n1+1) = 0, \Delta R(n,n1-1) = 0,$
    $\Delta R(n+1,n1-1) = 0, \Delta R(n-1,n1-1) = 0, \Delta R(n-1,n1) = 0,$
    $\Delta R(n-1,n1+1) = 0,$
        ElseIf $I = 1$
    $\Delta R(I,J-1) = 0, \Delta R(I,J) = 0, \Delta R(I,J+1) = 0, \Delta R(I+1,J-1) = 0,$
    $\Delta R(I+1,J) = 0, \Delta R(I+1,J+1) = 0, \Delta R(n,n1) = 0, \Delta R(n+1,n1) = 0,$
    $\Delta R(n,n1+1) = 0, \Delta R(n+1,n1+1) = 0, \Delta R(n,n1-1) = 0,$
    $\Delta R(n+1,n1-1) = 0, \Delta R(n-1,n1-1) = 0, \Delta R(n-1,n1) = 0,$
    $\Delta R(n-1,n1+1) = 0,$
        ElseIf $I = r$
                $\Delta R(I-1,J-1) = 0, \Delta R(I-1,J) = 0, \Delta R(I-1,J+1) = 0,$
                $\Delta R(I,J-1) = 0, \Delta R(I,J) = 0, \Delta R(I,J+1) = 0, \Delta R(n,n1) = 0,$
                $\Delta R(n+1,n1) = 0, \Delta R(n,n1+1) = 0, \Delta R(n+1,n1+1) = 0,$
                $\Delta R(n,n1-1) = 0, \Delta R(n+1,n1-1) = 0, \Delta R(n-1,n1-1) = 0,$
                $\Delta R(n-1,n1) = 0, \Delta R(n-1,n1+1) = 0,$
        Else
                $\Delta R(I-1,J-1) = 0, \Delta R(I-1,J) = 0, \Delta R(I-1,J+1) = 0,$
                $\Delta R(I,J-1) = 0, \Delta R(I,J) = 0, \Delta R(I,J+1) = 0,$
                $\Delta R(I+1,J-1) = 0, \Delta R(I+1,J) = 0, \Delta R(I+1,J+1) = 0,$
                $\Delta R(n,n1) = 0, \Delta R(n+1,n1) = 0, \Delta R(n,n1+1) = 0,$
                $\Delta R(n+1,n1+1) = 0, \Delta R(n,n1-1) = 0, \Delta R(n+1,n1-1) = 0,$
                $\Delta R(n-1,n1-1) = 0, \Delta R(n-1,n1) = 0, \Delta R(n-1,n1+1) = 0,$
        End
            End
        End
```

```
End
Detecting Maximum Neighborhood of MERC and Setting it and its neighbor and MERC and its neighborhood to Zero

If $(n > 1 \| n < r)$ And $(n1 == c)$
  If $n \sim= 1$ Or $n \sim= r$
     $G = [\Delta R(n+1, n1), \Delta R(n+1, n1-1), \Delta R(n, n1-1), \Delta R(n-1, n1-1), \Delta R(n-1, n1)]$
  $B = \max[G]$
  $[I, J] = \text{find}(\Delta R = B)$
   If $\Delta R(n, n1) \times (0.5) - B < 0.1$
      If $J = c$
            $\Delta R(I-1, J-1) = 0, \Delta R(I-1, J) = 0, \Delta R(I, J-1) = 0, \Delta R(I, J) = 0,$
            $\Delta R(I+1, J-1) = 0, \Delta R(I+1, J) = 0, \Delta R(n, n1) = 0, \Delta R(n+1, n1) = 0,$
            $\Delta R(n, n1+1) = 0, \Delta R(n+1, n1+1) = 0, \Delta R(n, n1-1) = 0,$
            $\Delta R(n+1, n1-1) = 0, \Delta R(n-1, n1-1) = 0, \Delta R(n-1, n1) = 0,$
            $\Delta R(n-1, n1+1) = 0,$
      ElseIf $I = r$
            $\Delta R(I-1, J-1) = 0, \Delta R(I-1, J) = 0, \Delta R(I-1, J+1) = 0,$
            $\Delta R(I, J-1) = 0, \Delta R(I, J) = 0, \Delta R(I, J+1) = 0, \Delta R(n, n1) = 0,$
            $\Delta R(n+1, n1) = 0, \Delta R(n, n1+1) = 0, \Delta R(n+1, n1+1) = 0,$
            $\Delta R(n, n1-1) = 0, \Delta R(n+1, n1-1) = 0, \Delta R(n-1, n1-1) = 0,$
            $\Delta R(n-1, n1) = 0, \Delta R(n-1, n1+1) = 0,$
      ElseIf $I = 1$
            $\Delta R(I, J-1) = 0, \Delta R(I, J) = 0, \Delta R(I, J+1) = 0, \Delta R(I+1, J-1) = 0,$
            $\Delta R(I+1, J) = 0, \Delta R(I+1, J+1) = 0, \Delta R(n, n1) = 0, \Delta R(n+1, n1) = 0,$
            $\Delta R(n, n1+1) = 0, \Delta R(n+1, n1+1) = 0, \Delta R(n, n1-1) = 0,$
            $\Delta R(n+1, n1-1) = 0, \Delta R(n-1, n1-1) = 0, \Delta R(n-1, n1) = 0,$
            $\Delta R(n-1, n1+1) = 0,$
      Else
```

```
                $\Delta R(I-1,J-1)=0, \Delta R(I-1,J)=0, \Delta R(I-1,J+1)=0,$
                $\Delta R(I,J-1)=0, \Delta R(I,J)=0, \Delta R(I,J+1)=0, \Delta R(I+1,J-1)=0,$
                $\Delta R(I+1,J)=0, \Delta R(I+1,J+1)=0, \Delta R(n,n1)=0, \Delta R(n+1,n1)=0,$
                $\Delta R(n,n1+1)=0, \Delta R(n+1,n1+1)=0, \Delta R(n,n1-1)=0,$
                $\Delta R(n+1,n1-1)=0, \Delta R(n-1,n1-1)=0, \Delta R(n-1,n1)=0,$
                $\Delta R(n-1,n1+1)=0,$
          End
        End
      End
    End
      If $Max(Max(\Delta R)) < 0.001$
        break;
        End
```

Numbering the Electrical Contact Points on the Structure,

```
  $m = 0$
  For $j = 1:8$
    For $i = 1:5$
      $m = m + 1$
      $h = 0.5 + 3 \times (i-1)$
          $k = 0.5 + 3 \times (8-j)$
          $r_i$_circle $= .4$
          $N = 256$
      $teta = (0:N) \times 2 \times pi/N$
      Plot ( r_circle * cos(teta) + h, r_circle * sin(teta) + k, 'w');
      text(h - 0.2, k, num2str(m), 'color', 'w')
```

```
                hold on
          End
End
```

Plot the Determined Locations and Severities of Damage

```
A(n,n1) = 0;
 row(tt) = n;      % saving the place
 column(tt) = n1;
 PL(n,n1) = 1;
Severity(n,n1) = A1(n,n1);
x = (n - 1) × 1.5 + 0.5;
x1 = 0.5 + 1.5 × (15 - n1);
plot(x,x1,'+')
DDD = max( Severity,[],1);
DDD = max(DDD)/9;
AA_pp(1,tt) = A1(n,n1);
NN(1,tt) = n;
NN1(1,tt) = n1;



For i = 1:size(AA_pp,2)

  If 8 * DDD < AA_pp(1,i)

          If
           AA_pp(1,i) < 9 * DDD + 0.05
          r_DDD = 0.4; N = 512;
          teta = (0:N) * 2 * pi/N;
          x = (NN(1,i) - 1) * 1.5 + 0.5;
          x1 = 0.5 + 1.5 * (15 - NN1(1,i));
         plot(x, x1, 'marker', 'o', 'MarkerFaceColor', Colour(9,:), 'MarkerSize',55 * r_DDD);
         hold on
         %fill(r_DDD * cos(teta) + x, r_DDD * sin(teta) + x1, 'r')


            End
```

```
    End
    If 7 * DDD < AA_pp(1,i)
If
      AA_pp(1,i) < 8 * DDD
      r_DDD = 0.4; N = 512;
      teta = (0 : N) * 2 * pi/N;
      x = (NN(1,i) - 1) * 1.5 + 0.5;
      x1 = 0.5 + 1.5 * (15 - NN1(1,i));
      plot(x, x1, 'marker' , 'o', 'MarkerFaceColor' , Colour(8, :), 'MarkerSize',50 * r_DDD);
      %fill(r_DDD * cos(teta) + x, r_DDD * sin(teta) + x1, 'r')
     % plot(r_DDD* cos(teta) + x, r_DDD * sin(teta) + x1, 'color' , Colour(8, :));
     hold on

        End
    End
    If 6 * DDD < AA_pp(1,i)
If
      AA_pp(1,i) < 7 * DDD
      QQ = 200;
      r_DDD = 0.4; N = 512;
      teta = (0 : N) * 2 * pi/N;
      x = (NN(1,i) - 1) * 1.5 + 0.5;
     x1 = 0.5 + 1.5 * (15 - NN1(1,i));
     plot(x, x1, 'marker' , 'o', 'MarkerFaceColor' , Colour(7, :), 'MarkerSize',45 * r_DDD);

        End
    End
If 5 * DDD < AA_pp(1,i)
```

```
If
      AA_pp(1,i) < 6 * DDD
      r_DDD = 0.4; N = 512;
      teta = (0 : N) * 2 * pi/N;
      x = (NN(1,i) - 1) * 1.5 + 0.5;
     x1 = 0.5 + 1.5 * (15 - NN1(1,i));
     %plot(r_DDD * cos(teta) + x, r_DDD * sin(teta) + x1, 'color', Colour(6,:));
      plot(x, x1, 'marker', 'o', 'MarkerFaceColor', Colour(7,:), 'MarkerSize',45 * r_DDD);

         End

  End

  If 4 * DDD < AA_pp(1,i)

If
      AA_pp(1,i) < 5 * DDD
      r_DDD = 0.4; N = 512;
      teta = (0 : N) * 2 * pi/N;
      x = (NN(1,i) - 1) * 1.5 + 0.5;
     x1 = 0.5 + 1.5 * (15 - NN1(1,i));
     %plot(r_DDD * cos(teta) + x, r_DDD * sin(teta) + x1, 'color', Colour(5,:));
      plot(x, x1, 'marker', 'o', 'MarkerFaceColor', Colour(5,:), 'MarkerSize',35 * r_DDD);

         End

   End

   If 3 * DDD < AA_pp(1,i)

If
      AA_pp(1,i) < 4 * DDD
      r_DDD = 0.4; N = 512;
      teta = (0 : N) * 2 * pi/N;
      x = (NN(1,i) - 1) * 1.5 + 0.5;
     x1 = 0.5 + 1.5 * (15 - NN1(1,i));
     %plot(r_DDD * cos(teta) + x, r_DDD * sin(teta) + x1, 'color', Colour(4,:));
     plot(x, x1, 'marker', 'o', 'MarkerFaceColor', Colour(4,:), 'MarkerSize',30 * r_DDD);

         End
```

```
          End

          If 2 * DDD < AA_pp(1,i)

      If
           AA_pp(1,i) < 3 * DDD
           r_DDD = 0.4; N = 512;
           teta = (0 : N) * 2 * pi/N;
           x = (NN(1,i) - 1) * 1.5 + 0.5;
          x1 = 0.5 + 1.5 * (15 - NN1(1,i));
          %plot(r_DDD * cos(teta) + x, r_DDD * sin(teta) + x1, 'color', Colour(3,:));
          plot(x, x1, 'marker', 'o', 'MarkerFaceColor', Colour(3,:), 'MarkerSize',25 * r_DDD);


             End

        End

        If 1 * DDD < AA_pp(1,i)

      If
           AA_pp(1,i) < 2 * DDD
           r_DDD = 0.4; N = 512;
           teta = (0 : N) * 2 * pi/N;
           x = (NN(1,i) - 1) * 1.5 + 0.5;
          x1 = 0.5 + 1.5 * (15 - NN1(1,i));
          %plot(r_DDD * cos(teta) + x, r_DDD * sin(teta) + x1, 'color', Colour(2,:));
           plot(x, x1, 'marker', 'o', 'MarkerFaceColor', Colour(2,:), 'MarkerSize',20 * r_DDD);
             End

       End

         If
           AA_pp(1,i) < 1 * DDD
           r_DDD = 0.4; N = 512;
           teta = (0 : N) * 2 * pi/N;
           x = (NN(1,i) - 1) * 1.5 + 0.5;
          x1 = 0.5 + 1.5 * (15 - NN1(1,i));
         % plot(r_DDD* cos(teta) + x, r_DDD * sin(teta) + x1, 'color', Colour(1,:));
         plot(x, x1, 'marker', 'o', 'MarkerFaceColor', Colour(1,:), 'MarkerSize',15 * r_DDD);
             End

    End
```

Appendix B

Flowchart of proposed technique presented in Chapter 4

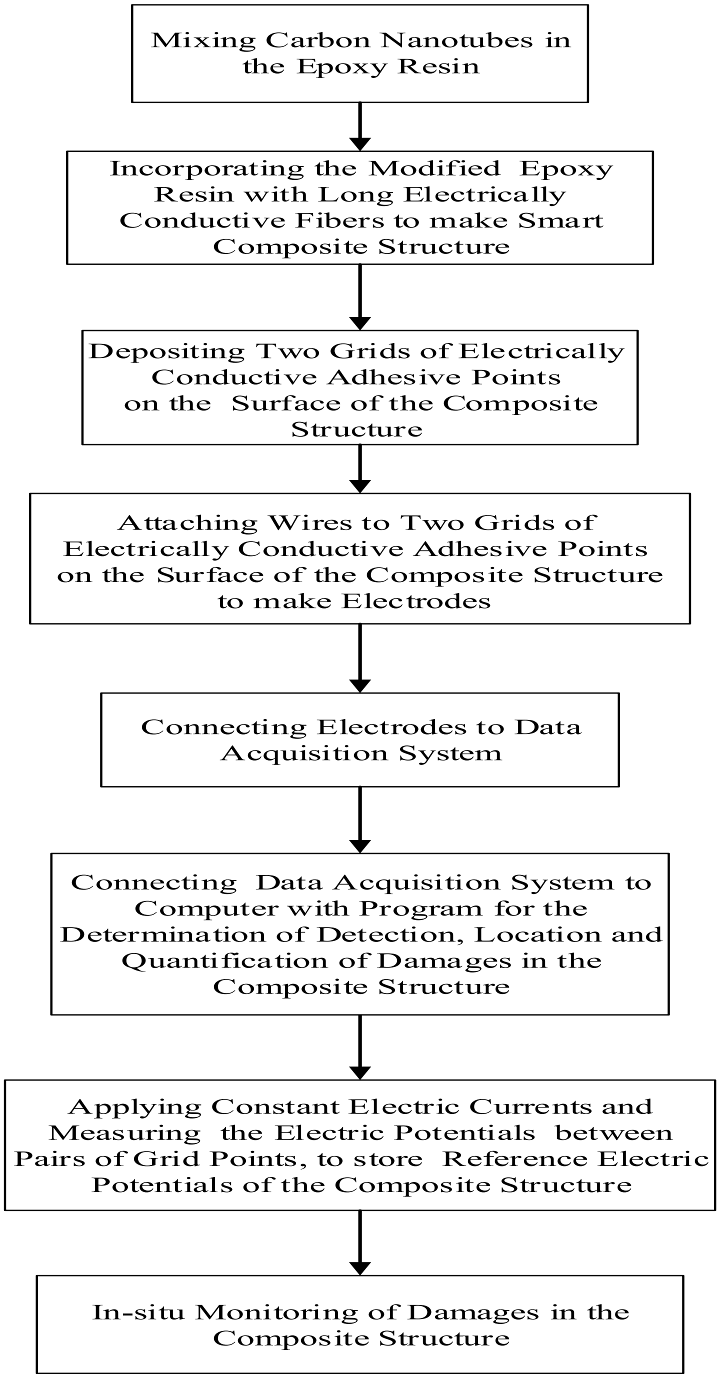

Structural health monitoring program for electrically conductive fiber/epoxy composite structures containing CNT

The computer program is made for electrically conductive fiber/epoxy composite structures containing CNT. In this program, electric potentials are used as in-put values for carbon fiber/epoxy composite structures containing CNT. In general, L, W and N are representation of Length, Width and Number of electrical contact points of structural composites, respectively. These are used to determine the number of rows and columns of the contact points, depending on the space between the contact points. Let V_i and V_f be the initial and final electric potentials between the probes, respectively. The real-time health monitoring system of a composite plate with L=22 inch, W=13 inch and N= 80 is schematically shown in Figure 4.2. The flowchart of computer program is illustrated in Figure B.1. The algorithm of this program is given in the following:

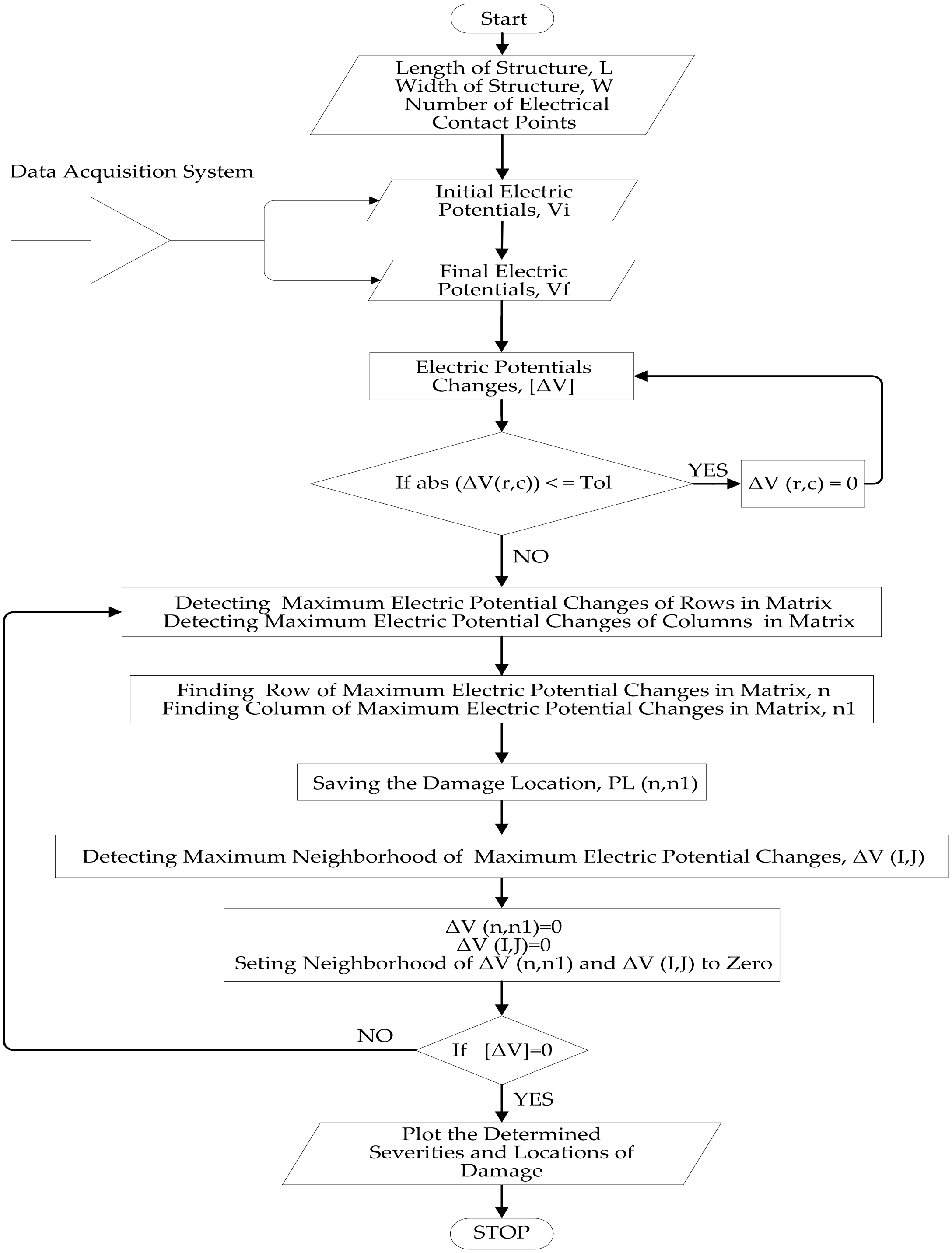

Figure B.1: Flowchart of SHM program for electrically conductive fibers reinforced polymer composite structures containing CNT

Algorithm B:

MEPC means Maximum Electric Potential Change

Let L and W be the length and width of structure, respectively.

Let *N* be the number of electrical contact points.

Let Tolerance be 0.0000001

***Main*: Read** $[V_i]_{(r\times c)}$ and $[V_f]_{(r\times c)}$ as the set of initial and final electric potentials, respectively.

```
    For $j = 1 \text{ to } c$
        For $i = 1 \text{ to } r$
        If $V_f(r,c) = 0$ then $\Delta V(r,c) = 0$
            Else
            $\Delta V = \frac{(1-\delta)V_f - (1+\delta)V_i}{(1+\delta)V_i} \times 100$
            End
      End
   End
        Replace $\Delta V(r,c) = \Delta V$
 Omit those electric potential changes which less than tolerance

For $tt = 1 \text{ to } 20$
```

```
            For $i = 1 \text{ to } r$
                For $j = 1 \text{ to } c$
              If $|\Delta V(r,c)| =< \delta$ then $\Delta V(r,c) = 0$
                  End
           End
      End
 Detecting MEPC of Columns in matrix

    $[m1, n1] = Max(Max[\Delta V])$

Detecting MEPC of Rows in matrix

       $[m, n] = Max(Max \Delta V(:, n1))$

Setting MEPC to Zero

       $\Delta V(n, n1) = 0$

Finding Row and Column of MEPC in matrix

   $row(tt) = n$
       $column(tt) = n1$
Saving the place of Damage Location

   $PL(n, n1) = 1$

 Finding coordinates of damage on the structure

    $x1 = (n - 1) \times 1.5 + 0.5$
```

```
$x = 0.5 + 1.5 \times (15 - n1)$
```

Applying Boundary Conditions:

Detecting Maximum Neighborhood of MEPC and Setting it and its neighbor and MEPC and its neighborhood to Zero

```
If $n = 1$ And $n1 = 1$ then $[G] = [\Delta V(n, n1+1), \Delta V(n+1, n1), \Delta V(n+1, n1+1)] = 0$
            $B = \max[G]$
            $[I, J] = \text{find}(\Delta V = B)$
  If $\Delta V(n, n1) \times (0.5) - B < 0.1$
    If $I \sim= 1$ And $J \sim= 1$
              $\Delta V(I-1, J-1) = 0, \Delta V(I-1, J) = 0, \Delta V(I-1, J+1) = 0,$
              $\Delta V(I, J-1) = 0, \Delta V(I, J) = 0, \Delta V(I, J+1) = 0,$
              $\Delta V(I+1, J-1) = 0, \Delta V(I+1, J) = 0, \Delta V(I+1, J+1) = 0,$
              $\Delta V(n, n1) = 0, \Delta V(n, n1+1) = 0, \Delta V(n+1, n1) = 0,$
              $\Delta V(n+1, n1+1) = 0,$
            End
        End
End
```

Detecting Maximum Neighborhood of MEPC and Setting it and its neighbor and MEPC and its neighborhood to Zero

```
If $(n = 1)$ And $(n1 = c)$ then $G = [\Delta V(n+1, n1), \Delta V(n, n1-1), \Delta V(n+1, n1-1)]$
                  $B = \max(G)$
                  $[I, J] = \text{find}(\Delta V = B)$
  If $\Delta R(n, n1) \times (0.5) - B < 0.1$
      If $I \sim= 1$ And $J \sim= c$
```

```
$\Delta V(I-1,J-1)=0, \Delta V(I-1,J)=0, \Delta V(I-1,J+1)=0,$
$\Delta V(I,J-1)=0, \Delta V(I,J)=0, \Delta V(I,J+1)=0,$
$\Delta V(I+1,J-1)=0, \Delta V(I+1,J)=0,$
$\Delta V(I+1,J+1)=0, \Delta V(n,n1)=0,$
$\Delta V(n+1,n1)=0, \Delta V(n,n1-1)=0,$
$\Delta V(n+1,n1-1)=0,$
            End
        End
    End
```

Detecting Maximum Neighborhood of MEPC and Setting it and its neighbor and MEPC and its neighborhood to Zero

```
  If $(n=1)$ And $(n1=c)$ then $G=[\Delta V(n,n1+1), \Delta V(n-1,n1), \Delta V(n-1,n1+1)]$
            $B=\max[G]$
            $[I,J]=\text{find}(\Delta V=B)$
        If $\Delta V(n,n1)\times(0.5)-B<0.1$
        If $I\sim=V$ And $J\sim=1$
                    $\Delta V(I-1,J-1)=0, \Delta V(I-1,J)=0, \Delta V(I-1,J+1)=0,$
                    $\Delta V(I,J-1)=0, \Delta V(I,J)=0, \Delta V(I,J+1)=0,$
                    $\Delta V(I+1,J-1)=0, \Delta V(I+1,J)=0,$
                    $\Delta V(I+1,J+1)=0, \Delta V(n,n1)=0,$
                    $\Delta V(n,n1+1)=0, \Delta V(n-1,n1)=0,$
                    $\Delta V(n-1,n1+1)=0,$
            End
        End
  End
```

Detecting Maximum Neighborhood of MEPC and Setting it and its neighbor and MEPC and its neighborhood to Zero

```
If $(n = r)\ \text{And}\ (n1 = c)$ then $G = [\,\Delta V(n, n1-1), \Delta V(n-1, n1), \Delta V(n-1, n1-1)]$
        $B = \max[G]$
          $[I, J] = \text{find}(\Delta V = B)$
    If $\Delta V(n, n1) \times (0.5) - B < 0.1$
      If $I \sim= r\ \text{And}\ J \sim= c$
            $\Delta V(I-1, J-1) = 0, \Delta V(I-1, J) = 0, \Delta V(I-1, J+1) = 0,$
            $\Delta V(I, J-1) = 0, \Delta V(I, J) = 0, \Delta V(I, J+1) = 0,$
            $\Delta V(I+1, J-1) = 0, \Delta V(I+1, J) = 0,$
            $\Delta V(I+1, J+1) = 0, \Delta V(n, n1) = 0,$
            $\Delta V(n-1, n1) = 0, \Delta V(n, n1-1) = 0,$
            $\Delta V(n-1, n1-1) = 0,$
      End
    End
  End
```

Detecting Maximum Neighborhood of MEPC and Setting it and its neighbor and MEPC and its neighborhood to Zero

```
  If $(n > 1 \| n < r)\ \text{And}\ (n1 > 1 \| n1 < c)$
    If $n \sim= 1$ Or $n \sim= r$
      If $n1 \sim= 1$ Or $n1 \sim= c$ then
      $G = [\,\Delta V(n+1, n1), \Delta V(n, n1+1), \Delta V(n+1, n1+1), \Delta V(n, n1-1), \Delta V(n+1, n1-1),$
      $\Delta V(n-1, n1-1), \Delta V(n-1, n1), \Delta V(n-1, n1+1)]$

  $B = \max[G]$
```

```
$[I, J] = \text{find}(\Delta V = B)$
    If $\Delta V(n, n1) \times (0.5) - B < 0.1$
      If $I = 1$
            $\Delta V(I, J-1) = 0, \Delta V(I, J) = 0, \Delta V(I, J+1) = 0,$
            $\Delta V(I+1, J-1) = 0, \Delta V(I+1, J) = 0, \Delta V(I+1, J+1) = 0,$
            $\Delta V(n, n1) = 0, \Delta V(n+1, n1) = 0, \Delta V(n, n1+1) = 0,$
            $\Delta V(n+1, n1+1) = 0, \Delta V(n, n1-1) = 0, \Delta V(n+1, n1-1) = 0,$
            $\Delta V(n-1, n1-1) = 0, \Delta V(n-1, n1) = 0, \Delta V(n-1, n1+1) = 0,$
      ElseIf $I = r$
            $\Delta V(I-1, J-1) = 0, \Delta V(I-1, J) = 0, \Delta V(I-1, J+1) = 0,$
            $\Delta V(I, J-1) = 0, \Delta V(I, J) = 0, \Delta V(I, J+1) = 0,$
            $\Delta V(n, n1) = 0, \Delta V(n+1, n1) = 0, \Delta V(n, n1+1) = 0,$
            $\Delta V(n+1, n1+1) = 0, \Delta V(n, n1-1) = 0,$
            $\Delta V(n+1, n1-1) = 0, \Delta V(n-1, n1-1) = 0,$
            $\Delta V(n-1, n1) = 0, \Delta V(n-1, n1+1) = 0,$
      ElseIf $J = 1$
            $\Delta V(I-1, J) = 0, \Delta V(I-1, J+1) = 0, \Delta V(I, J) = 0,$
            $\Delta V(I, J+1) = 0, \Delta V(I+1, J) = 0, \Delta V(I+1, J+1) = 0,$
            $\Delta V(n, n1) = 0, \Delta V(n+1, n1) = 0, \Delta V(n, n1+1) = 0,$
            $\Delta V(n+1, n1+1) = 0, \Delta V(n, n1-1) = 0,$
            $\Delta V(n+1, n1-1) = 0, \Delta V(n-1, n1-1) = 0,$
            $\Delta V(n-1, n1) = 0, \Delta V(n-1, n1+1) = 0,$
      ElseIf $J = c$
```

```
$\Delta V(I-1,J-1)=0, \Delta V(I-1,J)=0, \Delta V(I,J-1)=0,$
$\Delta V(I,J)=0, \Delta V(I+1,J-1)=0, \Delta V(I+1,J)=0,$
$\Delta V(n,n1)=0, \Delta V(n+1,n1)=0, \Delta V(n,n1+1)=0,$
$\Delta V(n+1,n1+1)=0, \Delta V(n,n1-1)=0, \Delta V(n+1,n1-1)=0,$
$\Delta V(n-1,n1-1)=0, \Delta V(n-1,n1)=0, \Delta V(n-1,n1+1)=0,$
            Else
$\Delta V(I-1,J-1)=0, \Delta V(I-1,J)=0, \Delta V(I-1,J+1)=0,$
$\Delta V(I,J-1)=0, \Delta V(I,J)=0, \Delta V(I,J+1)=0,$
$\Delta V(I+1,J-1)=0, \Delta V(I+1,J)=0, \Delta V(I+1,J+1)=0,$
$\Delta V(n,n1)=0, \Delta V(n+1,n1)=0, \Delta V(n,n1+1)=0,$
$\Delta V(n+1,n1+1)=0, \Delta V(n,n1-1)=0, \Delta V(n+1,n1-1)=0,$
$\Delta V(n-1,n1-1)=0, \Delta V(n-1,n1)=0, \Delta V(n-1,n1+1)=0$
            End
          End
        End
      End
  End
```

Detecting Maximum Neighborhood of MEPC and Setting it and its neighbor and MEPC and its neighborhood to Zero

```
  If $(n=1)$ And $(n1>1 \| n1<c)$
    If $n1 \sim= 1$ Or $n1 \sim= c$ then
            $G=[\Delta V(n+1,n1), \Delta V(n,n1+1), \Delta V(n+1,n1+1),$
            $\Delta V(n,n1-1), \Delta V(n+1,n1-1)]$
      $B=\max[G]$
      $[I,J]=\mathrm{find}(\Delta V=B)$
            If $\Delta V(n,n1)\times(0.5)-B<0.1$
```

```
        If $I = 1$
                  $\Delta V(I, J-1) = 0, \Delta V(I, J) = 0, \Delta V(I, J+1) = 0, \Delta V(I+1, J-1) = 0,$
                  $\Delta V(I+1, J) = 0, \Delta V(I+1, J+1) = 0, \Delta V(n, n1) = 0, \Delta V(n+1, n1) = 0,$
                  $\Delta V(n, n1+1) = 0, \Delta V(n+1, n1+1) = 0, \Delta V(n, n1-1) = 0,$
                  $\Delta V(n+1, n1-1) = 0, \Delta V(n-1, n1-1) = 0, \Delta V(n-1, n1) = 0,$
                  $\Delta V(n-1, n1+1) = 0,$
        ElseIf $J = 1$

$\Delta V(I-1, J) = 0, \Delta V(I-1, J+1) = 0, \Delta V(I, J) = 0; \Delta V(I, J+1) = 0,$
$\Delta V(I+1, J) = 0, \Delta V(I+1, J+1) = 0, \Delta V(n, n1) = 0, \Delta V(n+1, n1) = 0,$
$\Delta V(n, n1+1) = 0, \Delta V(n+1, n1+1) = 0, \Delta V(n, n1-1) = 0, \Delta V(n+1, n1-1) = 0,$
$\Delta V(n-1, n1-1) = 0, \Delta V(n-1, n1) = 0, \Delta V(n-1, n1+1) = 0,$
        ElseIf $J = c$

$\Delta V(I-1, J-1) = 0, \Delta V(I-1, J) = 0, \Delta V(I, J-1) = 0, \Delta V(I, J) = 0,$
$\Delta V(I+1, J-1) = 0, \Delta V(I+1, J) = 0, \Delta V(n, n1) = 0, \Delta V(n+1, n1) = 0,$
$\Delta V(n, n1+1) = 0, \Delta V(n+1, n1+1) = 0, \Delta V(n, n1-1) = 0, \Delta V(n+1, n1-1) = 0,$
$\Delta V(n-1, n1-1) = 0, \Delta V(n-1, n1) = 0, \Delta V(n-1, n1+1) = 0,$
        Else

$\Delta V(I-1, J-1) = 0, \Delta V(I-1, J) = 0, \Delta V(I-1, J+1) = 0,$
$\Delta V(I, J-1) = 0, \Delta V(I, J) = 0, \Delta V(I, J+1) = 0, \Delta V(I+1, J-1) = 0,$
$\Delta V(I+1, J) = 0, \Delta V(I+1, J+1) = 0, \Delta V(n, n1) = 0, \Delta V(n+1, n1) = 0,$
$\Delta V(n, n1+1) = 0, \Delta V(n+1, n1+1) = 0, \Delta V(n, n1-1) = 0, \Delta V(n+1, n1-1) = 0,$
$\Delta V(n-1, n1-1) = 0, \Delta V(n-1, n1) = 0, \Delta V(n-1, n1+1) = 0,$
                  End
              End
        End
  End
```

Detecting Maximum Neighborhood of MEPC and Setting it and its neighbor and MEPC and its neighborhood to Zero

```
If $(n = r)$ And $(n1 > 1 \| n1 < c)$
  If $n1 \sim= 1$ Or $n1 \sim= c$ then
$G = [\Delta V(n, n1+1), \Delta V(n, n1-1), \Delta V(n-1, n1-1), \Delta V(n-1, n), \Delta V(n-1, n1+1)]$
      $B = \max[G]$
      $[I, J] = \mathrm{find}(\Delta V = B)$
      If $\Delta V(n, n1) \times (0.5) - B < 0.1$
        If $I = r$
$\Delta V(I-1, J-1) = 0, \Delta V(I-1, J) = 0, \Delta V(I-1, J+1) = 0, \Delta V(I, J-1) = 0,$
$\Delta V(I, J) = 0, \Delta V(I, J+1) = 0, \Delta V(n, n1) = 0, \Delta V(n+1, n1) = 0,$
$\Delta V(n, n1+1) = 0, \Delta V(n+1, n1+1) = 0, \Delta V(n, n1-1) = 0,$
$\Delta V(n+1, n1-1) = 0, \Delta V(n-1, n1-1) = 0, \Delta V(n-1, n1) = 0,$
$\Delta V(n-1, n1+1) = 0,$
        ElseIf $J = 1$
$\Delta V(I-1, J) = 0, \Delta V(I-1, J+1) = 0, \Delta V(I, J) = 0, \Delta V(I, J+1) = 0,$
$\Delta V(I+1, J) = 0, \Delta V(I+1, J+1) = 0, \Delta V(n, n1) = 0, \Delta V(n+1, n1) = 0,$
$\Delta V(n, n1+1) = 0, \Delta V(n+1, n1+1) = 0, \Delta V(n, n1-1) = 0,$
$\Delta V(n+1, n1-1) = 0, \Delta V(n-1, n1-1) = 0, \Delta V(n-1, n1) = 0,$
$\Delta V(n-1, n1+1) = 0,$
        ElseIf $J = c$
```

```
$\Delta V(I-1,J-1)=0, \Delta V(I-1,J)=0, \Delta V(I,J-1)=0, \Delta V(I,J)=0,$
$\Delta V(I+1,J-1)=0, \Delta V(I+1,J)=0, \Delta V(n,n1)=0, \Delta V(n+1,n1)=0,$
$\Delta V(n,n1+1)=0, \Delta V(n+1,n1+1)=0, \Delta V(n,n1-1)=0,$
$\Delta V(n+1,n1-1)=0, \Delta V(n-1,n1-1)=0, \Delta V(n-1,n1)=0,$
$\Delta V(n-1,n1+1)=0,$
          Else
$\Delta V(I-1,J-1)=0, \Delta V(I-1,J)=0, \Delta V(I-1,J+1)=0, \Delta V(I,J-1)=0,$
$\Delta V(I,J)=0, \Delta R(I,J+1)=0, \Delta V(I+1,J-1)=0, \Delta V(I+1,J)=0,$
$\Delta V(I+1,J+1)=0, \Delta V(n,n1)=0, \Delta V(n+1,n1)=0,$
$\Delta V(n,n1+1)=0, \Delta V(n+1,n1+1)=0, \Delta V(n,n1-1)=0,$
$\Delta V(n+1,n1-1)=0, \Delta V(n-1,n1-1)=0,$
$\Delta V(n-1,n1)=0, \Delta V(n-1,n1+1)=0,$
           End
         End
    End
      End
```

Detecting Maximum Neighborhood of MEPC and Setting it and its neighbor and MEPC and its neighborhood to Zero

```
If $(n > 1 \| n < r)$ And $(n1 = 1)$
    If $n \sim= 1$ Or $n \sim= r$ then
        $G = [\Delta V(n+1,n1), \Delta V(n,n1+1), \Delta V(n+1,n1+1), \Delta V(n-1,n1),$
        $\Delta V(n-1,n1+1)]$
    $B = \max[G]$
    $[I,J] = \mathrm{find}(\Delta V = B)$
      If $\Delta V(n,n1) \times (0.5) - B < 0.1$
```

```
        If $J = 1$

$\Delta V(I-1, J) = 0, \Delta V(I-1, J+1) = 0, \Delta V(I, J) = 0, \Delta V(I, J+1) = 0,$
$\Delta V(I+1, J) = 0, \Delta V(I+1, J+1) = 0, \Delta V(n, n1) = 0, \Delta V(n+1, n1) = 0,$
$\Delta V(n, n1+1) = 0, \Delta V(n+1, n1+1) = 0, \Delta V(n, n1-1) = 0,$
$\Delta V(n+1, n1-1) = 0, \Delta V(n-1, n1-1) = 0, \Delta V(n-1, n1) = 0,$
$\Delta V(n-1, n1+1) = 0,$

        ElseIf $I = 1$

$\Delta V(I, J-1) = 0, \Delta V(I, J) = 0, \Delta V(I, J+1) = 0, \Delta V(I+1, J-1) = 0,$
$\Delta V(I+1, J) = 0, \Delta V(I+1, J+1) = 0, \Delta V(n, n1) = 0, \Delta V(n+1, n1) = 0,$
$\Delta V(n, n1+1) = 0, \Delta V(n+1, n1+1) = 0, \Delta V(n, n1-1) = 0,$
$\Delta V(n+1, n1-1) = 0, \Delta V(n-1, n1-1) = 0, \Delta V(n-1, n1) = 0,$
$\Delta V(n-1, n1+1) = 0,$

        ElseIf $I = r$
                $\Delta V(I-1, J-1) = 0, \Delta V(I-1, J) = 0, \Delta V(I-1, J+1) = 0,$
                $\Delta V(I, J-1) = 0, \Delta V(I, J) = 0, \Delta V(I, J+1) = 0, \Delta V(n, n1) = 0,$
                $\Delta V(n+1, n1) = 0, \Delta V(n, n1+1) = 0, \Delta V(n+1, n1+1) = 0,$
                $\Delta V(n, n1-1) = 0, \Delta V(n+1, n1-1) = 0, \Delta V(n-1, n1-1) = 0,$
                $\Delta V(n-1, n1) = 0, \Delta V(n-1, n1+1) = 0,$

        Else
                $\Delta V(I-1, J-1) = 0, \Delta V(I-1, J) = 0, \Delta V(I-1, J+1) = 0,$
                $\Delta V(I, J-1) = 0, \Delta V(I, J) = 0, \Delta V(I, J+1) = 0,$
                $\Delta V(I+1, J-1) = 0, \Delta V(I+1, J) = 0, \Delta V(I+1, J+1) = 0,$
                $\Delta V(n, n1) = 0, \Delta V(n+1, n1) = 0, \Delta V(n, n1+1) = 0,$
                $\Delta V(n+1, n1+1) = 0, \Delta V(n, n1-1) = 0, \Delta V(n+1, n1-1) = 0,$
                $\Delta V(n-1, n1-1) = 0, \Delta V(n-1, n1) = 0, \Delta V(n-1, n1+1) = 0,$

        End

            End

        End
```

End

Detecting Maximum Neighborhood of MEPC and Setting it and its neighbor and MEPC and its neighborhood to Zero

```
If $(n > 1 \| n < r)$ And $(n1 == c)$
  If $n \sim= 1$ Or $n \sim= r$
    $G = [\,\Delta V(n+1, n1), \Delta V(n+1, n1-1), \Delta V(n, n1-1), \Delta V(n-1, n1-1), \Delta V(n-1, n1)]$

  $B = \max[G]$
  $[I, J] = \text{find}(\Delta V = B)$
   If $\Delta V(n, n1) \times (0.5) - B < 0.1$
     If $J = c$
            $\Delta V(I-1, J-1) = 0, \Delta V(I-1, J) = 0, \Delta V(I, J-1) = 0, \Delta V(I, J) = 0,$
            $\Delta V(I+1, J-1) = 0, \Delta V(I+1, J) = 0, \Delta V(n, n1) = 0, \Delta V(n+1, n1) = 0,$
            $\Delta V(n, n1+1) = 0, \Delta V(n+1, n1+1) = 0, \Delta V(n, n1-1) = 0,$
            $\Delta V(n+1, n1-1) = 0, \Delta V(n-1, n1-1) = 0, \Delta V(n-1, n1) = 0,$
            $\Delta V(n-1, n1+1) = 0,$
     ElseIf $I = r$
            $\Delta V(I-1, J-1) = 0, \Delta V(I-1, J) = 0, \Delta V(I-1, J+1) = 0,$
            $\Delta V(I, J-1) = 0, \Delta V(I, J) = 0, \Delta V(I, J+1) = 0, \Delta V(n, n1) = 0,$
            $\Delta V(n+1, n1) = 0, \Delta V(n, n1+1) = 0, \Delta V(n+1, n1+1) = 0,$
            $\Delta V(n, n1-1) = 0, \Delta V(n+1, n1-1) = 0, \Delta V(n-1, n1-1) = 0,$
            $\Delta V(n-1, n1) = 0, \Delta V(n-1, n1+1) = 0,$
     ElseIf $I = 1$
            $\Delta V(I, J-1) = 0, \Delta V(I, J) = 0, \Delta V(I, J+1) = 0, \Delta V(I+1, J-1) = 0,$
            $\Delta V(I+1, J) = 0, \Delta V(I+1, J+1) = 0, \Delta V(n, n1) = 0, \Delta V(n+1, n1) = 0,$
            $\Delta V(n, n1+1) = 0, \Delta V(n+1, n1+1) = 0, \Delta V(n, n1-1) = 0,$
            $\Delta V(n+1, n1-1) = 0, \Delta V(n-1, n1-1) = 0, \Delta V(n-1, n1) = 0,$
            $\Delta V(n-1, n1+1) = 0,$
```

```
          Else
                    $\Delta V(I-1,J-1)=0, \Delta V(I-1,J)=0, \Delta V(I-1,J+1)=0,$
                    $\Delta V(I,J-1)=0, \Delta V(I,J)=0, \Delta V(I,J+1)=0, \Delta V(I+1,J-1)=0,$
                    $\Delta V(I+1,J)=0, \Delta V(I+1,J+1)=0, \Delta V(n,n1)=0, \Delta V(n+1,n1)=0,$
                    $\Delta V(n,n1+1)=0, \Delta V(n+1,n1+1)=0, \Delta V(n,n1-1)=0,$
                    $\Delta V(n+1,n1-1)=0, \Delta V(n-1,n1-1)=0, \Delta V(n-1,n1)=0,$
                    $\Delta V(n-1,n1+1)=0,$
          End
        End
     End
End
  If $\mathrm{Max}(\mathrm{Max}(\Delta V)) < 0.001$
      break;
      End
```

Numbering the Electrical Contact Points on the Structure,

```
$m=0$
For $j=1:8$
    For $i=1:5$
        $m=m+1$
        $h=0.5+3\times(i-1)$
            $k=0.5+3\times(8-j)$
            $r_i\_circle=.4$
             $N=256$
        $teta=(0:N)\times 2\times pi/N$
        Plot $(r\_circle*\cos(teta)+h, r\_circle*\sin(teta)+k,'w');$
```

```
        text(h - 0.2, k, num2str(m), 'color', 'w')
              hold on
         End
End
```

Plot the Determined Locations and Severities of Damage

```
A(n,n1) = 0;
 row(tt) = n;      % saving the place
 column(tt) = n1;
 PL(n,n1) = 1;
Severity(n,n1) = A1(n,n1);
x = (n - 1) × 1.5 + 0.5;
x1 = 0.5 + 1.5 × (15 - n1);
plot(x, x1, '+')
DDD = max( Severity,[],1);
DDD = max(DDD)/9;
AA_pp(1,tt) = A1(n,n1);
NN(1,tt) = n;
NN1(1,tt) = n1;



For i = 1 : size(AA_pp,2)
  If 8 * DDD < AA_pp(1,i)
        If
         AA_pp(1,i) < 9 * DDD + 0.05
        r_DDD = 0.4; N = 512;
        teta = (0 : N) * 2 * pi/N;
        x = (NN(1,i) - 1) * 1.5 + 0.5;
        x1 = 0.5 + 1.5 * (15 - NN1(1,i));
       plot(x, x1, 'marker', 'o', 'MarkerFaceColor', Colour(9, :), 'MarkerSize', 55 * r_DDD);
       hold on
       %fill(r_DDD * cos(teta) + x, r_DDD * sin(teta) + x1, 'r')
```

```
        End
    End
    If 7 * DDD < AA_pp(1,i)
If
      AA_pp(1,i) < 8 * DDD
      r_DDD = 0.4; N = 512;
      teta = (0 : N) * 2 * pi/N;
      x = (NN(1,i) - 1) * 1.5 + 0.5;
      x1 = 0.5 + 1.5 * (15 - NN1(1,i));
      plot(x, x1, 'marker', 'o', 'MarkerFaceColor', Colour(8,:), 'MarkerSize',50 * r_DDD);
      %fill(r_DDD * cos(teta) + x, r_DDD * sin(teta) + x1, 'r')
     % plot(r_DDD* cos(teta) + x, r_DDD * sin(teta) + x1, 'color', Colour(8,:));
     hold on

       End
    End
    If 6 * DDD < AA_pp(1,i)
If
      AA_pp(1,i) < 7 * DDD
      QQ = 200;
      r_DDD = 0.4; N = 512;
      teta = (0 : N) * 2 * pi/N;
      x = (NN(1,i) - 1) * 1.5 + 0.5;
     x1 = 0.5 + 1.5 * (15 - NN1(1,i));
     plot(x, x1, 'marker', 'o', 'MarkerFaceColor', Colour(7,:), 'MarkerSize',45 * r_DDD);

        End
    End
If 5 * DDD < AA_pp(1,i)
```

```
If
       AA_pp(1,i) < 6 * DDD
       r_DDD = 0.4; N = 512;
       teta = (0 : N) * 2 * pi/N;
       x = (NN(1,i) - 1) * 1.5 + 0.5;
      x1 = 0.5 + 1.5 * (15 - NN1(1,i));
      %plot(r_DDD * cos(teta) + x, r_DDD * sin(teta) + x1, 'color', Colour(6,:));
       plot(x, x1, 'marker', 'o', 'MarkerFaceColor', Colour(7,:), 'MarkerSize',45 * r_DDD);


         End

  End

  If 4 * DDD < AA_pp(1,i)

If
       AA_pp(1,i) < 5 * DDD
       r_DDD = 0.4; N = 512;
       teta = (0 : N) * 2 * pi/N;
       x = (NN(1,i) - 1) * 1.5 + 0.5;
      x1 = 0.5 + 1.5 * (15 - NN1(1,i));
      %plot(r_DDD * cos(teta) + x, r_DDD * sin(teta) + x1, 'color', Colour(5,:));
       plot(x, x1, 'marker', 'o', 'MarkerFaceColor', Colour(5,:), 'MarkerSize',35 * r_DDD);


         End

   End

   If 3 * DDD < AA_pp(1,i)

If
       AA_pp(1,i) < 4 * DDD
       r_DDD = 0.4; N = 512;
       teta = (0 : N) * 2 * pi/N;
       x = (NN(1,i) - 1) * 1.5 + 0.5;
      x1 = 0.5 + 1.5 * (15 - NN1(1,i));
      %plot(r_DDD * cos(teta) + x, r_DDD * sin(teta) + x1, 'color', Colour(4,:));
      plot(x, x1, 'marker', 'o', 'MarkerFaceColor', Colour(4,:), 'MarkerSize',30 * r_DDD);


          End
```

```
     End
     If 2 * DDD < AA_pp(1,i)
  If
       AA_pp(1,i) < 3 * DDD
       r_DDD = 0.4; N = 512;
       teta = (0 : N) * 2 * pi/N;
       x = (NN(1,i) - 1) * 1.5 + 0.5;
      x1 = 0.5 + 1.5 * (15 - NN1(1,i));
      %plot(r_DDD * cos(teta) + x, r_DDD * sin(teta) + x1, 'color', Colour(3, :));
      plot(x, x1, 'marker', 'o', 'MarkerFaceColor', Colour(3, :), 'MarkerSize',25 * r_DDD);


        End
    End
    If 1 * DDD < AA_pp(1,i)
  If
       AA_pp(1,i) < 2 * DDD
       r_DDD = 0.4; N = 512;
       teta = (0 : N) * 2 * pi/N;
       x = (NN(1,i) - 1) * 1.5 + 0.5;
      x1 = 0.5 + 1.5 * (15 - NN1(1,i));
      %plot(r_DDD * cos(teta) + x, r_DDD * sin(teta) + x1, 'color', Colour(2, :));
       plot(x, x1, 'marker', 'o', 'MarkerFaceColor', Colour(2, :), 'MarkerSize',20 * r_DDD);
        End
   End
    If
       AA_pp(1,i) < 1 * DDD
       r_DDD = 0.4; N = 512;
       teta = (0 : N) * 2 * pi/N;
       x = (NN(1,i) - 1) * 1.5 + 0.5;
      x1 = 0.5 + 1.5 * (15 - NN1(1,i));
     % plot(r_DDD* cos(teta) + x, r_DDD * sin(teta) + x1, 'color', Colour(1, :));
     plot(x, x1, 'marker', 'o', 'MarkerFaceColor', Colour(1, :), 'MarkerSize',15 * r_DDD);
        End
End
```

Bibliography

[1] T. W. Ebbesen, H. J. Lezec, H. Hiura, J. W. Bennett, H. F. Ghaemi, and T. Thio, "Electrical conductivity of individual carbon nanotubes," *Nature,* vol. 382, pp. 54-56, Jul 4 1996.

[2] S. Berber, Y. K. Kwon, and D. Tomanek, "Unusually high thermal conductivity of carbon nanotubes," *Physical Review Letters,* vol. 84, pp. 4613-4616, May 15 2000.

[3] R. S. Ruoff and D. C. Lorents, "Mechanical and Thermal-Properties of Carbon Nanotubes," *Carbon,* vol. 33, pp. 925-930, 1995.

[4] E. T. Thostenson and T. W. Chou, "Carbon nanotube networks: Sensing of distributed strain and damage for life prediction and self healing," *Advanced Materials,* vol. 18, pp. 2837-2841, Nov 3 2006.

[5] E. T. Thostenson and T. W. Chou, "Real-time in situ sensing of damage evolution in advanced fiber composites using carbon nanotube networks," *Nanotechnology,* vol. 19(215713), 2008.

[6] E. T. Thostenson, C. Y. Li, and T. W. Chou, "Nanocomposites in context," *Composites Science and Technology,* vol. 65, pp. 491-516, Mar 2005.

[7] E. T. Thostenson, Z. F. Ren, and T. W. Chou, "Advances in the science and technology of carbon nanotubes and their composites: a review," *Composites Science and Technology,* vol. 61, pp. 1899-1912, 2001.

[8] L. Böger, M. H. G. Wichmann, L. O. Meyer, and K. Schulte, "Load and health monitoring in glass fibre reinforced composites with an electrically conductive nanocomposite epoxy matrix," *Composites Science and Technology,* vol. 68, pp. 1886-1894, Jun 2008.

[9] M. Nofar, S. V. Hoa, and M. D. Pugh, "Failure detection and monitoring in polymer matrix composites subjected to static and dynamic loads using carbon nanotube networks," *Composites Science and Technology,* vol. 69, pp. 1599-1606, Aug 2009.

[10] T. W. Chou, *Microstructural Design of Fiber Composites* Cambridge: Cambridge University Press, 1992.

[11] D. Balageas, C.-P. Fritzen, and A. Guemes, *Structural health monitoring*: ISTE L td, 2006.

[12] S. Takeda, Y. Aoki, T. Ishikawa, N. Takeda, and H. Kikukawa, "Structural health monitoring of composite wing structure during durability test," *Composite Structures,* vol. 79, pp. 133-139, Jun 2007.

[13] D. Balageas, C. P. Fritzen, and G. A, *structural health monitoring*: ISTEL td, 2006.

[14] G. Y. Baaklini, "Nondestructive evaluation, structural health monitoring and optical diagnostics at NASA Glenn: A summary," *Emerging Technologies in Non-Destructive Testing V,* pp. 3-5, 2012.
[15] V. Giurgiutiu and C. Soutis, "Enhanced Composites Integrity Through Structural Health Monitoring," *Applied Composite Materials,* vol. 19, pp. 813-829, Oct 2012.
[16] S. Sugimoto, T. Aoki, Y. Iwahori, and T. Ishikawa, "Nondestructive evaluation of composites using Micro-Focused X-Ray CT Scanner," *Review of Progress in Quantitative Nondestructive Evaluation, Vols 24A and 24B,* vol. 760, pp. 1081-1086, 2005.
[17] W. Obitayo and T. Liu, "A Review: Carbon nanotube-Based Piezoresistive strain sensor," *Journal of Sensors* vol. 652438, pp. 1-15, 2012.
[18] J. M. Park, D. S. Kim, J. R. Lee, and T. W. Kim, "Nondestructive damage sensitivity and reinforcing effect of carbon nanotube/epoxy composites using electro-micromechanical technique," *Materials Science & Engineering C-Biomimetic and Supramolecular Systems,* vol. 23, pp. 971-975, Dec 15 2003.
[19] W. Zhang, V. Sakalkar, and N. Koratkar, "In situ health monitoring and repair in composites using carbon nanotube additives," *Applied Physics Letters,* vol. 91, Sep 24 2007.
[20] X. Zhu, P. Rizzo, A. Marzani, and J. Bruck, "Ultrasonic guided waves for nondestructive evaluation/structural health monitoring of trusses," *Measurement Science & Technology,* vol. 21, Apr 2010.
[21] J. Veilleux, S. E. Kruger, K. T. Wu, and A. Blouin, "Multi-element, high-temperature integrated ultrasonic transducers for structural health monitoring," *Smart Sensor Phenomena, Technology, Networks, and Systems Integration 2013,* vol. 8693, 2013.
[22] Y. J. Sun, Y. H. Zhang, C. S. Qian, and Z. J. Zhang, "Near-Field Ultrasonic Phased Array Deflection Focusing Based CFRP Wing Box Structural Health Monitoring," *International Journal of Distributed Sensor Networks,* 2013.
[23] G. Birkelbach, I. J. Aldave, I. Lopez, and W. Grill, "Integral ultrasonic structural health and load monitoring on a fiber reinforced polymer based composite helicopter tail boom," *Health Monitoring of Structural and Biological Systems 2012,* vol. 8348, 2012.
[24] Z. Kral, W. Horn, and J. Steck, "Crack Propagation Analysis Using Acoustic Emission Sensors for Structural Health Monitoring Systems," *Scientific World Journal,* 2013.
[25] M. Nishino, Y. Harada, T. Suzuki, and H. Niino, "Acoustic damage detection in laser-cut CFRP composite materials," *Laser Applications in Microelectronic and Optoelectronic Manufacturing (Lamom) Xvii,* vol. 8243, 2012.
[26] P. Rizzo and F. L. di Scalea, "Acoustic emission monitoring of carbon-fiber-reinforced-polymer bridge stay cables in large-scale testing," *Experimental Mechanics,* vol. 41, pp. 282-290, Sep 2001.

[27] D. G. Aggelis, N. M. Barkoula, T. E. Matikas, and A. S. Paipetis, "Acoustic structural health monitoring of composite materials: Damage identification and evaluation in cross ply laminates using acoustic emission and ultrasonics," *Composites Science and Technology,* vol. 72, pp. 1127-1133, Jun 8 2012.

[28] R. Austin, P. Ziehl, J. Yu, and D. Forsyth, "Development and Validation of Acoustic Emission Structural Health Monitoring for Aerospace Structures," *Structural Health Monitoring 2013, Vols 1 and 2,* pp. 2123-2129, 2013.

[29] R. K. Verma, R. G. Kander, and B. S. Hsiao, "Acoustic-Emission Monitoring of Damage Using High Amplitude Gains in Carbon-Fiber-Reinforced Poly(Ether Ketone Ketone)," *Journal of Materials Science Letters,* vol. 13, pp. 438-442, Mar 15 1994.

[30] G. P. McCombe, J. Rouse, R. S. Trask, P. J. Withers, and I. P. Bond, "X-ray damage characterisation in self-healing fibre reinforced polymers," *Composites Part a-Applied Science and Manufacturing,* vol. 43, pp. 613-620, Apr 2012.

[31] J. M. Menendez, P. Munoz, J. M. Pintado, and Guemes, "Damage detection in composite materials by FBGs," *Second European Workshop on Optical Fibre Sensors: Proceedings,* vol. 5502, pp. 451-454, 2004.

[32] H. T. Zhao, Q. B. Wang, Y. Qiu, J. A. Chen, Y. Y. Wang, and Z. M. Fan, "Strain transfer of surface-bonded fiber Bragg grating sensors for airship envelope structural health monitoring," *Journal of Zhejiang University-Science A,* vol. 13, pp. 538-545, Jul 2012.

[33] P. Munendhar and S. K. Khijwania, "Two Dimensional Fiber Bragg Grating Based Vibration sensor for Structural Health Monitoring," *Proceeding of International Conference on Recent Trends in Applied Physics & Material Science (Ram 2013),* vol. 1536, pp. 1324-1326, 2013.

[34] Y. Shimada and A. Nishimura, "Development of Optical Fiber Bragg Grating Sensors for Structural Health Monitoring," *Journal of Laser Micro Nanoengineering,* vol. 8, pp. 110-114, Jan 2013.

[35] J. J. Bai, J. X. Li, J. Zhang, X. Y. Zhang, L. Wang, and Y. Wu, "Smart Structural Health Monitoring Based on Detecting Picometer-scale Wavelength Shift of Fiber Bragg Grating," *Micro-Nano Technology Xiv, Pts 1-4,* vol. 562-565, pp. 1346-1352, 2013.

[36] Y. Chen, Y. Q. Ni, X. W. Ye, H. X. Yang, and S. Zhu, "Structural health monitoring of wind turbine blade using fiber Bragg grating sensors and fiber optic rotary joint," *Sensors and Smart Structures Technologies for Civil, Mechanical, and Aerospace Systems 2012, Pts 1 and 2,* vol. 8345, 2012.

[37] E. Kirkby, R. de Oliveira, V. Michaud, and J. A. Manson, "Impact localisation with FBG for a self-healing carbon fibre composite structure," *Composite Structures,* vol. 94, pp. 8-14, Dec 2011.

[38] Y. Y. Hung, "Shearography: a new optical method for strain measurment and nondestructive testing," *Optical engineering,* vol. 21, p. 391, 1982.

[39] X. J. Wang, S. K. Wang, and D. D. L. Chung, "Sensing damage in carbon fiber and its polymer-matrix and carbon-matrix composites by electrical resistance measurement," *Journal of Materials Science,* vol. 34, pp. 2703-2713, Jun 1 1999.

[40] D. C. Seo and J. J. Lee, "Damage detection of CFRP laminates using electrical resistance measurement and neural network," *Composite Structures,* vol. 47, pp. 525-530, Dec 1999.

[41] R. Schueler, S. P. Joshi, and K. Schulte, "Damage detection in CFRP by electrical conductivity mapping," *Composites Science and Technology,* vol. 61, pp. 921-930, 2001.

[42] M. Kupke, K. Schulte, and R. Schuler, "Non-destructive testing of FRP by d.c. and a.c. electrical methods," *Composites Science and Technology,* vol. 61, pp. 837-847, 2001.

[43] A. S. Kaddour, F. A. R. Alsalehi, S. T. S. Alhassani, and M. J. Hinton, "Electrical-Resistance Measurement Technique for Detecting Failure in CFRP Materials at High-Strain Rates," *Composites Science and Technology,* vol. 51, pp. 377-385, 1994.

[44] A. Todoroki, "The effect of number of electrodes and diagnostic tool for monitoring the delamination of CFRP laminates by changes in electrical resistance," *Composites Science and Technology,* vol. 61, pp. 1871-1880, 2001.

[45] S. Wang and D. D. L. Chung, "Mechanical damage in carbon fiber polymer-matrix composite, studied by electrical resistance measurement," *Composite Interfaces,* vol. 9, pp. 51-60, 2002.

[46] A. Todoroki, Y. Mizutani, and Y. Suzuki, "Fatigue damage detection of CFRP using the electrical resistance change method," *International J. of Aeronautical & Space Sci.,* vol. 14, pp. 350–355, 2013.

[47] L. Hou and S. A. Hayes, "A resistance-based damage location sensor for carbon-fibre composites," *Smart Materials & Structures,* vol. 11, pp. 966-969, Dec 2002.

[48] H. Simon and J. Frank, "Electrical damage detection system for a self-healing polymeric composite."

[49] B. P. Rice, "Sensing system for monitoring the structural health of composite structures."

[50] M. F. Yu, O. Lourie, M. J. Dyer, K. Moloni, T. F. Kelly, and R. S. Ruoff, "Strength and breaking mechanism of multiwalled carbon nanotubes under tensile load," *Science,* vol. 287, pp. 637-640, Jan 28 2000.

[51] M. F. Yu, B. S. Files, S. Arepalli, and R. S. Ruoff, "Tensile loading of ropes of single wall carbon nanotubes and their mechanical properties," *Physical Review Letters,* vol. 84, pp. 5552-5555, Jun 12 2000.

[52] N. Yao and V. Lordi, "Young's modulus of single-walled carbon nanotubes," *Journal of Applied Physics,* vol. 84, pp. 1939-1943, Aug 15 1998.

[53] M. M. J. Treacy, T. W. Ebbesen, and J. M. Gibson, "Exceptionally high Young's modulus observed for individual carbon nanotubes," *Nature,* vol. 381, pp. 678-680, Jun 20 1996.

[54] K. Sun, M. A. Stroscio, and M. Dutta, "Thermal conductivity of carbon nanotubes," *Journal of Applied Physics,* vol. 105, Apr 1 2009.

[55] J. K. W. Sandler, J. E. Kirk, I. A. Kinloch, M. S. P. Shaffer, and A. H. Windle, "Ultra-low electrical percolation threshold in carbon-nanotube-epoxy composites," *Polymer,* vol. 44, pp. 5893-5899, Sep 2003.

[56] A. Rochefort, P. Avouris, F. Lesage, and D. R. Salahub, "Electrical and mechanical properties of distorted carbon nanotubes," *Physical Review B,* vol. 60, pp. 13824-13830, Nov 15 1999.

[57] G. T. Pham, Y. B. Park, Z. Liang, C. Zhang, and B. Wang, "Processing and modeling of conductive thermoplastic/carbon nanotube films for strain sensing," *Composites Part B-Engineering,* vol. 39, pp. 209-216, 2008.

[58] N. Hu, Y. Karube, M. Arai, T. Watanabe, C. Yan, Y. Li*, et al.*, "Investigation on sensitivity of a polymer/carbon nanotube composite strain sensor," *Carbon,* vol. 48, pp. 680-687, Mar 2010.

[59] N. Hu, Y. Karube, C. Yan, Z. Masuda, and H. Fukunaga, "Tunneling effect in a polymer/carbon nanotube nanocomposite strain sensor," *Acta Materialia,* vol. 56, pp. 2929-2936, Aug 2008.

[60] S. L. Gao, R. C. Zhuang, J. Zhang, J. W. Liu, and E. Mader, "Glass Fibers with Carbon Nanotube Networks as Multifunctional Sensors," *Advanced Functional Materials,* vol. 20, pp. 1885-1893, Jun 23 2010.

[61] M. Nofar, "Failure detection and monitoring in polymer matrix composites subjected to static and dynamic loads using carbon nanotube networks," Master thesis, Mechanical and industrial engineering, Concordia university, 2008.

[62] M. Nofar, S. V. Hoa, and M. Pugh, "Self sensing glass/epoxy composites using carbon nanotubes," in *ICCM 17 Edinburgh*.

[63] H. Hena-Zamal, "Monitoring Fatigue Damage Behavior of Glass/Epoxy Composites Using Carbon Nanotubes as Sensors," Master thesis, Mechanical and industrial engineering, Concordia University, 2011.

[64] H. Hena-Zamal and S. V. Hoa, "Fatigue Damage Behavior of Glass/Epoxy Composites Using Carbon Nanotubes as Sensors," presented at the 26th ICAF Symposium, Montreal, 2011.

[65] L. M. Gao, T. W. Chou, E. T. Thostenson, Z. G. Zhang, and M. Coulaud, "In situ sensing of impact damage in epoxy/glass fiber composites using percolating carbon nanotube networks," *Carbon,* vol. 49, pp. 3382-3385, Aug 2011.

[66] A. Raghavan, S. S. Kessler, C. T. Dunn, D. Barber, S. Wicks, and B. L. Wardle, "Structural health monitoring using carbon nanotube (CNT) enhanced composites," presented at the IWSHM, 2009.

[67] A. Proper, W. Zhang, S. Bartolucci, A. A. Oberai, and N. Koratkar, "In-Situ Detection of Impact Damage in Composites Using Carbon Nanotube Sensor Networks," *Nanoscience and Nanotechnology Letters,* vol. 1, pp. 3-7, Mar 2009.

[68] A. Baltopoulos, N. Polydorides, A. Vavouliotis, V. Kostopoulos, and L. Pambaguian, "Sensing capabilities of multifunctional composite materials using

carbon nanotubes," presented at the IAC-10.C2.9.2 Prague CZ 61st International Astronautical Congress, 2010.

[69] V. Kostopoulos, A. Vavouliotis, P. Karapappas, P. Tsotra, and A. Paipetis, "Damage Monitoring of Carbon Fiber Reinforced Laminates Using Resistance Measurements. Improving Sensitivity Using Carbon Nanotube Doped Epoxy Matrix System," *Journal of Intelligent Material Systems and Structures,* vol. 20, pp. 1025-1034, Jun 2009.

[70] J. Masters, "Damage detection in composite materials " presented at the American Society for Testing and Materials, Philadelphia PA 1992.

[71] G. Park, C. R. Farrar, F. L. di Scalea, and S. Coccia, "Performance assessment and validation of piezoelectric active-sensors in structural health monitoring," *Smart Materials & Structures,* vol. 15, pp. 1673-1683, Dec 2006.

[72] C. Li, E. T. Thostenson, and T. W. Chou, "Sensors and actuators based on carbon nanotubes and their composites: A review," *Composites Science and Technology,* vol. 68, pp. 1227-1249, May 2008.

[73] L. M. Gao, T. W. Chou, E. T. Thostenson, and Z. G. Zhang, "A comparative study of damage sensing in fiber composites using uniformly and non-uniformly dispersed carbon nanotubes," *Carbon,* vol. 48, pp. 3788-3794, Nov 2010.

[74] N. D. Alexopoulos, C. Bartholome, P. Poulin, and Z. Marioli-Riga, "Structural health monitoring of glass fiber reinforced composites using embedded carbon nanotube (CNT) fibers," *Composites Science and Technology,* vol. 70, pp. 260-271, Feb 2010.

[75] I. D. Rosca and S. V. Hoa, "Highly conductive multiwall carbon nanotube and epoxy composites produced by three-roll milling," *Carbon,* vol. 47, pp. 1958-1968, Jul 2009.

[76] S. Wicks, D. Barber, A. Raghavan, C. T. Dunn, L. Daniel, S. S. Kessler*, et al.*, "Health monitoring of carbon nanotube (CNT) hybrid advanced composite for space applications," presented at the MIT Copyright 2009.

[77] L. Vanderpauw, "A method of measuring the resistivity and Hall coefficient on lamellae of arbitrary shape," pp. 220-224, 1958.

[78] J. D. Weiss, R. J. Kaplar, and K. E. Kambour, "A derivation of the van der pauw formula from electrostatics," *Solid-state Electron,* vol. 52, pp. 91-98, 2008.

[79] D. D. L. Chung, "Structural health monitoring by electrical resistance measurement," *Smart Materials & Structures,* vol. 10, pp. 624-636, Aug 2001.

[80] K. Schulte and C. Baron, "Load and Failure Analyses of CFRP Laminates by Means of Electrical-Resistivity Measurements," *Composites Science and Technology,* vol. 36, pp. 63-76, 1989.

[81] A. Todoroki, M. Tanaka, and Y. Shimamura, "Electrical resistance change method for monitoring delaminations of CFRP laminates: effect of spacing between electrodes," *Composites Science and Technology,* vol. 65, pp. 37-46, Jan 2005.

[82] S. K. Wang, D. D. L. Chung, and J. H. Chung, "Impact damage of carbon fiber polymer-matrix composites, studied by electrical resistance measurement,"

Composites Part a-Applied Science and Manufacturing, vol. 36, pp. 1707-1715, 2005.

[83] A. Todoroki, Y. Tanaka, and Y. Shimamura, "Multi-probe electric potential change method for delamination monitoring of graphite/epoxy composite plates using normalized response surfaces," *Composites Science and Technology,* vol. 64, pp. 749-758, Apr 2004.

[84] A. Iwasaki and A. Todoroki, "Statistical evaluation of modified electrical resistance change method for delamination monitoring of CFRP plate," *Structural Health Monitoring-an International Journal,* vol. 4, pp. 119-136, Jun 2005.

[85] D. Wang and D. D. L. Chung, "Comparative evaluation of the electrical configurations for the two-dimensional electric potential method of damage monitoring in carbon fiber polymer-matrix composite," *Smart Materials & Structures,* vol. 15, pp. 1332-1344, Oct 2006.

[86] D. J. Wang, S. K. Wang, D. D. L. Chung, and J. H. Chung, "Comparison of the electrical resistance and potential techniques for the self-sensing of damage in carbon fiber polymer-matrix composites," *Journal of Intelligent Material Systems and Structures,* vol. 17, pp. 853-861, Oct 2006.

[87] D. J. Wang, S. K. Wang, D. D. L. Chung, and J. H. Chung, "Sensitivity of the two-dimensional electric potential/resistance method for damage monitoring in carbon fiber polymer-matrix composite," *Journal of Materials Science,* vol. 41, pp. 4839-4846, Aug 2006.

[88] S. K. Wang, D. J. Wang, D. D. L. Chung, and J. C. H. Chung, "Method of sensing impact damage in carbon fiber polymer-matrix composite by electrical resistance measurement," *Journal of Materials Science,* vol. 41, pp. 2281-2289, Apr 2006.

[89] A. Todoroki, Y. SHIMAZU, and Y. MISUTANI, "Electrical Resistance Reduction of Laminated Carbon Fiber Reinforced Polymer by Dent Made by Indentation without Cracking," *Journal of Solid Mechanics and Materials Engineering* vol. 6, 2012.

[90] Y. Suzuki, A. Todoroki, R. Matsuzaki, and Y. Mizutani, "Impact-damage visualization in CFRP by resistive heating: Development of a new detection method for indentations caused by impact loads," *Composites Part a-Applied Science and Manufacturing,* vol. 43, pp. 53-64, Jan 2012.

[91] A. Naghashpour and S. Van Hoa, "A technique for real-time detection, location and quantification of damage in large polymer composite structures made of electrically non-conductive fibers and carbon nanotube networks," *Nanotechnology,* vol. 24 (455502), Nov 15 2013.

[92] A. Naghashpour and S. Van Hoa, "In situ monitoring of through-thickness strain in glass fiber/epoxy composite laminates using carbon nanotube sensors," *Composites Science and Technology,* vol. 78, pp. 41-47, Apr 1 2013.

[93] A. Todoroki, D. Haruyama, Y. Mizutani, Y. Suzuki, and T. Yasuoka, "Electrical Resistance Change of Carbon/Epoxy Composite Laminates under Cyclic Loading under Damage Initiation Limit," *Open Journal of Composite Materials,* vol. 4, pp. 22-31, 2014.

[94] J. D. Kraus and K. R. Carver, *Electromagnetics*, second edition ed. McGraw-Hill, 1973.

[95] A. Todoroki and Y. Tanaka, "Delamination identification of cross-ply graphite/epoxy composite beams using electric resistance change method," *Composites Science and Technology,* vol. 62, pp. 629-639, 2002.

[96] R. Pipes and N. Pagano, "Interlaminar stresses in composite laminates under uniform axial extension," *J Compos Mater* vol. 4, pp. 538–548, 1970.

[97] N. J. Salamnon, "An Assessment of the Interlaminar Stress Problem in Laminated Composites," *Journal of Composite Materials,* vol. 14, pp. 177-194, 1980.

[98] S. Takeda, Y. Okabe, T. Yamamoto, and N. Takeda, "Detection of edge delamination in CFRP laminates under cyclic loading using small-diameter FBG sensors," *Composites Science and Technology,* vol. 63, pp. 1885-1894, Oct 2003.

[99] B. Fiedler, F. H. Gojny, M. H. G. Wichmann, W. Bauhofer, and K. schulte, "Can carbon nanotubes be used to sense damage in composites?," *ANN CHIM SCI MATER* vol. 22, pp. 81-94, 2004.

[100] J. M. Whitney, I. M. Daniel, and R. B. Pipes, "Experimental mechanics of fiber reinforced composite materials," *Society for Experimental Mechanics Monograph,* vol. 4., 1984.

[101] P. L. N. Murthy and C. C. Chamis, "Free-Edge Delamination - Laminate Width and Loading Conditions Effects," *Journal of Composites Technology & Research,* vol. 11, pp. 15-22, Spr 1989.

[102] P. G. Ifju, J. E. Masters, and W. C. Jackson, "The use of Moiré interferometry as an aid to standard test method development for textile composite materials," *Compos Sci Technol* vol. 53, pp. 155-163, 1995.

[103] Y. Guo, D. Post, and B. Han, "Thick Composites in Compression - an Experimental-Study of Micromechanical Behavior and Smeared Engineering Properties," *Journal of Composite Materials,* vol. 26, pp. 1930-1944, 1992.

[104] C. L. Nailadi, D. F. Adams, and D. O. Adams, "An experimental and numerical investigation of the free edge problem in composite laminates," *Journal of Reinforced Plastics and Composites,* vol. 21, pp. 3-39, 2002.

[105] M. W. Hyer, *Stress Analysis of Fiber-Reinforced Composite Materials*: Destech publications.

[106] http://www.mflstraingauges.com/index_gauge_types.html.

[107] A. Allaoui, S. V. Hoa, and M. D. Pugh, "The electronic transport properties and microstructure of carbon nanofiber/epoxy composites," *Composites Science and Technology,* vol. 68, pp. 410-416, Feb 2008.